UNIVERSITAT DE BARCELONA

Nanostructured systems of thymol for dermatological and topical treatments

Camila Folle

UNIVERSITAT DE BARCELONA

FACULTAT DE FARMACIA I CIÈNCIES DE L'ALIMENTACIÓ

Nanostructured systems of thymol for dermatological and topical treatments

Sistemas nanoestructurados de timol para tratamientos dermatológicos y tópico enfermedades neurodegenerativas

Camila Folle

BARCELONA 2021

UNIVERSITAT DE BARCELONA

DOCTORAL PROGRAM

Researcg, Development and Control of Drugs

Nanostructured systems of thymol for dermatological and topical treatments

Report presented by Camila Folle to apply for the title of Doctor from the University of Barcelona

Directors

Dra. María Luisa García López Dra. Ana Cristina Calpena Capmany

PhD student

Camila Folle

Tutor

Ana Cristina Calpena Capmany

Barcelona, 2021

Abbreviation list

AM	Antimicrobial
AOX	Antioxidant
ATP	Adenosine triphosphate
BHT	Butylated hydroxytoluene
B-NPs	Blank Nanoparticles
B-NP-T-	Blank Nanoparticles surface covered TW
B-NP-L-	Blank Nanoparticles surface covered PL
B-NP-P-	Blank Nanoparticles surface covered P188
B-NP-P-C+	Blank Nanoparticles surface covered P188/CS
CS	Chitosan
CTR	Control
DCF	2,7-dichlorofluorescein
DLS	Dynamic light scattering
DMEM	Dulbecco's Modified Eagle's medium
DPPH	2,2-diphenyl-1-picrylhydrazyl
DS	Deep skin
DSC	Differential Scanning Calorimetry
EE	Entrapment efficiency
EO	Essential oil
EPD	Epidermidis
PR	Phenol Red
FS	Fat skin
FBS	Fetal bovine serum
FDA	Food and drug administration
GC	Gel carbomer
GC-TH	Carbomer gel of thymol
GC-TH-NP	Carbomer gel of thymol NPs
GC-TH-NLC	Carbomer gel of thymol NLCs
GH	Gel hydroxypropilmethylcellulose
GP-TH	Pluronic gel of thymol
GP-TH-NP	Pluronic gel of thymol NPs
GP-TH-NLC	Pluronic gel of thymol NLCs
GH-TH-NP	HPMC gel of thymol NPs
GH-TH-NLC	HPMC gel of thymol NLCs
GLY	Gliceryn
GP	Gel pluronic
HPLC	High-performance liquid chromatography
HPMC	Hydroxypropilmethylcellulose
LNPs	Lipid Nanoparticles
MB	methylene blue
McF	Mac Farland standard
MO	Microorganism
MTT	(3-(4,5-Dimethylthiazol-2-yl)- 2,5-diphenyl tetrazolium bromide)
MW	Molecular weight

NLC	Nanosctructured lipid carrier
NLRP3	NOD-like receptor pyrin 3
NPs	Nanoparticles
NS	Nanosphere
NSAIDs	Non-steroidal anti-inflammatory drugs
OD	Optical density
PG	Propylenglycol
PI	Polydispersity index
PL	Phosphatidylcoline
PLGA	Poly-(D,L)lactic-co-glycolic acid
PNPs	Polymeric nanoparticles
PR	Phenol Red
RHOD	Rhodamine
ROS	Reactive oxygen species
SC	Stractum corneum
SDL	Skin deeper layers
SEM	Scanning Electron Microscopy
TEM	Transmission electron microscopy
TH	Thymol
THO	Thyme Oil
TH-NLC-PP-	Thymol-loaded NLC surface covered P407
TH-NPs	Thymol-loaded Nanoparticles
TH-NP-T-	Thymol-loaded Nanoparticles surface covered TW
TH-NP-P-	Thymol-loaded Nanoparticles surface covered P188
TH-NP-P-C+	Thymol-loaded Nanoparticles surface covered P188/CS
TH-NP-PP-	Thymol-loaded Nanoparticles surface covered P407
TH-NP-PP-C+	Thymol-loaded Nanoparticles surface covered P407/CS
TH-NP-L-	Thymol-loaded Nanoparticles surface covered PL
THO-NPs	Thyme oil loaded Nanoparticles
THO-NP-P-	Thyme oil loaded Nanoparticles surface covered P188
THO-NP-P-C+	NPP-Th (P188)
THO-NP-L-	NPP+Th (P188+CS)
TW	Tween 20
WH	Wound healing
XRD	X-Ray diffraction
Zav	Average particle size
ZP	Zeta potential

ABSTRACT

The skin is the major organ of the human body, which protect the internal tissue from environmental changes, maintaining the body temperature and avoiding penetration of contaminants. Therefore, the skin barrier is highly restrictive and constitutes the major challenge for most of the compounds to be administered dermally. Moreover, the skin possesses resident microbiota, which perform several roles in the skin functionality, more specifically, maintain the sebum levels, the acid pH and protect the skin against other pathogenic microorganism. The healthy skin is a result of an equilibrium of resident microbiota. Their unbalanced proliferation may lead to skin disorders such as infection and inflammation, either caused by internal disfunction or external contaminants. Antimicrobial actives from natural source, such as plant material, are a promoting approach for the treatment of skin infection, should be considered to avoid antibiotic, class of drug, which along the treatment normally lead to microbial resistance.

Natural products are the most favourable active types, since they may not develop side effects, and in the case of antimicrobial agents, they are unlikely to lead to microbial resistance, as most of the antibiotic class of drugs. Plant material are suitable choices, due to their high content of antioxidant compounds, which most of them are phenolic aromatic molecules, which normally possess antimicrobial and anti-inflammatory activities, the key treatment requirement for skin infections.

Thymol (TH), is a multifunctional monoterpene of aromatic phenolic structure, found naturally occurring in plant extracts or on its white crystalline synthetic form. The effects of TH are largely attributed to its antioxidant properties, via free radical scavenging thus enhancing endogenous antioxidant activities and chelation of metal ions.

Nanostructured systems, such as polymeric and lipid nanoparticles, may contribute as a novelty approach for management of skin diseases. Nanotechnology offers several advantages to improve active compounds bioavailability after topical administration, since small particle diameters tend to penetrate the deep skin, withdraw the drug in a controlled manner and be mainly retained in the deeper layers. Moreover, they constitute an excellent potential candidate in skin disorders, especially for acne treatment, due to their ability to penetrate inside the follicle and provide for long-term release of actives inside the lesions.

According to the above, the main objective of this work was the development and physicochemical and biopharmaceutical characterization of polymeric and lipid nanostructured systems containing TH for the treatment of skin infections, mainly focused to the acne. The study consisted on modified surface composition of the nanosystem, in other to enhance the therapeutic efficacy of this novel approach. Polymeric and lipid nanoparticles of thymol provided suitable physicochemical morphometry, sustained release, and slow-rate penetration of TH into the hair follicle, being highly retained inside the

skin. The therapeutical efficacy was achieved with good results as antimicrobial activity against *Cutibacterium acnes* and minor effect towards *Staphylococcus epidermis*, the major resident of the healthy skin microbiota. Moreover, the development of surface-modified polymeric NPs with thymol performed enhanced *in vitro* anti-inflammatory, antioxidant, and wound healing activities in human keratinocyte cells (HaCaT). Moreover, semi-solid formulations with the nanosystem incorporated had proven to diminish the trans-epidermal water loss due to the film-forming developed on the skin surface. Sebum reduction activity was also recorded in oily skin, presenting outstanding results.

To conclude, nanostructured systems of thymol provided good antimicrobial activity for acne treatment without affecting the healthy skin microbiota. The surface-modification of TH-NPs had proven to be suitable to be used as anti-inflammatory, antioxidant, and wound healing agents, constituting a promising therapy for treating acne infection and associated inflammation. According to the results obtained, the nanostructured systems of thymol and the semi-solid formulations which they were incorporated, demonstrated an outstanding strategy for skin disorders, being considered a novelty approach as a natural treatment of acne. These formulations could be useful for daily application as a complement with other cosmetic and personal hygiene products, for prevention or treatment of also other microbial skin infections.

INDEX

1. Introduction…… 1

1.1. Skin: Anatomy and Physiopathology…….. 3

1.1.1. Skin Structure……...……... 3

1.1.2. Skin Microbiota…..…… 7

1.1.3. Skin Exposome……..… 12

1.1.4. Skin Regenerative Processes…… 14

1.1.5. Skin Penetration Route…… 14

1.1.6. Skin Diseases…… 17

1.2. Natural Products in Pharmacotherapy…… 27

1.2.1. Thyme Oil……..…….... 28

1.2.2. Thymol……..…..……. 29

1.3. Nanoparticles for Skin Delivery…..…….. 32

1.3.1. Biodegradable Polymeric Nanoparticles…..……... 32

1.3.2. Biodegradable Lipid Nanoparticles……..…….. 34

1.3.3. Skin Penetration of Nanoparticles……..……. 36

2. Hypothesis and Objectives…….…….. 39

2.1. Hypothesis……..… 41

2.2. Objectives…….. 42

3. Materials and Methods……. 43

3.1. Product and Reagents……..… 45

3.2. Instrumental…….…….. 47

3.3. Preparation of Nanoparticles…… 48

3.3.1. Preparation and Optimization of Thymol-Loaded Polymeric NPs……..... 48

3.3.2. Preparation of Thymol Loaded Lipid Nanoparticles…… 49

3.3.3. Preparation of Semi-Solid Formulations of Developed Nanoparticles...……. 51

3.4. Analytical Methods……... 52

3.4.1. Physicochemical Characterization of Thymol NPs…….. 52

3.4.2. Nanoparticles Interaction Studies……..……..... 54

3.4.3. Stability Studies…… 55

3.4.4. Rheological Studies…….. 57

3.5. Biopharmaceutical Behaviour…… 59

3.5.1. *In vitro* Release…… 59

3.5.2. *Ex.vivo* Skin Permeation…… 60
3.6. Biochemical Studies……. 62
3.6.1. Cytotoxicity of Thymol Nanoparticles……..…… 62
3.6.2. Cellular Uptake of Thymol Nanoparticles.....…… 62
3.7. Therapeutical Efficacy…….……. 63
3.7.1. *In vitro* and *Ex vivo* Antimicrobial Efficacy……..……...…… 63
3.7.2. *In vitro* and *Ex vivo* Antioxidant Activity…….…… 66
3.7.3. *In vitro* and Anti-Inflammatory Efficacy…… 67
3.7.4. *In vitro* Wound Healing Efficacy…… 69
3.7.5. *In vivo* Efficacy Studies……. 69
4. Results……. 71
4.1. Thymol-Loaded PLGA Nanoparticles…… 73
4.1.1. Formulation, Characterization and Optimization…… 73
4.1.2. Biopharmaceutical Behaviour……. 79
4.1.3. Biochemical studies…… 81
4.1.4. Therapeutic Efficacy…… 83
4.2. Surface-Functionalized Thymol-Loaded PLGA NPs…… 88
4.2.1. Physicochemical Characterization……88
4.2.2. Biopharmaceutical Behaviour…….. 93
4.2.3. Therapeutic Efficacy and Biochemical studies…….93
4.3. Thyme Oil Loaded PLGA Nanoparticles…… 103
4.3.1. Physicochemical Characterization…….. 103
4.3.2. Biochemical studies…… 104
4.3.3. Therapeutic Efficacy……... 105
4.4. Semi-Solid Formulations of Thymol and Thyme Oil PLGA NPs……. 109
4.4.1. Physicochemical and Rheological Characterization of Semi-Solid Formulations…….. 109
4.4.2. Biopharmaceutical Behaviour……. 113
4.4.3. Therapeutic Efficacy……118
4.5. Thymol-Loaded Nanostructured Lipid Carriers……125
4.5.1. Formulation, Characterization and Optimization……..125
4.5.2. Surface-Functionalization of TH-NLC and Physicochemical Characterization……. 131
4.5.3. Physicochemical and Rheological Characterization of Semi-Solid Formulations…….. 134
4.5.4. Biopharmaceutical Behaviour…….. 136
4.5.5. Biochemical studies…….. 139
4.5.6. Therapeutic Efficacy……141

5. Discussions…… 147
5.1. Polymeric NPs…….. 149
5.1.1. Thymol-Loaded PLGA NPs…….……..... 149
5.1.2. Surface-Functionalized Thymol-Loaded PLGA NPs…...……. 152
5.1.3. Thyme-Oil-Loaded PLGA NPs……. 154
5.1.4. Semi-Solid Formulations of Polymeric NPs……. 156
5.2. Lipid NPs……. 160
5.2.1. Nanostructured Lipid Carriers of Thymol…….…….. 1660
6. Conclusions…… 165
7. References..…….. 169
8. Appendix……. 185
8.1. Published Article……. 187
8.2. Accepted Article (in press)…….. 211

1. INTRODUCTION

1.1 SKIN: ANATOMY AND PHYSIOPATOLOGY

The skin is the largest body organ (a surface area of 1.5 - 2.0 m^2) which constitutes the extern interface of the human body with the environment, performing an important role as mechanical and physical barrier. Hence, is considered an energized organ that protects the organism against environmental factors and regulates heat and water loss from the body (Uchechi, Ogbonna, and Attama 2014). The skin functions are focused on thermoregulation, immunological and sensorial mediations, fluid homeostasis, as well as social and protective activities. These functions are related to the complex multiple layers containing highly specified cells and structures (Zhang et al. 2013). Moreover, the skin barrier function plays the most important role in drug development and pharmacokinetic implications for topical administration (Calpena, Clares, and Fernández 2011).

Furthermore, the skin participates in the internal and external environment, being exposed to challenges such as pollution, allergen, microbial agents, ageing, infections, inflammations, sensitization, UV damage and water impairment. Nevertheless, it provides metabolic functions that can be associated to stress, nutrition, hormonal disorder, among others. The internal water balance and excretory systems (eccrine) are also involved on skin activity. For these reasons, a healthy skin is fully dependant on the internal and external balance, based on the protective barrier. Nevertheless, the penetration of active ingredient inside the skin is limited due to the barrier function, and therefore, enhanced penetration techniques are the keys for an effective skin treatment.

1.1.1. Skin Structure

The skin is a complex organ consisting of three anatomical layers: epidermis, dermis, and subcutaneous fat tissue (hypodermis), that perform important functions between the external environment and the internal organism (**Figure 1**). The multiple layers of the skin provide different types of protection. The most superficial skin layer, the epidermis, provides waterproofing and acts as a barrier to infection. The middle layer, the dermis, contains blood vessels, nerves, and glands that are important for our skin's function. The inner layer of the skin contains fat that acts as a shock absorber, protecting the body from internal injury and trauma.

The skin thickness varies over the body, corresponding to the thinnest part the eyelids (less than 0.1 mm thick) and the thickest to the palms, foot soles and upper back more than 5.0 mm (Zhang et al. 2013).

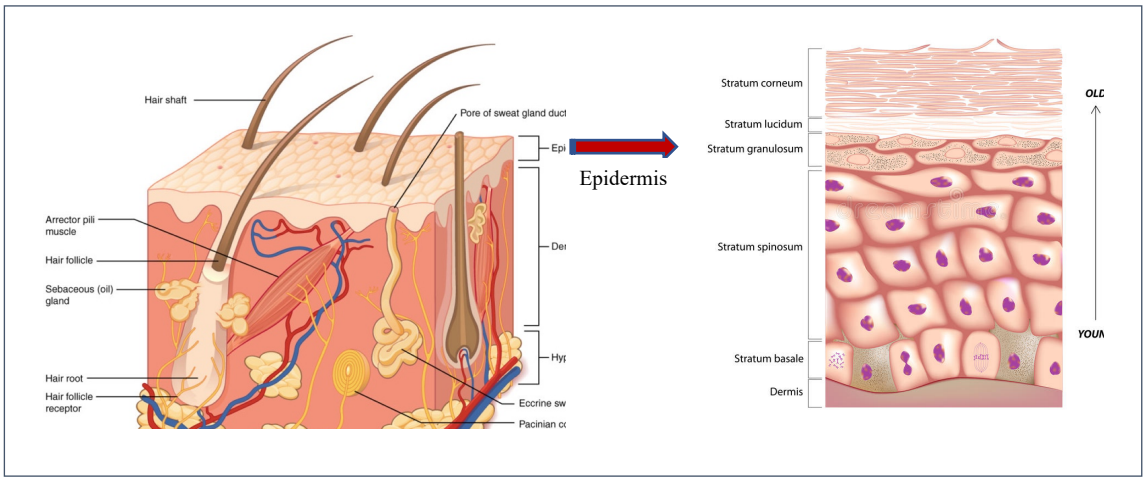

Figure 1.1. Skin structure

(https://courses.lumenlearning.com/suny-wmopen-biology2/chapter/structure-and-function-of-skin/)

Epidermis

The epidermis, constitutes the outermost layer, being responsible for physical barrier protection against exogenous attack such as microbial pathogens and pollutants. It is composed of the keratinized stratified squamous and non-vascularized flat epithelium, with an average thickness ranged from 0.02 to 0.2 mm (depending on the anatomical area). The main epidermal cells are the keratinocytes (95% of cells) while melanocytes, Langerhans cells and Merkel cells account for the remaining 5%. The keratinocytes, as they rise to the surface, become wider and flatter, gradually losing the nucleus and organelles, becoming enriched in keratin (Wertz 1996). The total water content on the entire epidermis is lower than the dermis, corresponding to only 20 - 30 %. The main skin functions are protection against external environment, occlusive, preventing body water loss (dehydration), and receptor for epidermal metabolic products (Calpena et al. 2011). It is made up of two main layers: the stratum corneum (comprising the external barrier in contact with the external environment) and the stratum germinativum (the rest of the epidermis down to the top layer of the dermis). Based on the location, five different layers of the epidermis can be identified, from the inner base to the surface (**Figure 1.1**):

- ***Stratum Basale*** is a single layer of cells linked by desmosomes and a basal lamina supported by hemidesmosomes, responsible for actively constant regeneration of the entire epidermal cell layers, produced by continuous replication. This layer is composed not only by keratinocytes but also melanocytes (skin melanin), Langerhans cells (immune system) and Merkel cells (neuro-endocrine system).

- ***Stratum Spinosum*** is formed by cells that are linked by intercellular bridges to spine mode with cytoplasmic continuity.
- ***Stratum Granulosum*** is composed of cells that contain granules of keratohyalin which by degradation produces hygroscopic substances responsible for the natural hydration of the skin. The granules also contain glycolipids and sterols, which are excreted into the extracellular medium, being the main responsible for the impermeability of the epidermis.
- ***Stratum Lucidum*** is located between the granular and the corneous layers where cells lose organelles by protease and nuclease. This tight junction creates an impermeable moisture barrier to most drug molecules above 500 kDa and also hydrophilic (Bos and Meinardi 2000). Moreover, the outermost layer of the entire epidermis is the main access tool for active ingredients to be able to penetrate across the skin. This complies with several implications that formulations must enhance the suitability of vehicles to enable the active pathways through this protective barrier.
- ***Stratum corneum (SC)*** constitutes the epidermis external layer and is made up of highly flattened cells keratinized, called corneocytes, which have lost their nuclei and cytoplasmic organelles and can be considered physically dead cell (Palmer and DeLouise 2016). These insoluble bundled keratins are surrounded by a cell envelope, stabilized and held together by crosslinked proteins and covalently bound lipids (Schneider et al. 2009). These lipids combined with constant peeling and renewal are the main responsible for the barrier function (Tanner and Marks 2008). Among these lipids, 70 - 80% corresponds to neutral ones. More specifically, usually present in SC, 14 % free sterols, 19.3 % free fatty acids, 25.2 %; triglycerides, 5.4 % cholesterol and fatty esters, 4.8 % squalene, 6.1 %; alkanes, 18 % sphingolipids (ceramides and glucosylceramides), and 5% polar lipids (phosphatidylethanolamine, phosphatidylcholine, phosphatidylserine and sphingomyelin) (Lampe et al. 1983). This epicutanous emulsion or hydrolipidic coverage is formed from metabolic products from sebaceous secretions of keratinocytes and the water from sweat glands. This helps to maintain the protective microbiota and cutaneous functions (Pappas 2009). This external structure also behaves as a biological affinity-selective membrane for substances penetrating across the skin layers.

Since the skin is the most accessible organ of the body and it is designed to isolate the organism from the external milieu (Calpena et al. 2011). For this reason, all skin penetration issues are major related to the ability to cross the SC, hence the tight impermeable junction thought the granular layer. However, there are pharmaceutical development of excipients that yield optimal permeation and cutaneous absorption of the actives. In fact, this remarkable taught characteristic

is crucial to protect our internal system form the external aggressions, such as hazard chemicals, pathogens, and pollutants.

Nevertheless, the hair follicle, the sebaceous gland and the sweat glands are deeply located through the entire length of the dermis, with the base located on the hypodermis junction however, their cellular enrolment are confined by the epidermis layers, except the SC.

The epidermis is separated from the dermis by a thin ***cutaneous basement membrane***, lesser than <200 nm across, composed of an intricate network of macromolecules that link the keratin intermediate filaments, of basal keratinocytes, with collagen fibres in the superficial dermis, thus, providing the epidermis-dermis adhesion.

Dermis

It is the internal layer of the skin, with 0.5-5 mm thick (depending on the body site), formed by an amorphous matrix highly irrigated, rich in glycosaminoglycans with high wetting power that nourishes and hydrates the epidermis, acting as their support. It is formed by fibrous protein collagen, elastin, immune cells, fibroblasts (also involved on the cell regeneration and wound healing activity), lymphatic vessels, nerves, and many other components. The dermis is, therefore, a highly irrigated and sensitive tissue. Since the tightest level of the skin barrier is found on the epidermis, once actives reach the dermis, it enables their access to the blood vessels, thus enter the systemic circulation, but firstly, they must be able to cross the SC barrier (Calpena et al. 2011).

Hypodermis

The subcutaneous tissue or hypodermis is the lower base of the entire skin which separates the dermis from the underlying tissues, nerves, and muscles. It is a highly moisten and fatty tissue, where the elastic fibres and the vascularized system are present. The hypodermis contains the fibroblasts, adipose tissue (fat cells), connective tissue, larger nerves, blood vessels, and macrophages. It is also the base of the hair follicles and the origin of the sebaceous glands, which play a crucial role in the passage of drugs to systemic circulation, since in these areas, the thickness of the SC decreases and may eventually disappear(Wilkes, Brown, and Wildnauer 1973). However, the fat deposit may behave as a deep compartment for the drug, delaying its entry in the blood circulation (Calpena et al. 2011).

Skin Appendages

Skin appendages (adnexa) are considered skin-associated structures that perform several specific functions, such as sensation, lubrication, and heat loss. Among these, the most involved in drug skin penetration are hair (sensation, heat loss, filter for breathing, protection), sebaceous glands (secrete sebum onto hair follicle, which grease skin and hair), and sweat glands (secrete sweat).

- *Hair follicle:* is a derivative of the epidermis formed by two parts: the follicle and the hair shaft. Hair follicles are angled settled into the dermis, with the bulb (germinal matrix) touching the hypodermis-dermis junction (Graham-Brown and Bourke 2006). It is formed from the base on the fat tissue, surrounded by the epidermis into the dermal layer, up until the external barrier. They are composed of papilla, matrix, root sheath, hair fibre and bulge. Also, they are associated with arrector pili muscles that pull hairs straight. Besides producing hair, the hair follicles contain several types of stem cells that play an important role in wound healing and re-epithelialization. The follicle is the essential unit for the hair generation by a continuous growth and rest sequence (hair cycle).
- *Sebaceous glands*: microscopic exocrine glands that opens into a hair follicle to secrete an oily or waxy matter (sebum), which lubricates the hair and skin, maintaining the dermal oil balance.
- *Sweat glands*: Eccrine system which secretes sweat, regulating body temperature, associated to apocrine glands involved with hair follicles, in certain restricted regions of the body, such as axilla, and nails (Zhang et al. 2013).

1.1.2. SKIN MICROBIOTA

The skin microbiota is an ecosystem of bacteria on the skin's surface and internal layers that constitutes the entire microbiota, composed of several microorganisms (MOs) There Mos are present on skin, being considered resident or transient. More specifically, it refers to microbes including bacteria, fungi, protozoa, viruses, and mites living, which are generally non-pathogenic It works to protect against external pathogens that could affect skin and overall health. There are evidence of relationship between bacteria, skin cells and immune cells, which reinforce and repair the skin barrier, improve defences against infection and diminishes excessive inflammations (Grice and Segre 2011). When the microbiota is balanced, the skin looks and feels healthy, and present a balanced immune system.

The *transient microbiota* colonizes the skin superficial layers and are likely to be removed by hygiene routine. Those do not normally proliferate but sporadically, leading to an infection disease. Their transmissibility and activity are dependent on the number of present species and their concentration on the surface, as well as on the skin moisture. The *resident microbiota* are consistent skin survivals, mainly found on the surface, under the superficial cells of the SC. They are normally gram-positive bacteria, not regarded as pathogens and they survive longer on intact skin than gram-negative transient species. The protective microbiota functions are believed to be microbial antagonism activity and nutrient competition for the stability of the dermal ecosystem, preventing the adherence of pathogens (Kampf G and Kramer A 2004).

Skin is colonized by beneficial microorganisms and serves as a physical barrier to prevent the invasion of pathogens. In circumstances where the barrier is broken or when the balance between commensals and pathogens is disturbed, skin or even systemic diseases can be developed.

- *Staphylococcus epidermidis* is a non-pathogenic bacterium most abundant on the entire human skin. It is found mostly concentrated on the external layers but is also found ubiquitous. In fact, *S. epidermidis* may have a probiotic function by preventing colonization of more pathogenic bacteria such as *S. aureus* (Otto 2009).
- *Cutibacterium acnes* (previously known as Propionibacterium acnes), a rod-shaped Gram-positive and aerotolerant anaerobic bacterium, is a resident microbiota, which maintains the balance of the skin microbiota, its acidity and sebum levels, and is mainly located on the deeper layers of the skin surrounding the hair follicle. Although, it can also be found on the proximities of the external epidermidis in lower concentrations.

The skin is an active immune organ whose function is augmented by the presence of commensal microbiota. Keratinocytes and dermal appendages release antimicrobial peptides (AMPs) and proteins, which provide defence against pathogenic microbes. There are several other types of MOs related to our skin microbiota, depending on the region. For example, *C. acnes* are mainly found on facial skin, whereas *S. aureu*s are mainly found on skin hand, underarms, or other sweat excretory regions. The top three bacterial species for each skin site are shown in **Figure 1.2**. Dry and sebaceous sites are colonized predominantly by *C. acnes*, whereas moist sites and the foot are colonized chiefly by Corynebacterium tuberculostearicum (Coates et al. 2019).

Other skin microbiota constituents are fungi, yeast and some viruses. Among fungi, the most common resident, is *Pityrosporum (Malassezia) spp* (Noble 1993), the pathogen on seborrheic dermatitis, that proliferates within an impairment of sebum production on the scalp.

Normal human skin microbiota is colonized by a total aerobic bacterial count, expressed as colony forming units (CFU)/cm^2, ranging from above 1 x 10^6 (scalp), 5 x 10^5 (axilla), and 4 x 10^4 CFU/cm^2 (abdomen) to 1 x 10^4 CFU/cm^2 (forearm) (Selwyn 1980).

The skin and its annexes constitute the main structural defence barrier of the organism, against external agents, to which is constantly exposed. There is a constant balance between microorganism and host, so the impairment of this balance can promote the development of infections.

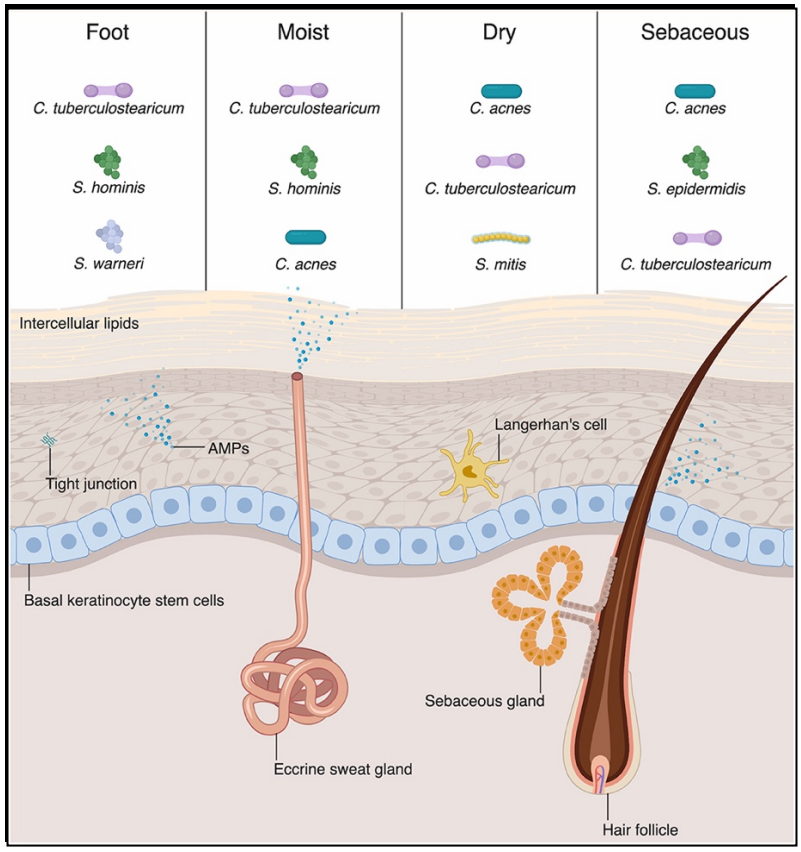

Figure 1.2: Skin microbiota. The top three bacterial species for each skin site (Coates et al. 2019).

However, when an unbalanced function of the sebaceous glands occurs, this bacterium proliferates, behaving as pathogenic and leading to acne development. Therefore, it can be considered a dual activity on the skin microbiota, being a non-pathogenic essential for sebum control, as well as active pathogenic on acne infection and inflammation. Moreover, *Staphylococcus aureus* are transient skin bacteria, which can be naturally found at low concentrations on the outermost layers of the skin, as well as they can be acquired by direct contact to contaminated surfaces. They are able to remain harmless to health but could also be mildly or severely pathogenic, leading to strengthened skin infection diseases. Patients with chronic dermatitis are particularly likely to have skin areas colonized with *S. aureus* (Aly, Maibach, and Shinefield 1977).

Associated with the natural skin microbiota of the skin we highlight two important species of transient MOs:

Gram positives: *Staphylococcus aureus* and *Streptococcus pyogenes*. Therefore, involved in skin infections if balance is not maintained.

- *S. Aureus,* a Gram-positive coccus, has great pathogenic potential due to the large amount of toxins and enzymes it is able to produce such as cytotoxin (induces the lysis and marked inflammation) and the epidermolytic toxin (produces skin erythema and epidermal separation).
- *S. pyogenes, a Gram-positive coccus,* is a microorganism that can be found forming part of the microbiota of the upper airways and in certain wet and hot areas of the skin surface. It is sometimes able to produce skin infections whose invasiveness and aggressiveness will depend mainly on the host's immune system and the characteristics of the microorganism.

Gram negative bacteria like *P. aeruginosa* and *E.* coli are not responsible for primary dermal infections but are related to secondary infections that can be triggered after a previous bacterial infection that facilitates the entry of other microorganisms, that will generate symptoms and infections associated with their bacterial nature.

- *P. aeruginosa,* a Gram-negative bacillus, which in culture media produces blue-green colonies due to pigment production, is widely spread in nature in intimate association with wet media. It can often affect skin structures by producing folliculitis, nail infections, and surgical wound infections.
- *Escherichia coli*, a Gram-negative bacterium, is found naturally in the intestinal flora of hot-blooded organisms. When the skin is physically altered, it can become a focus of entry into the body and trigger infections caused by this bacterium, such as cellulites, surgical site infections, after burn injuries infections, among others (Petkovšek et al. 2009).

In the skin immunological activity, the microbial ligands for tool-like receptors (TLRs) include bacterial cell wall components and genetic material. TLR4 mediates host responses to gram-negative bacterial lipopolysaccharide, whereas TLR2 mediates responses to gram-positive bacteria peptidoglycan (Kim 2005). The lower sensitivity of the gram-negative bacteria to the action of the AM agent could be due to the outer membrane that surrounds the wall of lipopolysaccharides (LPS) in these microorganisms restricting the diffusion of hydrophobic compounds (Vaara 1992). Cell wall and cytoplasmic membrane, structure is made of different layers of polysaccharides, fatty acids, and phospholipids, which can be easily permeabilized. This can be associated with loss of ions and reduction of membrane potential, collapse of the proton pump and depletion of the ATP (Bakkali et al. 2008). Lipid constituents of cell membrane are important for its functionalities such as barrier function and play a role in a variety of processes in the bacterial cell (Trombetta et al. 2005).

The skin microbiota is related to the immune system through resident dendritic cells resulting from complement activation (**Figure 1.3**). The immune system is enhanced by the quorum-sensing process between bacterial populations, which can limit the overgrowth of potential pathogens, or by the production of certain antibiotics, such as lugdunin (c). Microbiotic homeostasis, dependent on the production of AMPs both by bacteria themselves and by host cells, such as keratinocytes and sebocytes (b and d).

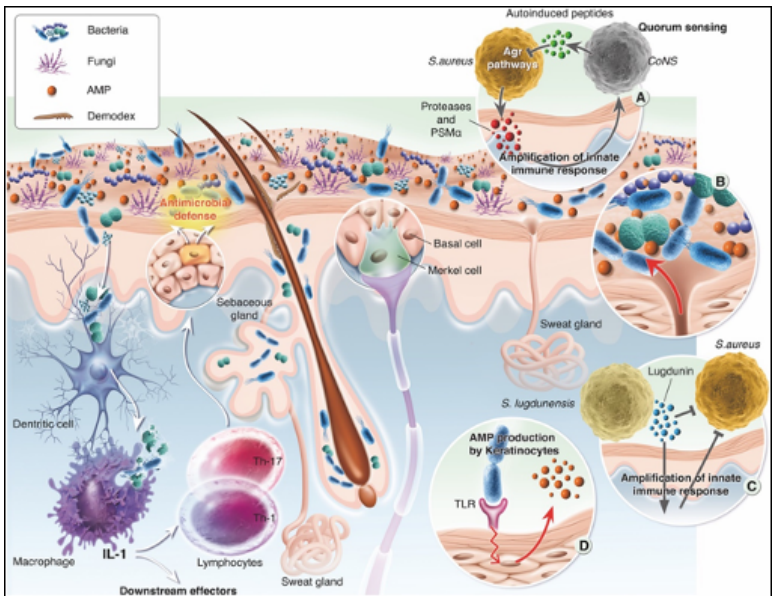

Figure 1.3. .Skin microbiota the immune system (Boxberger et al. 2021)

1.1.3. SKIN EXPOSOME

Some authors previously defined exposome as all life-course environmental exposures (including lifestyle factors) from prenatal period onwards (Wild 2005). Others stated that exposome is the sum of all exposures throughout life, where the environment is the body's internal chemical environment and exposures are all biologically active chemicals in this internal environment (Rappaport 2011). Others define exposome as a mixture of environmental exposures, including factitious and naturally occurring chemicals and physical agents, macrolevel factors (including population density and sanitation) and lifestyle factors (Buck Louis and Sundaram 2012). Others highlight the 'eco-exposome' as a concept from the contact-point between the stressor and the receptor, inwards the organism and outwards to general environment. Exposome has also considered as the cumulative measurement of environmental influences and biological associated responses throughout the lifespan including environment exposures, diet, behaviour and endogenous processes (Miller and Jones 2014).

The skin exposome refers to a group of internal and external exposures brough together including solar UV rays, air pollution, tobacco smoke, stress, unbalanced nutrition, cosmetic products, excessive washing and rubbering with strong surfactants, among others (Salsberg et al. 2019). These factors contribute to cutaneous disorders such as aging, sensitivity, pustules, disruption of optimal skin barrier function and internal skin cells conditions. The exposome can directly affect the skin microbiota, leading to an impaired balance of skin host activity, as well as diminishing the activity of the internal functional cells. Therefore, healthy skin requires a good skin balance internally and externally (**Figure 1.4**)

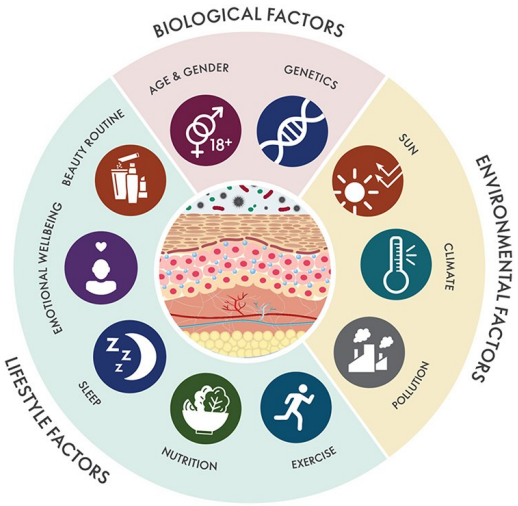

Figure 1.4.Schematic map of the biological, environmental, and lifestyle factors influencing skin health and skin aging (Khmaladze et al. 2020)

Skin Hygiene & Contamination

The control of hygiene develops and crucial role to maintain the skin barrier balance, as well as protecting the internal composition. Microorganisms, chemical pollutants, and other contaminants are strongly harmful to the skin structure and functions. In general, to maintain the skin clean and disinfected avoid inflammation, infection, and aging. Frequently the use of washing soaps (anionic surfactants) and sanitizer gels (alcohol-based), to maintain cleanness and anti-septic conditions, are required. However, excessive use may be too aggressive to the skin barrier conditions, by damaging the SC lipids, losing moisture content, and impairing penetration activity. Moreover, excessive use of these products will impair the microbiota activity and may also lead to malfunctioning and skin disorders.

Skin Aging

Skin aging can induce the loss of internal moisture, degradation of functional proteins and lipids, lowering the cellular activity or cell-death. The skin aging is not only applied to appearance of wrinkles and expressions marks, but to the main context of all cellular loss of function that may also be prone to some disease, due to the unbalanced activity.

Skin Oxidative Damage

Reactive oxygen species (ROS), including singlet oxygen ($^1O_2$), superoxide ion ($O_2^{-}\cdot$), hydroxyl ion ($OH\cdot$), and hydrogen peroxide (H_2O_2), are highly reactive and toxic molecules, generated in cells under normal metabolic conditions. Besides living cells possess an excellent scavenging mechanism to avoid excess ROS, these can cause oxidative damage to proteins, lipids, enzymes, and DNA (Amiri 2012).

The skin is constantly exposed to oxidative stress induced by reactive oxygen species (ROS), developed by endogenous sources involving enzymatic activity of neutrophils, and by external pro-oxidant stimuli, such as solar UV irradiation (Briganti and Picardo 2003). All these factors further associate somehow to skin impaired function hence an inflammatory response as well as cell death. The skin is equipped with antioxidant defence mechanisms against ROS-mediated oxidative damage, contributing to barrier integrity, which is essential for healthy skin condition. The cellular redox environment plays a pivotal role in skin homeostasis being able prevent oxidative injury of structural lipids and proteins, avoiding an imbalance on pro-oxidant/antioxidant stimuli.

Permeabilization of outer and inner mitochondrial membranes leads to cell death by apoptosis and necrosis (Armstrong 2006). A suggestion of phenolic-like pro-oxidant activity seems that chain reactions from the cell wall or the outer cell membrane invade the whole cell of varied organelles such as mitochondria and peroxisomes. Phenolic compound oxidation appears to take place in the cytosol in contact with peroxidase/H_2O_2, producing phenoxyl radical that may co-oxidize glutathione (GSH) (Bakkali et al. 2008).

1.1.4. Skin regenerative processes

Skin regeneration is the recovery of moisture, and restructure of lipids and protein on the entire skin structure. Renewed epidermal cells are constantly reproducing on the basal layer and migrating to the SC, where they are found dead. The youngest the organism, the fastest it occurs, and it slows down within age, due to loss of functions due to excessive oxidative stress. Functional molecules lead degradations and skin needs to be protected from any oxidative stress generated in other to maintain regular function of healthy cells.
Cell regeneration works towards cicatrisations processes in open wounds, while healing the inflammation and infections.

1.1.5. Skin penetration route

Transdermal penetration is not only a route of administration for dermatological and cosmetic products, but also an alternative for delivering several oral drug types, to avoid loss of activity by first-path metabolism that occurs by-passing the hepatic system. However, it is relevant that the skin structure is very tight and complexed, with several lipids and protein molecules cross-linked together, which are the main challenge for selecting molecules to penetrate. Some molecules are impermeable due to its solubility or due to its molecular size, since it is known that large molecules are unable to cross into the deeper layers of the skin (Bos and Meinardi 2000). In fact, there are several types of excipients that are designed vehicles for enhanced penetration of actives, as well as a broad range of delivery systems that overcome most of these issues.

Transdermal drug delivery plays an important role when topical, regional, or systemic effects are desired. To enhance drug transdermal absorption, different methodologies have been investigated, developed, and patented. It is known that the SC usually limits drug permeation. Thus, it involves diffusion through the intact epidermis and/or via skin appendages (hair follicles and sweat glands). Although, the latter hold only 0.1 % of the total skin surface area (Uchechi et al. 2014).

The permeation barrier properties of human skin are mostly attributed to the SC bricks (corneocytes) and mortar (intercellular lamellar lipid bilayers), being the rate-limiting selective barrier. Transdermal delivery approaches directly deliver drugs to the skin target cells and smaller amounts of drugs are needed to produce a therapeutic effect. The cutaneous penetration pathways are through intercellular/intracellular routes, followed by the viable epidermis and dermis via partitioning/diffusion and through the appendage pathways. Compounds with moderate lipophilicity, with optimum partition coefficient log P value (octanol-water) between 1.0 and 4.0) a permeability coefficient greater than $0.5.10^{-3}$ cm/h as well as a molecular weight less than 500 Daltons, are able to permeate the SC and into the skin deeper layers (SDL) (Zhang et al. 2013).

Mostly a drug follows a passive diffusion process for percutaneous absorption, which can be explained by Fick's first law of diffusion:

$$J= DKC/h$$

where J, the diffusion flux, is the amount of the substance going through a unit area during a small interval of time; D is the diffusion coefficient (or diffusivity) of the compound in the membrane; is concentration gradient which is the driving force that leads to molecular movement into skin; C is de drug concentration, which is divided by the overall thickness of the skin (*h*) (Couto et al. 2014).

Absorption of hydrophilic compounds is limited by the lipophilicity of the SC; however, the dermis is much more hydrophilic. Therefore, transdermal administration is more ideal for substances with intermediate polarity. Drug concentration and solubility of the vehicle are directly proportional to the penetration rate and drug dissociation depends on the pH of the skin and of the formulation. Molecular weight impacts upon drug diffusion where small molecules are likely to crosslink, whereas larger the molecules lower the diffusion rate. Although, the lipophilic nature of the drug plays the more important role.

Passive and active skin penetration

Active skin penetration enhancement is categorized into electrical, mechanical, and other energy-related techniques, such as microneedle, SC abrasion, ultrasound, or electroporation techniques. Passive penetration enhancement includes optimization of formulation and drug carriers to increase the flux by increasing the diffusion coefficient and solubility of the drug in the skin by adding chemical penetration enhancers to the formulation. However, those cause temporary disorder of the intercellular SC lipids structure and reduce skin resistance. Another

strategy is using nano-sized carriers (Zhang et al. 2013). Ideally and most appropriate, feasible and suitable approaches to improve skin penetration are the formulation enhancers vehicles and the use of nanotechnology.

Different routes for skin penetration involve transcellular and intercellular permeation (through SC), and trans-appendageal (via hair follicle, sebaceous and sweet glands) as can be seen in **Figure 1.5.**

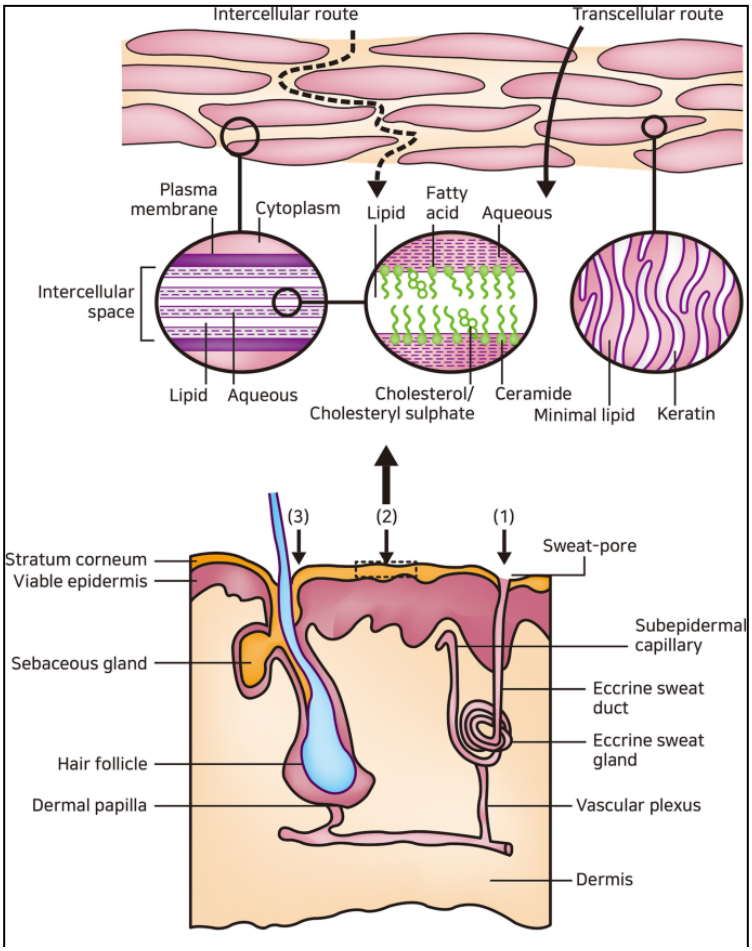

Figure 1.5: Skin penetration routes: 1) Sweat duct, 2) Transepidermal transport (across SC). 3) Hear follicle and associate sebaceous gland (Kim et al. 2020)

Intercellular lipid route

Interlamellar regions in the SC are less ordered lipids and more flexible hydrophobic chains, therefore, forming non-planar spaces between crystalline lipid lamellae and their adjacent outer membrane cells. Transepidermal diffusion of the lipidic and amphiphilic molecules depend on

fluid lipids in skin barrier, occupying those spaces for the insertion and migration. The hydrophilic molecules diffuse along surfaces (interlamellar spaces), less abundant in water content (Uchechi et al. 2014).

Transcellular route

Intracellular macromolecular matrix within the SC does not contribute directly to the skin diffusive barrier but supports mechanical stability and thus intactness. Regions of poor cellular and intercellular lipids correspond to lowest skin resistance to hydrophilic transport. This pathway leads between clusters of corneocytes at the locations where such cellular groups show no lateral overlap (Uchechi et al. 2014).

Follicular penetration

The hair follicle is of great interest in the treatment of skin diseases. For this reason, such pathways have been considered of great interest on topical administration of nanoparticles. Hair follicles type and quantity, as well as for glands, are relevant for drug penetration since the SC thickness decreases on these appendices, considered an important access route. These numbers are variable depending on the anatomical region (Calpena et al. 2011). Evaluation of follicles anatomical sites have previously featured their own characteristics, where the surface coverage was minimum on the forearm (0.09 %) and highest at the forehead (1.28 %). This area had also presented the highest follicular reservoir, similarly to the SC (Schneider et al. 2009). Moreover, non-damaged skin hair follicles are considered the keys for solid NPs penetration, although, its upper tight pathway prevents particles from invading living cells, instead, it stores the NPs until be cleared by hair growth or sebum production (Zhu et al. 2019).

1.1.6. Skin diseases

Skin is the largest organ of human body, and under certain conditions, it can suffer varied alterations and diseases which main characteristics are infection, inflammation, edema, redness, allergy, and pustule. The most popular diseases accomplished with inflammatory processes are atopic dermatitis, vitiligo, psoriasis, eczema, and acne. In the case of infectious diseases, the most popular diseases are caused by bacteria such as cellulitis, folliculitis, and acne, or caused by fungi such as candida, mycosis, and dermatitis seborrheic. All skin infections lead to alteration in the immunologic system responses, thus can be also considered as inflammation.

The skin immunological activity includes microbial ligands for toll-like receptors (TLR). Host responses to gram-positive bacteria peptidoglycan and gram-negative bacterial lipopolysaccharide are mediated by TLR-2 and TLR-4, respectively (Kim 2005).

Skin Inflammation

Skin inflammation is an innate and non-specific skin immunological responses towards external and internal environment changes or aggressions. In most of the recent cases, the skin exposome and skin microbiota has been involved as potential precursors of skin sensitivity or other immune unbalanced reactivity.

All inflammatory processes on the skin are developed by activation of defensins for acquired immunity reaction that serve as an immediate defence system. An array of induced immune-regulatory and pro-inflammatory mediators amplify direct damaging effects on molecules and cells, including DNA, proteins and lipids, causing immunosuppression.

The skin anti-inflammatory mechanism of action consists in modulating the expression of certain genes in order to produce an increase in anti-inflammatory proteins and inhibit pro-inflammatory cytokines release.

Cytokines are small proteins which modulate the innate and adaptive immune responses, regulate, cell activation and proliferation, proliferation, haematopoiesis, survival, and migration of leukocytes. They are produced by epithelial cells, macrophages, and CD4, CD8 T cells. They can be classified as proinflammatory such as interferon (INF)-γ, tumour necrosis factor (TNF)-α, interleukin (IL)-1β, IL-6, IL-8 and IL-17., or as anti-inflammatory such as IL-4, IL-10, IL-11, and IL-1 antagonist receptors. In acute inflammation these mediators are present for short periods of time, whereas in chronic, there is an imbalanced production of pro-inflammatory ones, and the anti-inflammatory cytokines fail to attenuate.

Chemokines, a small protein cytokine subtype, act to recruit monocytes/macrophages, neutrophils, and T cells from the circulation to areas of infection. T cells play an essential role in immunity through their role as both regulators and effectors of the adaptive immune response. Antigen specific receptors are located on the cell surface of T lymphocytes and function to recognize foreign pathogens. Moreover, neutrophils promote wound healing due to secretion of cytokines, chemokines and growth factors to abolish bacteria and adjust wound microenvironment through oxygen metabolism (Xue and Falcon 2019).

Contact dermatitis is a common dermatological disorder caused by continuous skin direct contact with external factors (allergens and irritants), characterized by inflammation, redness,

erythema, burning and itching. It is also characteristic the formation of vesicles and pustules (Zhang et al. 2013), due to an impaired oil balance, produced as consequence of the inflammatory process. For this reason, natural anti-inflammatory, antioxidants, and anti-microbial agents could be the key ingredients for preventing or mediate symptoms.

In the other hand, skin sensitivity is defined by an immune reaction of the skin against external environment, resulting inflammation. The main characteristics are red, itchy, bumpy rash. Some people carry this skin characteristics by genetic factor, besides it is necessary previous exposure to specific substances for symptom development. In fact, global environmental pollution is more and more hazard along the past years, hence, a broad range on non-genetic factors triggering such skin reactions. The external aggressive factors hence skin reactions and, as consequence, there is an unpaired function on the skin cells, leading to inflammation.

Skin Infections

Skin infection normally occurs in open wounds, where the SC is completely damaged, and the internal content is exposed to contaminants such as bacteria and fungi. Some are pathogenic and leading to a severe infection, but in contrast, some are skin microbiota-based organism that proliferates under an internal unbalance. Environment surfaces are massively covered by pathogenic and non-pathogenic living organisms and the lack of hygiene may lead to skin infection and consecutive inflammation.

There are two main **fungi disease**, among several others, that affects the skin, mucosa, and nails, being them, mycosis caused by filamentous fungi called dermatophytes and candidiasis caused by the yeast *C. albicans*.

- ***Dermatophytes*** are microorganism responsible for most skin infections due to their capability to invade keratinized tissues (skin, hair and nails) and to overcome the skin defence mechanisms. *Trichophyton rubrum* and *Trichophyton mentagrophytes* are the main dermatophytes responsible for superficial (cutaneous) mycosis (also called tinea) by producing extracellular keratinases, which hydrolyses keratin. In skin, the pathogenic procedure starts with adherence of conidia (arthroconidia) to the keratinized skin surface structures, with further proliferation and spreading of the fungal mycelium (hyphae) through the orifices of the epidermal surface (Barros, Santos, and Hamdan 2007; Smijs and Pavel 2011). The cutaneous lesion formed are likely to be mainly superficial, however, in some immuno-compromised cases, it might be able to expand to the deeper layers (Inaoki et al. 2015). The ideal treatment for this class of infections requires an antimycotic agent with the ability to eradicate the dermatophytes that are acting inside the skin structure to enable reconstitution of the keratinized tissue.

- ***Candidiasis*** occurs in the presence of excessive heat and humidity that changes the barrier conditions of the tissue, lowering the skin defence activity and leading to a proliferation of the relevant host microorganism, causing a local infection. The symptoms include thickening of the skin, hyperkeratosis, and erythema (Kühbacher, Burger-Kentischer, and Rupp 2017).

The most popular **bacterial skin infections** are cellulitis and folliculitis.

- ***Cellulitis*** usually refers to a local deeply skin infection due to bacterial invasion in the fat tissue with subsequent proliferation, caused by gram-positive bacteria: mainly *streptococcus pyogenesis*, *B-haemolytic Streptococcus dysgalactiae* (subspecies *equisimilis*) and can also be involved *Staphylococcus aureus* (Siljander et al. 2008).
- ***Folliculitis*** normally caused by *S. aureus*, is an inflammatory reaction in the superficial follicular opening or the perifollicular hair follicles and its conditions can be classified according to their anatomical location. Acute inflammation manifests pustules whereas chronic leads hyperkeratosis and formation of keratotic plug (Luelmo-aguilar and Santandreu 2004).

Acne

Acne vulgaris is one of the most prevalent skin inflammatory disorders affecting around 9.5% of the population worldwide (Sachdeva et al. 2021; Williams, Dellavalle, and Garner 2012) mainly at young puberty aged adolescents, diminishing the affectation with age. It can be considered a multifactorial disease, with a complex pathophysiology in which several internal and external factors are involved, such as irregular keratinocyte proliferation and differentiation, increased sebum production by active sebaceous glands and imbalances in the skin microbiota (related to Cutibacterium acne). In addition, exogenous factors (exposome) such as hormones, drugs, nutrition, stress or smoke habits, can also trigger acne development (Ajay Bhatia, Jean-Francoise Maisonneuve, and David H. Persing 2004; Claudel et al. 2019). This combination of factors leads to skin lesions such as whiteheads, blackheads, pustules and cysts developing into swelling and inflammation (Boukraâ, Abdellah, and Ait-Abderrahim 2013).

This multifactorial chronic disease of pilosebaceous follicles (due to excessive sebum and bacteria proliferation responses), which commonly affects the face, neck, upper back, chest and upper arms is considered a non-infectious disease influenced by imbalanced skin microbiome, leading to various inflammatory pathways (Dreno et al. 2015). It is characterized by both

polymorphic non-inflammatory lesions (open or closed comedones) and inflammatory lesions like papules, pustules, nodules, cysts, leading to scarring as a common sequel.

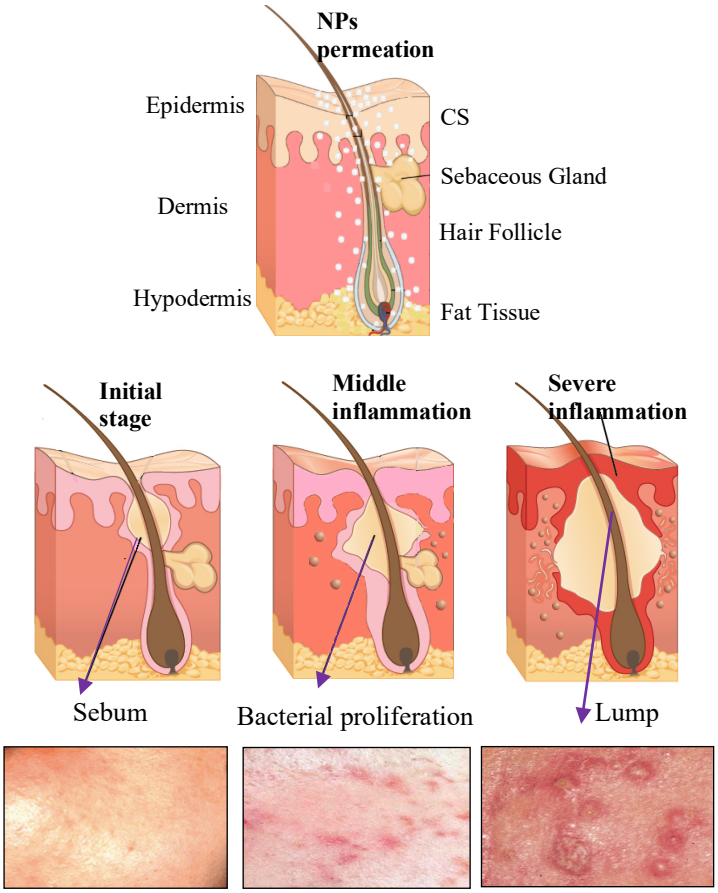

Figure 1.6 Mechanism of acne. Dermal lesions

Skin Microbiota and exposome in Acne

The microbiota of the sebaceous areas, such as face forehead, takes shape during puberty as hormonal changes activate the sebaceous glands. In sebum rich sites such as scalp, face, chest and back, C. acnes takes up to 90 % of microbiota in pilosebaceous units. C. acnes is a normal resident of healthy skin, mainly located surrounding the hair follicle, which is likely to proliferate under unbalanced function of the sebaceous glands, contributing to inflammation and acne development (Ajay Bhatia et al. 2004). Hence, C. acnes has a dual activity. This skin commensal strain is essential for sebum control and maintenance of the acidic pH of the pilosebaceous follicle by hydrolysing sebum triglycerides and via propionic acid secretion (Flowers and Grice 2020; Platsidaki and Dessinioti 2018). Moreover, it can block the skin

colonization by other pathogens, such as Staphylococcus aureus and Streptococcus species. However, it can act as a pathogen under dysbiosis conditions that help its overgrowth in active sebaceous glands (Rozas et al. 2021).

Imbalanced skin microbiome, including C. acnes overgrowth, trigger innate immune system activation, leading to cutaneous inflammation. Consequently, the great array of induced immune-regulatory and pro-inflammatory mediators amplify direct damaging effects on molecules and cells, including DNA, proteins, and lipids, causing immunosuppression (Bharti and Vadlamudi 2021).

Exposome factors act on the natural skin barrier and on the skin microbiota, enhancing sebum production, hyperkeratinisation, microbiome dysbiosis, activation of the innate immunity reflecting on worsening acne. Previous authors concluded under clinical trial investigation with acne patients, that exposome factors including nutrition, medication, pollutants, climatic factors, and psychosocial and lifestyle factors may impact on the course and severity of acne and on the treatment efficacy (Dréno et al. 2018).

Superoxide or hydroxyl ions, and hydrogen peroxide are highly reactive molecules generated in normal cell metabolism. Moreover, acne-related strains generate ROS and raise inflammation in keratinocytes. Then, it can cause oxidative damage to proteins, lipids, enzymes, and DNA (Amiri 2012; Briganti and Picardo 2003). These factors reflect on impaired skin function, thus an inflammatory response and cell death. Therefore, the skin is constantly exposed to induced oxidative stress. However, intrinsic antioxidant defence mechanisms contribute to barrier integrity, which is essential for a healthy skin. The cellular redox environment plays a key role in skin homeostasis, preventing oxidative damage of lipids and proteins, and avoiding an imbalanced pro-oxidant/antioxidant stimulus. The oxidation of phenolic compounds normally takes place in the cytosol, in contact with peroxidase/H_2O_2. This would produce phenoxyl radical and may co-oxidize glutathione (Bakkali et al. 2008). Consecutive inflammation may affect the skin internal components and their functions. Moreover, cicatrisation processes rely on cell regeneration while healing the infection and the inflammatory responses.

Sebum in acne

The responsible factors for acne development are, the hyperactivity of sebaceous glands producing elevated levels of sebum; hyperkeratosis by blockage of the hair follicle and the etiopathogenic factors of excessive microbiota reproduction (Kapuścińska and Nowak 2015).

Normal human sebum is mainly composed of a constellation of lipid, such as triacylglycerols, wax esters, squalene, and free fatty acids with minor amounts of cholesterol, sterol esters, and diacylglycerols (Zouboulis, Jourdan, and Picardo 2014). In fact, acne does not occur within low sebum secretion. Most fatty acids in sebum are covalently bound in triacylglycerols, whereas in acne their release amount is increased by 50 % due to triacylglycerol lipase activity, a virulence factor that is upregulated in *C. acnes* biofilms (Coenye, Peeters, and Nelis 2007). The most abundant fatty acids of sebum are the saturated fatty acid (palmitic acid 25 %) and the monounsaturated fatty acid (sapienic acid 22%) (Melnik 2018). Besides sebum composition is severely altered in acne, and ROS produced by neutrophils are involved in the irritation and disrupting the follicular wall, leading a progressive inflammatory response Compared to normal skin, linoleic acid decreases and palmitic acid increases significantly in comedones. In fact, ROS overflow might be associated with the lipids present in the sebum where linoleic acid inhibits effect of superoxide radical anion, hydroxyl radical and hydrogen peroxide, whereas palmitic acid only decreases the generation of the last one. Hence, the pathogenesis of acne inflammation from an oxidative tissue injury standpoint may have palmitic acid involved (Briganti and Picardo 2003). A mediated production of monounsaturated oleic acid is a crucial step in virulence factor of biofilm formation, playing a critical role for bacterial adherence, since it has been found to be an essential nutrient for resident *C. acnes* microbiota (Melnik 2018). Hence, the pathogenesis of acne inflammation from an oxidative tissue injury standpoint may have palmitic acid involved (Briganti and Picardo 2003).

Squalene triterpenoid is suggested to function as a singlet oxygen quencher that protects skin surface from lipid peroxidation, however, when this suffers oxidation it generates squalene peroxides, which exerts comedogenic effects. It is thus thought to be the link to bacterial colonization. Moreover, skin surface squalene photo-oxidation products have been previously found to mediate metabolic and inflammatory responses to solar UV in HaCaT (Kostyuk et al. 2012).

It is also known to enhance epidermal calcium influx in keratinocytes, inducing abnormal keratinization and barrier function associated with increased release of IL-1α in comedones (Katsuta et al. 2009). Furthermore, uric acid increases IL-1β expression through a TLR4-mediated pathway. Thus, increased sebum in acne may activate uric acid–mediated inflammasome.

Hyper-keratinization might be initiated via IL-1, suggesting keratinocyte activation cycles, and hence, hyper-proliferation (Dréno et al. 2018). Hyper-keratinization leads to sebaceous gland obstruction clogging the follicle in function of lipids, bacteria, and induced cytokines. In addition to *C. acnes* being a gram-positive bacterium, it possesses a featured cell wall and outer envelope that synthesizes phosphatidylinositol. Its surrounding peptidoglycan containing a cross-linkage peptide chain may allow recognition of receptors contributing to inflammation, secreting TNF-α, IL-1α and IL-8 (Kim 2005). In particular, IL-8 together with other factors, may attract neutrophils to the pilosebaceous unit.

Acne Infection and Inflammation

On keratinocytes*, C. acnes* activates TLR-2 and TLR-4 leading to the activation of MAPK and NF-kB pathways. Moreover, they produce interleukins such as IL-1, IL-6, IL-8 and TNF-α. Then, ROS production is stimulated, when CD-36 recognizes *C. acnes*, clearing away the bacteria and inducing the inflammation (Lee, Byun, and Kim 2019). In acute inflammation, these mediators are present for short periods of time, whereas in chronic inflammation, there is an imbalanced production.

Recognition of *C acnes*, by the immune system acts via defence against pathogen-associated molecular patterns (PAMPs) and damage-associated molecular patterns (DAMPs). On keratinocytes, *C. acnes* activates TLR-2 and TLR-4 leading to the activation of MAPK and NF-kB pathways, inducing inflammation mediated by proinflammatory interleukins, such as TNF-α, IL-1, IL-6, IL-8, and IL-12 (Rosen and Friedman 2014). Previous studies indicated that interleukin-1α (IL-1α) plays a crucial role in comedogenesis (Ingham et al. 1992). For this reason, prone acne skin faces abnormal metabolic dysfunction including release of others pro-inflammatory cytokine. *C acnes* is a potent trigger of IL-1b generation via inflammasome activation (NLRP3), previously demonstrated in keratinocytes, as well as sebocytes (Li et al. 2014).

Low oxygen levels allow *C. acnes* to grow stimulating keratinocytes to produce and release cytokines, as the duct ruptures and, into the dermis, triggers an intense local reaction of the innate immune system. The neutrophils and lymphocytes in the follicular epithelium contribute to breakdown of the follicular wall, with disturbance of the barrier function, as a result of sebum production, such as deficiency of linoleic acid, and production of pro-inflammatory cytokines by the sebocytes (Dreno et al. 2015).

Proliferation in the epithelium elevates CD3 þ, CD4 þ T cells in the perifollicular and papillary dermis with the number of macrophages greatly increased in papules. When occurring before

hyper-proliferation of keratinocytes, some of these changes are similar to a type IV delayed hypersensitivity response (Jeremy et al. 2003). For hyper-keratinization, it might be initiated via IL-1, suggesting keratinocyte activation cycles, leading to hyper-proliferation (Dreno et al. 2015). Hyperkeratinisation leads to sebaceous gland obstruction clogging the follicle in function of androgens, lipids, bacteria, cellular debris, and cytokines induced. Studies also suggested that sebaceous glands are neuroendocrine inflammatory organs, with hyperplasia in response to androgen hormones, and that the sebaceous gland activity is androgen-estrogen ratio dependant (Bagatin et al. 2019).

In a microcomedo, the bacteria break the lipid into free fatty acids causing further blockage of follicles and triggers an inflammatory response through activation of expression of TLR. In perifollicular inflammation its involved macrophages, neutrophils and CD4+ lymphocytes and hence, formation of inflammatory acne lesions called papules, pustules, nodules, and cysts.

The *C. acnes* inflammation triggers immune reaction via activation of toll-like receptor-2 (TLR2), involved in host defence of innate immune system against invading micro-organisms (Kim 2005). Consequently, expression of immune response genes, including various cytokines and chemokines, including production of IL-12 and IL-8. The major proinflammatory cytokine produced by monocytes in response to invading gram-positive organisms is known to be IL-12. Through the activation of TLRs, *C. acnes* can also induce, in cultured human epidermal keratinocytes, human b-defensin-2 expression. Thus, an AMP is produced in the skin, in response to microbial infection (Nagy et al. 2005), with properties of modifying cell migration, maturation and also induction of cytokines. In acne inflammation events, it is also known the release of various exogenous proteases, producing IL-1a, IL-8, and TNF-a via protease-activated receptor-2 (PAR-2) on keratinocytes (Tanghetti 2013).

Besides *C. acnes* is a gram-positive bacteria type, it has a unique featured cell wall and outer envelope that synthesizes phosphatidyl inositol, distinguishing from the others. Additionally, its surrounding peptidoglycan containing a cross-linkage peptide chains (L,L -diaminopimelic acid and D-alanine) which may allow for the recognition receptors contributing to inflammation, secreting TNF-α,IL-1α and IL-8 (Kim 2005). In particular, IL-8 together with other factors, may attract neutrophils to the pilosebaceous unit.

Levels of the proinflammatory cytokine IL-1 were also upregulated perifollicularly (Jeremy et al. 2003). Integrin expression has been demonstrated in the epidermis uninvolved follicles and inflamed lesions, whereas the basement membrane was still intact. This evidence considers vascular endothelial cell activation and involvement of inflammatory responses in early-stage acne lesion.

Acne treatment

The commonly treatment for acne during the past decades were the use of antibiotics, despite their lead to microbial resistant post-treatment and side-effects. Some antibiotics used for acne treatment significantly debated the activity of neutrophil-derived ROS, previously reported (Briganti and Picardo 2003). However, the use natural products have increased in the recent days, due to their natural origin that avoid side effects, improving patients' acceptance to the treatment.

Acne lesions often cause skin discolorations and scar formation, even once post-healed. Therefore, a skin regenerative active ingredient, such as the antioxidants are great candidates to be used in acne treatments. Even though, the antioxidant activity on skin is an approach on restoring skin homeostasis, maintaining its internal conditions relatively constant and stable, modulate SC barrier function and prevent skin irritation.

Lactic acid in the body is the result of metabolites produced from the lactate system or anaerobic glycolysis due to imperfect glucose breakdown. Increased the levels of lactic acid in the body can lead to decreased blood pH. The improvement framework is to maintain the balance of the internal environment (homeostasis). Increased levels of lactic acid in muscle and blood will have an adverse effect on cell activity due to the disruption of the performance of a number of enzymes acting on neutral or base pH as catalysts in various metabolic processes (Nanang et al. 2018). Therefore, it could be thought that on acne treatment, the good balance of present oil and local skin pH can lead to fast recovery of the injury.

Natural anti-inflammatory, antioxidants and antimicrobial agents could be the key for preventing or ameliorating acne associated symptoms (Amiri 2012). In this area, natural compounds are gaining increased importance. Among them, Thymol (TH) is a monoterpene with a phenolic structure associated with several activities such as antioxidant, antimicrobial, antifungal, antiseptic as well as anti-inflammatory (Nagoor Meeran, Jagadeesh, and Selvaraj 2016; Najafloo et al. 2020; Pivetta et al. 2018). Previous researches (Briganti and Picardo 2003) showed the capability of thymol to increase elasticity and porosity, which are essential on cicatrizing/healing processes. Since skin bacteria are hosted by the dermis compartment, located near the follicle region, the probability of the drug NPs to target their action site is high (Alvarez-Román et al. 2004; Boukraâ et al. 2013).

1.2. NATURAL PRODUCTS IN PHARMACOTHERAPY

Natural products played a critical role in drug discovery and development, especially for antibacterial and antitumor agents (Atanasov et al. 2021). For several generations in different cultures, traditional knowledge of medicine has based on the empirical use of medical plants as the primary means to maintain health, preventing and treating diseases especially in rural communities. According to the World Health Organization (WHO), 80% of the people in rural areas are dependent on herbal plants and other medicinal plants for the treatment of diseases such as rheumatism, swelling, insects bites, pains, among others (Singh 2019). Obviously, in this century, natural products will continue to be extremely important as sources of novel pharmacologically active compounds. People living in urban areas use medicines that; directly or indirectly come from medicinal plants. In this way, 11% of the 252 drugs considered as basic and essential by the WHO, were exclusively of flowering plant origin (Veeresham 2012). Natural products have a wide range of diversity of multidimensional chemical structures, being their therapeutic role justified by the presence of their bioactive molecule.

Medicinal plants also represent an important activity today, since the main product of interest obtained from these plant species are their essential oils (EOs). An essential oil can be considered as a volatile substance with aroma and flavour that is obtained from plants by physical processes. They generally have a great variability in their composition and can present up to more than 100 components that can be aliphatic compounds of low molecular weight (alkanes, alcohols, aldehydes, ketones, esters, and acids), sesquiterpenes, monoterpenes, phenols...

Most of the production of EOs are destined as raw material of cosmetics, food industry (flavouring and preservatives), pharmaceutical industry (antimicrobials) and other novel fields such as in the production of bioinsecticide (Roldan, Díaz, and Duringer 2010). Currently, several industries are promoting the development of natural products, for sustainable use of natural resources. For this reason, the interest as well is focused on the use of EOs as a natural alternative source of preservatives various dermopharmaceutical and cosmetic formulations. Nevertheless, the main activity of the EOs is due to the main components such as flavonoids, terpenoids, etc., which, mostly performs antioxidant, antimicrobial, anti-inflammatory and anti-virus effect. So, to design an effective formulation, not only essential oils, but also, their majority compound should be considered.

1.2.1. THYME OIL

The genus Thyme, an aromatic evergreen from the Lamiaceae family used as culinary herbal and for different medicinal purposes for many centuries, comprises a wide variety (300-400) of species presents in many parts of the world but is more indigenous to Europe. Among these, *Thymus vulgaris* is native to the Mediterranean regions and is the common species planted in Arabic world in addition to certain African countries

Thymus vulgaris' EO has a complex chemical composition as well as other oils, with hydrocarbon monoterpene families (37.42%) and oxygenated monoterpenes (37.36%) those who have the most representation **(Table 1.1**). According to the European Pharmacopoeia, the limit percentages of its components are as follows: thymol 36-55%, carvacrol 1-4%. terpinene 5-10%, cymene 15-28% and s-myrcene 1-3%. Of all these, the compounds with the greatest antimicrobial activity are thymol and carvacol.

The composition of thyme oil (THO) (**Table 1.1**) from a particular specie of plant can depending on the harvesting seasons, ecological and climatic conditions, and/or geographical source, and it may have variation from year to year.

Table 1.1. Major components of *T. vulgaris* essential oil (%)

Thymol	Carvacol	Terpinene	Cymene	Linalool	References
44.7	2.4	16.5	18.6	-	(Porte and Godoy 2008)
23 - 64	2 - 8	18 - 50	8 - 44	3 - 4	(Satyal et al. 2016)
7.44 - 14.32	2.46 -4.55	0.18 - 2.12		1.59 - 3.20	(Özgüven and Tansi 1998)
29.4	4.2	0.3	21.6	0.7	(Nowak et al. 2013)
46.6	-	0.3	38.9	3.8	(De Lira Mota et al. 2012)
30.61	1.49	27.31	10.9	-	(Roldan et al. 2010)
46.2	-	14.1	9.9	4	(Özcan and Chalchat 2004)
30.86	3.37	-	30.53	2.73	(Grigore et al. 2010)

(Major components of Thymus vulgaris essential oil (Mandal and Debmandal 2016)

Some of the species have been used in traditional medicine, presenting a growing prominence in the formulations of the Pharmacopoeia, especially the common thyme (Thymus vulgaris. L) from which the EOs which is an extremely concentrated substance and of multipurpose use in the pharmacological industry for its various properties:

- Antioxidant Activity: It has free-radical scavenger activity, in which thymol and carvacrol of the essence are considered involved, as well as flavonoids and other polyphenols.
- Antiseptic Activity: it is proven that its phenolic components (thymol and carvacrol) have antibacterial activity against Gram-positive and Gram-negative germs due to its capacity for action on the plasma membrane. The antibacterial action of thyme is enhanced by its ability to produce a stimulation of leucopoiesis and an elevation of thrombocyocyte values in the blood, so it is also considered that its use as an enhancer of the action of other immunostimulants may be interesting. (Lopez, 2006).
- Activity Anti-inflammatory: In topical application, the essential oil, especially carvacrol has an inhibitory action of prostaglandin biosynthesis. This justifies the inclusion of thyme essence in preparations for the treatment of muscle and osteoarticular pains.

Thyme EO, a rich nature in monoterpene compounds, could be considered a potential candidate act as a natural preservative in formulations, due to its strong antimicrobial activity, in addition to generating its beneficial effects for skin protection, preventing bacterial skin infections. Also, thyme essential oil is considered GRAS, so it is not considered harmful to health (Falcone et al., 2005).

Since thymol is the main constituent of THO, it is understood that the main activities are performed by this compound. In fact, in some cases there might be a synergic effect within the other components of the extract that may enhance its activity.

1.2.2. THYMOL

Thymol (TH), a natural monoterpene found in Lamiaceae plants, especially oreganos and thymes, frequently used as flavours but highlighting their naturally occurring antimicrobial, antioxidant, and antiseptic agents. It is a primary phenolic component of thyme essential oil and has a rapid antimicrobial activity due to its direct action into the cell membrane. TH can be found naturally as the main component in *Thymus vulgaris* and *Thymus daenesis* essential oils and extracts, as well as other plant species. In can be found in a range of 10 - 40 %. and it is also present in many other species such as oreganum.

Structure

TH is a monoterpene of aromatic phenolic structure (5-methyl-2-(propan-2-yl) phenol), represented by a phenolic group that gives it a highly hydrophobic profile. The molecular formula is $C_{10}H_{14}O$, composed of C = 79.95 %, H = 9.39 %, O = 10.65 %, with molecular weight of 150.21 g/mol, density of 0.9699 g/l and a refractive index of 1.5204. (P. S. Nagle*, Y. A. Pawar, A. E. Sonawane, A. P. Nikum 2013). The melting point and the boiling point are 51.5

ºC and 233 ºC, respectively. TH is a volatile compound with strong and characteristic odour. This compound is an isomer of carvacrol (2-methyl-5 (methyl-5) phenol), so it has a similar chemical structure, changing only the position of the hydroxyl group. The chemical formula and structure of TH are reflected in **Figure 3.6.**

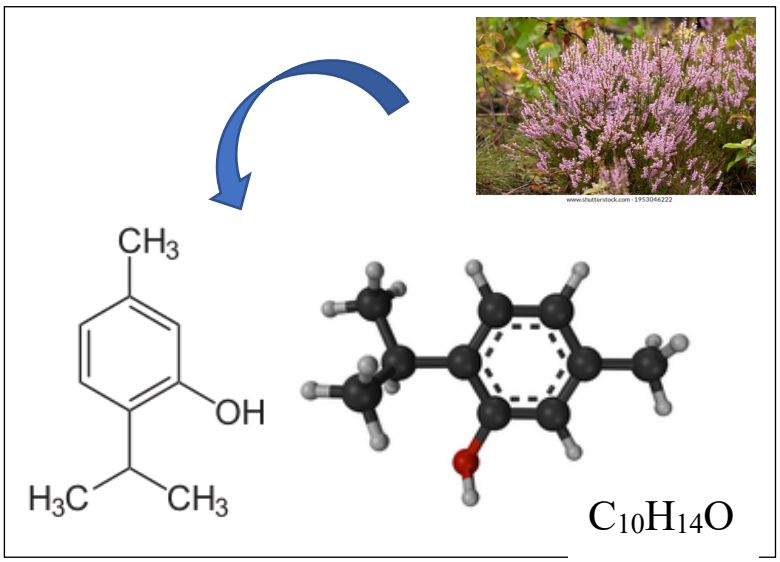

Figure 1.7: Structure of Thymol 5-Methyl-2-(propan-2-yl) phenol.

It can be found naturally occurring in plant extracts or on its white crystalline synthetic form. Synthetic TH can be obtained by the reaction of m-cresol and propene in the gas in the presence of an acidic catalyst containing oxides (Nagoor Meeran et al. 2017). Alternatively, thymol could be biosynthesized by the hydroxylation of p-cymene after the aromatization of g-terpinene to p-cymene (Poulose and Croteau 1978). It is highly soluble in alcohols, alkaline solutions, and other organic solvents due to the deprotonation of phenol, but it is slightly soluble in water at neutral pH. It also has low solubility in the hydrophobic domain of the bacterial cytoplasmic membrane due to its hydrophobicity (Trombetta et al. 2005).

Activity and Mechanism of action

Thymol, used as preservatives in cosmetics and food by its antimicrobial activity (Wattanasatcha, Rengpipat, and Wanichwecharungruang 2012) is considered safe in cosmetics formulations up to 0.5%, according to the Cosmetic Ingredients Review (CIR). The noteworthy effects of thymol are largely attributed to different activities exhibit by this compound:

- **antimicrobial** (depends on the lipophilic or hydrophilic character of the essential oil),
- **anti-inflammatory** (via inhibiting recruitment of cytokines and chemokines),

- **antioxidant** (via scavenging of free radicals, enhancing the endogenous enzymatic and non-enzymatic antioxidants and chelation of metal ions) and
- **antihyperlipidemic** (via increasing the levels of high-density lipoprotein cholesterol and decreasing the levels of low-density lipoprotein cholesterol and low density lipoprotein cholesterol in the circulation and membrane stabilization) (via maintaining ionic homeostasis) effect. (Nagoor Meeran et al. 2017).

Given the large number of chemical components present in EOs, it is likely that their antimicrobial life cannot be attributed to a single component as there may be a synergy between all oil components. Additionally, the mechanism of action in bacterial cells also would be multifactional. Oils rich in phenolic compounds have a characteristic that the structures of their active compounds have an aromatic ring, a hydroxyl group (or other groups such as tert-butyl or isopropal), that alter the polarity and topography of the molecule and therefore, can change its affinity by different binding sites in the bacterium. Potassium loss is the first indication of damage to the membranes of microorganisms. This confirms the fact that membrane disruption contributes to the mode of action of phenolic groups such as thymol. Therefore, the mode of action of most EOs, with antibacterial activity, lies in its ability to alter and damage the integrity of the cell membrane, affects the pH of the intracellular medium and the balance of organic ions. The site of action appears to be the phospholipid layer and alterations of biochemical mechanisms can trigger alterations in the transport of electrons, protein translocation, phosphorylation and other enzyme-dependent reactions. Some components of EOs apparently act at the level of proteins embedded in the cytoplasmic membrane, such as ATPases.

The extent of bacteria membrane damage induced by TH can be related to its intrinsic hydrophobicity, with log Po/w higher than 3 (Ultee, Bennik, and Moezelaar 2002) characteristic of components affecting deeply in the cell membrane (Frans Weber 1995). Due to its slight hydrophilicity, it could diffuse through the polysaccharide matrix of bacteria biofilm, destabilizing it due to intrinsic antimicrobial properties (Nostro et al. 2007). Since these products are usually sensitive to light, oxygen, humidity, and high temperatures, nanotechnology can be consider an attractive tool to increase their chemical stability and activity (Bilia et al. 2014).

1.3. NANOPARTICLES FOR SKIN DELIVERY

Different dosage forms based on nanotechnology, developed in the last years, constitute a new approach for skin drug delivery, as a new tool for management of some dermal disorders. In this way, several kinds of carriers such as micelles, liposomes, nanoemulsions, lipid and polymeric NPs have been developed to increase percutaneous absorption of therapeutic agents and reducing side effect (Shim et al. 2004).

Transdermal drug delivery depends on the ability of carriers to overcome the skin barrier and reach deeper tissue layers. Having into account that the skin appendages comprise around 0.1 % of fractional area for skin drug permeation, investigations are focused to develop new strategies to improve, not only on the drug passage through the appendages, but also through the stratum corneum.

Biodegradable nanoparticulate systems based on, polymeric and lipid NPs constitute one of the most studied colloidal systems for prolonged dermal applications, improving active penetration. These colloidal systems, with an average particle size ranged between 10 and 1000 nm, are able to increase drug bioavailability and reducing its toxicity.

1.3.1. Biodegradable polymeric nanoparticles

Polymeric NPs are nanostructured systems formed by natural or synthetic polymer chains with a matrix (nanospheres) or vesicular (nanocapsules) structure (**Figure 1.8**). Nanosphere systems composed of a matrix structure, where the drug can be adsorbed, entrapped, or solved into the polymeric matrix, are the most extended.

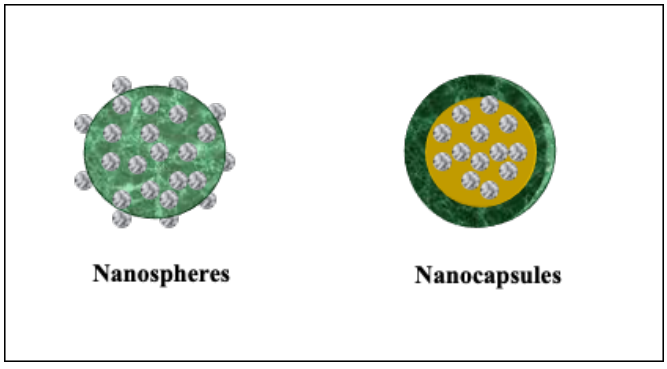

Figure 1.8. Polymeric biodegradable nanoparticles

Among all the polymers, poly-(D,L)-lactic-co-glycolic acid (PLGA), approved by the European and American drug agencies (EMA and FDA, respectively) have been widely used as a biomaterial in medical prostheses and surgical sutures (Anderson and Shive 2012). Also, in recently developments of colloidal carriers due to its biocompatibility, biodegradability and non-toxicity, higher reproducibility, easily formulated and suitable for control and prediction of the degradation kinetics. This polymer constitutes an ideal carrier for long-term administration treatments. Additionally, polyethylene glycol (PEG) chains surrounding the NPs increase its mucoadhesive properties and facilitates transport across the biological barriers (Liu et al. 2008).

Methods for preparation of polymeric NPs

Polymeric nanospheres can be produced by different methods, depending on the physicochemical characteristics of active, and polymer selected, to achieve an efficient entrapment of the active (Pinto Reis et al. 2006). Although, polymeric NPs can be prepared by emulsion-polymerization reaction of monomers, the most widely used methods recently (Emulsification/solvent evaporation, solvent displacement/interfacial deposition, and salting out**)** are based on preformed polymers.

The emulsification/solvent evaporation method, applied to liposoluble drugs, consists of a first step where the polymer solution in an organic solvent is emulsified using high-energy homogenization into an aqueous phase and a second step based the solvent evaporation and induction of the polymer precipitation as nanospheres. Morphometrical properties of NPs can be modified adjusting the stirring rate, the dispersing agent as well as the temperature and the viscosity and type of organic solvent (Pinto Reis et al. 2006).

Solvent displacement and interfacial deposition methods

These methods are based on spontaneous emulsification of the organic internal phase containing the dissolved polymer into the aqueous external phase (Pinto Reis et al. 2006).

- ***Solvent displacement*** involves the precipitation of a preformed polymer from an organic solution and the diffusion of the organic solvent in the aqueous medium, in the presence or absence of a surfactant. Polymer deposition on the interface between the water and the organic solvent, caused by fast diffusion of the solvent, leads to the instantaneous formation of a colloidal suspension. Thus, it can form nanospheres or nanocapsules.
- ***Interfacial deposition*** is based on the polymer deposits at the interface between the disperse oil droplets and the aqueous phase, forming nanocapsules. An aqueous solution is used as

the dispersing medium. This mixture is injected slowly into a stirred aqueous medium, resulting in the deposition of the polymer in the form of nanoparticles.

Emulsification/solvent diffusion

This method was proposed in literature based on the use of organic solvents, and then it was adapted to the following salting-out procedure. The encapsulating polymer is dissolved in a partially water-soluble solvent, such as propylene carbonate, and saturated with water to ensure the initial thermodynamic equilibrium of both liquids. In fact, to produce the precipitation of the polymer, and the consequent formation of nanoparticles, it is necessary to promote the diffusion of the solvent of the dispersed phase by dilution with an excess of water, when the organic solvent is partly miscible with water, or with another organic solvent in the opposite case. Subsequently, the polymer-water saturated solvent phase is emulsified in an aqueous solution containing stabilizer, leading to solvent diffusion to the external phase and the formation of nanospheres or nanocapsules, according to the oil-to-polymer ratio. Finally, the solvent is removed by evaporation according to its boiling point (Pinto Reis et al. 2006).

Salting-out

This method is based on the separation of a water-miscible solvent from aqueous solution via a salting-out effect. It can be considered as a modification of the emulsification/solvent diffusion. Polymer and drug are initially dissolved in a solvent, such as acetone, which is subsequently emulsified into an aqueous gel, containing the salting-out agent and a colloid. This oil/water emulsion is diluted with a sufficient volume of water or aqueous solution to enhance the diffusion of acetone into the aqueous phase, thus inducing the formation of nanospheres. Both the solvent and the salting-out agent are then eliminated by crossflow filtration. Salting out does not require an increase of temperature and, therefore, may be useful when heat-sensitive substances have to be processed. The greatest disadvantages are exclusive application to lipophilic drugs and the extensive nanoparticle washing steps.

1.3.2. Biodegradable lipid nanoparticles

Solid lipid nanoparticles (SLN) have been considered one of the promising strategies for the treatment of dermal disorders (Khater et al. 2021). These systems, characterized by a solid lipid core stabilized by surfactants in aqueous dispersion, are suitable to load lipophilic drug molecules. SLN show high physical stability, protection of labile drugs against degradation and excellent *in vivo* tolerability due to their biocompatibility. However, these systems generally show a low drug payload capacity and high drug expulsion during storage, due to the

polymorphic transitions of lipid molecules, toward more stable configurations during its shelf live (Souto, Mehnert, and Müller 2006). These disadvantages can be overcome by surface modification of the particles and, more recently, using nanostructured lipid carriers (NLC), a second generation of lipid particles containing of solid lipids and liquid lipids, leading to special nanostructures (**Figure 1.9**), with improved drug incorporation and release properties (Müller, Radtke, and Wissing 2002).

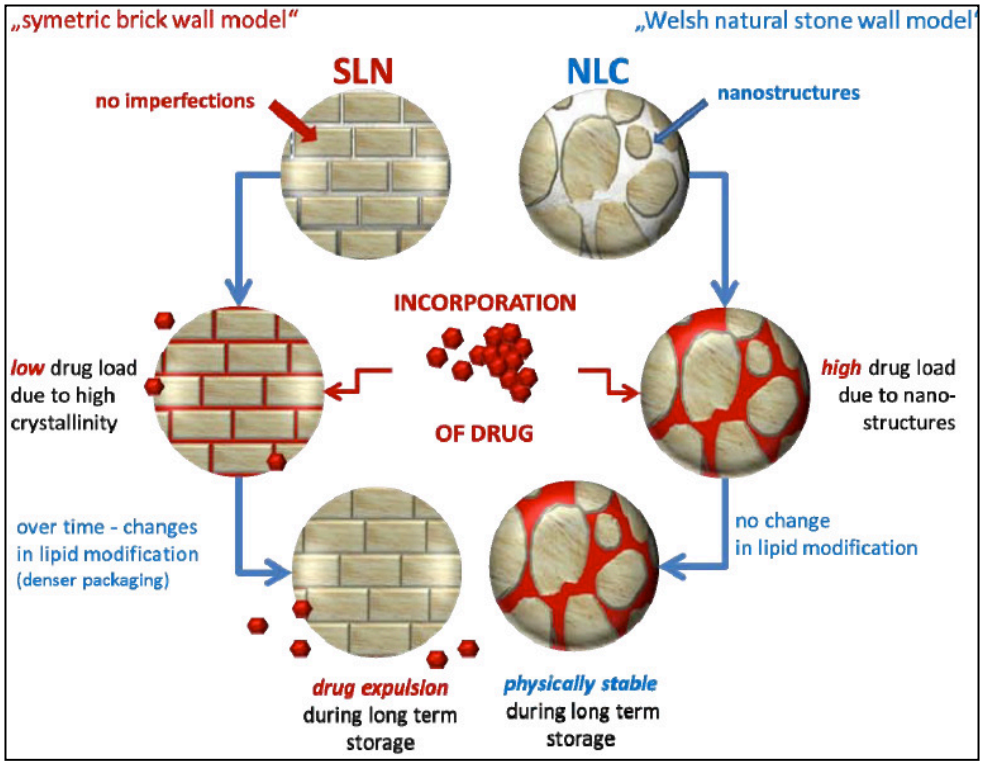

Figure 1.9: Lipid nanoparticles (SLN and NLC), adapted from (Patel et al., 2013)

Components

The main components of lipid nanoparticles (lipids and surfactants) have a great influence on the product quality, being their selection related to the physicochemical properties of the drug and the selected administration route.

- The characteristics of **lipid components** (e.g., structure, hydrophobicity, and crystalline modifications), are important for production of lipid nanoparticles. Lipids, which a highly ordered crystalline lattice, increase drug expulsion, and so, lipids with complex structures, containing fatty acid chains of different lengths, could be considered a good selection to improve long-term stability, and increase the loading capacity. In general, a combination of

long and short chain fatty acids is preferred to reduce the average size of particles (Sánchez-López et al. 2017).

- ***Surfactants*** are required to assure the stability of lipid nanoparticles in aqueous dispersion. The surfactant molecules, located between the lipid and water phases, may also contribute to induce specific surface-chemical properties and to modulate the biopharmaceutical profile of the drug-loading particles. Several factors, such as hydrophilic-lipophilic balance (HLB) values, cytotoxicity, and their effect on the lipid polymorphism and particle size, should be considered in the selection of surfactants, for production of lipid nanoparticles intended for skin administration. Surface modification of lipid nanoparticles has an important role to modulate the interaction with the skin. A cationic surface charge improves the electrostatic interaction with the negatively charged epithelium enhancing residence time and the drug's bioavailability. Surfactant composition also influences the in vivo biodegradation of the lipid matrix, as well as the mean particle diameter. The most used surfactants include biological membrane lipids (lecithin, phospholipids), bile salts, biocompatible non-ionic molecules (ethylene oxide/propylene oxide copolymers, sorbitan esters, fatty acid ethoxylates), and mixtures, among others.

Methods for preparation of lipid NPs

For production lipid NPs, different factors, such as the particle average size and surface electrical charge, degree of crystallinity and lipid polymorphism, have been considered the main key factors influencing the long-term stability of lipid nanoparticles and the drug release profile.

Different methods of high and low energy based on solidified emulsion technologies, were described for production of lipid NPs (SLN and NLC). Among this, the most widely used are the high-shear homogenization and ultrasound, the high pressure (hot and cold homogenization), solvent emulsification/evaporation, and the microemulsion-based approach (Mehnert, 2001). Furthermore, for the desire of encapsulation for hydrophilic actives, the most suitable method that can be applied is a multiple-emulsion/melt dispersion technique, using the correct proportions, temperature and mixtures of different surfactants suitable HLB for W/O and O/W emulsification, with the additional high-shear techniques (Becker Peres et al. 2016). In this case, it will provide small aqueous portions emulsified inside the lipid core.

1.3.3. Skin penetration of nanoparticles

Generally, is assumed that the SC is the main barrier for skin absorption following two possible pathways: through the corneocytes (bricks) or along the intercellular spaces along the lipid matrix (mortar), being crucial the hydrophilicity/lipophilicity of the absorbent (**Figure 1.5**).The

transappendageal route (via hair follicle, sebaceous and sweet glands) can also be consider for some active an polymeric nanoparticles (Schneider et al. 2009).

Nanotechnology has the advantage on transdermal delivery to be able to penetrate across the SC barrier and reach SDLs, overcoming conventional barrier penetration issues as previously stated. They can also be designed according to the target cells of interest. They play an important role on being more effective with lower dosages applied, as well as lower toxicity reaching the systemic level. Many factors can be considered for nano-based delivery systems, such as particle size, size distribution and surface charge. Particle size and shape affect drug release, physical stability, and cellular uptake. Moreover, the surface charge of NPs plays an important role on physical stability of the particles in solution, as well as can influence on their penetration ability across the skin layers or on the attachment to cell membrane for internalization. The surface charge could potentially control binding to specific cells or tissues (Uchechi et al. 2014). Skin cellular surfaces are negatively charged due to phosphatidylcholine and carbohydrates with negatively charged groups. NPs with higher surface positive charge show strong affinity to cellular membrane due to electrostatic interactions between the anionic membrane and cationic NPs, facilitating the uptake. In the other hand, the high cellular uptake of negatively charged NPs is related first to the non-specific adsorption on the cell membrane and formation of a clusters (Honary and Zahir 2013). For instance, NPs with predominant positive charge could enhance transdermal penetration (Uchechi et al. 2014). In fact, on positively charged sites, electrostatic interaction by adsorption of the negatively charged particles may lead to local neutralization favouring endocytosis for cellular uptake (Yin Win and Feng 2005).

Different studies revealed that **polymeric nanoparticles** were found accumulated preferentially in the follicular openings, with increased distribution in a time and size-dependent manner, being favoured to smaller particle size (Alvarez-Román et al. 2004). Other research described the influence of microparticle size in skin penetration by differential stripping. Nanoparticles can act as efficient drug carriers through the follicle or serve as follicle blockers to stop the penetration of topically applied substances (Uchechi et al. 2014). Moreover, the localization of nanoparticles in the hair follicles may promote proliferation and differentiation of hair follicle stem cells, being potentially addressed to the treatment of dermatological conditions and wound healing (Zhang et al. 2013). No evidence for uptake of this vectors outside the follicles was observed, whose transport was clearly impeded by the SC (Alvarez-Román et al. 2004). In addition, it has been previously described that hairless animal did not show any NPs penetration

into the skin, indicating that the hair follicles are an essential pathway for skin invasion of particulate materials (Schneider et al. 2009).

The mechanism of transdermal permeation of lipid NPs is still unclear, however, previous authors explain the interactions between lipid nanoparticles and skin lipids by dynamic diffusion process (Gu et al. 2018). Other authors proposed that the main mechanism of lipid NPs skin penetration is related to their close contact with the SC superficial junctions, penetrating between corneocytes bricks (Khater et al. 2021). This permits superficial spreading of the active, consequently forming an adhesive layer with occlusive properties. This effect may reduce corneocyte packing, due to SC hydration, improving drug partitioning and allowing lipid exchange between the nanosystem and the SC. In fact, recent researcher stated a potential of lipid NPs to penetrate by the follicles, due to the sebum affinity with the lipid composition of the nanocarrier (Souto et al. 2020), since they are also present in the human sebum composition (triglycerides, diglycerides, wax esters, free fatty acids, cholesterol and its derivatives) (Lauterbach and Müller-Goymann 2015).

2. HYPOTHESIS AND OBJECTIVES

2.1. HYPOTHESIS

The microbiome plays an important role in maintaining skin health. The most frequent skin disorders involve inflammation or infections. A skin infection generally will lead to an inflammation, which is a sign of an immune response in the body. The skin microbiota is able to interact with the immune system, helping to maintain skin homeostasis by growth inhibition of pathogenic bacteria on the skin, decreasing the inflammation. Acne is a common inflammatory skin disorder of the hair follicle that involves hyperseborrhea, abnormal follicular keratinization and *C. acnes* proliferation in the pilosebaceous unit. The associate infection is generally treated with antibiotics to kill excess skin bacteria, reducing redness and inflammation, resulting in unbalanced skin microbiota and microbial resistance. Therefore, natural compounds with anti-inflammatory, antioxidants, and antimicrobial agents, such as thymol (TH), could be the key for preventing or reducing the associated symptoms.

Despite its multifunctional properties, TH presents good affinity for skin penetration, since its molecule may cause mobility of the intercellular lipids of the stratum corneum. For this reason, the timeframe this compound remains inside the skin might be short. Moreover, this compound is sensitive to oxygen and light which can undergo oxidation long storage, decreasing its potential effects against acne. Therefore, drug delivery systems, based on nanotechnology, could be a novelty approach for skin disease management. Nanotechnology offers several advantages to improve active compounds bioavailability after topical administration, since small particle diameters tend to penetrate the deep skin, withdraw the drug in a controlled manner, be mainly retained in the deeper layers and prolong their passage inside the skin. Among these systems, nanoparticles (NPs) constitute an excellent candidate in skin disorders, especially for acne treatment, due to their small particle diameter, able to penetrate inside the follicle and prolonged release active compounds inside the lesions. Although, the efficacy of the nanosystems could be slower than the free form at the beginning of the treatment, however, due their prolonged release, it is expected to potentiate the long-term activity. Since NPs release slowly the active in the target site, it might be an advantage on not disturbing the entire skin microbiota, since its good balance is the main key for treating skin disorders.

For this reason, polymeric and lipid nanoparticles encapsulating TH or THO (natural active compounds), with antimicrobial and antioxidant properties, could be considered a novelty approach for acne treatment, replacing the use of antibiotics, and so avoiding the disturbances on the healthy skin microbiota or microbial resistance.

2.2. OBJECTIVES

The present work is focused on the development of novel polymeric and lipid nanostructured systems containing thymol (TH) for topical administration, enhancing its anti-inflammatory, antimicrobial, antioxidant, and wound healing efficacy against acne.

The main objective of this research is the development and physicochemical characterization of different dosage forms of thymol, based on nanoparticulate systems, able to improve acne treatment, analyzing their biopharmaceutical and toxicological behavior as well as their therapeutic efficacy.

To achieve this objective, the research has been divided into several stages, which constitute the *specific objectives*:

- Development, and optimization by DoE of biodegradable PLGA NPs encapsulating TH, prepared by solvent-displacement technique.
- Development, and optimization of lipid NPs encapsulating TH, prepared by high energy procedures.
- Surface modification of nanoparticle containing TH or THO to improve efficacy and incorporation in gels to enhance nanostructured system stability.
- Physicochemical characterization of developed systems, analysing, their morphology, morphometry (average size, polydispersity index), surface charge, encapsulation efficiency, stability at different temperatures and rheological behaviour
- Interaction studies between active and polymeric or lipid matrix by thermal and/or spectroscopic methods.
- Biopharmaceutical behaviour, analysing, *in vitro* the release profile of TH from different colloidal dosage forms developed and *ex vivo* skin permeation.
- In vitro cytotoxicity studies, determining cell viability of human epidermal keratinocyte cell lines (HaCaT) and cell up-take of developed NPs
- Determination of therapeutic efficacy of developed nanoparticles, analyzing in vitro antimicrobial, antioxidant, anti-inflammatory activity as well as the in vivo determination of biomechanical properties on human skin and skin barrier and sebum regulation efficacy

3. MATERIALS AND METHODS

3.1. PRODUCTS AND REAGENTS

Materials used for the development, physicochemical and biopharmaceutical characterization of polymer and lipid nanoparticles, including manufacturers, are shown in **Table 3.1**. Milli-Q-water and double distilled water were used after filtration in a Millipore system (Millipore Sigma, Burlington, Massachusetts, USA). All the other chemicals and reagents, used in the study, were of analytical grade.

Tabla 3.1: Preparation, optimization, and characterization of Thymol nanoparticles

	Products and reagents	**Manufacturer**
Active	Thymol (TH)	Sigma-Aldrich (Madrid, Spain)
	Thyme oil (THO)	Ventós (Barcelona)
Polymeric NPs Preparation	Poly(D,L-lactide-co-glycolide) PLGA Resomer®RG 504H (Carboxylic terminal group, MW:38000 54000Da molar ratio lactide:glycolide 50:50)	Evonik Industries, Evonik Corp. (Birmingham, USA).
	Tween®20 (Tw20)	Sigma-Aldrich (Madrid, Spain)
	Poloxamer 188 (P) and Poloxamer 407 (PP)	BASF (Barcelona, Spain)
	Chitosan (C)	HMC+ (GmbH, Germany)
	Phosphatidylcholine (L)	Lipoid® (GmbH, Germany)
Semi-solid formulations	Glycerin	Sigma Aldrich (Madrid, Spain)
	Propylene glycol	Sigma Aldrich (Madrid,Spain)
	Carbomer®934	Fagron Ibérica.Barcelona, Spain
	Hydroxypropylmethylcellulose (HPMC)	Sigma Aldrich (Madrid,Spain)
Lipid NPs Preparation	Compritol CG® 888 ATO (Glyceryl behenate)	Gattefossé (Madrid, Spain))
	LAS (PEG-8 Caprylic/Capric Glycerides)	Gattefossé (Cedex, Spain))
	Mygliol®812 (Caprylic/Capric Triglyceride)	Sigma Aldrich (Madrid, Spain)
Analysis and Interactions	Disposable folded capillary cells (ZP)	Iesmat (Spain)
	Tryptone Soy Agar	Oxoid UK
	Sabouraud Dextrose Agar	Oxoid UK
	Uranyl acetate	Fisher Scientific (Spain)
	Kromasil®column (C18, 5 µm, 150x4.6 mm)	Tecknokroma. (Spain)
	Amicon®Ultra, 0.5 centrifugue filter devices	Millipore
	DSC perforated aluminium pans	Mettler Toledo (Spain)
Bio-pharmaceutical behavior	Methylcellulose membranes (Dialysis Tubing –Visking Inf Day 15.9 mm, MWCO: 12–14.000 Da	Medicell Membranes Ltd Code DTV12000.03.000, Size 3 (London, UK)
	Skin samples from abdominal plastic surgery	Hospital de Barcelona, SCIAS, Barcelona, Spain
	Transcutol P	Gattefossé (Cedex, France)
	Fluoromount G® mounting medium	Invitrogen, Thermo Fisher Scientific, USA).
	3M Tegaderm™, 6x7cm, 10u,	3M Spain, S.A.

The main products and reagents involved in toxicological assays, cellular uptake, and therapeutic efficacy, including manufacturers, are reflected in **Table 3.2**.

Tabla 3.2: Products and reagents for toxicity studies and therapeutic efficacy of developed NPs

	Products and reagents	**Manufacturer**
Toxicological Behavior and Cellular uptake	Human keratinocytes cell lines (HaCaT)	Cell Lines Service (CLS, Eppelheim, Germany
	High glucose DMEM	Dulbecco's Modified Eagle's Medium (Thermofisher)
	Wheat germ agglutinin (WGA) Alexa-488	Molecular Probes
	MTT (3-(4,5-Dimethylthiazol-2-yl)-2,5-diphenyl tetrazolium bromide)	Sigma-Aldrich Chem. Co, (St. Louis, MO, USA)
	4',6-diamidino-2-phenylindole (DAPI)	Sigma Aldrich, Spain
	trypan blue	Sigma Aldrich, Spain
	MTT (3-(4,5-Dimethylthiazol-2-yl)-2,5-diphenyl tetrazolium bromide)	Sigma Aldrich, Spain
	AnaeroGen™ 2.5L, Oxoid,)	Basingstoke, UK
	PFA (paraformaldehyde)	Sigma Aldrich, Spain
Therapeutic Efficacy	Clindamycin Clorhidrate,	Acofarma, Llobregat, Spain
	Mueller Hinton Broth and Brain Heart Infusion	Oxoid (Basingstoke, UK)
	Chlostridium reinforced medium (CRM)	Oxoid (Basingstoke, UK)
	Berens Cosmetic diluent	Scharlab UK
	96-well polypropylene microtiter plate	Costar, Corning Incorp. USA
	Methhylene blue (MB)	Fisher Scientific (Spain)
	DPPH (2,2-diphenyl-1-picrylhydrazyl)	Sigma Aldrich, Spain
	BHT (butylated-hydroxytoluene)	Sigma Aldrich, Spain
	Osmium tetroxide	Sigma Aldrich, Spain
	EPON resin	Sigma Aldrich, Spain
	H_2DCFDA Fluorogenic dye (2',7'-dichlorodihydrofluorescein diacetate)	Merck Spain
	DMEM medium (absent of phenol red and FBS)	Fisher Scientific (Spain)
	ELISA Immunoassay (BD OptEIA™ SET Human IL-8, IL-6.	BD Biosciences
	RNA extraction kit	Qiagen RNeasy (Germantown, Maryland)
	High-Capacity cDNA Reverse Transcription kit	Applied Biosystems

Table 3.3 Oligonucleotide´s primers

Gene	**Forward (5′-3′)**	**Reverse (5´-3´)**
TNF-α	CTGCTGCACTTTGGAGTGAT	AGATGATCTGACTGCCTGGG
IL-1α	GAAGAGACGGTTGAGTTTAAGCC	CAGGAAGCTAAAAGGTGCTGA
IL-1β	GTGGCAATGAGGATGACTTGTTTC	TAGTGGTGTCGGAGATTCGTA
IL-8	CTGATTTCTGCAGCTCTGTG	GGGTGGAAAGGTTTGGAGTATG
IL-6	AGCCACTCACCTCTTCAGAAC	GCCTCTTTGCTGCTTTCACAC
Keratin 16 (K16)	CAGCGAACTGGTACAGAGCA	GTTCTCCAGGGATGCTTTCA

3.2 INSTRUMENTAL

The instrumental (and manufacturer) used for different assays involved in the development of polymeric and lipid nanoparticles containing TH are shown in **Table 3.4**.

Table 3.4 Instrumental for development of TH-loaded nanoparticles

	Instrumental	Manufacturer
Formulations Preparation (NPs, NLCs, gels)	Multi-position magnetic stirrer Magnetic stirrer multiplace with heating	IKA (Germany) OVAN.Thermo Fisher Sci.UK
	Elma digital ultrasonic cleaners®	Schmidbauer GmbH (Germany)
	Rotatory evaporator (R-210/215)	Buchi (Flawil Switzerland)
	High-pressure homogeniser Stansted FPG 12800	Stansted, United Kingdom
	Ultra-Turrax T25	IKA (Germany)
	Ultrasonic®probe	Sonics & Materials, INC. USA
	Unguator®emulsifier	Microcaya (Bilbao, Spain)
Analysis and characterization of NPs	Size and zeta potential analyzer ZetaSizer Nano ZS	Malvern Instruments (Malvern UK)
	TEM (transmission electron microscopy)	JEOL 1010,Tokyo, Japan
	SEM (scanning electron microscopy)	JEOL JSM-7001F
	Confocal microscopy (Leica TCS SPII), 63X oil immersion objective	Leica Microsystems
	HPLC (Diode array detector)	Waters 2695
	Centrifuge 5415C, Geratebau Eppendorf	GmbH, Engelsdorf, Germany
	Turbiscan®Lab Expert (Stability analyzer)	Formulaction S.A, (L'Union, France)
	Rheometer Haake®Rheo Stress 1	Thermo Fisher Sci., Kalsruhe, Germany
	Differential scanning calorimetry (DSC) Mettler M3 Microbalance	Mettler, TA 4000 system (Greifensee, Switzerland)
	X-ray diffractometer (XRD)	Siemens D500 system (Karlsruher, Germany)
	pH-meter Crison, GLP 21	Crison Instruments Barcelona (Spain)
	Optical Leica DM 1000 LED light microscope	Leica Microsystems Wetzlar, Germany
Biophrmaceutic Behaviour	Diffusion Franz cells, FDC-400	Vidra-Foc (Barcelona, Spain)
	Cryostat microtome (LEICA CM3050 S) -20 °C. Glass-slides Superfrost® Plus	Menzel-Glaser,Thermo Sci. USA
Toxicological behaviour	Modulus® Microplate Photometer	Turner BioSystems Inc.SunnyvaleUSA
	Automated cell counter	Invitrogen, Thermofisher
Therapeutic efficacy	Corneometer (CM 825)	C+K electronic Gmbh,Germany
	DermaLab® module	Cortex Techn (Hadsund, Denmark)
	Sebumeter	Cutometer® dual MPA 580, C+K electronic Gmbh, Germany)
	NanoDrop TM-2000 spectrophotometer	Thermo Fisher Scientific Waltham, Massachusetts (USA)
	UV-Vis Spectrophotometer	Shimazu (Kyota, Japan)
	Shaker incubator Innova 4080	New Brunswick Scientific (New Jersey, USA)
	Varioskan plate reader	Thermo Fisher Sci., Rockford, USA
	StepOne Plus PCR cycler SYBR® Green PCR Master Mix	Applied Biosystems Thermofisher Sci.

3.3 PREPARATION OF NANOPARTICLES

3.3.1. Preparation and Optimization of Thymol-Loaded Polymeric NPs

Thymol (TH) or thymol oil (THO) loaded PLGA NPs (TH-NPs), containing a matrix structure (nanospheres), were prepared by solvent displacement evaporation, as described by Fessi et al. (Fessi et al. 1989) and illustrated in **Figure 3.1**. Briefly, 25 mg of active (TH or THO) were added to an organic solution containing acetone and 90 mf of the co-polymer (PLGA). This organic phase was subjected to 5 min sonication, in an ultrasonic bath (Elma Digital Ultrasonic Cleaners® Frechen, Germany), to ensure complete dissolution of compounds. The organic phase was then, added dropwise into an aqueous phase containing 40 mg of tween 20 (TW) as stabilizer, under continuous moderate magnetic stirring (700 rpm) for 15 min. The formation of nanoparticles was observed by the change from transparent to white opaque solution. Organic solvent (acetone) was removed under constant reduced pressure, using a rotatory evaporator (Rotavapor® R-210/215 (Buchi, Flawil, Switzerland) for 20 min at 90 mbar and NPs were concentrated to a volume of 10 mL. In the case of obtaining a double concentrated TH-NP (0.5 % of TH), additional 5 mL of water was evaporated. The pH of aqueous phase, prior to NPs formation, and the pH of the final formulation were adjusted by using a pHmeter (MicropH 2001, Crison). Empty NPs (B-NPs) were prepared using the same procedure but without the addition of active (TH or THO).

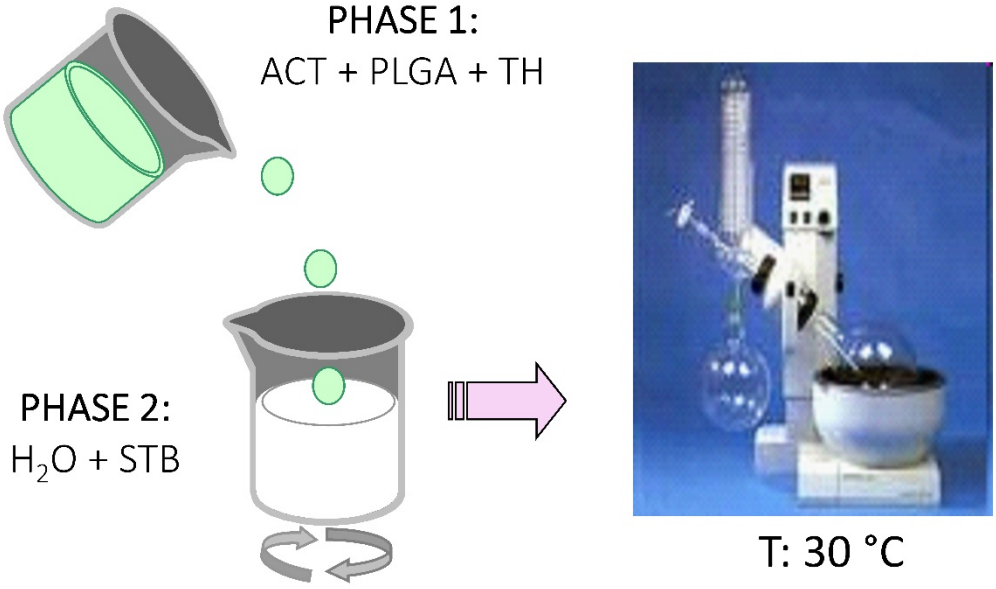

Figure 3.1. Preparation of TH-NPs by solvent displacement evaporation method.

Thymol free solutions were either prepared in an hydroalcoholic solution by dissolving 25 mg in 2 mL of ethanol, competed with 8 ml of water (0.25 %) or using TW at 0.4 or 1.6 %, completed with water to 10 ml total.

Surface of TH-PLGA-NPs was modified by using several compounds. In order to prepare the surface modified polymeric NPs, the organic phase composed by PLGA, and TH was dissolved in acetone and the aqueous phase consisted on either phosphatidylcholine (PL), Poloxamer 188 (P188) or Poloxamer 407 (P407), namely TH-NP-L-, TH-NP-P- and TH-NP-PP-, respectively, for negatively charged particles. Additionally, positively charged particles were also produced containing chitosan (CS), namely TH-NP-P-C+ or TH-NP-PP-C+, where the aqueous solution contained 1 % acetic acid. The organic phase was added dropwise into the aqueous phase, under continuous stirring, as described before.

A full factorial central design with three levels and five factors has been developed to enable optimization of TH-NP-T- (Vega et al. 2006). The experimental design consisted of 16 formulations with variable factorial points (-1/+1), axial points (-1.68/+1.68) and central points (0), consisting of 8, 6 and 2 formulations respectively. The amount of drug (TH), surfactant (TW) and the pH of the aqueous phase were submitted to variance, while PLGA was set a fixed value of 9 mg/mL. These were performed in triplicate. Variable points are shown in **Table 3.5**, where the active ingredient and the surfactant concentrations are expressed in µg/ml.

Table 3.5: Parameters of factorial design

Factorial Design					
Factors	***-1.68***	***-1***	***0***	***+1***	***+1.68***
Active	1.16	1.5	2	2.5	2.84
Surfactant	1.32	2	3	4	4.68
pH	5.16	5.5	6	6.5	6.84

3.3.2. Preparation of Thymol Loaded Lipid Nanoparticles

Nanostructure Lipid Carrier (NLC) was the lipid system chosen to encapsulate TH, due to the ability of higher loading capacity than solid lipid nanoparticles (SLN). Before the preparation of the nanoparticles, the compatibility of the mixture of the total lipids (solid and liquid proportion) and the amount of TH to be encapsulated, was assess by DSC. The selected solid lipid

(SL) was glyceryl behenate (Compritol CG ATO 888) (C188) and the liquid lipids (LL) tested were PEG-8 Caprylic/Capric Glycerides (LAS) (LL1) or Caprylic/Capric Triglyceride (Mygliol 812) (MGL) (LL2). Briefly, mixtures (SL:LL) were analyzed alone (60:40, 70:30, 80:20 and 90:10) being a total lipid portion of 2 % and with a total of thymol amount of 0.5 %. The DSC measurement was set up where samples were heated from 5 °C to 100 °C at 10 °C/min under a nitrogen atmosphere. Data were evaluated from the peak areas with Mettler STARe V 9.01 DB software. Thymol-loaded lipid nanoparticles (TH-NLCs) were produced by high energy procedures, probe ultrasonication or high-pressure homogenization, by using a Sonics Ultrasonic® probe and a High-pressure homogenizer Stansted FPG 12800, respectively (**Figure 3.2**). Briefly, to produce TH.NLC-T-, the aqueous phase containing 1 % or 1.6 % Tw20 was heated above 80 ºC as well as the lipid phase containing 0.5 % of Thymol and 2 % total lipid mixture, ranging from 60:40 to 90:10 proportion (SL:LL). The aqueous phase was then added into the lipid phase and a pre-emulsion was generated using an Ultra-Turrax T25 (IKA, Staufen, Germany) for 2 min by at 5000 rpm followed by ultrasonication during 20 min at 40 % amplitude or high-pressure homogenization (3 cycles at 700 mbar) and immediately cooled down under cold running water for 5 minutes. Samples were kept overnight for further characterization analysis. Samples were then optimized by design of experiment (DoE), 2^2-star factorial design. Based on previous results obtained, a central point (0) and two variable factors (-1/+1) were selected (SL:LL and TW %).

Surface modification of TH-NLC was performed by adding or replacing TW using PL or P407 and, additionally, to obtained positively charged NLC's, either CS at 0.05 % or benzalkonium chlodire (BZ), a positively charge surfactant at 0.1 %, were added. The prior stock CS solution was previously prepared in 1 % acetic acid.

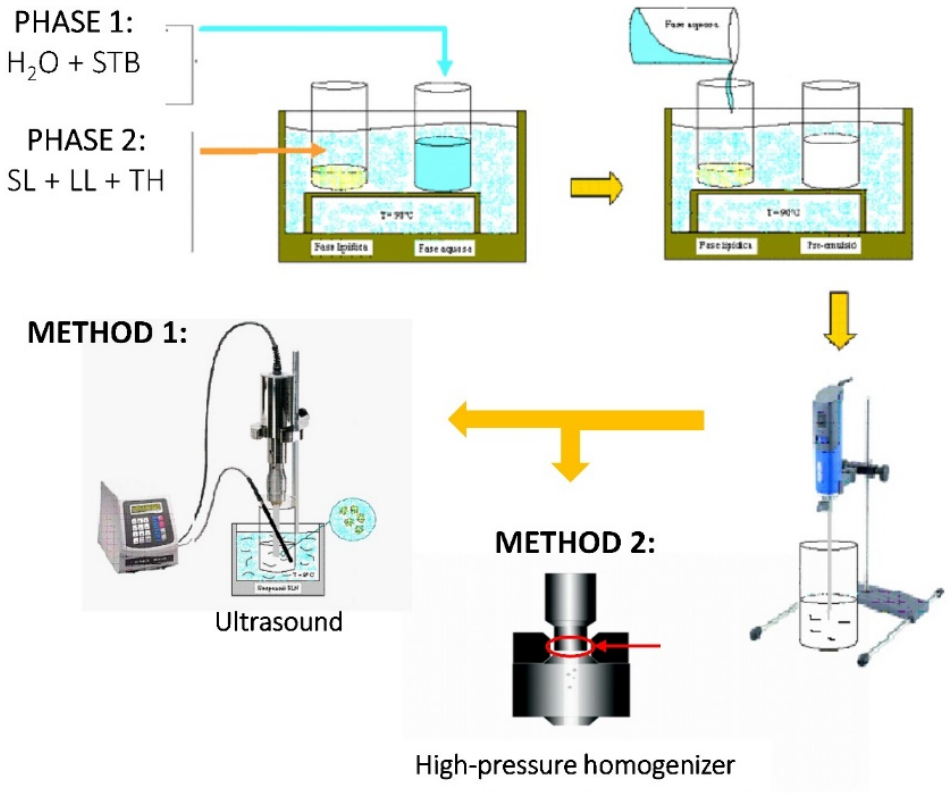

Figure 3.2. Preparation of TH-NLC by ultrasound or high-pressure homogenization methods.

3.3.3. Preparation of Semi-Solid Formulations of Developed Nanoparticles

In the preparation of the gels, TH-NPs, THO-NPs or TH-NLCs (at 0.25 % or 0.5 %) were incorporated at 40 or 50 % of the total water content, obtaining a final concentration of thymol of 0.1 or 0.25 %, respectively. For thymol gels, TH was previously dissolved in 5 % glycerine or propylene glycol, under sonication, then completed with water. Carbomer gels (GC) were formulated by previously dissolving Carbopol 0.6 - 1 % in water under constant magnetic stirring and then adding 5% of glycerine or propylene glycol. Then, the mixture was allowed to stand overnight, and the pH was adjusted to 5.0 – 6.5 with NaOH 2N. For the hydroxypropyl methylcellulose (HPMC) gels (GH), this was dissolved in the water phase (2 – 5 %) and 5 % of glycerine or propylene glycol was added. For the pluronic gel (GP), P407 (20 %) was dissolved in cold water under continuous stirring. Then, the mixture was allowed to stand overnight at 4 °C, then glycerine or propylene glycol (5 %) was added and mixed under vigorous stirring. The gel was formed when the temperature reached RT. All gel mixtures were performed using Unguator®emulsifer.

3.4 ANALYTICAL METHODS

3.4.1. Physicochemical Characterization of Thymol NPs

Morphometrical properties of NPs (average particle size, Zav and polydispersion index, PI) were determined by photon correlation spectroscopy, using the dynamic light scattering technique (McConnell 1981) that allows measurements to be made with a wide range of sizes (0,6 nm - 4 μm). This spectroscopic technique is based on the measurement of the variations in the intensity of the scattered light, due to the Brownian movement of the particles in the sample. These fluctuations are not constant, so that the amount of light dispersed by the solution oscillates over time. The information obtained through scattered light can be related to the diffusion coefficient, which, in turn, allows information on the size and shape of the particles.
The Brownian movement of the particles or molecules in suspension causes the laser light to disperse in different intensities. From the analysis of these intensity fluctuations, the speed of the Brownian movement is obtained and, therefore, the particle size ratio using the Stokes-Einstein equation:

$$D = \frac{kB \text{ x } T}{6\pi * \pi * r} \qquad /3.1/$$

where, kB is the Boltzmann constant (1,3806504x10^{-23} J / K), T the absolute fluid temperature); π, the fluid viscosity and r the radius of the particle. PI is the measure of the particle size distribution ranging from 0 to 1, low values (<0.200) indicate a mono-dispersed system.
For the determination of NPs morphometry, a ZetaSizer Nano ZS (Malvern Instruments; Malvern, UK) was used. The values were obtained from the average of three measurements (in 10 mm diameter cells at 25ºC) from three different batches of each formulation. Before measurement, all samples were diluted with milli-Q water (1/20) to represent an adequate dispersion intensity.

The **surface charge** of NPs, which is an indirect parameter of aggregation measured as zeta-potential (ZP), was determined by electrophoretic mobility (μE) of charged particles subjected to an electric field, applying Henry's equation (Vega E. et al, 2008):

$$\mu E = \frac{\sum Zpot.f(K\alpha)}{6\pi\eta} \qquad /3.2/$$

where μE is the electrophoretic mobility, Ɛ is the dielectric constant of the medium, η is the viscosity of the medium, K is the Debye-Hückel parameter, and f (Kα) is a correction, factor

considering the thickness of the double layer and diameter of the particle. The unit of K is a reciprocal length 1 / K is described as the thickness of the electrical double layer. This technique allows working at high concentrations of up to 60 % by volume, without prior dilution of the sample. However, in the ZP determination, if the formulation has aggregates, in many cases it is advisable to dilute the sample until obtaining a constant value

The **morphology** of the nanoparticles and the degree of homogeneity of the sample was accessed by *transmission electron microscopy* (TEM), in a JEOL JEM1010, (Tokyo, Japan). Images were taken *using 20,000 to 100,000* × magnifications with Megaview III (Soft using Megaview III (Soft Imaging Systems, GmbH, Münster, Germany).

The sample preparation was performed in a cupper grid that acts as a support and subjected to a negative staining. The grid was placed in contact with a drop of the NPs suspension diluted 1/4 for 60 seconds, followed by 3 dilution cycles in milli-Q water drops for 30 s each, then contrasted with 2 % Uranyl acetate for 60 seconds. Samples were dried overnight in a desiccator at room temperature. The morphological examination of the NPs was performed using TEM JEOL 1010 instrument.

Scanning electron microscopy (SEM) was used to access the morphology TH-NPs and TH-NLCs incorporated into carbomer gels. This instrument uses pumping electrons beam instead of beam light to form an image. It has a great shallow depth of field, which allows a large focus to be focused part of the sample. It also produces high resolution images, so that the smallest characteristics of the sample can be examined with large amplification (Balk 1988). Due the fact that the sample are required to be conductive, it is coated with a carbon layer or a layer thin of a metal to give it a conductive character. The solid sample was deposited on a metal support for subsequent sputtering cupper coating. Then, samples were visualized by SEM microscope (JSM-7001F, JEOL) (Sosa et al. 2019).

Quantitative analysis was performed by reverse-phase high-performance liquid chromatography (HPLC), by a modification of the method described previously (Ghasemi Pirbalouti et al. 2011). Studies were carried out in Waters System (2695) with UV PDA Waters® 2996 detector, using a Kromasil® column (C18, 5 µm, 150x4.6 mm). The mobile phase consisted of acetonitrile:water under gradient conditions of 30:70 / 58:42 / 30:70 during 20 min. Thymol was determined at wavelength of 275 nm.

The encapsulation of TH was measured indirectly by quantification of unloaded amount after filtration centrifugation of samples. NPs were diluted 1:10 in Milli-Q water:ethanol (90:10) and centrifuged (Centrifuge 5415C, Geratebau Eppendorf GmbH, Engelsdorf, Germany) for 10 min

at 14000 rpm, using Millipore filter device (Amicon® Ultra, 0.5 mL 100K, Merck Millipore Ltd., Carrigtwohill Co. Cork IRL). The filtered fractions were quantified by HPLC, and the EE was determined by the equation (3.3):

$$EE\% = \frac{TH\ (total\ amount) - TH(free)}{TH(total\ amount)}\ x\ 100$$

A calibration curve was freshly prepared for each experiment by dissolving 10 mg of TH in 1 ml of methanol diluted 1:10 obtaining a stock solution of 1000 µg/ml. All further dilutions were performed in methanol:water (70:30). The calibration curve normally ranged from 1 to 250 µg/ml.

3.4.2 NPs Interaction Studies

Interaction studied were carried out with TH-NP and blank NPs (B-NP) by previous ultracentrifugation (Beckmann-Coulter ultracentrifuge) of the samples at 15.000 rpm during 30 min, followed by drying in a desiccator. The possible interactions between TH and PLGA were assessed by differential scanning calorimetry (DSC). Thermograms were obtained on a DSC823e System (Mettler-Toledo, Barcelona, Spain). A pan with indium (purity ≥ 99.95 %; Fluka, Switzerland) was used to check the calibration of the calorimetric system and an empty pan was used as a reference (Sánchez-López et al. 2016). Samples were heated from 10 °C to 100 °C at 5 °C/min under a nitrogen atmosphere. Data were evaluated from the peak areas with Mettler STARe V 9.01 DB software (Mettler-Toledo). The physical state (amorphous or crystalline) of TH and TH-NP was analyzed by X-ray diffraction (XRD). Samples were sandwiched between 3.6 µm films of polyester and exposed to Cu K α radiation (λ = 1.5418 Å) with work power (45 kV, 40 mA). Diffractograms were recorded on a PANalytical X'Pert PRO MPD θ/θ, powder diffractometer of 240 mm of radius, using PIXcel detector (active length = 3.347 º). The measure time was defined 200 s per step, 2θ/θ scans from 2 to 60 º2θ with a step size of 0.026 º2θ (Silva-Abreu et al. 2018).

***Differencial Scanning Calorimetric (DSC)**:*

This technique analyzes any thermal transitions of compounds being affected within the NPs production. It is a thermodynamical tool for direct assessment of the heat energy uptake, which occurs in a sample within a regulated increase or decrease in temperature. The calorimetry is particularly applied to monitor the changes of phase transitions.

Thermal transition temperatures (Tt, melting points) of the samples are also determined in solution, solid, or mixed phases such as suspensions. It studies a single molecular transition of a molecule from one conformation to another. The difference in the input energy required to match the temperature of the sample to that of the reference would be the amount of excess heat absorbed or released by the molecule in the sample (during an endothermic or exothermic process, respectively). As a result of the presence of the molecule of interest, more energy is required to bring the sample to the same temperature as the reference; hence, the concept of heat excess comes into the place (Gill, Moghadam, and Ranjbar 2010).

Thermodynamic changes between the NPs and compounds alone were reflected on the Thermograms obtained by differential scanning calorimetry using DSC823e Mettler TA 4000 System (Greifensee, Switzerland). The dried forms of TH, TH-NP and B-NP were weighed (Mettler M3 Microbalance) in perforated aluminum pans and heated from 10 °C to 100 °C at 5 °C/min under a nitrogen atmosphere. Data was evaluated by peak areas with Mettler STARe V 9.01 DB software.

X-Ray Diffraction (XRD)

This technique was used to analyze the physical form of the thymol-loaded NPs and its components alone.

The physical state (amorphous or crystalline) of TH and TH-NP was analysed by X-ray diffraction (XRD). The crystalline or amorphous state of substances is one of the physicochemical characteristics that determines its biopharmaceutical behavior. Therefore, XRD is used to assess the structure of the molecule present inside the nanostructured systems.

Powder of thymol, thymol NPs and blank NPs were each sandwiched between 3.6 μm films of polyester an exposed to Cu K α radiation (λ = 1.5418 Å) with work power (45 kV, 40 mA). The diffractograms were recorded on a PANalytical X'Pert PRO MPD θ/θ, powder diffractometer of 240 mm of radius, using PIXcel detector (active length = 3.347 º). The measure time was defined 200 s per step, 2θ/θ scans from 2 to 60 º2θ with a step size of 0.026 º2θ (Silva-Abreu et al. 2018).

3.4.3 Stability Studies

The physical stability analysis of the developed formulations was carried out by means of an optical analyzer Turbiscan®Lab Expert, (Formulation, L'Union, France), based on the analysis of the multiple light scattering by concentrated solutions of said systems.

The sample to be analyzed is contained in a cylindrical glass cell that is placed in an upright position. The detection head consists of a source of pulsed near IR radiation (l = 850 nm) and two synchronized detectors of transmitted and scattered light. The transmission detector receives the light that passes through the sample (at an angle of 0° with respect to the incident radiation), while the dispersion detector receives it dispersed by the sample at 135° with respect to the incident radiation. The detection head scans the entire sample cell (50 mm in length), acquiring transmission and dispersion data every 40 μm (1625 acquisition and dispersion acquisitions in each scan). The profile obtained, in the percentage curves of transmitted (T) or scattered (BS) light depending on the height of the cell, allows to characterize the homogeneity of the sample and therefore determine destabilization phenomena. The method is based on the variation of the droplet volume fraction (migration) or the diameter (coalescence) that results in a variation of the scattered or transmitted light (Lemarchand et al. 2003).
Stability studies were performed with TH-NP-T- stored at 4 ºC (for 12 months) and at a RT (room temperature) and 37 ºC (for 3 months), determining the backscattering profile to predict sample short-term stability, faster than at naked. The stability was studied by measuring backscattering of near-infrared pulsed light (λ = 880 nm), bottom-to-top of the Turbiscan® cell containing TH-NPs, to predict the behavior of the NPs in solution. Additionally, measurements of morphometry **(**Zav, PI), surface charge (ZP), pH of the formulations (pH Meter, GLP 21, Crison Barcelona, Spain) and TEM images were also monitored at selected times. The EE stability was also measured at the end of 6 months storage.

The short-term stability of surface functionalized TH-NPs, TH-NLCs and carbomer gels containing the particles were also measured by Turbiscan® to predict particle´s physical stability.

Stability studies were also performed with surface functionalized TH-NPs and THO-NPs stored at 4 °C, measuring the morphometry **(**Zav, PI) and surface charge (ZP) for 6 months.

Short-term accelerated stability studies were applied to surface functionalized TH-NPs and their carbomer gels, recording measurements of morphometry **(**Zav, PI), surface charge (ZP), pH of the formulations after 1 month storage at 4, 25, 30 and 40 °C. Statistical analysis was performed by one-way ANOVA, Dunnett´s multiple comparison test, compared to values of freshly prepared formulations. Semi-solid formulations were evaluated stability of appearance and pH along storage.

To analyse the microbial preservative activity of TH during storage, selected samples (aqueous and gels) stored for a period of either 6 up to 36 months, either at RT or 4 °C where used. For direct measurement, 0.1 mL or g of each sample was transferred into the plates or, additionally, samples where diluted 1:10 in neutralizing solution (Berens Cosmetic Diluent, Scharlab, UK), then 1 mL was transferred into the plates. The total viable count was carried out by inclusion on TSA (Tryptone Soy Agar, Oxoid, UK) for bacteria or Sabouraud Dextrose Agar (Oxoid, UK) for fungi and yeasts. Plates were incubated at 35 ± 2 °C for 3 days or at 28 ± 2 °C for 7 days, respectively. This methodology was designed based on specifications of the European Pharmacopeia monographs (2.6.12. Microbiological examination of non-sterile products: total viable aerobic count).

3.4.4 Rheological studies

The flux type and viscosity of the formulations (20 g) was determined with cone-and-plate geometry (rotor C60/2-Ti 60 mm diameter, 2°angle) using Thermo Scientific, Haake Rheo Stress 1rheometer (Haake, Kalsruhe, Germany). The shear stress (τ) and viscosity (η) at 25 ± 0.1 °C were measured continuously to evaluate the shear stress (Pa) as a function of shear rate γ (s−1). The shear rate ramp was programmed (constant rate 100 s−1 during 1 min) including the ramp-up period from 0 to 100 s^{-1} in 3 min, and ramp-down backwards. Runs were performed in duplicate and data measurement were analyzed by Haake RheoWin®Data Manager V 3.3 (software) (Suñer-Carbó et al. 2017).

Using the rheometer, the material to be studied is subjected to different types of controlled deformations and the stresses are measured. One of the most important rheological properties is the viscosity. The fluids are classified by their behavior according to the shear force used.
Multiple models have been developed previously to understand rheological behavior of Newtonian or non-Newtonian fluids in the absence of nanoparticles, such as, Newton‘s, Ostwald De-Waele, Cross‘s and Herschel-Bulkley, among others. In fact, addition of solid particles to fluids, may lead to increased viscosity. According to Einstein’s theory on hydrodynamic viscosity, an increase in fluid viscosity should occur upon addition of solid particles being directly proportional to the volume fraction of solids added (Taborda et al. 2017).

Semi-solid formulations of TH, TH-NP and TH-NLC were analyzed. Samples were measured twice, in duplicate, for comparable results. Different mathematical models were applied to flow

curves to identify the best fit model to describe the flow type of each formulation. These mathematical models and their corresponding equations are shown in **Table 3.6**.

Table 3.6: Mathematical models developed to rheological behavior

MODEL	EQUATIONS	
Newton	$\tau = \eta \cdot \dot{y}$	τ = shear stress, η = dynamic viscosity, ẏ = strain rate
Bingham	$\eta = \frac{\eta p + \tau o}{y}$	η = apparent viscosity ηp = Plastic viscosity τ0 = Creep threshold or shear stress when the deformation rate tends to zero ẏ = Deformation rate
Ostwald de Wae	$\eta = K * y^{(N-1)}$	η = apparent viscosity K= consistency coefficient ẏ= Warp speed N = flow behavior index.
Herschel-Bulkley	$\eta = \frac{\tau o}{y + K * y^{(N-1)}}$	η = apparent viscosity, τ0 = Creep threshold or shear stress when the deformation velocity tends to zero ẏ = Deformation velocity K = consistency coefficient N = flow behavior index.
Cross	$\eta = \eta\infty + \frac{\eta o - \eta\infty}{(\tau\gamma)^m}$	η = apparent viscosity η0 and η∞ = asymptotic values of viscosity at very low and very high shear rate, γ = ……. and *m* =
Cross-Wiliamson	$\eta = \eta\infty + \frac{(\eta o - \eta\infty)}{(1 + \left(\frac{y}{yb}\right)^N)}$	η = apparent viscosity, η0 and η∞ = asymptotic values of viscosity at very low and very high shear rate ẏ = Warp speed, ẏb = warp speed at a point b, N = behavior index of flow

3.5 BIOPHARMACEUTICAL BEHAVIOUR

The biopharmaceutical behavior of TH, TH-NPs, TH-NLCs and their gels formulations were studies using vertical diffusion Franz cells as illustrated in **Figure 3.3**.

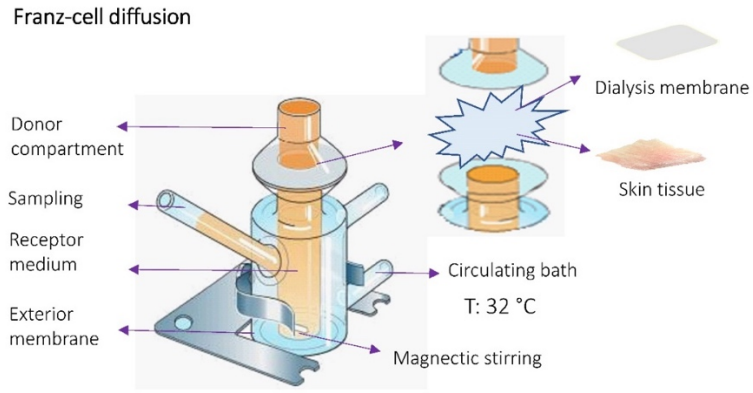

Figure 3.3. Vertical diffusion Franz cells for evaluation of drug release and skin permeation, using a methylcellulose membrane or an *ex vivo* tissue, respectively.

3.5.1. *In vitro* Release

The *in-vitro* release study was performed Franz cells (FDC-400, Vidra-Foc, Barcelona, Spain) using, methylcellulose membranes (Dialysis Tubing – ViskingCode DTV12000.03.000, Size 3, Inf Day 20/32"– 15.9 mm, MWCO– 12–14.000 Da, Liverpool Road, London, UK) clamped between donor/receptor compartments (2.54 cm^2). Samples of TH, TH-NP, TH-NLC or gels formulations were added to the donor phase and the receptor phase was filled with Transcutol P®:water (50:50), kept under constantly stirring at 32 °C, to mimic skin, maintaining sink conditions. Aliquots of 300 µL were collected at selected times, during a range of time up to 72 h, replaced with the same amount of receptor medium (Abrego et al. 2015). Sample were analyzed by HPLC and processed with the following mathematical models using GraphPad®:

Boltzmann Sigmoidal	*Y=Bottom+(Top-Bottom)/ (1+exp((V50-X)/Slope))*
Hiperbole	*Y=Bmax*X/(Kd+X)*
First Order	*Y=Ymax*(1-exp(-K*X))*
Peppas	*Y=K*(X^n)*
Higuchi	*Y=K*(X^(1/2))+P*

where, Y is amount of TH; Top, Bottom, Bmax and Ymax are the Y values at the plateaus; V50 is the time taken to reach halfway between the plateaus, X is time (min), Slope is the steepness of the curve; and K and Kd are kinetic rate constants.Statistical analysis was performed by one-way ANOVA, Tukey´s multiple comparison test or unpaired t student test.

3.5.2. *Ex vivo* Skin Permeation

Ex vivo human skin permeation study was also performed in vertical diffusion Franz described above. Skin samples (0.64 or 2.54 cm², 0.4 mm thick) were obtained from abdominal plastic surgery (Hospital de Barcelona, SCIAS, Barcelona, Spain), following a protocol approved by the Bioethics Committee of the Barcelona-SCIAS Hospital. Skin samples were clamped on each Franz cells with the SC and the dermis facing the donor and receptor compartment, respectively (Carvajal-Vidal et al. 2019). The donor compartment was filled with TH, TH-NP, TH-NLC or gel formulations (0.25 % of TH). Amounts of thymol penetrating through the skin, collected at selected times, were measured by HPLC and data analyzed by GraphPad®.

Statistical analysis was performed by one-way ANOVA Tukey´s multiple comparison tes or unpaired t test. The skin permeation parameters were calculated by the equation /3.4/:

$$J = Kp \,.\, C_0 \qquad /3.4/$$

where J is the flux, Kp is the permeability coefficient and C_0 is the initial concentration of the active (Alvarado et al. 2014)

In the case of using a "damaged skin", skin samples were previously scratched with sandpaper on the SC. In the case of using a full skin, including the fat tissue, the skin tissue was 0.8-1 mm thick. In the case of using rhodamine-labelled TH-NPs (R-TH-NPs), samples were protected from the light during the entire experiment.

Skin Tape Stripping and skin extraction

The amount of active retained inside the skin was assessed by tape striping and skin extraction techniques. The skin tape stripping was performed to measure the amount of TH retained on the SC and on the deeper layers of the skin (DS), where the second corresponds to the remaining part of the epidermis and the dermis. Firstly, skin samples were washed with sodium lauryl sulphate (0.02 %) and rinsed with distilled water, dried, cut, and weighted. For determination of the amount retained in the SC, tape stripping assay was developed based on previous authors with minimal modifications (Rehman et al. 2015). Extraction of the amount in the SC was performed by stripping of 7 first layers from the same region of SC, using a transparent label dressing (3M Tegaderm®, 6x7cm, 10u, Spain, S.A.). The strips were added into 4 mL of ethanol and placed into an ultrasonic bath (JP, Selecta) for 20 min for compound extraction, cooled down and quantified by HPLC. Data was processed by GraphPad®. For determination of the total amount retained inside the deeper layers (DS), the rest of the skin was perforated, added into 1 or 2 mL of ethanol:water (50:50) and then

kept in the ultrasonic bath for 20 min (Alvarado et al. 2015). After 10 min storage at -30°C, the amount of thymol extracted was determined by HPLC and calculated using the recovery factor previously obtained.

Skin Recovery Assay

A stock solution of thymol was prepared (250 μg/ml) and added (1 ml) to a weighted skin sample (0.012 ± 0.001 g). After sonication for 20 min, samples were kept in a 32 °C bath for 6 h. A sample of the stock solution alone was used as control. Samples were washed with sodium lauryl sulphate (0.02%), rinsed with distilled water, dried and weighted, while the remaining solution was kept for analysis (A*f*). Skins were stippled by needle-holes, weighted, and then added to 1 ml of Ethanol, followed by 20 min sonication (A_i). Results were measured by HPLC, and skin recovery was calculated by the equation:

$$Recovery\ (\%) = \frac{\frac{As}{wf}}{\frac{Ai - Af}{wi}}\ x\ 100$$

where, A_i is the total initial amount applied, A_s is the amount extracted from the skin, A_f is the final amount in the supernatant, w_i and w_f are the initial and final skin weights.

Permeation route study

To determine the permeation route of TH-NP, vertical diffusion Franz cells were used as described before. *Ex vivo* pig skin penetration was obtained from the animal house (Bellvitge, University of Barcelona), used in accordance with the protocol approved by the Ethics Committee of the University of Barcelona. For this study, rhodamine-labelled PLGA (R-PLGA) was synthesized as previously described (Gonzalez-Pizarro et al. 2019). R-PLGA was used at 0.01 % into TH-NP, added in the organic phase with PLGA. The rhodamine-labelled thymol-loaded NPs (R-TH-NPs) were applied onto the ex-vivo pig skin 0.64 cm2 (donor compartment) and allowed penetration for 24 h. Skin samples were washed, fixed in PBS containing 4 % paraformaldehyde (PFA) for 4 h, followed by cryoprotection into PBS with 30 % sucrose for 24 h, snap-frozen in isopentane at – 50 °C, then kept overnight at - 80 °C. Samples were mounted in O.C.T.® Compound (Tissue-Tek®, Sakura) and sliced with cryostat microtome (LEICA CM3050 S) at -20 °C onto glass-slides Superfrost® Plus (Menzel-Glaser, Thermo Scientific, USA), covered with Fluoromount G® (Invitrogen, Thermo Fisher Scientific, USA). Samples were visualized by confocal laser scanning microscopy (Zeiss LSM 880), using objective lens 10X 0.45. Images were acquired using Zen Black 2.3 software performing z-stack sections and thus processed with ImageJ software.

3.6.BIOCHEMICAL STUDIES

Cell culture

Human keratinocytes (HaCaT) cells were cultured in high glucose DMEM (Dulbecco's Modified Eagle's Medium (Thermofisher), supplemented with 10 % fetal bovine serum (FBS), 2 mM L-glutamine, 100 units/mL penicillin G and 100 µg/mL streptomycin. Cells were incubated at 37 °C and 5 % CO2 and experiments were performed when cells reached 80 – 90 % of confluence.

3.6.1. Cytotoxicity

The cytotoxicity of TH-NPs, THO-NPs and TH-NLCs were performed determining cell viability of human epidermal keratinocyte cell lines (HaCaT), (Cell Lines Service. CLS, Eppelheim, Germany). MTT (3-(4,5-Dimethylthiazol-2-yl)-2,5-diphenyl tetrazolium bromide) assay was used to determine the cell viability, by reduction of tetrazolium salt by intracellular dehydrogenases of viable living cells. Samples were tested at determined range of concentrations. In the case of washed particles (-w), these were previously washed thrice to remove excess of free TW (centrifugation at 14000 rpm for 15 min). Briefly, HaCaT cells were seeded in 96-well plates with 100 µL of culture medium (DMEM) at a density of 2 × 105 cells/well, adjusted in automated cell counter (Countess, Invitrogen, Thermofisher). Cells were incubated with samples for 24 h. at 37°C and 5 % CO_2. Then, the medium was removed and MTT (Sigma-Aldrich Chemical Co, St. Louis, MO, USA) was added at 0.25 % in PBS. After 2 h incubation, the medium was replaced by 100 µL DMSO (99 % dimethyl sulfoxide, Sigma-Aldrich) (Diaz-Garrido et al. 2019). Cell viability was then measured at wavelength of 570 nm in a Modulus®Microplate Photometer (Turner BioSystems Inc., Sunnyvale, CA, USA). Results were expressed as percentage of cell survival relative to untreated cells.

3.6.2. Cellular uptake of TH-NPs

The cellular uptake of NPs was assayed in HaCaT cells seeded in an 8-well µ-slide (Ibidi®) following the same methodology as described before. Cells were incubated with or without R-TH-NPs for 2 h at the indicated concentration, using FBS/phenol red free medium. Cell membranes were stained with wheat germ agglutinin (WGA) Alexa-488 (Molecular Probes) at 1 µg/mL for 15 min followed by fixation with paraformaldehyde 3 % for 25 min. Cell nuclei were stained with 4',6-diamidino-2-phenylindole (DAPI, Sigma Aldrich, Spain) at 0.5 µg/mL for 15 min. Internalization of NPs in HaCaT cells was assessed by confocal microscopy (Leica TCS SPII), 63X oil immersion objective lens (Gonzalez-Pizarro et al. 2019). Images were processed using Fiji image software.

3.7.THERAPEUTIC EFFICACY

3.7.1. *In vitro* and *Ex vivo* Antimicrobial Efficacy

Bacteria Culture

S. epidermidis was grown overnight 37 °C in Mueller Hinton Broth (MHB) culture medium (Oxoid, Basingstoke, UK). Prior to each experiment, the inoculum was prepared in PBS adjusted to 0.5 MacFarland (McF) standard, to obtain a suspension with a cell density at the range of 1.5 x 10^8 colony forming units/mL (CFU/mL). Microbial count of *S. epidermis* was performed in TSA plates, incubated at 37 °C. The *C. acnes* was cultured in Brain Heart Infusion (BHI) medium (Oxoid, Basingstoke, UK) for 48 hours at 37 °C under anaerobic conditions using parches (AnaeroGen®, Oxoid, Basingstoke, UK) and indicator (Oxoid, Basingstoke, UK). Prior to each experiment, the inoculum was prepared in PBS adjusted to 0.5 McF. Microbial count of *C. acnes* was performed in clostridium reinforced medium (CRM) plates, as recommended for anaerobia growth, incubated at 37 °C.

In vitro Microbial Activity by Minimal Inhibitory Concentration (MIC)

The MIC of TH, TH-NP and TH-NLC were determined using the broth microdilution assay (Koeth and Miller 2019). Briefly, double concentrated sample dilutions were prepared and added (100 µL) to double concentrated culture medium (100 µL) in a 96-well polypropylene microtiter plate (Costar, Corning Incorporated, Corning, USA). Inocula were prepared to yield a final concentration of 5 x 10^5 CFU/mL. For *S. epidermidis,* 10 µL were transferred to inoculate wells with final TH concentrations of 2 to 1024 µg/mL, followed by incubation at 37 °C for 18 to 20 h. For *C. acnes,* 20 µL was used to inoculate wells with concentrations ranging from 2 to 1000 µg/mL and the plate was incubated at 37 °C for 48 h under anaerobiosis. Thus, the MBC was performed by transferring 10 µL of each sample presenting no visible growth of *C. acnes* into BHI plates. These were further incubated as described before. Growth controls were used for the above experiments: presenting antimicrobial sterility (negative) and absent of antimicrobial (positive). Clindamycin was also used as an active control for both microorganisms.

In vitro Microbial Activity by Decimal Reduction Time (D)

The determination of the decimal reduction time assay, explores the antimicrobial activity of TH, TH-NPs or TH-NLCs on reducing bacteria viability at determined contact times

(MacGowan et al. 1996). For *C. acnes*, formulations were diluted with water up to 250, 500 and 1000 µg/mL representing the MIC, 2X MIC and 4X MIC, respectively. In the case of gel formulation, these were used at 1000 µg/mL. For *S. epidermidis*, formulations (aqueous and gels) were used at 1000 µg/mL, representing twice as MIC. Inocula were prepared in PBS at 10^8 CFU/mL and used to inoculate (100 µL) each experimental sample of 10 mL, incubated at 32 °C. The determined times were 0, 1, 2, 3 and 6 h or 0, 3, 8, 24 and 48 h for *C. acnes* and *S. epidermidis*, respectively. After incubations of each time set, an aliquot of 1 mL of each sample was neutralized in 9 mL of Berens diluent (Scharlab, Barcelona, Spain) for 15 minutes, then, diluted in PBS on subsequent 10-folds. Drop count method (10 µL) was performed in CRM and TSA agar plates, *for C. acnes* and *S. epidermidis*, respectively, incubated at 37 °C as described before. Bacterial viability was expressed as logCFU against time (h). The decimal reduction time, the time taken to reduce a decimal of the initial value, was determined calculating the inverse of the slope (1/b).

In vitro Microbial Activity by Suspension Test

A fresh inoculum of *C. acnes* was prepared in PBS adjusted to an optical density of 0.72 at 550 nm, using a UV-visible spectrophotometer (Shimadzu Corp., Kyoto, Japan). The assay was carried out in a total volume of 1 mL containing TH, THO, TH-NPs, THO-NPs or TH-NLCs (900 µL) at a final concentration of 250 µg/mL and fresh bacterial inoculum (100 µL). Samples were kept at 37 °C in a shaker incubator (Innova 4080) for 30 min. Then, 100 µL of each test tube was neutralized in 900 µL of Berens cosmetic diluent (Scharlab) for 15 min (Messager et al. 2001). Ten-fold dilutions in PBS (10 µL) were added to clostridium reinforced medium agar dishes for enumerating bacteria by the drop count method. Microbial count was performed after incubation for 48 h under anaerobic conditions at 37 °C. Bacterial viability was expressed as CFU/mL.

In vitro Microbial Activity by Suspension Test using SEM

The antimicrobial activity was also evaluated by SEM. For this, *C. acnes* was cultured for 48 h in BHI culture media in an incubator shaker (Innova® 4080, New Brunswick Scientific) at 37 °C under anaerobic conditions. The concentrated inoculum was transferred (900 µL) to each tube containing 100 µL of TH, TH-NP, GC-TH and GC-TH-NP at 0.1 %, or sterile distilled water (control), and incubated in the shaker for 1 h. After samples were centrifuged (10000 g for 5 min), supernatants were discarded and the concentrated pellets were placed into poly-l-lysine coated coverslips, kept at room temperature for 24 h (Mazia, Schatten, and Sale 1975). Samples were fixed for 4 h with phosphate buffer 0.1 M pH 7.4, containing 4 % paraformaldehyde and

2.5 % glutaraldehyde, then post-fixed with 1 % osmium tetroxide (with potassium ferrocyanide) for 1 h, at 4 °C. After dehydration with alcohol gradients, samples were dried at critical point (Emitech K850), mounted on a conductor adhesive disc (Carbon tabs, Agar Scientific), followed by carbon coating under evaporation (Emitech 950). Images were analyzed by SEM (scanning electron microscopy, Jeol JSM-7001F).

Ex vivo Antimicrobial Efficacy by Microbial Count

The bacteria viability was evaluated on treated human skin explant obtained from abdominal plastic surgery (Hospital de Barcelona, SCIAS, Barcelona, Spain) with, based on other researcher with modifications (Messager et al. 2001). Skin samples were cut in 0.6 cm2, washed with ethanol followed by sterile PBS, for 2 and 10 s, respectively, to remove possible existing bacteria. Once dried with sterile filter paper, skins were placed into petri dishes with the SC facing up, onto PBS-wet sterile filter paper to keep dermis moisture. Two experiments (prevention and treatment) were set up for 24 h incubation at 32 °C, in the presence of humidity. A fresh overnight culture of C. acnes was suspended in PBS (1.5 x 108 CFU/mL) and skin samples were inoculated with 10 µL. For the pre-treatment study, NPs or TH were applied on skin samples (30 µL) and incubated at 32 °C for 8 h, followed by inoculation with C. acnes (30 µL) for 16 h. For the post-treatment study, skins were first inoculated for 30 min and then treated with products for 24 h. At the end of the experiment, skin samples were neutralized in Berens diluent (1 mL) for neutralization (15 min) followed by extraction for 10 min using a sonication bath (JP, Selecta, Spain). The extraction method was previously optimized by testing the control at varied extraction times (3 to 15 min), controlling bacteria viability by sonication process. Positive controls were also performed using PBS. Dilutions 10-fold were performed and 100 µL of each sample was spread individually onto CRM agar plates and incubated under anaerobiosis at 37 °C for 48 h. Viable bacteria count was expressed as log/CFU per treated skin.

The analysis of bacteria viability on dosage-dependent study on treated skin was also performed. using the same technique as described above, with further modifications (Messager et al. 2001). A fresh overnight culture of C. acnes was prepared in PBS and skin samples were inoculated (10 µL). After 30 min, 30 µL of TH or TH-NP were administered as a single or repeated dosage (1, 2 or 3), at selected times (0, 12 and 18 h), completing a total incubation of 24 h at 32 °C, in the presence of humidity. Then, skin samples were neutralized and extracted as described above. These were diluted 10-folds and transferred to CRM plates by drop-count method (10 µL). Plates were incubated under anaerobic conditions at 37 °C for 48 h. Viable bacteria were expressed as CFU per treated skin.

Ex vivo Antimicrobial Efficacy by TEM

A simulation of skin infection was performed in fresh human skin explant (Hospital de Barcelona, SCIAS, Barcelona, Spain) and analyzed by transmission electron microscopy. The fat tissue of skin samples, obtained from human abdominal plastic surgical, was removed manually with sterile surgical razors. Skin samples were cut and placed on a 0.64 cm2 Franz diffusion cell. The receptor compartment was filled with PBS, and the skin was inoculated with 20 µL of *C. acnes* (10^8 CFU/mL) and incubated for 16 h at 32 °C, followed by treatment with TH or TH-NP (100 µL) for 8 h incubation. For electron microscopy, skin samples were fixed for 2 h with 4 % paraformaldehyde and 2.5 % glutaraldehyde in 0.1 M sodium cacodylate buffer (pH 7.4), postfixed with 1 % osmium tetroxide for 2 h at 4 °C, stained in 0.5 % uranyl acetate for 45 min at 4 °C and finally, dehydrated gradually in 30 to 100 % ethanol (Messager et al. 2004). Samples were infiltered in EPON resin [Eponate 12 (23.5 g), dodecenyl succinic anhydride DDSA (12.5 g) and Methyl nadic anhydride MNA (14 g)]. Inclusions were performed gradually diluted in ethanol and finally for 3 h using a catalyst [DMP-30 (2,4,6-tris(dimethylaminomethyl)phenol), 0.37 g]. Polymerization was carried out for 48 h at 60 °C. Blocks were sliced in thin sections with Ultracut microtome (LEICA), further fixed on copper grids and stained with uranyl acetate 2 % for 10 min. Analysis was performed by TEM and images were obtained with Megaview III.

3.7.2. *In vitro and Ex vivo* Antioxidant Activity

In vitro Antioxidant activity by DPPH

The scavenging capacity of TH and surface functionalization components was evaluated using DPPH (2,2-diphenyl-1-picrylhydrazyl) assay, based on other authors with some modifications (Aman et al. 2013). Samples were dissolved and diluted in methanol at concentrations ranging from 0.1 to 10 mg/mL, and DPPH, a free radical compound, was prepared in 80% methanol at 0.1 mM. Sample dilutions were transferred into a 96-well plate (200 µL/well) and 20 µL of the DPPH stock solution was added into each well. BHT (butyl-hydroxytoluene), a known antioxidant compound was used as endogenous control.

Samples without DPPH were used as blank. Samples were incubated in the dark for 45 min on a mechanical shaker. The UV-VIS absorbance was measured at 517 nm and data were calculated using the equation:

$$\% = \frac{Ac - (As - Ab)}{Ac}\ x\ 100$$

where *Ac, As* and *Ab are* the absorbances of the control, sample and blank, respectively.

Ex vivo Antioxidant Activity by Methylene Blue Reduction

A colorimetric assay was performed using methylene blue dye to test the *ex vivo* antioxidant activity of TH, THO and surface functionalized TH-NPs and THO-NPs. Methylene blue, in combination with an antioxidant molecule, reduces into a colorless lecomethylene blue (Fernández-García, Heluani-Gahete, and Wellinger 2016). Pig skin samples were cut into 2 cm^2 and placed into a 6-well plate containing 0.5 mL of PBS, with the stratum corneum (SC) facing up. Then, a methylene blue solution at 0.01% was applied on the surface of each skin sample and incubated for 4 h at 32 °C, in the presence of humidity. Skin fragments were washed with PBS and the SC was dried with filter paper. Samples were applied onto the skin (30 µL) and further incubated for 1 h. The control sample was treated with distilled water. Images were recorded at initial and 1 h post-treatment to assess differences in methylene blue reduction.

In vitro Antioxidant Activity in HaCaT cells

The antioxidant activity of TH, THO, TH-NP, THO-NPs and B-NPs was also assayed in HaCaT cells by quantification of ROS using the fluorogenic probe H2DCFDA. Cells were seeded in 96-well plates at 2 × 105 cells/well (100 µL) for 72 h. Cells were loaded with the fluorogenic dye H_2DCFDA (2',7'-dichlorodihydrofluorescein diacetate) at 25 µM diluted in DMEM medium absent of phenol red and FBS, for 45 min in the dark. This fluorogenic dye passively diffuses into the cells, being deacetylated by intracellular esterase and emits fluorescence upon oxidation by reactive oxygen species (ROS) (Liu et al. 2016). Then, cells were washed with PBS and incubated for 2 h with TH, TH-NPs, or B-NPs. After this period, 10 µL of H_2O_2 20 mM was added to each well. Untreated cells with or without H_2O_2 were used as positive and negative controls, respectively. Fluorescence was measured at excitation and emission wavelengths of 485 and 530 nm, respectively. Data were acquired at times t0 up to 120 min. Data of the positive control (H_2O_2) at 2 h, were used to normalize values (%). Background fluorescence of the negative control was subtracted from all measurements.

3.7.3. *In vitro* Anti-Inflammatory Efficacy

Cytokine quantification by ELISA Assay in TNF-α-Induced Inflammation

HaCaT cells were seeded in 12-well plates at a density of 2 × 105 cells/well and grown until 80–90% confluence. Cells were then treated with TH, TH-NPs and surface compounds alone for 2 h, followed by stimulation with 50 µM TNF-α for 2 h to induce inflammation (Carvajal-Vidal et al. 2019). The medium was replaced by fresh FSB-free medium, and cells were incubated

overnight. Supernatants were collected, and quantification of secreted interleukin-6 (IL-6) was carried out by using ELISA Human kit (BD OptEIA® Set Human IL-6) following manufacturer instructions. Absorbance was measured at 450 and 560 nm using a plate reader.

Statistical analysis was performed using GraphPad® and data were expressed as mean ± SD. Data are at least from three independent biological experiments. Three separated wells were processed for each independent experiment.

Cytokine quantification by ELISA using C. acnes Induced Inflammation

This experiment was performed as described in the previous section, but *C. acnes* fresh inoculum was added instead of TNF-α. Bacteria was grown until the stationary phase (5 days incubation under anaerobiosis in BHI culture medium). Then bacterial cells were harvested and diluted in FSB-free DMEM medium, adjusted to OD 1.2 at 550 nm. Different dilutions of this inoculum were added to HaCaT cells and incubated overnight. Quantification of IL-8 in cell culture supernatants was assayed by using ELISA Human kit (BD OptEIA® Set Human IL-8, BD Biosciences, New Jersey, US) following manufacturer instructions (Zhu et al. 2019).

Real-Time Quantitative Polymerase Chain Reaction (RT-qPCR)

HaCaT cells were adjusted to a density of 2 × 105 cells/well and seeded in 12-well plates. After 48 h, cells were treated with TH, THO, TH-NPs, THO-NPs or B-NPs for 2 h. Next, cells were stimulated for 4 h with *C. acnes* prepared in FBS-free DMEM medium, adjusted to OD 1.2 at 550 nm. HaCaT cells without any treatment were used as a negative control and cells incubated only with *C. acnes* as a positive control. Total RNA was isolated from cells using an RNA extraction kit (Qiagen RNeasy, Germantown, Maryland) following the manufacturer's guide (Qiagen, Crawley, UK) and quantified by the ratio of absorbance values at 260 and 280 nm using a NanoDrop TM-2000 spectrophotometer (Thermo Fisher Scientific, Waltham, MA, USA). cDNA was synthesized from RNA (1 μg) by using the High-Capacity cDNA Reverse Transcription kit (Applied Biosystems, Foster City, CA, USA) in a final volume of 20 μL. Quantitative PCR reactions were performed in a StepOne Plus PCR cycler (Applied Biosystems, Foster City, CA, USA) by using SYBR® Green PCR Master Mix (Applied Biosystems, Foster City, CA, USA) and specific human oligonucleotide primers for IL-1α, IL-1β, IL-6, IL-8, TNF-α and β-actin (endogenous control, primers specified in Table S1 of Supplementary Materials). Control reactions were performed in the absence of RNA. The standard PCR program was conducted by one denaturation cycle for 10 min at 95 °C followed by 40 cycles of 15 s at 95 °C and 1 min at 60 °C. Relative gene expression was calculated as fold change compared to sample control by means of $2^{-\Delta\Delta Ct}$ formula (Diaz-Garrido et al. 2019).

3.7.4. *In vitro* Wound Healing Efficacy

Wound healing activity in HaCaT cells by the Scratch Assay

In order to study wound healing activity of the developed TH-NPs, prevention and treatment were assessed. In order to study wound healing prevention, HaCaT cells were seeded in 12-well plates at a density of 5×10^4 cells/well and grown for 24 h until 70–80% confluence. Cells were treated for 2 h with free TH, THO, their surface functionalized derivative NPs or functionalization compounds, washed with PBS and further incubated for 24 h. Then, scratches were performed in the middle of each well using a 200 µL pipette tip, washed with PBS, refilled with FBS-free culture medium and incubated for 24 h (Governa et al. 2019; Jangpromma et al. 2016). Contrast phase images of the scratches were obtained at the beginning of the experiment (T0) and after 24 h using a fluorescent microscope, and the wound area was measured using ImageJ software.

In the previous assay, the capacity to prevent wound healing was assessed, whereas in a second assay, wound healing treatment was examined by applying the formulations after the lesion was caused. For this second experiment, HaCaT cells were seeded and grown for 24 h. After creating the scratches as previously mentioned, cells were washed with PBS and refilled with DMEM containing 1% FBS. Images at this timepoint were recorded by using fluorescent microscope at 10X (LEICA DFC300FX). Cells were then treated with either TH, surface functionalized TH-NP or surface functionalization compounds for 2 h and further incubated for 24 h in 1% FBS culture medium (Mengoni et al. 2017). Images at 24 h were recorded and processed using ImageJ software.

3.7.5. In vivo Efficacy Studies

Biomechanical Properties on Human Skin

This study was assessed by trans-epidermal water loss (TEWL) measurement DermaLab® module (Cortex Technology, Hadsund, Denmark) and skin hydration by Corneometer (CM 825, C+K electronic Gmbh, Germany). The measurement was determined prior and post varied times followed application of different formulations in a climate-controlled room (ambient temperature 25 ± 2 ºC, relative humidity 45%). Subjects were allowed a 30 min adaptation period prior to the measurements. Abnormalities in the structures related to disruption of the epidermal permeability barrier function were assayed by TEWL ($g/cm^2 \cdot h$). Statistical data was processed by GraphPad using ANOVA non-parametric system, Wilcoxon paired test (Carvajal-Vidal et al. 2020).

In vivo Sebum Regulation Efficacy

Sebum skin level of participants were assessed by Sebumeter (Cutometer® dual MPA 580, C+K electronic Gmbh, Germany). In the first study, a selection of volunteers with oily skin (n = 7) were examined. Measurements were taken prior to application and during 1.5 h. In the second study, a long-term treatment volunteers with oily acne-prone skin (n = 10) were examined recording the average basal level prior to application and after 28 days during treatment with daily applications. Sebum quantification was given by $\mu g/cm^2$. Statistical data was processed by GraphPad using ANOVA non-parametric system, Wilcoxon paired test.

4. RESULTS

4.1. Thymol-Loaded PLGA Nanoparticles

TH was loaded to polymeric NPs, based on PLGA, by solvent displacement method, described previously (3.3.1), with the aim to attain a prolonged release of active on the site of action and protects the, improving its bioavailability on the skin. Although, free TH presents good skin penetration ability, since its molecule may cause mobility of the intercellular lipids of the SC, the timeframe this compound remains inside the skin might be short. Moreover, it is sensitive to oxygen and light, and might undergo oxidation on long-term storage, decreasing its potential effects against acne.

Among all the polymers, PLGA, approved by EMA and FDA agencies, as a biomaterial in medical prostheses and surgical sutures (Anderson et al., 2012), was selected for the development of TH colloidal carriers due to its properties such as biocompatibility, biodegradability non-toxicity, higher reproducibility, and control and prediction of the degradation kinetics.

4.1.1. Formulation, Characterization and Optimization

The **optimization** of TH-NP-T- was obtained by developing a full composite factorial design of five levels and three factors. Studied independent variables were the amount of TW and TH as well as pH formulation. The latter was chosen due both to Thymol pKa (10.6) which, as previously reported in other studies, can influence in the EE (Sánchez-López et al. 2016), (Sánchez-López et al. 2017). The results of full factorial design on the physicochemical characterization and the entrapment efficiency of TH polymeric NPs are shown in **Table 4.1.** The Zav values ranged from 162 to 235 nm, being PI comprised between 0.06 and 0.12. Based on the criteria for monodispersed systems (PI < 0.1), all the formulations presented homogeneity of the particulate system (Vega et al. 2013). The surface charge of TH-NP-T-, measured as ZP, ranged from -22 to -31 mV. This negative ZP is related to the negative surface charge associated to PLGA, the main NPs compound (Sánchez-López et al. 2016), (Gómez-Segura et al. 2020) (Kim et al. 2005), (Zhang et al. 2012). Moreover, ZP is related to the stability of colloidal dispersions, for this reason, the developed formulations with values closest to -30 mV, were considered the most stables. The EE of designed formulations ranged from 71 to 83 %.

Surface response charts of the DoE, performed by Statgraphics® software, are shown in **Figure 4.1**. The statistical analysis (ANOVA) only presented significant differences for the particle size ($p < 0.01$), influenced by both, pH of the aqueous phase and ratio of surfactant/pH (**Figure 4.1A**). The responses at a fixed TH concentration (2.5 mg/mL) are illustrated for Zav, ZP and EE (**Figure 4.1B-D**), respectively. Results show that the highest EE was achieved at the lowest pH, while for ZP, the absolute high values were reached when the pH and surfactant were simultaneously low or high. Considering all

the evaluated parameters, the formulation F4, containing 0.25 % of TH and 0.4 % TW, has been optimized to carry out further experiments.

Table 4.1. Values of the 2^3 + star central composite factorial design, parameters, and responses

Independent Variables				Dependent Variables/Responses			
	TH	**TW**	**pH**	**Zav** (nm)	**PI**	**ZP** (mV)	**EE** (%)
Factorial Points							
F1	-1	-1	-1	217.9 ± 1.2	0.112 ± 0.001	-30.7 ± 0.9	76.35 ± 1.53
F2	1	-1	-1	234.9 ± 2.1	0.093 ± 0.004	-29.9 ± 0.4	79.16 ± 0.18
F3	-1	1	-1	176.2 ± 1.0	0.075 ± 0.023	-27.7 ± 1.3	76.67 ± 2.17
F4	**1**	**1**	**-1**	**174.0 ± 0.6**	**0.081 ± 0.012**	**-28.3 ± 0.8**	**80.07 ± 3.65**
F5	-1	-1	1	162.0 ± 0.4	0.072 ± 0.011	-26.2 ± 0.3	79.64 ± 3.79
F6	1	-1	1	163.5 ± 1.4	0.071 ± 0.009	-23.6 ± 0.5	73.52 ± 1.83
F7	-1	1	1	183.9 ± 0.4	0.087 ± 0.020	-29.5 ± 0.1	78.41 ± 2.51
F8	1	1	1	172.4 ± 1.1	0.094 ± 0.009	-26.6 ± 0.3	76.60 ± 5.60
Axial Points							
F9	*1.68*	*0*	0	174.2 ± 0.6	0.061 ± 0.018	-25.2 ± 0.4	77.01 ± 3.07
F10	*-1.68*	*0*	0	176.7 ± 1.1	0.083 ± 0.033	-23.6 ± 0.3	73.55 ± 2.93
F11	*0*	*1.68*	0	187.1 ± 0.8	0.024 ± 0.006	-23.1 ± 0.6	71.38 ± 0.62
F12	*0*	*-1.68*	0	167.4 ± 2.1	0.046 ± 0.021	-26.1 ± 0.4	76.92 ± 2.47
F13	*0*	*0*	1.68	164.6 ± 1.1	0.057 ± 0.010	-23.1 ± 0.8	72.44 ± 1.66
F14	*0*	*0*	-1.68	202.6 ± 3.5	0.063 ± 0.045	-22.5 ± 1.1	82.89 ± 6.01
Central Points							
F15	0	0	0	175.4 ± 2.1	0.053 ± 0.013	-24.5 ± 0.6	74.94 ± 1.77
F16	0	0	0	176.3 ± 1.9	0.072 ± 0.016	-25.3 ± 0.7	78.14 ± 0.49

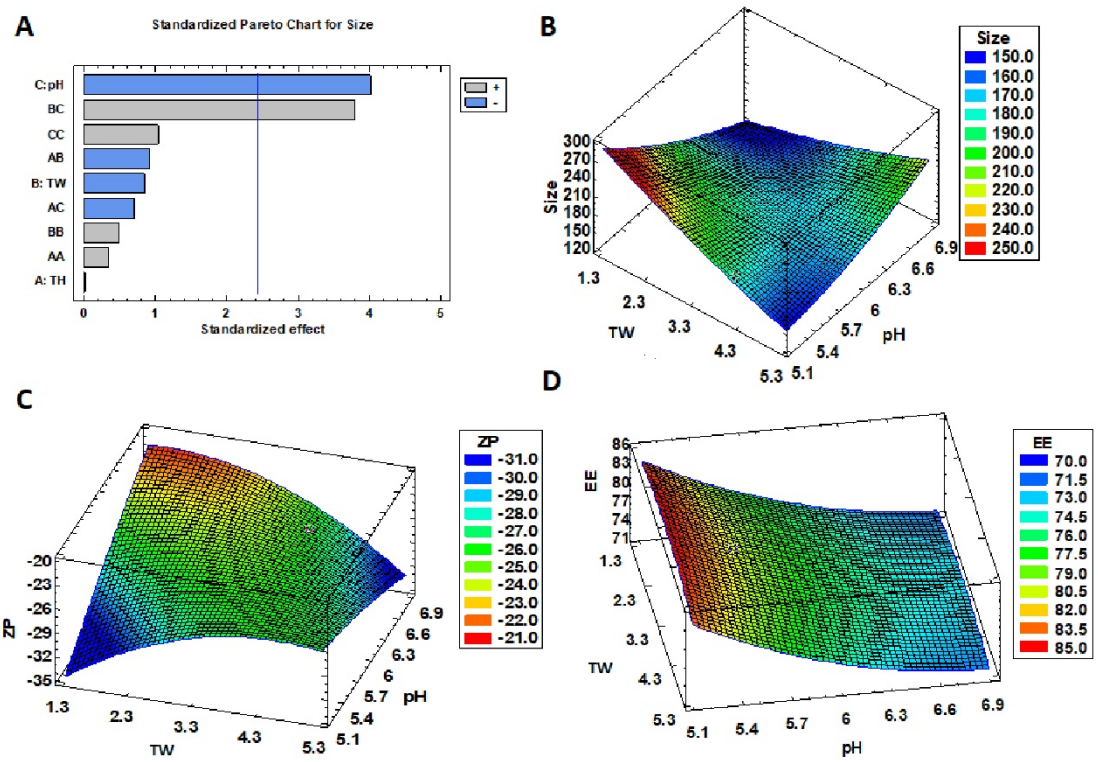

Figure 4.1. Factorial design with TH-NP-T-fixed at 2.5 mg/mL TH: (A) Pareto's chart for particle size (ANOVA) and surface response for (B) Zav particle size (nm), (C) ZP (mV) and (D) EE (%).

Morphology and Stability of TH-NP-T-

The morphology of TH-NP-T-evaluated by transmission electron microscopy (TEM), is shown in **Figure 2A**. The NPs maintained their structure for 1 month at 4 and 25 °C (**Figure 4.2B, 2C**, respectively), and additionally, for 12 months at 4 °C (**Figure 4.2D**). The arrows indicate small particle aggregation which was confirmed by a slightly increased of particle size, as indicated in Table 2. This is also related to the decrease of ZP, since electrostatic forces between surface-charged NPs decrease when stored in aqueous media. Temperature showed to accelerate particle destabilization by decreased ZP. A slight decrease of the pH value was also observed, probably due to a partial hydrolysis of the polymer. All these phenomena agree with the predicted backscattering profile shown in **Figure 4.3**, where NPs sedimentation was observed by the first left peak at the bottom of the vial, being reversible by agitation. Moreover, it can be observed that at 37 °C the signal greatly decreases, presenting the aqueous NPs destabilization at higher temperatures. Additionally, the EE was maintained at 4 and 25 °C for 6 months, whereas at 37 °C, it has decreased by 2.5 of the initial value. The parameters of all storage conditions were within stable criteria, presenting shelf-life best before 6 months stored at 4 °C. Samples presented no microbial growth within storage, confirming a preservative effect of thymol.

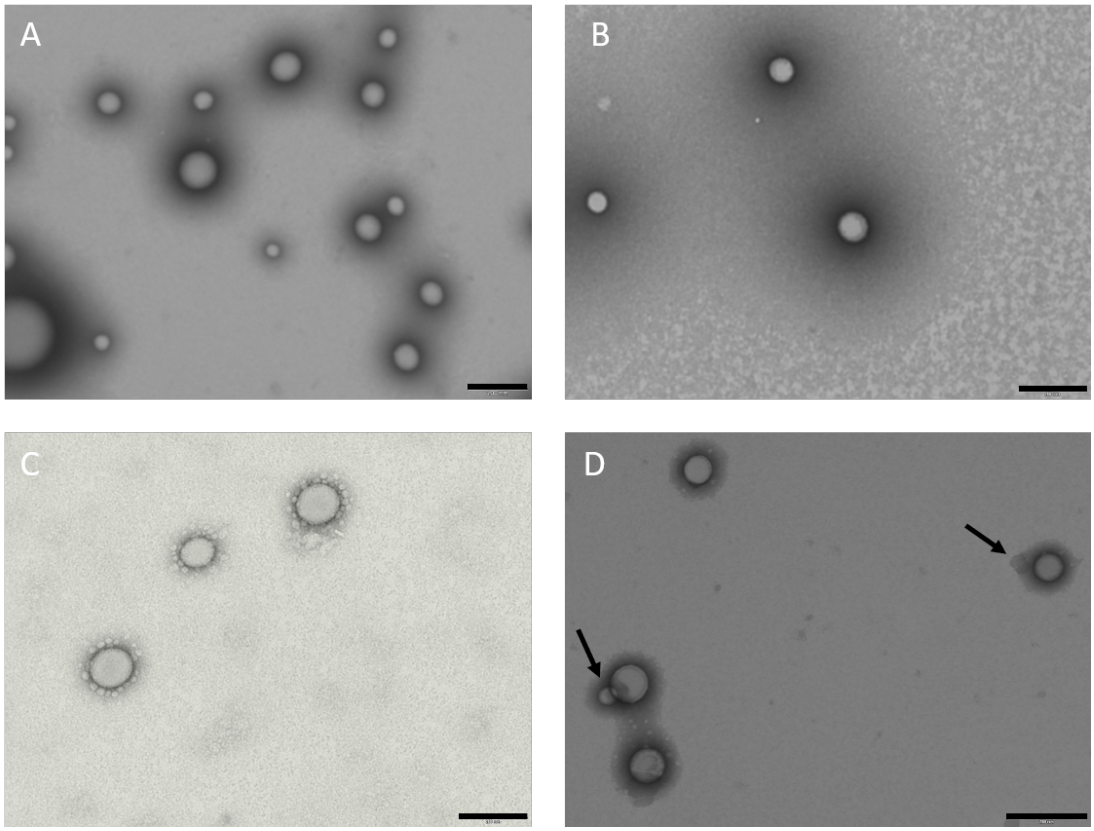

Figure 4.2. Morphology of the NPs by TEM: (A) t0, (B) 1 month at 4 °C (C) 1 month at 25 °C and (D) 12 months at 4 °C. Arrows indicate aggregation. Scale bar: 200 nm.

Table 4.2: Physicochemical stability of TH-NP stored at different temperatures (4, 25 and 37 ºC) measured at 0, 1, 3, 6 and 12 months.

	t (m)	Zav (nm)	PI	ZP (mV)	pH
4 °C	**0**	**158.8 ± 1.7**	**0.068 ± 0.027**	**-24.7 ± 1.0**	**4.20**
	1	158.6 ± 1.8	0.108 ± 0.046	-20.1 ± 0.6	4.07
	3	159.0 ± 2.1	0.101 ± 0.034	-17.1 ± 0.1	3.90
	6	168.6 ± 1.7	0.152 ± 0.033	-15.3 ± 0.1	3.68
	12	204.5 ± 1.3	0.231 ± 0.015	-11.1 ± 0.7	3.61
25 °C	1	162.3 ± 0.4	0.119 ± 0.015	-19.1 ± 0.1	3.91
	3	182.3 ± 1.4	0.145 ± 0.020	-10.3 ± 0.2	3.64
37 °C	1	177.4 ± 1.2	0.128 ± 0.012	-15.3 ± 0.6	3.32
	3	216.4 ± 2.8	0.205 ± 0.001	-8.56 ± 0.3	2.95

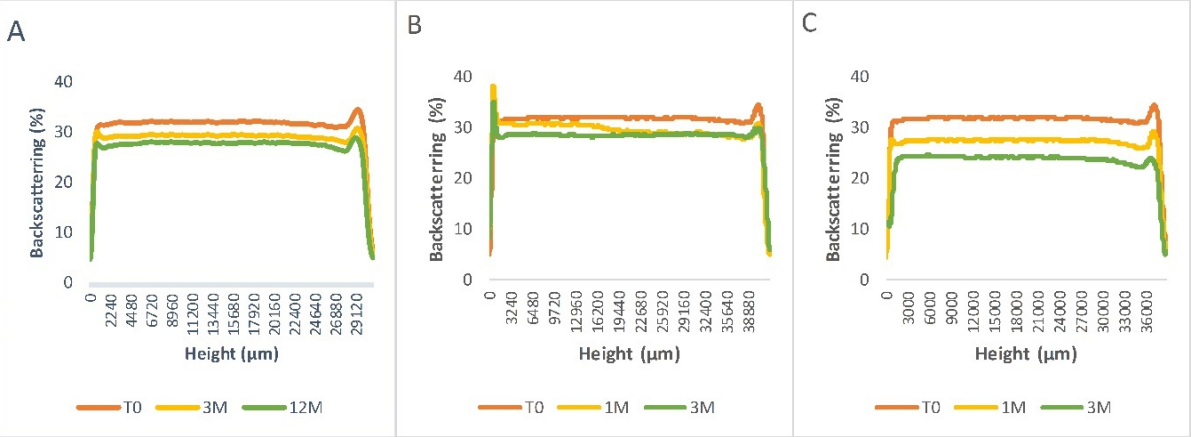

Figure 4.3. Stability behaviour of TH-NP-T- light backscattering measured by Turbiscan®Lab, stored at. (A) 5 °C (up to 12 months) (B) RT (up to 3 months and (C) 37 °C (up to 3 months). The scans run from the bottom to the top of the vial, from the left to the right, hourly for 24 h. Data was plot as the mean values of the total hourly scans performed.

Interaction Studies

The interactions between TH and PLGA, carried out by differential scanning calorimetry (DSC) and X-ray diffraction (XRD), are shown in **Figure 4.4**. DSC thermograms of TH showed an endothermic peak at 52 °C, which corresponds to its melting transition (**Figure 4.4A**). A minimal displacement of endotherm was presented by polymer alone and blank NPs (B-NP). However, TH-NP-T-presented an onset peak displaced at 40 °C, due to thymol-PLGA interaction. The XRD diffractograms (Figure **4.4B**) show TH on its crystalline form, expressed by the sharp diffraction peaks. TH-NP-T- is displayed as non-sharp peaks, confirming that thymol was dispersed in the polymer matrix in its amorphous form (molecular dispersion), also showing a similar profile to the B-NP-T-.

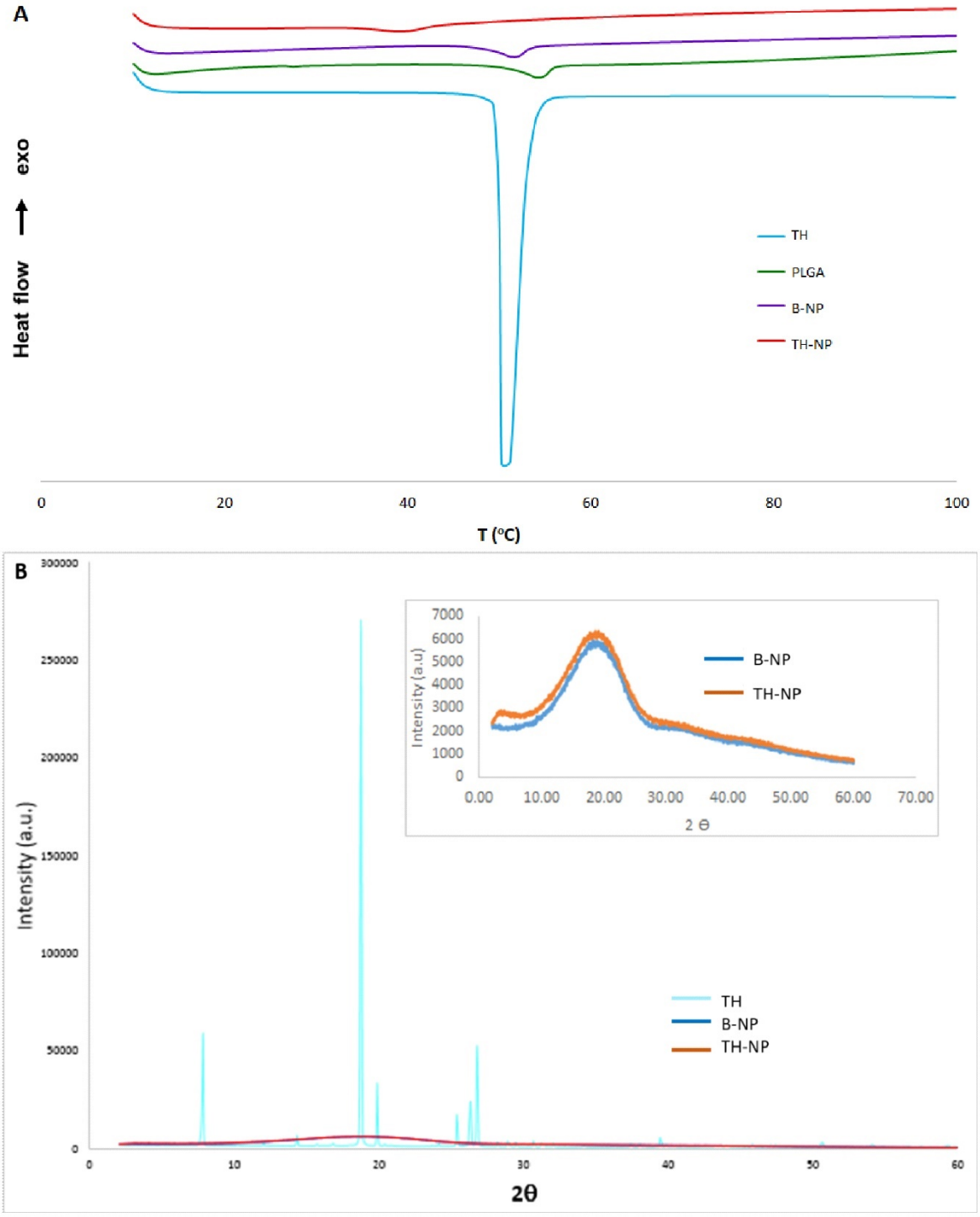

Figure 4.4. Interaction studies of TH-NP, B-NP, and compounds separately: (A) DSC thermograms and (B) X-ray diffraction patterns.

4.1.2. Biopharmaceutical Behaviour

In vitro Release

The *in vitro* release profile of TH from TH-NP-T- against free TH, carried out in Franz diffusion cells, is shown in **Figure 4.5**. As can be observed, the release of free TH through the dialysis membrane was faster, while TH-NP provided a slow-rate prolonged release. Kinetic data was adjusted to Boltzmann Sigmoidal equation showing that TH reached 50 % (V50) of total amount released within a short period of time (1.5 h), while TH-NP-T- only achieved the same within 23 h. The total amount of TH released in 24 h was 55 % and 35 % for TH and TH-NP, respectively, presenting statistically significant differences ($p < 0.01$).

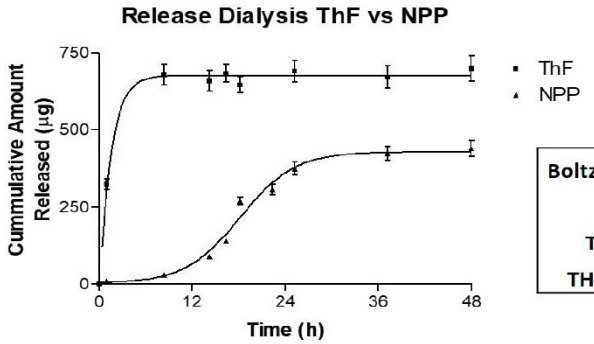

Boltzmann Sigmoidal	% Released-24h	TOP	V50	r^2
TH	54.7 ± 5.9*	683.9	1.5	0.9986
TH-NP	35.1 ± 3.2	440.3	22.8	0.9973

Figure 4.5. Release profile of TH and TH-NP-T- adjusted to Boltzmann Sigmoidal equation. Total amount released in 24 h expressed as % Mean ± SD (n = 3). Statistical analysis one-way ANOVA t-student test (*p < 0.01).

*Ex vivo S*kin Permeation

The *ex-vivo* skin permeation of TH and TH-NP-T-were performed in normal healthy skin and, additionally, in damaged skin, where the SC was previously scratched to mimic skin barrier disorder. The corresponding kinetics of both skin types are shown in **Table 4.3**. The permeation flux (*J*) of TH and TH-NP-T-were increased by 2.1 and 2.6 times, respectively, on damaged compared to healthy skin, where all samples presented significant statistical differences ($p < 0.001$) between them. In both cases, damaged and healthy skins, TH presented significantly ($p < 0.001$) faster penetration rate compared to TH-NP-T-, being increased by 1.6 and 1.3 times, respectively. The total amount penetrated (*Ap*) was significantly higher ($p < 0.001$) in damaged skin. In the other hand, the total amount retained inside the skin (*As*) was similar for both samples comparing healthy to damaged skins and there were significant differences ($p < 0.001$) comparing TH-NP-T-with TH.

Table 4.3. *Ex-vivo* skin permeation parameters

	Healthy Skin		Damaged Skin	
	TH	**TH-NP**	**TH**	**TH-NP**
J (μg/cm²/h)	12.68 ± 1.73	8.03 ± 0.55 *a*	26.43 ± 2.13 *a b d*	21.03 ± 0.92 *a b*
Kp (cm/h)	5.07E-03 ± 6.91E-03	3.21E-03 ± 2.19E-04 *a*	1.06E-02 ± 3.51E-04 *a b d*	8.41E-03 ± 3.69E-04 *a b*
Ap (μg/cm²)	106.43 ± 9.96	96.39 ± 12.68	272.36 ± 14.02 *a b d*	202.58 ± 11.65 *a b*
As (μg/cm²)	6.19 ± 1.45	10.85 ± 1.12 *a c*	5.92 ± 0.92	10.83 ± 2.13 *a c*
At (μg/cm²)	**112.61 ± 11.41**	**107.24 ± 13.80**	**278.28 ± 14.93 *a b d***	**213.78 ± 13.78 *a b***
SSD (p < 0.01)	*a*	*b*	*c*	*d*

J: flux, Kp: permeability constant, Ap: total amount penetrated, As: total amount retained inside the skin, At: total amount penetrated and retained inside the skin, SSD: statistically significant differences.

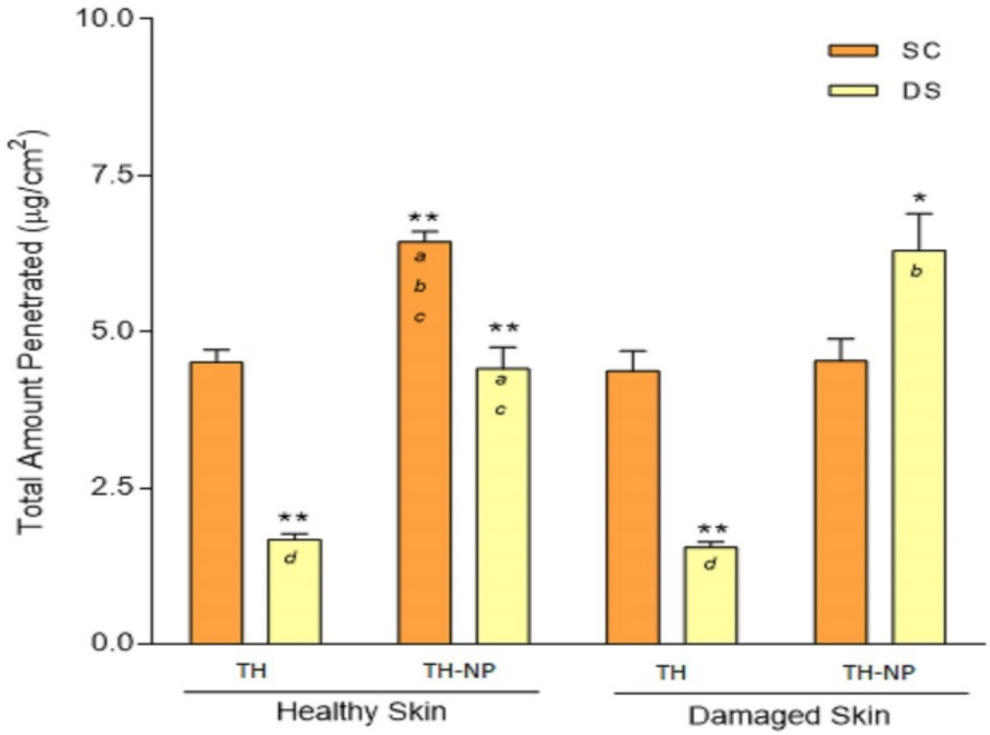

Figure 4.6. Total amount of TH and TH-NP penetrated in 24 hours in healthy and damage skin. SC: stratum corneum (tape stripping), DS: deep skin (extraction). Values represent the Mean ± SD (n=3). Statistical analysis for each localization via one-way ANOVA Tukey´s Multiple Comparison Test. Different letters inside the bars indicates significant differences between groups (*p < 0.01 and **p < 0.001).

The total amount of thymol penetrated within 24 h (**Figure 4.6**), was split into SC and DS. The amount found in the SC was the same for TH on both skin types and similarly to TH-NP-T-on damaged skin. However, for TH-NP, the retained amount was significantly higher ($p < 0.01$) on normal skin, in agreement with the slow-rate penetration, presenting delayed entry of the particles. In the other hand, it can be observed that TH-NP-T-presented significantly ($p < 0.001$) higher amounts retained in DS on both skin types, compared to TH. Meanwhile, TH-NP-T-on damaged skin was significantly higher than normal skin ($p < 0.01$).

Ex-vivo skin permeation route was studied by confocal microscopy using rhodamine-labelled TH-NP-T- (R-TH-NP-T-) after 24 h permeation. (**Figure 4.7**). The results obtained showed that R-TH-NP-T- successfully penetrated inside the skin hair follicle, where acne pathogen infection and inflammation occur. The image (**Figure 4.6B**) illustrates that R-TH-NP-T- were found concentrated in the hair follicle and presented delayed entry accumulation in the SC.

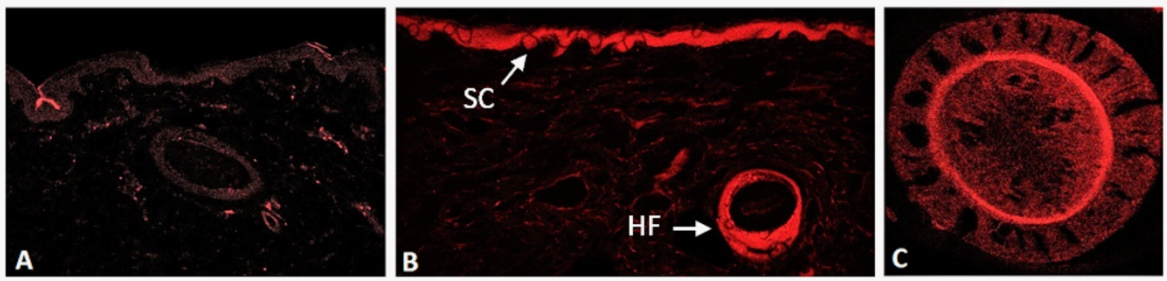

Figure 4.7. Confocal microscopy images of pig skin R-TH-NP-T- penetration after 24 h: untreated skin control (A), and treated with R-TH.NP-T-, showed on SC and hair follicle (B) and the hair follicle cross-section (C).

4.1.3. Biochemical studies

Cytotoxicity in HaCaT Cells

The cytotoxicity of TH-NP-T-was evaluated on HaCaT cells, incubated for 24 h with concentrations up to 1 mg/mL (**Figure 4.8**). Results showed that TH-NP-T-was not cytotoxic at concentrations up to 50 µg/mL, as cell viability was kept close to the untreated control cells. A 20 % reduction in cell viability was observed at 100 µg/mL and close to 90 % reduction at concentrations ≥ 250 µg/mL. Different results were obtained with washed nanoparticles (TH-NP-T-w), which was not cytotoxicity at 100 µg/mL and caused only a 25 % reduction in cell viability at 250 µg/mL. Differences between TH-NP-T- and TH-NP-T-w indicate that the presence of free TW in the samples could cause toxicity to HaCaT cells

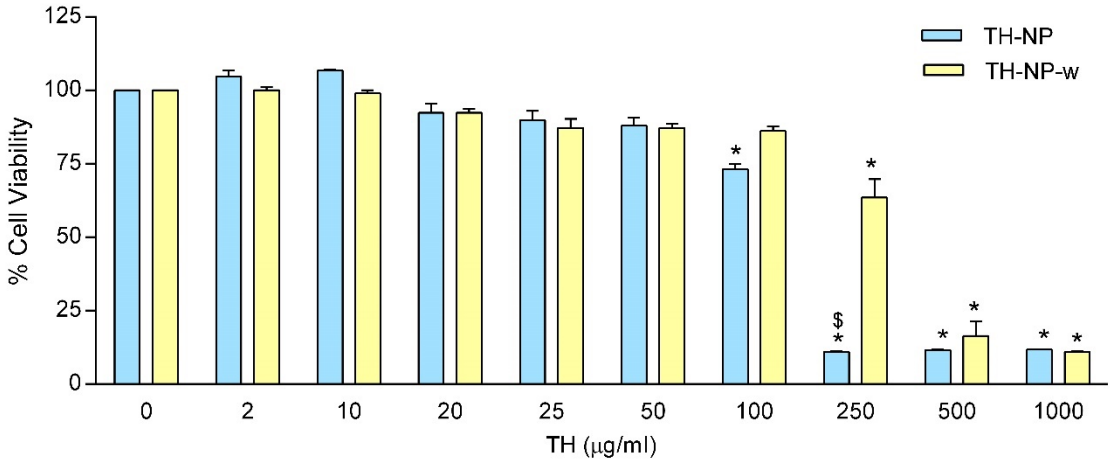

Figure 4.8. Cell viability of HaCaT keratinocytes by MTT assay, after 24 h incubation with TH-NP-T- and the washed NPs (TH-NP-T-w) at different concentrations. Values represent the Mean ± SD (n = 3). Statistical analysis one-way ANOVA Tukey 's Multiple Comparison Test, *$p < 0.01$ versus control and $^{\$}p < 0.01$ versus TH-NP-T-w.

Cellular Uptake of TH-NP

The cellular uptake of R-TH-NP-T- (20 µg/mL) was analysed in HaCaT cells. At this nanoparticle concentration, cell viability was over 90 %. After 2 hours incubation, fluorescence was detected by confocal microscopy in cells treated with R-TH-NP-T-but not in untreated control cells (**Figure 4.9**). The cell membrane and the nucleus are represented as green and blue, respectively. In the merged images, it can be observed that the internalized nanoparticles were mainly localized in the cytoplasm.

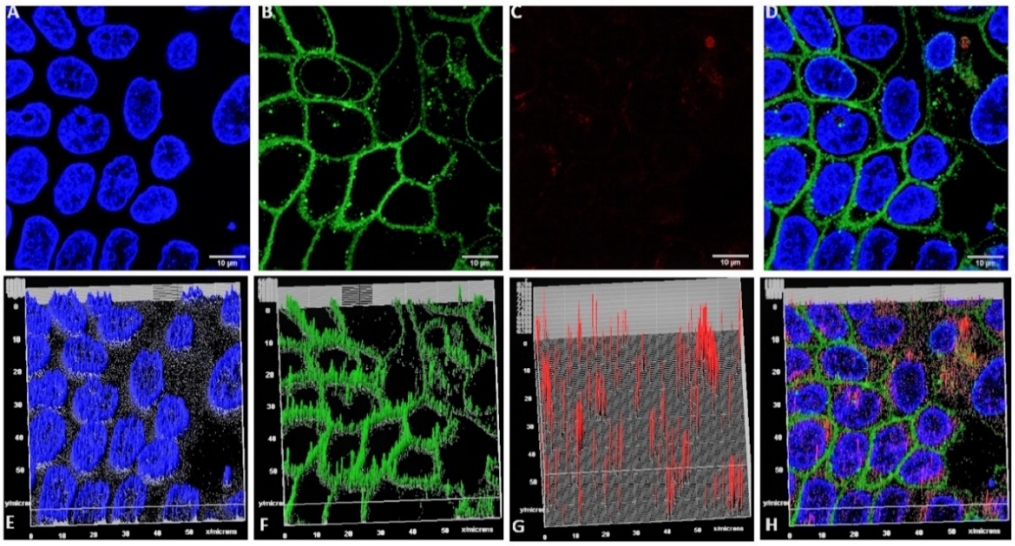

Figure 4.9. Confocal microscopy analysis of HaCaT cells: (A) nuclei and (B) membranes, incubated with (C) R-TH-NP-T- and (D) merged A, B and C. (E-H) 3D-surface plot of A-D, respectively.

4.1.4. Therapeutic Efficacy

In vitro Antioxidant Efficacy in HaCaT Cells

The antioxidant activity of TH and TH-NP-T-, performed in HaCaT cells, was successfully achieved by reducing the amount of reactive oxygen species (ROS) generated. While B-NP-T- did not present activity, TH and TH-NP-T-showed a 20 % and 32 % of ROS reduction, respectively, within 2 h treated with H_2O_2 (**Figure 4.10**). Moreover, TH-NP-T-was statistically significant compared to TH.

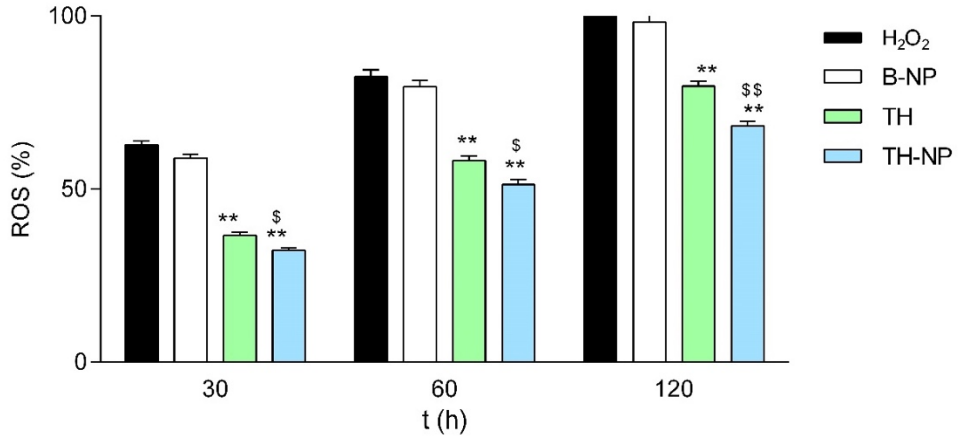

Figure 4.10. Time course analysis of ROS production induced by H_2O_2 (2 mM) in HaCaT cells treated with TH or TH-NP-T-. The ROS production (100 %) was set with the values obtained with cells challenged with H_2O_2 for 2 h. Data were expressed (%) as the Mean ± SD (n = 8). Statistical analysis was performed by one-way ANOVA Tukey's Multiple Comparison Test, **$p < 0.001$ versus controls at 2 h; $^{\$}p < 0.05$ and $^{\$\$}p < 0.001$ between TH and TH-NP-T- treated cells.

In vitro Antimicrobial Efficacy

The minimal inhibitory concentration (MIC) was determined for TH and TH-NP-T-on *S. epidermidis* being both 512 µg/mL For *C. acnes,* TH and TH-NP-T-displayed the same MIC and minimal bactericidal concentration (MBC) values, being 250 µg/mL and 400 µg/mL, respectively. Therefore, no differences were observed in the concentrations between samples, but there were relevant differences between microorganisms. In the other hand, clindamycin, a strong antibiotic drug commonly used to treat severe acne, presented MIC < 2 µg/mL for both microorganisms. For this reason, this type of drug is able to treat acne, however, it affects the healthy resident bacteria of the skin.

The bacterium viability reduction, evaluated by determination of decimal reduction time (D), treated with TH or TH-NP-T-in a timely manner, is illustrated in **Figure 4.11**. In the case of *C. acnes,* the decrease of viable bacteria correlated with the applied dose (**Figure 4.11A**). Although the effect of TH

and TH-NP-T-were similar, the activity of TH-NP-T-was slightly sustained at lower dosages. At the MIC concentrations, they present minimal reduction activity, whereas, at concentrations higher than MBC, the reduction was boosted for all tested samples. Meanwhile, *S. epidermidis* presented very slow viability reduction when incubated with TH and TH-NP-T-at twice the MIC (**Figure 4.11B**), the same highest concentration tested for *C. acnes*. It can be observed that TH completely reduced *S. epidermidis* viability within 8 h, whereas TH-NP-T-treated cultures still presented living colonies within 24 h.

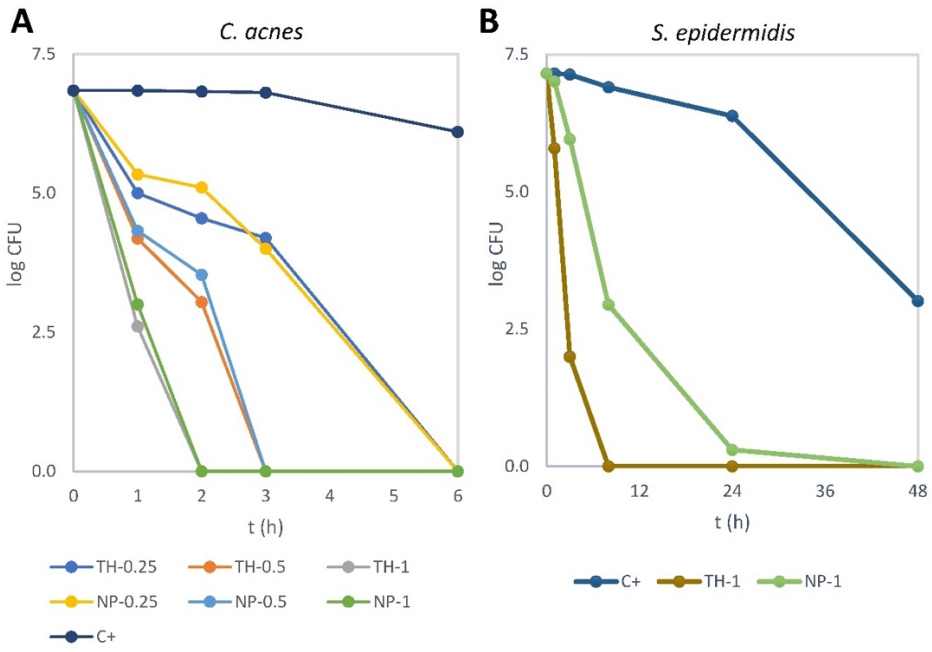

Figure 4.11. Bacterial viability reduction of (a) *C. acnes* 6 hours contact with TH or TH-NP-T- (dosage dependant) at 0.25, 0.5 and 1 mg/ml, (b) *S. epidermidis* 48 hours contact with THF or TH-NP-T- at 1 mg/ml. Data is expressed as $\log_{10}$CFU of mean values.

Data of decimal reduction time (D), the time taken to reduce a decimal part of the of bacterial viability, is shown in **Table 4.4**. In the case of *C. acnes,* differences could be observed comparing the variable dosages applied. However, variations between TH and TH-NP-T- were not detected. In the case of *S. epidermidis*, TH-NP-T- presented statistically significant differences compared to TH. Moreover, comparing the activity between both microorganisms, at the same dosage, only TH-NP-T- presented statistically significant differences for *S. epidermidis* against *C. acnes*.

Moreover, the structure of *C. acnes* (**Figure 4.12A**), evaluated by scanning electron microscopy (SEM), presents a rod-shape and smooth membrane. Treatment with TH or TH-NP-T- (**Figure 4.12B-C**) resulted on elongated cells, thickened cell envelope, and blebs formed on the surface.

Table 4.4. Decimal reduction time (D) for *C. acnes* and *S. epidermidis* viability

	TH (mg/mL)			**TH-NP-T-**(mg/mL)		
	0.25	**0.50**	**1.00**	**0.25**	**0.50**	**1.00**
C. acnes						
r^2	0.9654	0.9743	0.9812	0.9964	0.9984	0.9949
k (logCFU/h)	1.00 ± 0.11	2.03 ± 0.19	3.48 ± 0.08	1.02 ± 0.12	1.96 ± 0.43	3.44 ± 0.03
D (min)	**60.5 ± 6.5**	**29.6 ± 2.7**	**17.3 ± 0.4**	**59.0 ± 7.0**	**31.4 ± 6.9**	**17.4 ± 0.1**
S. epidermidis						
r^2			0.9944			0.9886
k (logCFU/h)			1.75 ± 0.02			0.54 ± 0.01
D (min)			**34.2 ± 0.4**			**111.1 ± 2.9*$**

*CFU: colony forming units. One-way ANOVA (t test): statistically significant differences *p > 0.001 versus TH, $p > 0.0001 against C. acnes, same dosages.*

.

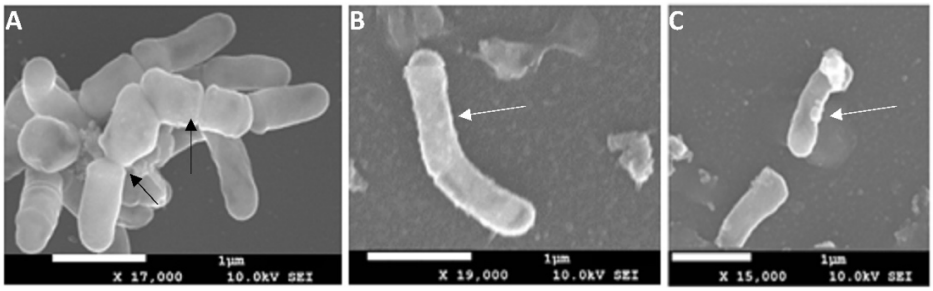

Figure 4.12. SEM micrographs of *C. acnes* (A) control and treated for 1 hour with (B) TH or (C) TH-NP. Black arrows indicate bacteria division and white arrows membrane disruption.

Ex vivo Antimicrobial Efficacy

The *ex-vivo* antimicrobial efficacy of TH and TH-NP-T- on *C. acnes* skin inoculated, as prevention or treatment for 24 h, were successfully determined. In both studies, all samples presented significant differences against the control. The activity was found greater as prevention than treatment, in both cases, where TH-NP-T- presented higher activity than TH, statistically significant (**Figure 4.13A**). In

the case of multiple dose treatment (**Figure 4.13B**), administration of a single dose showed significantly higher activity for TH than TH-NP-T. However, within 2 and 3 dosages, TH-NP-T- showed better efficacy, statistically significant compared to a single dose and against TH at the same dosages applied. Meanwhile, TH was only significant comparing 3 dosages to 1. Moreover, the highest efficiency of the experiment was achieved by 3 doses of TH-NP-T-.

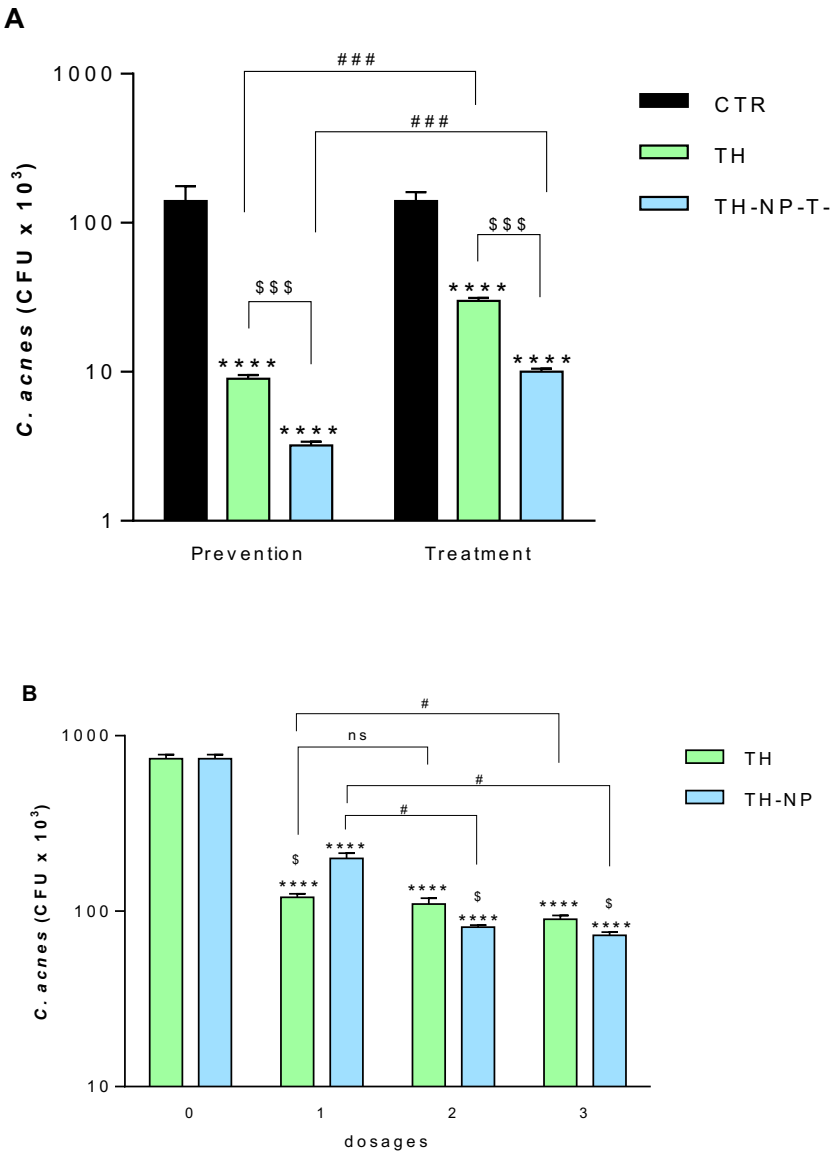

Figure 4.13. Bacteria viability on *ex vivo* treated skin with TH or TH-NP-T- for 24 h. Values represent viable count of *C. acnes* as the Mean ± SD (n=3). (A) Prevention and treatment: statistical analysis one-way ANOVA Tukey's Multiple Comparison Test (****$p < 0.0001$ versus control); unpaired t test ($^{\$\$\$}p < 0.001$ for TH versus TH-NP-T- and $^{\#\#\#}p < 0.001$ for preventions versus treatments. (B) Dose-dependent with 3 applied doses at times 0, 12 and 18 h of incubation: one-way ANOVA Tukey's Multiple Comparison Test (****$p < 0.0001$ versus control and $^{\$}p < 0.01$ for TH versus TH-NP-T- at the same dosage; unpaired t test ($^{\#}p < 0.05$ for multiple dosage versus a single dose.

The simulation of skin infection and treatment was carried out on *ex-vivo* fresh human skin explants, by inoculating *C. acnes* for 16 h, followed by 8 h treatment with TH or TH-NP. **Figure 4.14A** illustrates the untreated skin, while **Figure 4.14B** shows the *C. acnes* inoculated and penetrated within the skin layers. The treatment with TH (**Figure 4.14C**) demonstrated a fast and strong activity towards the bacteria membrane, presenting surrounding it, a great loss of intercellular material which may indicate damaged membrane. In the case of TH-NP-T- (**Figure 4.14D**), a slower effect with less amount of cellular leakage could be observed. The minor effects of NPs within 8 h treatment might be related to the slow-rate release and penetration.

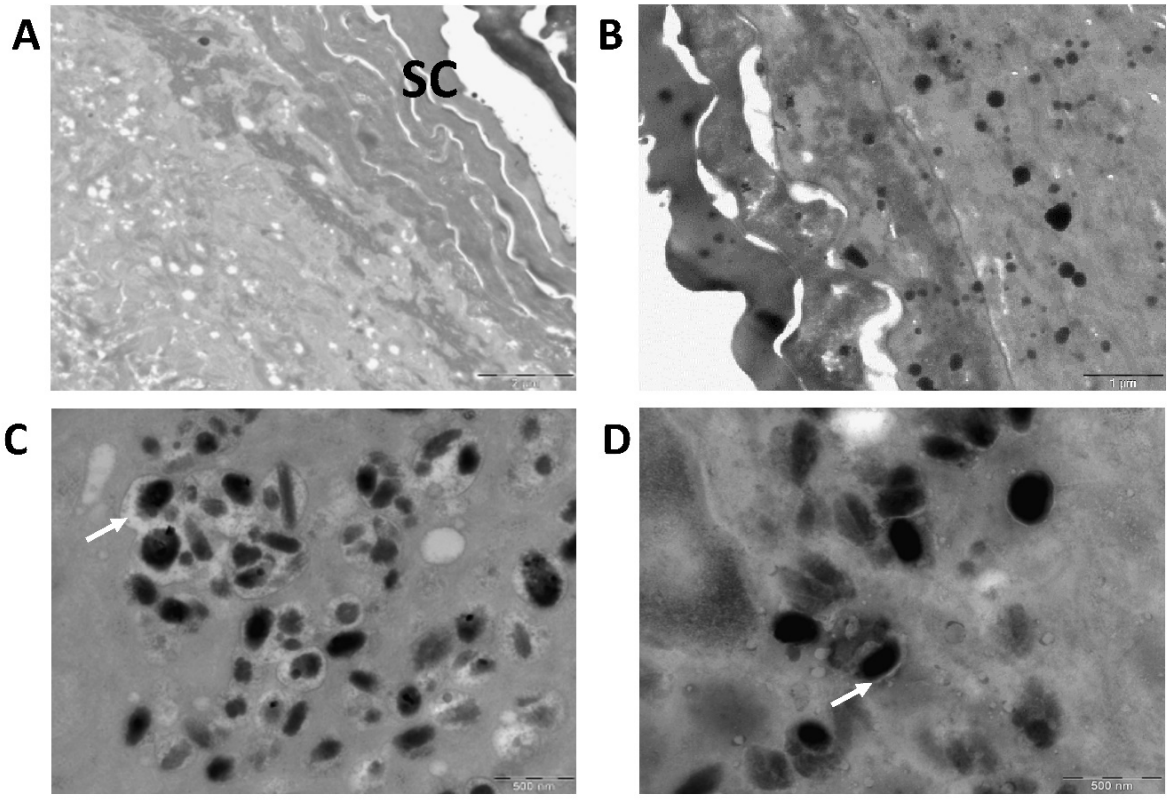

Figure 4.14. TEM images of normal human *ex vivo* skin: (A) untreated, (B) inoculated with *C. acnes (black)*, treated with (C) TH and (D) TH-NP-T-. White arrows indicate the loss of bacterial intracellular material. Scale bars: 2 µm (A), 1 µm (B) and 500 nm (C and D).

4.2. Surface-Functionalized Thymol-loaded PLGA Nanoparticles

4.2.1. Physicochemical Characterization

TH-NPs were prepared using the solvent displacement method and surface functionalized with different compounds (TH-NP-L-, TH-NP-P-; TH-NP-PP-, TH-NP-P-C+, TH-NP-PP-C+). Their physical-chemistry characterization is shown in **Table 4.5**. All formulations presented good homogeneity below 0.2 indicating monodisperse systems and high entrapment efficacy values around 80% leading to 2 mg/mL of TH encapsulated inside the NP (Vega et al. 2013). Moreover, Zav was adequate for skin topical administration and pH was slightly acidic in all the cases. Regarding ZP, the TH-NP-L-, TH-NP-P- and TH-NP-PP- show negative surface charges and, in contrast, the formulations functionalized with chitosan showed highly positive surface charge which may be able to favor interaction with negatively charged skin tissues.

Table 4.5. Surface functionalized Physicochemical parameter of TH-loaded PLGA NPs formulations, surface functionalized with (TH-NP-L-: phosphatidylcholine; TH-NP-P-: Poloxamer 188; TH-NP-PP-: Poloxamer 407; TH-NP-P-C+: Poloxamer 188 and Chitosan; TH-NP-PP-C+: TH-NPs Poloxamer 407 and Chitosan).

	Zav ± SD (nm)	PI ± SD	ZP ± SD (mV)	pH ± SD
NPP-P-	180.2 ± 6.5	0.066 ± 0.037	−28.9 ± 1.0	4.15 ± 0.10
NPP-P-C+	316.5 ± 3.8	0.123 ± 0.035	43.4 ± 0.6	3.15 ± 0.10
NPP-PP-	206.9 ± 9.9	0.101 ± 0.041	−17.8 ± 0.7	4.29 ± 0.10
NPP-PP-C+	297.3 ± 22.9	0.150 ± 0.068	19.6 ± 0.8	3.16 ± 0.10
NPP-L-	235.8 ± 29.7	0.063 ± 0.018	−32.1 ± 0.2	4.08 ± 0.10

Stability of Thymol Loaded Nanoparticles

TH-NPs stability with different surface functionalization compounds (TH-NP-L-, TH-NP-P-; TH-NP-PP-, TH-NP-P-C+, TH-NP-PP-C+) were measured in order to assess their short-term stability. Physical-chemical properties were measured after one-month of storage at 4, 25, 30 and 40 °C. As can be observed in **Figure 4.15**, after 1 month it was corroborated that the most suitable storage temperature was 4 °C since no statistically significant differences were observed regarding the average size of TH-NPs. Even though ZP and pH of chitosan functionalized TH-NPs show significant differences after one month, its values are still adequate for topical administration. In addition, it can be observed that at higher temperatures such as 30 or 40 °C, all the parameters vary significantly as it has been previously

reported by other authors developing PLGA NPs (Elena Sánchez-López et al. 2018; Elena Sánchez-López, Ettcheto, et al. 2017)

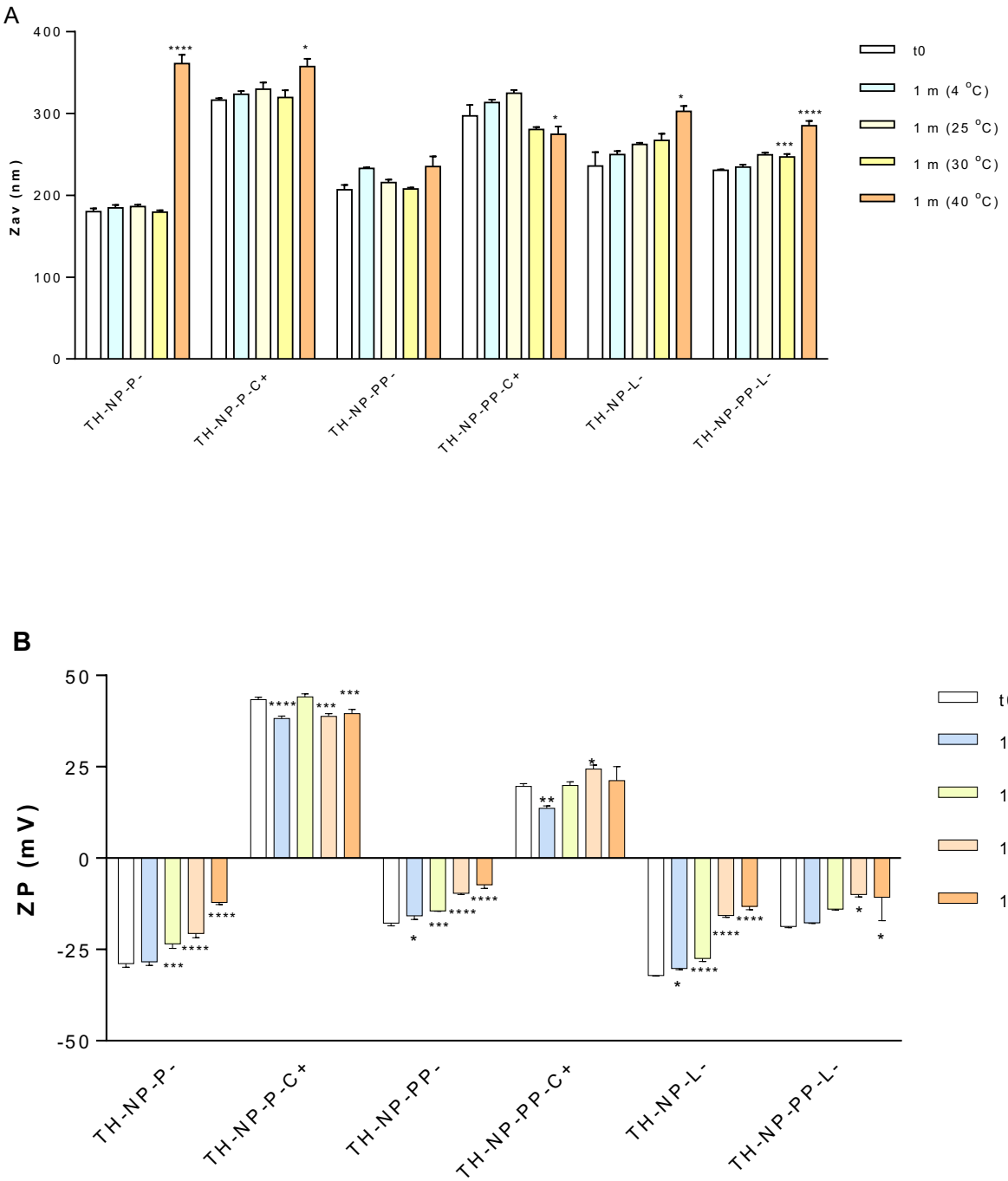

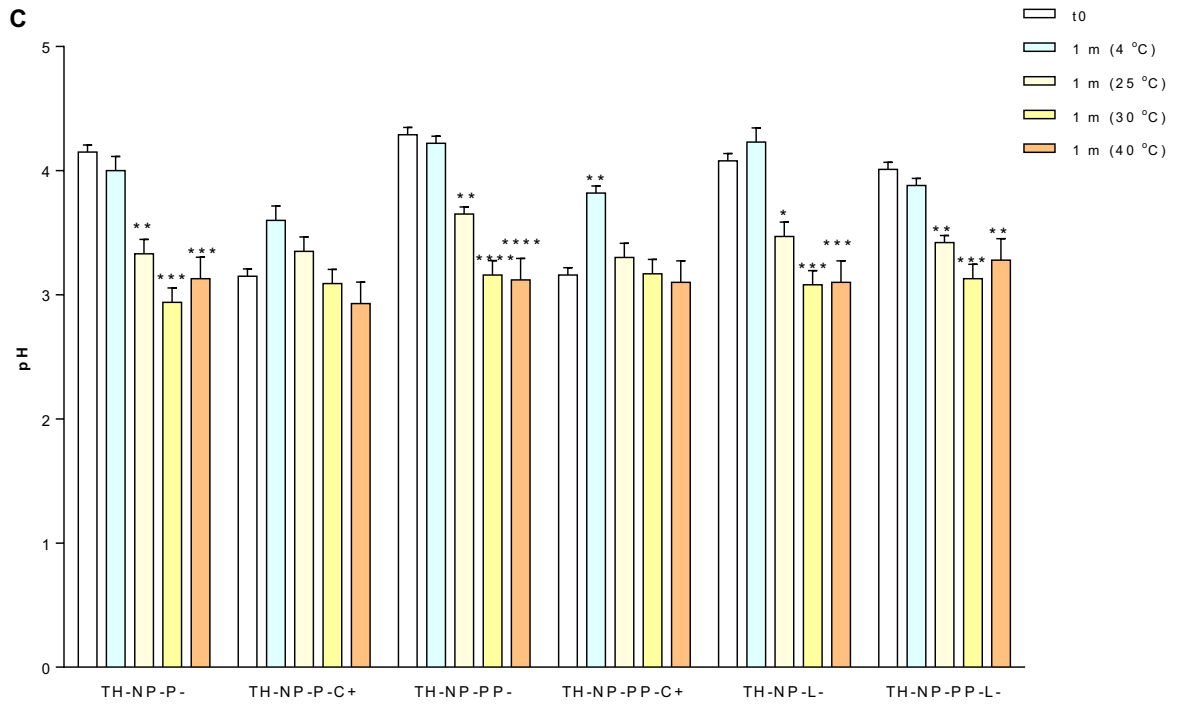

Figure 4.15. One-month stability of TH NPs with different surface functionalization strategies at 4, 25, 30 and 40 °C. (**A**) Average size, (**B**) Zeta potential (ZP), (**C**) pH values. Statistical significance was analyzed against freshly prepared formulations (one month), * $p < 0.05$; ** $p < 0.01$; *** $p < 0.001$; **** $p < 0.0001$.

Since the most suitable temperature for surface functionalized TH-NPs storage was found to be 4 °C, 6-month stability was studied at this temperature. Results obtained in **Table 4.6** show differences in the stability of the different functionalized NPs. It can be observed that after 6 months, TH-NP-P- vary its parameters. Even though, Zav of TH-NP-P- remains below 200 nm and PI below 0.1, ZP decreases significantly after 6 months of storage. A similar behavior is observed when chitosan was added to the formulation (TH-NP-P-C+) observing stability until 3-months of storage. TH-NP-PP- also show a ZP decrease after 3 months although their chitosan functionalized formulations (TH-NP-PP-C+) not vary their properties until 6 months. In the case of TH-NP-L-, NPs modified their physicochemical properties prior to 3 months after their preparation.

Table 4.6. Physicochemical values of TH-NPs with different surface functionalization stored at 4 °C.

	Month	Zav (nm) ± SD	PI ± SD	ZP ± SD (mV)
TH-NP-P-	0	172.9 ± 1.9	0.066 ± 0.037	−24.5 ± 0.9
	1	177.7 ± 2.2	0.071 ± 0.015	−20.9 ± 0.5
	3	183.8 ± 3.6	0.082 ± 0.005	−18.3 ± 0.7
	6	191.5 ± 1.5	0.091 ± 0.015	−14.3 ± 0.6
TH-NP-P-C+	0	337.3 ± 7.4	0.123 ± 0.035	23.6 ± 0.3
	1	365.4 ± 3.2	0.141 ± 0.011	23.2 ± 0.9
	3	392.9 ± 8.0	0.158 ± 0.037	21.0 ± 0.3
	6	419.6 ± 11.5	0.197 ± 0.066	17.2 ± 0.2
TH-NP-PP-	0	184.0 ± 0.9	0.101 ± 0.041	−22.2 ± 0.6
	1	191.2 ± 0.7	0.098 ± 0.022	−18.2 ± 0.6
	3	189.1 ± 10.1	0.099 ± 0.015	−12.1 ± 0.4
	6	220.0 ± 10.8	0.123 ± 0.33	−8.4 ± 0.7
TH-NP-PP-C+	0	221.1 ± 3.3	0.149 ± 0.036	10.5 ± 0.6
	1	224.1 ± 5.3	0.150 ± 0.068	9.8 ± 0.6
	3	256.1 ± 5.3	0.152 ± 0.077	7.3 ± 0.7
	6	348.5 ± 17.2	0.189 ± 0.023	6.1 ± 0.5
TH-NP-L-	0	178.5 ± 0.6	0.063 ± 0.018	−41.2 ± 1.8
	1	180.9 ± 1.4	0.076 ± 0.019	−39.7 ± 0.5
	3	214.7 ± 2.7	0.114 ± 0.032	−29.7 ± 0.5
	6	201.9 ± 3.4	0.132 ± 0.027	−23.9 ± 0.8

In addition, backscattering profile of surface-functionalized TH-NPs was analyzed by Turbiscan®Lab and results are shown in **Figure 4.16**. All optimized TH-NPs underwent a slight sedimentation that was reversible by agitation. This sedimentation might be the cause of the physicochemical modifications previously observed (**Table 4.6**). Moreover, since the difference between the obtained profiles was below 10%, this indicates a suitable stability of all the functionalized TH-NPs. However, in order to ensure long-term stability, TH-NPs lyophilization and incorporation into semi-solid formulations would be contemplated in further studies.

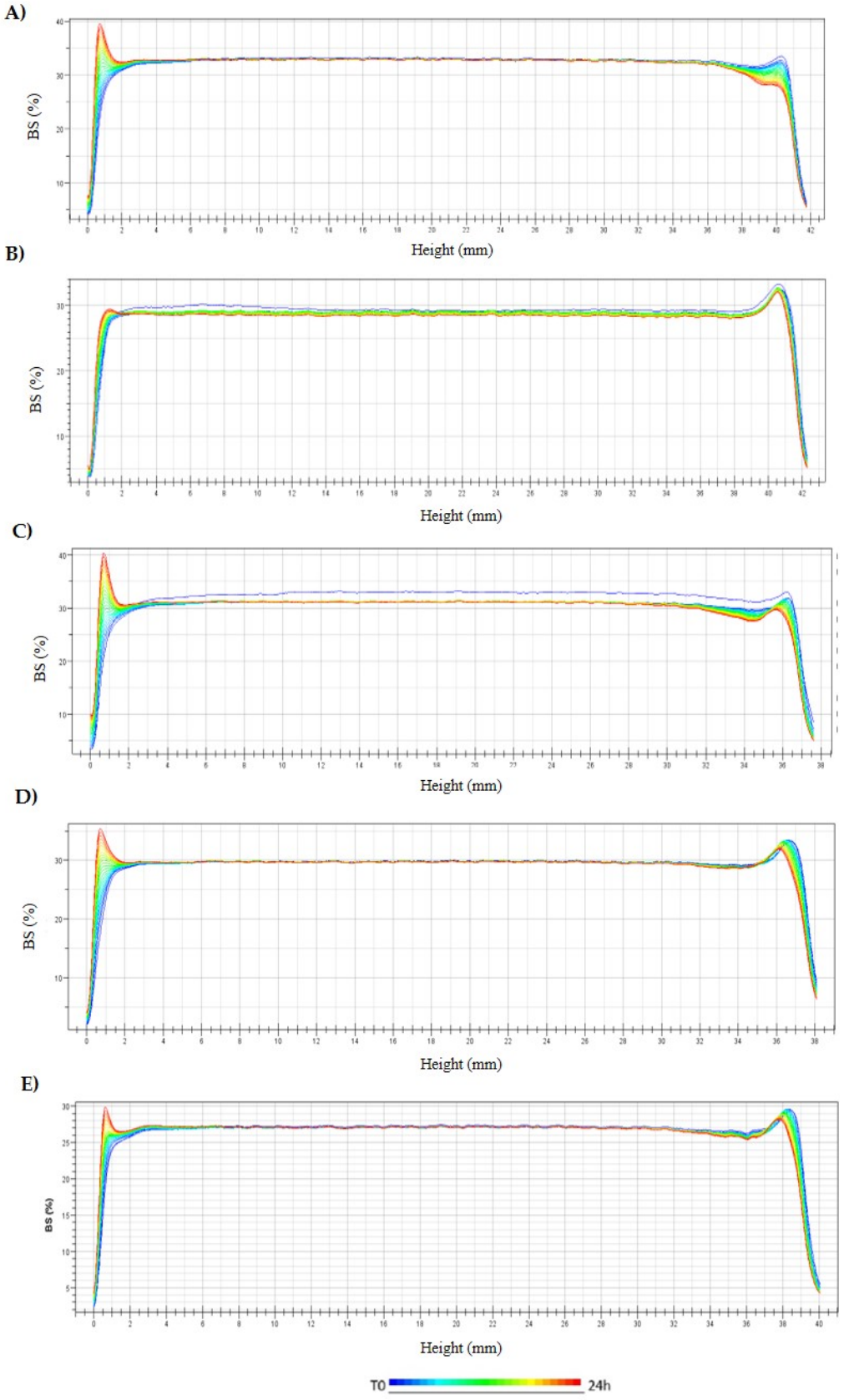

Figure 4.16. Backscattering profile of NPs measured monthly for 6 months after storage at 4 °C. (**A**) TH-NP-L-, (**B**) TH-NP-P-, (**C**) TH-NP-P-C+, (**D**) TH-NP-PP- and (**E**) TH-NP-PP-C+.

4.2.2. Biopharmaceutical Behaviour

Ex vivo Skin Penetration of Thymol Loaded Nanoparticles

As can be observed in **Figure 4.17**, all tested R-TH-NPs successfully penetrated into the skin hair follicle within 24 h. This is of extreme relevance since it is the main site where acne associated infection and inflammation occurs. Moreover, it can be observed that penetration was not influenced by the surface charge carried out since both negatively and positively charge TH NPs were able to penetrate through the skin follicle *ex vivo*.

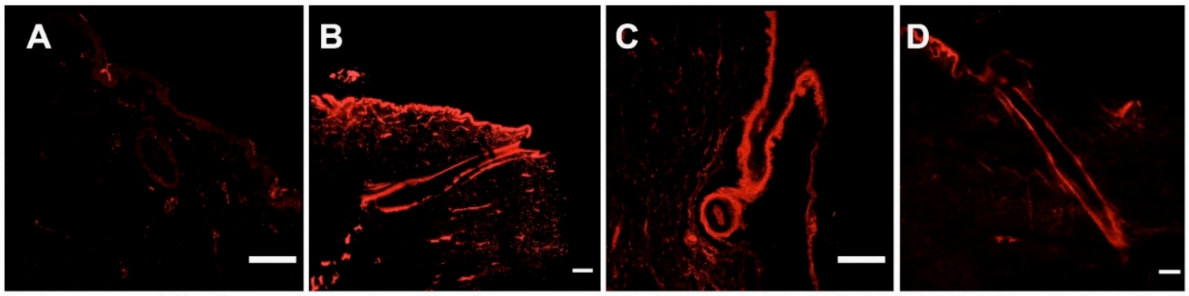

Figure 4.17. Pig skin hair follicle penetration of R-TH-NPs in 24 h by confocal microscopy. (**A**) untreated (control), (**B**) R-TH-NP-L-, (**C**) R-TH-NP-P- and (**D**) R-TH-NP-P+. Scale bar: 200 µm.

4.2.3. Therapeutic Efficacy and Biochemical studies

Ex vivo Methylene Blue Reduction

The antioxidant efficiency of TH and surface functionalized TH-NPs was evaluated in the *ex vivo* pig skin model by measuring qualitatively the methylene blue reduction, which results in a colorless compound (**Figure 4.18**). Results showed that all the assessed TH-NPs showed antioxidant activity, greater than that of free TH. No qualitative differences between TH-NPs were observed.

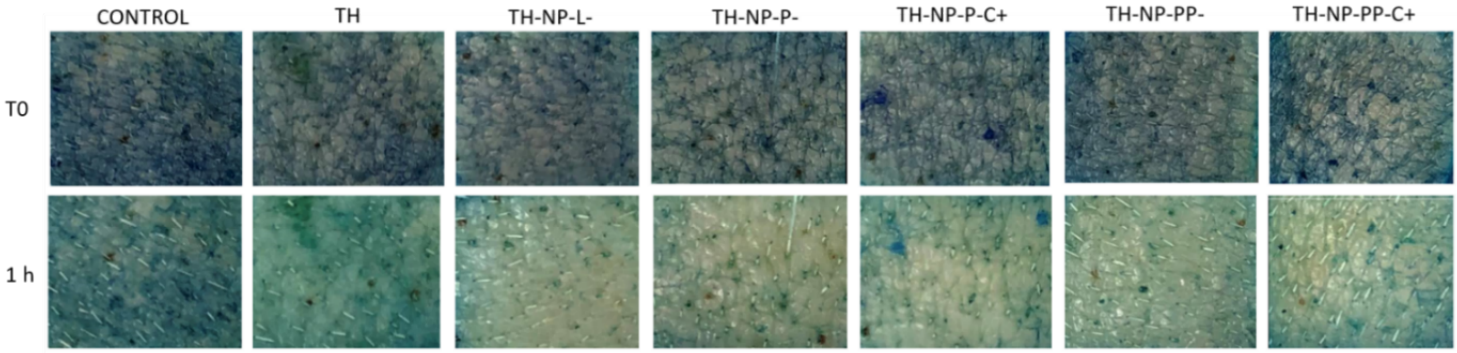

Figure 4.18. *Ex vivo* antioxidant activity by methylene blue reduction in pig skin surface. Images recorded at time 0 and after 1 h incubation at 32 °C with water (control), TH, TH-NP-L-, TH-NP-P-, TH-NP-P-C+, TH-NP-PP- and TH-NP-PP-C+).

In vitro Antioxidant Activity

The *in vitro* antioxidant activity of the different compounds used to prepare the formulations was evaluated individually by the DPPH assay (**Figure 4.19**). Results expressed as free radical scavenging capacity (%) showed that TH has similar antioxidant activity as the control BHT, although slightly higher. When tested separately, the surface compounds P188, P407 and PL displayed slightly *in vitro* free radical scavenging activity, although it was much lower than the activity of TH and BHT in all dosages tested.

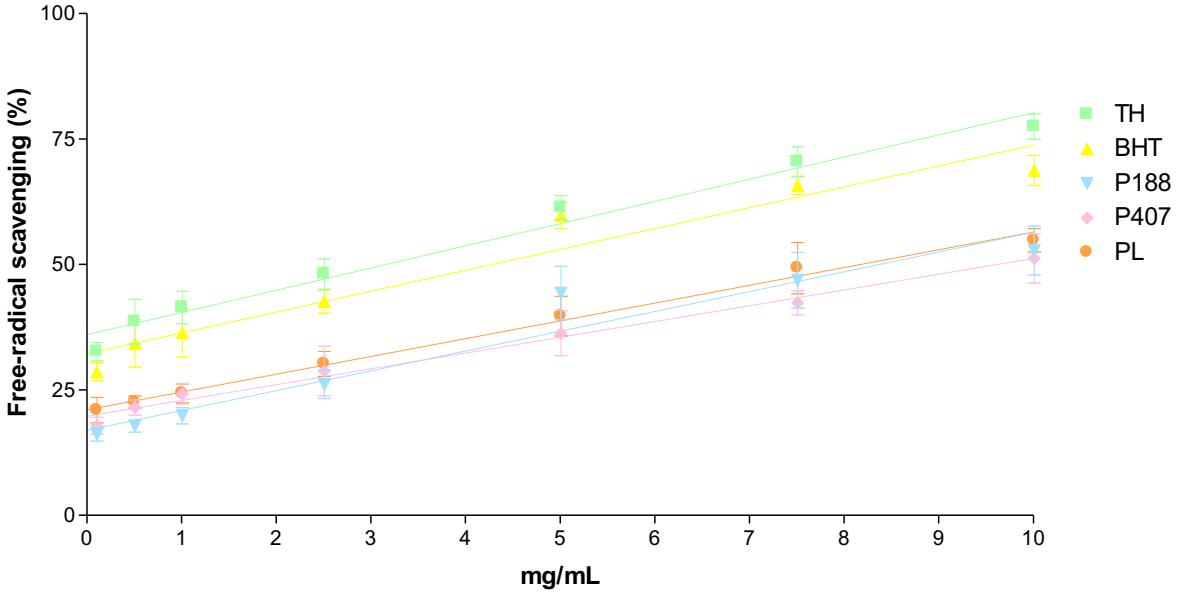

Figure 4.19. Antioxidant activity of TH, BHT and surface compounds alone (P188, P407 and PL) assessed by the DPPH free-radical scavenging assay. The 100 % ROS was obtained by the value of the control (H_2O_2) in 2 h.

In vitro Antimicrobial Efficacy

The *in vitro* antimicrobial activity of optimized surface functionalized TH-NPs against *C. acnes* was studies by suspension test. Results were similar to that of TH and in all the cases, statistically significant differences for all samples were obtained against the positive control (**Figure 4.20**). The higher antimicrobial activity was obtained with TH-NP-P-, although no statistically significant differences were observed between the different formulations.

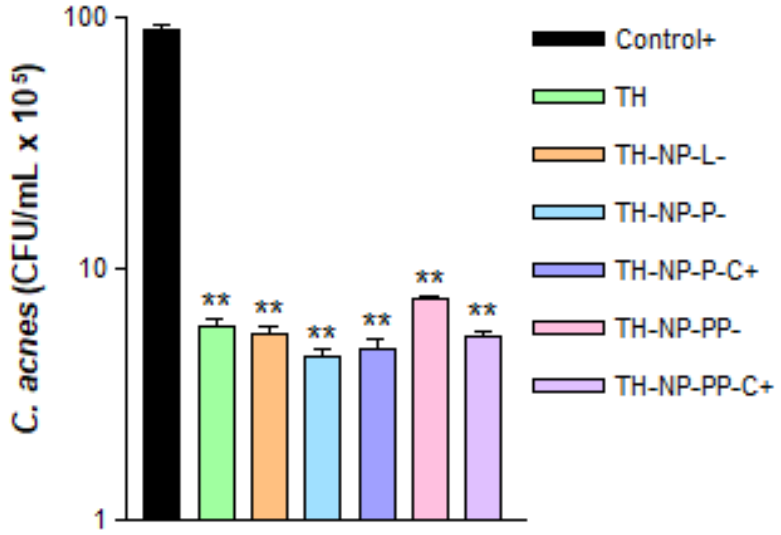

Figure 4.20. Antimicrobial activity of TH-NPs against *C. acnes* measured by the suspension test. Values represent microbial counts in CFU/mL after 30 min incubation and are expressed as Mean ± SD (n = 3). Statistical analysis was carried out via one-way ANOVA, with Tukey's Multiple Comparison Test: **, $p <$ 0.001 against control (*C. acnes* without any treatment).

Cytotoxicity and Cellular Uptake of Thymol Loaded NPs in HaCaT Cells

Cytotoxicity of TH-NPs was evaluated on HaCaT cells using the MTT assay. Cells were incubated for 24 h with TH or each TH-NP at concentrations of 2, 10 or 20 µg/mL. The surface compounds alone (P, PP, L) were tested at concentrations equivalent to those present in each formulation. Results showed that none of the samples were cytotoxic as cell viability was kept close to the untreated control cells, above 90% (data not shown).

Cellular uptake was evaluated for R-TH-NP-L-, R-TH-NP-P- and R-TH-NP-P-C+ (20 µg/mL) in HaCaT cells in order to evaluate composition and surface charge influence on cellular uptake. After 2 h incubation, TH-NPs-associated fluorescence was detected by confocal microscopy in cells treated with any of the R-TH-NPs tested (**Figure 4.21**). The cell membrane was stained with WGA (green) and the nucleus (blue) with DAPI. In the merged images the internalized TH-NPs were mainly localized in the cytoplasm in all the cases.

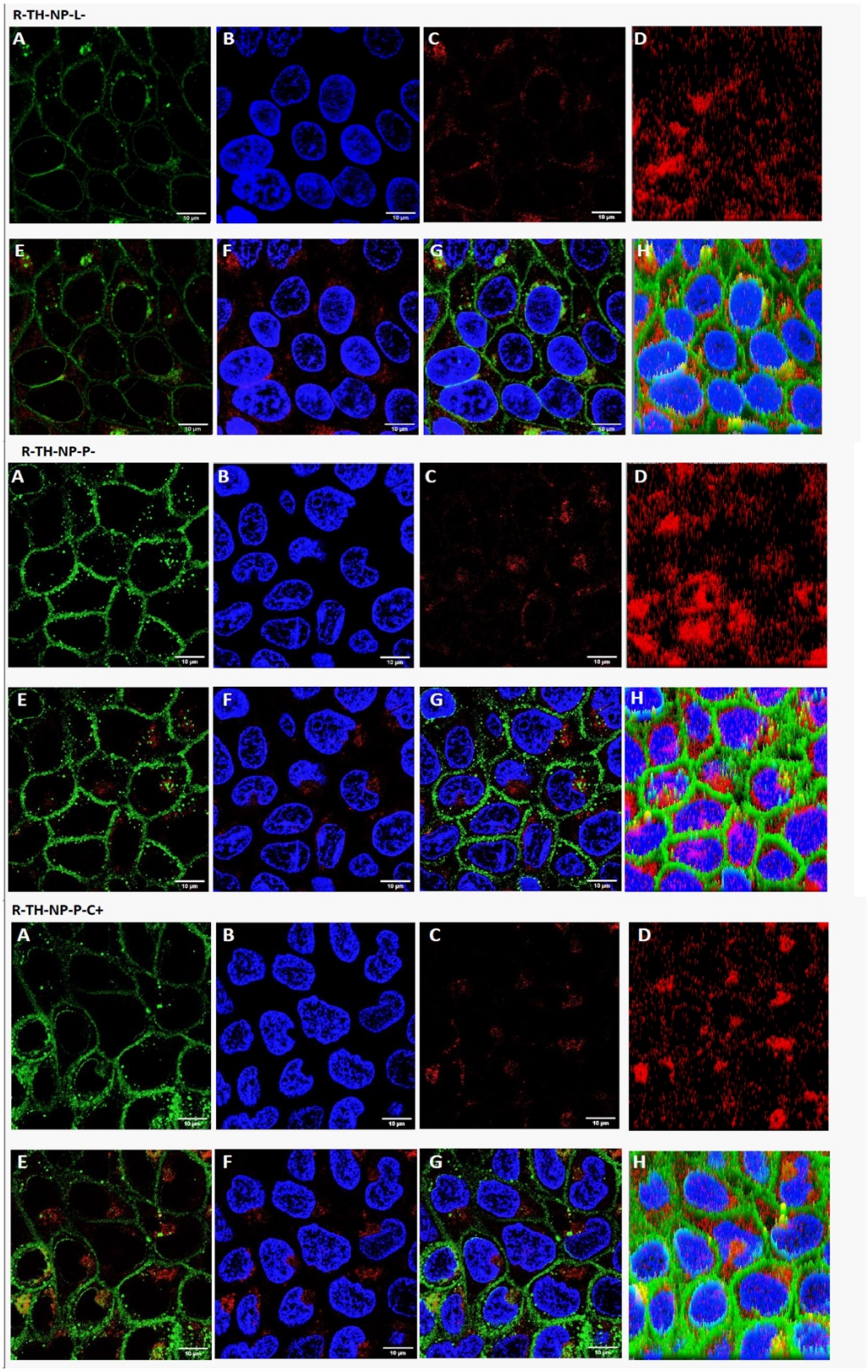

Figure 4.21. Cellular uptake by confocal microscopy analysis of HaCaT cells incubated with the indicated rhodamine-labelled NPs. (**A**) membrane staining with WGA, (**B**) nuclei staining with DAPI; (**C**) fluorescence of internalized R-TH-NPs, (**D**) 3D-plot of C, (**E**) merged A and C, (**F**) merged B and C, (**G**) merged A, B and C, (**H**) 3D-plot of G. Scale bar represents 10 μm.

Anti-Inflammatory Activity of Thymol Loaded NPs in HaCaT Cells Treated with TNF-α

The anti-inflammatory activity of the formulated NPs was evaluated in the TNF-α-induced inflammation model using HaCaT cells. Secretion of IL-6 was quantified by ELISA in cell supernatants of untreated control HaCaT cells (basal IL-6 expression), TNFα-treated HaCaT cells in the absence (positive control of inflammation) or in the presence of the different NPs. Free TH and surface compounds (C, L, P, PP) were also tested in parallel (**Figure 4.22**). Results showed that TH significantly reduced TNF-α-induced secretion of IL-6. All surface compounds analyzed individually, except PP, have similar anti-inflammatory activity as TH. Additionally, all TH-NPs, except TH-NP-PP-, presented higher anti-inflammatory activity than free compounds. The most effective NPs were the positively charged formulations, containing C. However, only TH-NP-P-C+ displayed a significant difference compared to TH.

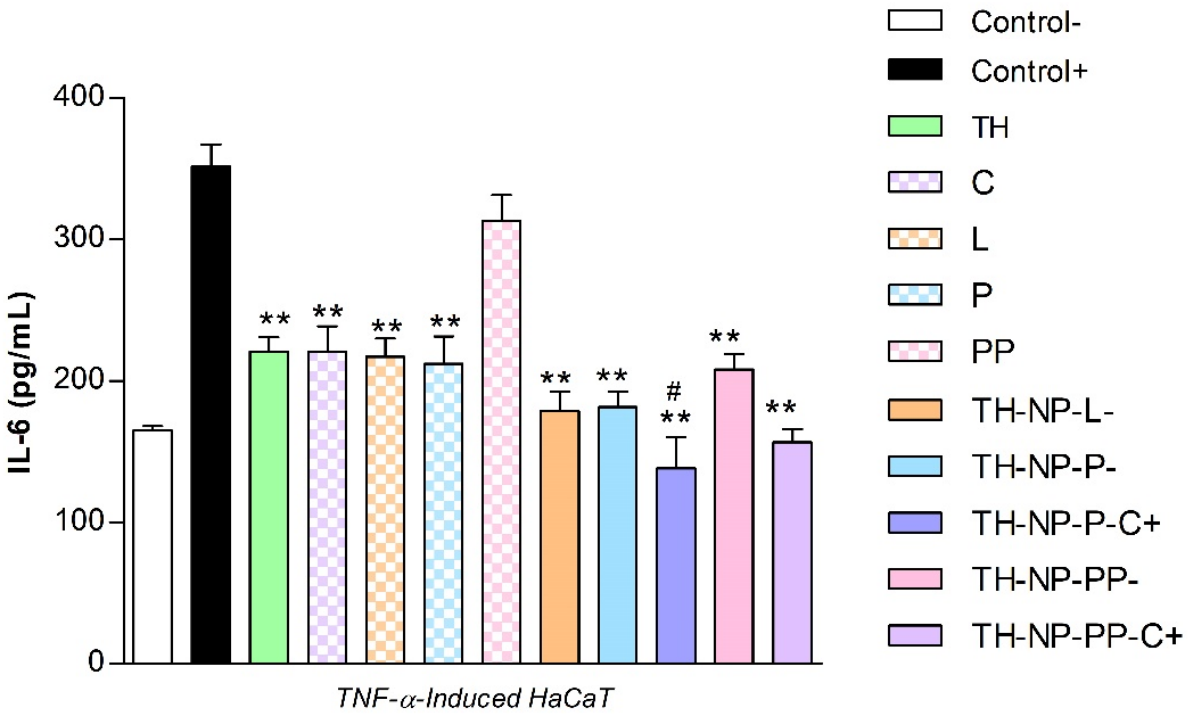

Figure 4.22. Quantification of secreted IL-6 by ELISA in TNF-α-stimulated HaCaT cells pre-incubated with formulated NPs and free compounds. Values of IL-6 (pg/mL) are the Mean ± SD, $n = 3$. Negative control: HaCaT cells without any treatment; Positive control: HaCaT cells treated only with TNF-α. Statistical analysis was performed by via one-way ANOVA, followed by Tukey's Multiple Comparison Test. ** $p < 0.001$ compared to positive control, and $^{\#}$ $p < 0.01$ compared to TH.

Anti-Inflammatory Activity of Thymol Loaded NPs in HaCaT Cells Treated with *C. acnes*

The inflammatory capacity of *C. acnes* was assessed in HaCaT cells treated with different dilutions of a *C. acnes* stock inoculum prepared in DMEM medium (OD 1.2 at 550 nm). Inflammation was evaluated by quantification of secreted IL-8 by ELISA. Results showed that *C. acnes* triggered IL-8 secretion in a dose- dependent manner **(Figure 4.23)**

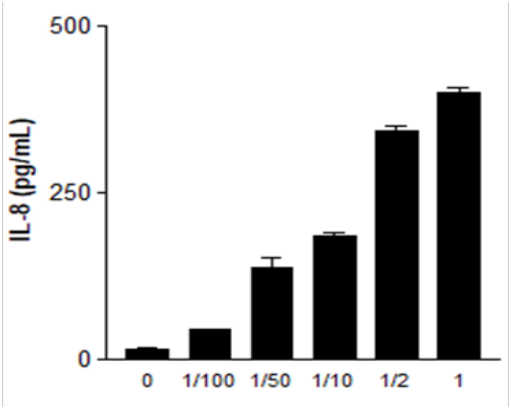

Figure 4.23. Dose-dependent inflammatory capacity of *C. acnes*. HaCaT cells were incubated for 24 with the indicated dilutions of the *C. acnes* stock inoculum (adjusted to OD 1.2 at 550 nm). Value 1 indicates no dilution. Secreted IL-8 was quantified in the cell culture supernatant by ELISA. Values of IL-8 (pg/mL) are the Mean ± SD, n=3.

From these results, the undiluted *C. acnes* stock inoculum prepared in DMEM medium (OD 1.2 at 550 nm) was optimized to be added directly to HaCaT cells to induce inflammation in further experiments aimed at evaluating the anti-inflammatory potential of TH-NPs. In this context, expression of genes encoding the inflammatory cytokines TNF-α, IL-1α, IL-1β, IL-6 and IL-8 was analysed by RT-qPCR after *C. acnes* infection in HaCaT cells pre-treated with TH, TH-NPs or B-NPs (NPs without TH). Cells challenged only with *C. acnes* were used as a positive control of the inflammatory response. Results are illustrated in **Figure 4.24**. Infection by *C. acnes* strongly induced the expression of all pro-inflammatory cytokines tested. According to its anti-inflammatory properties, TH significantly decreased the expression of all of them.

Infection by *C. acnes* strongly induced the expression of all pro-inflammatory cytokines tested (positive control). According to its anti-inflammatory properties, TH significantly decreased the expression of all of them. In general, all TH-NPs have anti-inflammatory activity, being able to reduce the mRNA levels of the different cytokines to a greater or lesser degree depending on the type of TH-NPs and the cytokine analyzed. Some TH-NPs have an anti-inflammatory activity greater than that of free TH. Statistically significant differences with respect the reduction caused by TH were apparent when analyzing the expression of IL-1α and IL-6. In the case of the TH-NP-P-C + formulation, statistical differences with respect to TH were also significant for TNF-α and IL-8. The results showed that B-

NPS can also significantly reduce the expression of all cytokines except IL-1α. However, the anti-inflammatory activity was less than that exhibited by the equivalent TH-NP. The only TH-NP that did not show significant differences with respect the equivalent B-NP is the TH-NP-L formulation.

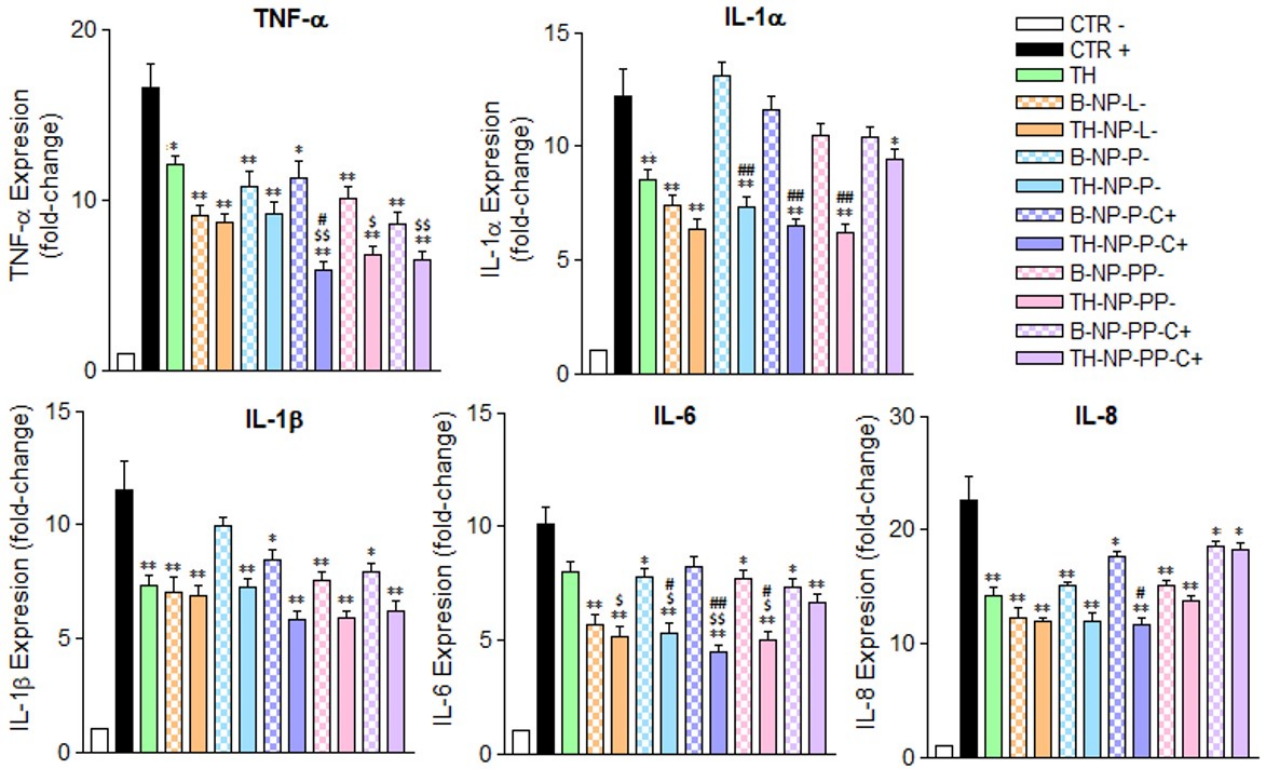

Figure 4.24. Gene expression levels of inflammatory cytokines in *C. acnes* infected HaCaT cells. Before the addition of undiluted *C. acnes* inoculum (adjusted to OD 1.2 at 550 nm), HaCaT cells were pre-incubated with TH or the indicated NPs. Relative mRNA levels of (**A**) IL-6, (**B**) IL-8, (**C**) IL-1α, (**D**) IL-1β and (**E**) TNF-α were measured by RT-qPCR, using β-actin as the reference gene. Values (Mean ± SEM, $n = 3$) are expressed as fold-change compared to untreated HaCaT cells (control-). Statistical analysis was performed via one-way ANOVA, followed by Tukey's Multiple Comparison Test ($p < 0.05$ *or $p < 0.001$**): versus positive control (control+); ($p < 0.05^{\$}$ or $p < 0.001^{\$\$}$): versus TH and ($p < 0.05^{\#}$ or $p < 0.001^{\#\#}$): versus the respective B-NP.

Antioxidant Activity via ROS Quantification in H_2O_2-Induce H2DCFDALabelled HaCaT

The antioxidant activity of TH-NPs was evaluated by ROS quantification in HaCaT cells stressed with hydrogen peroxide. Treatment with any of the surface functionalized TH-NPs significantly reduced intracellular ROS to a greater extent than TH (**Figure 4.25**). TH displayed antioxidant activity at all assay times. Moreover, the surface compounds tested individually did not show significant antioxidant activity (**Figure 4.25A**), indicating their inability to act as free radical scavengers at the cellular level.

In the case of the B-NPs (**Figure 4.25B**), they showed a ROS scavenging activity similar to TH up to 60 min after H_2O_2 challenge. Even though no significant differences were found, TH-NP-L- showed an increased antioxidant activity that may be due to PL coating potentiation of TH antioxidant effects (J. Y. Kim et al. 2015). However, this activity was lost at 120 min of incubation since ROS values were similar to that of H_2O_2-treated cells. Therefore, surface functionalization compounds could increase TH-NPs antioxidant activity at the cellular level potentiating their effects. In the other hand, all TH-NPs displayed greater antioxidant activity than TH and B-NPs, with minimal variances between them (**Figure 4.25C**).

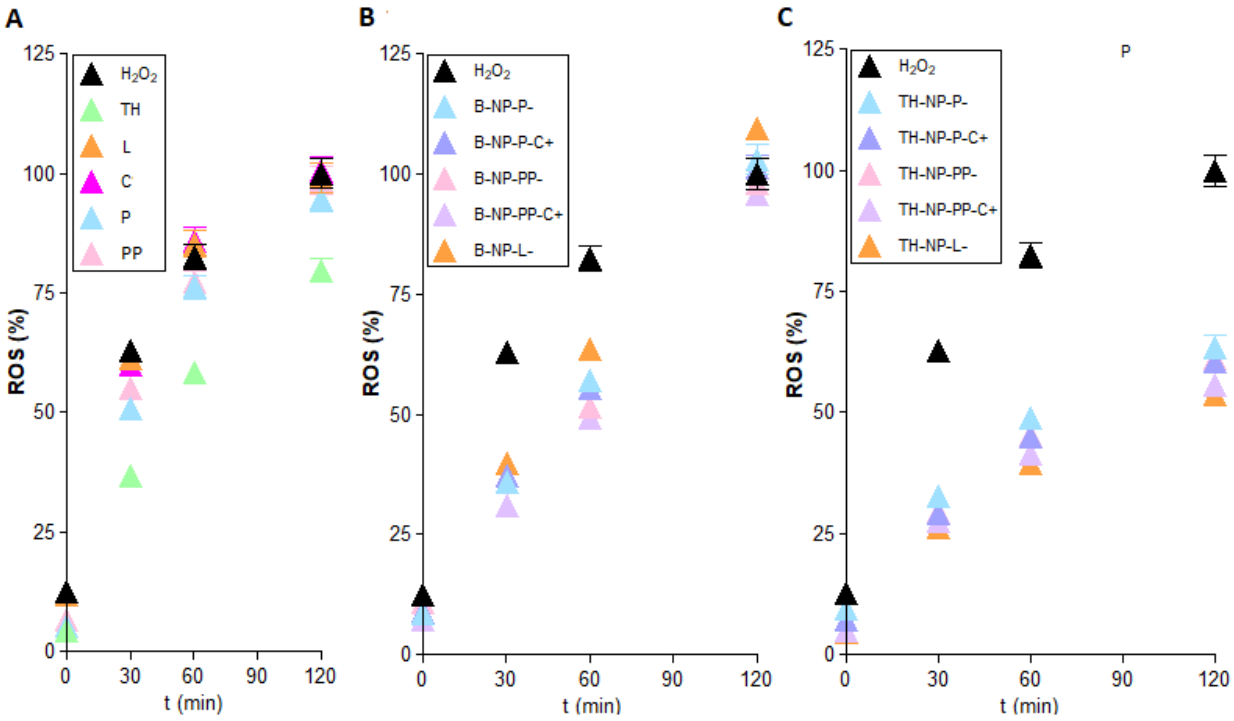

Figure 4.25. Antioxidant activity of (**A**) TH and free surface compounds, (**B**) B-NPs (blank NPs) and (**C**) TH-NPs evaluated in HaCaT cells challenged with H_2O_2. ROS were quantified using the fluorescent probe H2DCFDA. Data are expressed as the Mean ± SD (n = 8) of the amount of quantified ROS (%), assigning the value of 100 to the amount of ROS generated after 120 min treatment with H_2O_2.

Wound Healing Activity

In this study, the wound healing activity of the samples was analyzed in HaCaT cells following two different protocols. The first study was focused on studying prevention wound healing capacity. In this experiment, a 2 h treatment with TH-NPs and the coating compounds was applied 24 h prior to the

scratch (**Figure 4.26**). Images were recorded at the time of the scratch (T0) and after 24 h incubation. Results showed that all samples increased cell regeneration and possess wound healing activity compared to control. TH-NPs (**Figure 4.26 E-I**) presented higher activity than TH (**Figure 4.26B**), specially un the case of TH-NP-PP-C+. The surface compounds alone had minor effects. Therefore, using this assay, wound healing prevention of surface modified TH-NPs has been demonstrated.

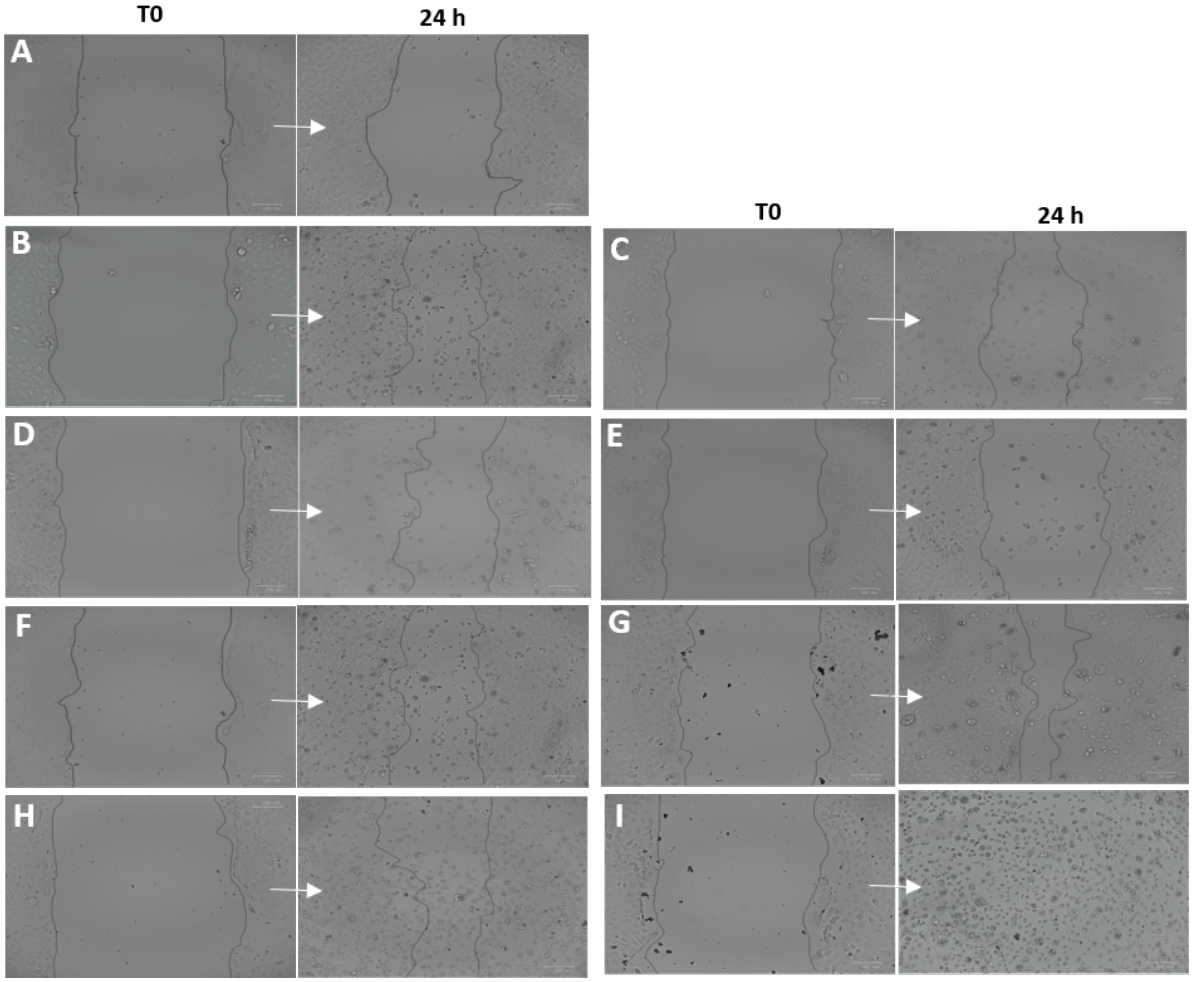

Figure 4.26. Wound healing activity in HaCaT pre-scratch treatment (wound healing prevention). Scratches were monitored at T0 and after 24 h incubation. (**A**) control, (**B**) Free TH, (**C**) chitosan, (**D**) phosphatidylcholine, (**E**) TH-NP-L-, (**F**) TH-NP-P-, (**G**) TH-NP-P-C+, (**H**) TH-NP-PP- and (**I**) TH-NP-PP-C+.

The second protocol was performed in order to study wound healing treatment. Cell regeneration and wound healing efficacy after 24 h incubation are illustrated in **Figure 4.27**. Results indicate that surface-functionalized TH-NPs showed greater wound healing activity than control TH and all other individually tested compounds. Additionally, depending on their surface composition, an increase in cell proliferation and wound closure could be observed specially in the case of Chitosan coated TH-

NPs. Therefore, this test confirms that TH-NPs could also be used for wound healing treatment. Meanwhile, B-NPs and surface compounds alone presented minimal activity thus indicating synergic effect between TH and surface functionalization compounds.

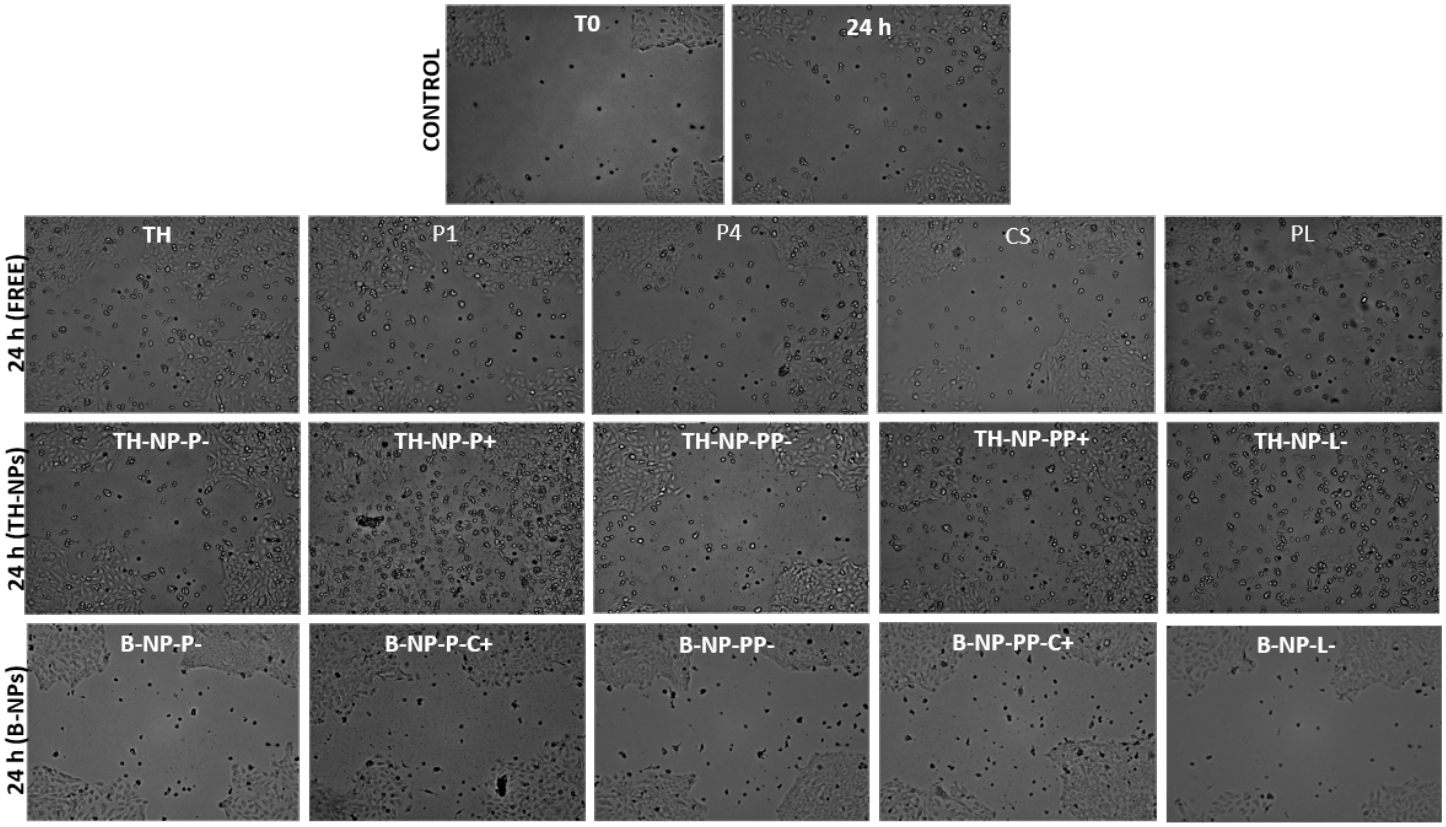

Figure 4.27. Recorded images of wound healing activity in HaCaT cells under post-scratch treatment (wound healing treatment). (**A**) Control T0, (**B**) Control after 24 h incubation, (**C**) Free TH, (**D**) Poloxamer 188, (**E**) poloxamer 407, (**F**) chitosan, (**G**) phosphatidylcholine, (**H**) TH-NP-P-, (**I**) TH-NP-P-C+, (**J**) TH-NP-PP-, (**K**) TH-NP-PP-C+, (**L**) TH-NP-L-, (**M**) B-TH-NP-P-, (**N**) B-NP-P-C+, (**O**) B-NP-PP-, (**P**) B-NP-PP-C+, (**Q**) TH-NP-L-.

4.3. Thyme Oil Loaded PLGA Nanoparticles

4.3.1. Physicochemical Characterization

THO-NPs were prepared using the solvent displacement method and surface functionalized with different compounds (THO-NP-L-, THO-NP-P- and THO-NP-P-C+). Their physicochemical characterization and stability for 6 months, stored at 4 °C are shown in **Table 4.7**. All formulations presented suitable polydispersity values, below 0.2, indicating monodisperse and homogeneous systems (Vega et al. 2013). Moreover, Z_{av} was adequate for skin topical administration.

Table 4.7. Physicochemical values of Thyme oil loaded PLGA NPs formulations surface functionalized with PL, P188 and P188-CS, respectively (THO-NP-L-, THO-NP-P- and TH-NP-P-C+), and their stability for 6 months stored at 4 °C.

	t (months)	Zav (nm)	PI	ZP (mV)
THO-NP-L-	0	193.3 ± 1.1	0.153 ± 0.029	-32.1 ± 0.9
	3	228.9 ± 19.6	0.154 ± 0.061	-24.3 ± 0.8
	6	254.8 ± 3.6	0.173 ± 0.018	-18.1 ± 0.5
THO-NP-P-	0	181.2 ± 4.9	0.052 ± 0.014	-22.8 ± 0.2
	3	193.2 ± 3.1	0.123 ± 0.032	-17.1 ± 0.3
	6	190.6 ± 4.13	0.123 ± 0.056	-13.9 ± 0.6
THO-NP-P-C+	0	237.5 ± 2.9	0.168 ± 0.028	24.3 ± 0.7
	3	326.9 ± 9.6	0.167 ± 0.06	20.1 ± 0.2
	6	344.4 ± 8.3	0.174 ± 0.02	16.5 ± 0.4

In vitro Antimicrobial Efficacy

The *in vitro* antimicrobial activity of optimized surface functionalized THO-NPs against *C. acnes* was evaluated by the suspension test within 30 min contact. All samples presented statistically significant reduction of bacteria viability, compared to the control. Results of THO-NPs presented no differences between them, however, THO showed a complete microbial growth depletion (**Table 4.8**). The strong and fast antimicrobial activity of THO against *C. acnes* may be related to the synergic effect its entire composition.

Table 4.8. Antimicrobial activity of THO and THO-NPs against *C. acnes* measured by the suspension test. Values represent microbial counts in CFU/mL after 30 min incubation and are expressed as Mean ± SD (*n* = 3). Statistical analysis was carried out via one-way ANOVA, with Tukey's Multiple Comparison Test; (*): against control (*C. acnes* without treatment) and (“): against THO.

SAMPLE	CFU x 10^3/mL	SSD
CTR (*)	8800	
THO (")	< 1	* ($p < 0.0001$)
THO-NP-L-	740 ± 80	*" ($p < 0.0001$)
THO-NP-P-	740 ± 90	*" ($p < 0.0001$)
THO-NP-P-C+	430 ± 60	*" ($p < 0.0001$)

4.3.2. Biochemical studies

In vitro Cytotoxicity of THO and THO-NPs in HaCaT Cells

Cell viabiliby was carried out by MTT assay, evaluating THO and functionalizaed THO-NPs at concentrations of 2, 10 and 20 µg/mL **(Figure 4.28).** Results presented no citotoxic effects of any of the concentrations tested, as cell viability were maintained above 80 %.

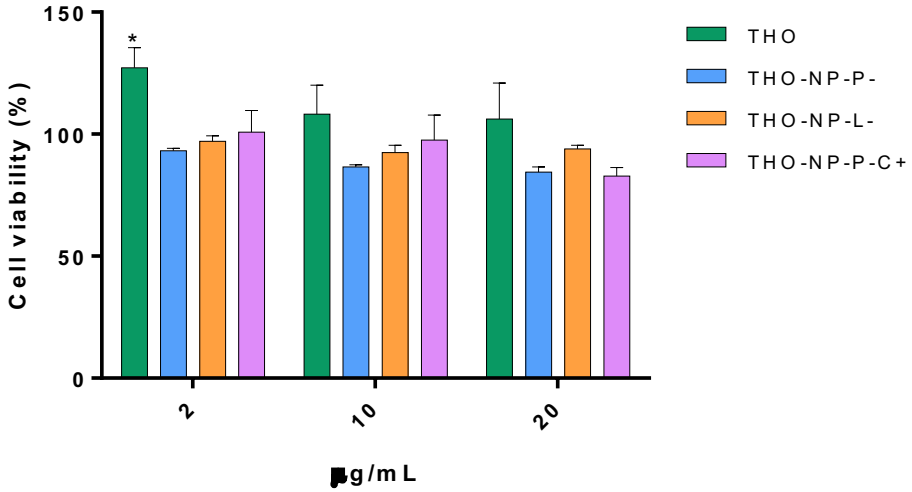

Figure 4.28. Cell viability of HaCaT cells after incubation for 24 h with THO or surface functionalized THO-NPs at different concentrations. Cell viability was assayed by the MTT reduction method; 100 % viability was set with the values obtained with the untreated control cells. Values represent the Mean ± SEM (n = 3). Statistical analysis one-way ANOVA Tukey ‘s Multiple Comparison Test, (*$p < 0.05$).

4.3.3. Therapeutic Efficacy

Anti-Inflammatory Activity in HaCaT Cells Infected with *C. acnes*

To study the anti-inflammatory activity of THO and surface/functionalized THO-NPs against *C. acnes* induced inflammation, a stock inoculum prepared in DMEM medium (OD 1.2 at 550 nm) and it was added directly to HaCaT cells. Expression of genes encoding the inflammatory cytokines TNF-α, IL-1α, IL-1β, IL-6 and IL-8 were analysed by RT-qPCR after *C. acnes* infection in the cells pre-treated with THO or THO-NPs for 2 h. Cells challenged only with *C. acnes* were used as a positive control of the inflammatory response.

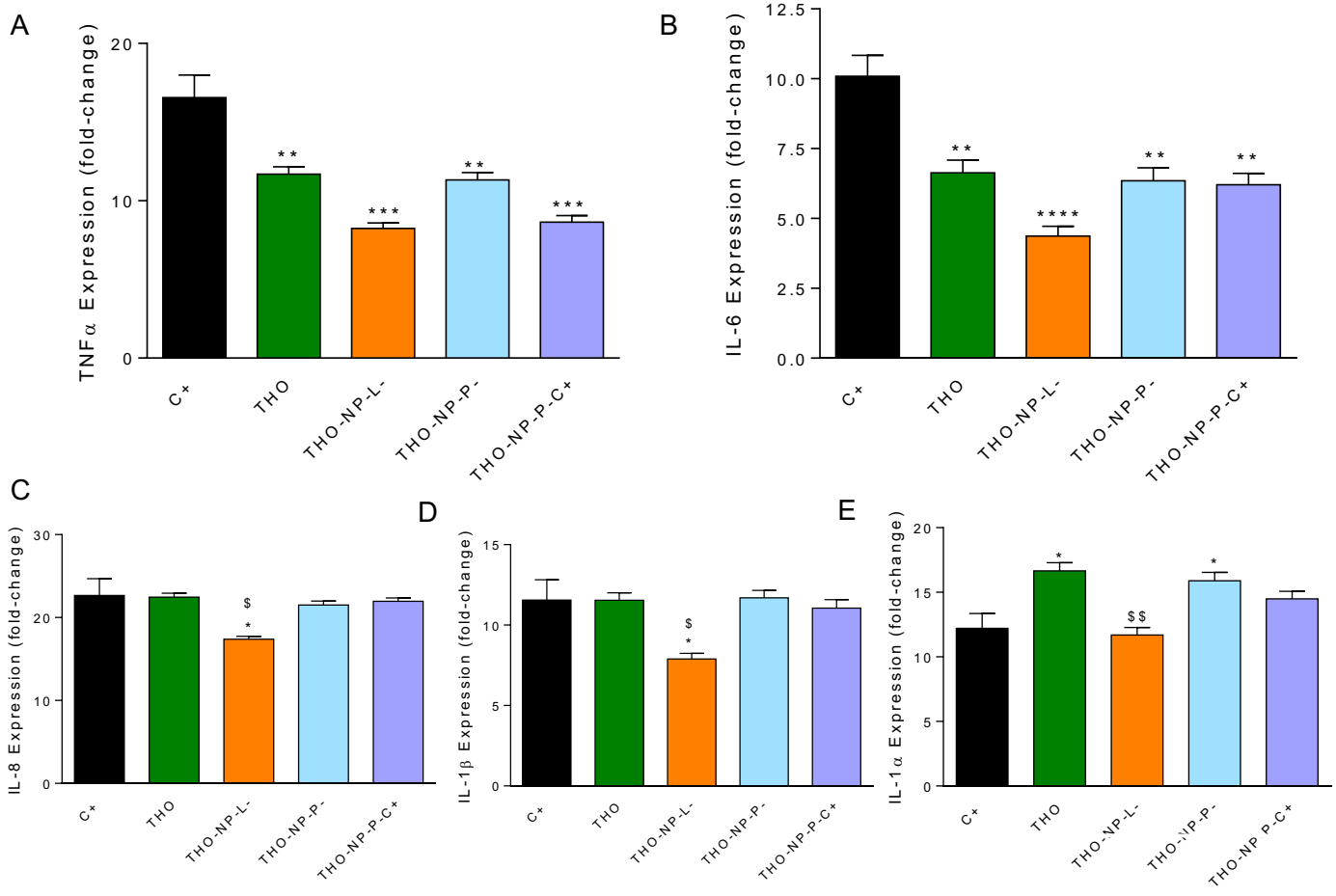

Figure 4.29. Gene expression levels of inflammatory cytokines in *C. acnes*-infected HaCaT cells. Before the addition of undiluted *C. acnes* inoculum (adjusted to OD 1.2 at 550 nm), HaCaT cells were pre-incubated with THO or THO-NPs. Relative mRNA levels of (**A**) TNF-α, (**B**) IL-6, (**C**) IL-8, (D) IL-1α and (E) IL-1β were measured by RT-qPCR, using β-actin as the reference gene. Values (Mean ± SEM, $n = 3$) are expressed as fold-change compared to untreated HaCaT cells (control-). Statistical analysis was performed via one-way ANOVA, followed by Tukey's Multiple Comparison Test (*$p < 0.05$, **$p < 0.01$, ***$p < 0.001$ or ****$p < 0.0001$): versus positive control (C+) and ($^{\$}p < 0.05$ or $^{\$\$}p < 0.01$): versus THO.

Results are illustrated in **Figure 4.29**, where THO-NP-L- presented higher activity for all gene tested, except for IL-1α, but it presented statistically significant differences compared to THO that surprisingly increased compared to the control. Moreover, no activity was found for IL-8 and IL-1β with any sample, except THO-NP-L- which also presented significant differences compared to THO.

Antioxidant Activity via ROS Quantification in H_2O_2-Induced H2DCFDA-Labelled HaCaT

The free-radical scavenging capacity of THO was previously studied compared to TH and BHT by DPPH assay. Results (**Figure 4.30A**) showed that THO has much higher activity than TH and BHT, since it is composed by several antioxidant compounds.

The antioxidant activity of THO and THO-NPs were evaluated by ROS quantification in HaCaT cells stressed with hydrogen peroxide (**Figure 4.30B**). Treatment with any of the surface functionalized THO-NPs significantly reduced intracellular ROS, without significant differences between them. However, THO displayed significantly higher antioxidant activity than THO-NPs. That could be explained by the fact that THO is a lipid and has high affinity to the cellular membrane and, additionally, it is composed by several antioxidant molecules, which might make the activity synergically higher and faster. In the case of THO-NPs, they would take slightly longer until release the encapsulated THO, and therefore, the activity in the timeframe of this experiment was lower.

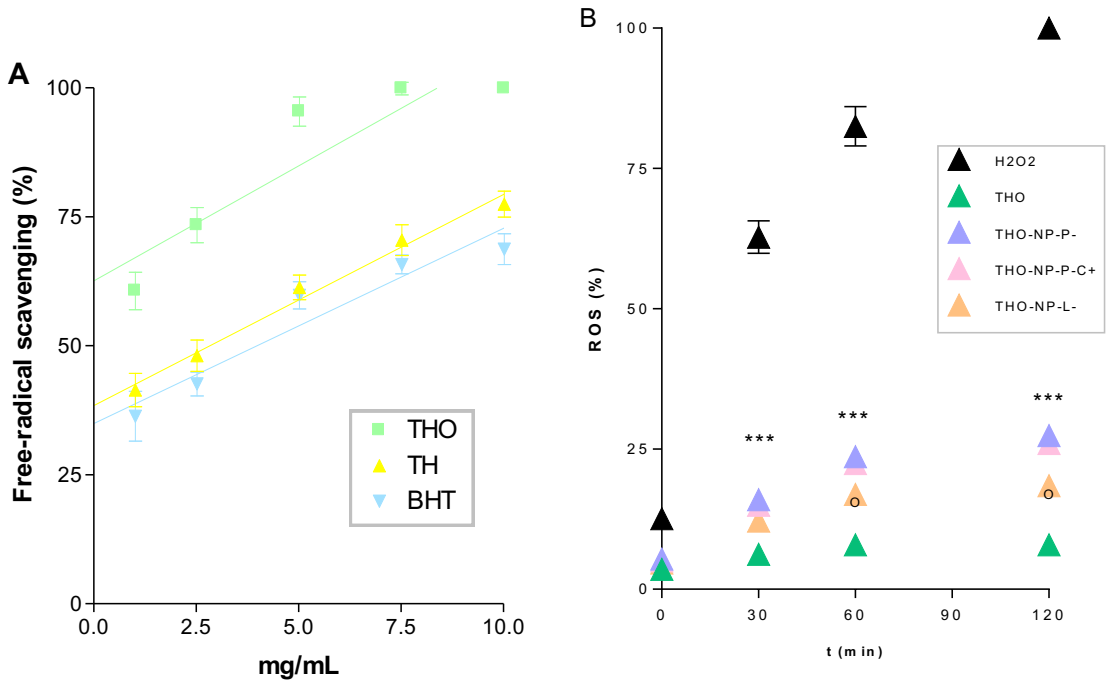

Figure 4.30. Antioxidant activity of THO and THO-NPs evaluated in HaCaT cells challenged with H_2O_2. ROS were quantified using the fluorescent probe H2DCFDA. Data are expressed as the Mean ± SD (n = 8) of the amount of quantified ROS (%), assigning the value of 100 to the amount of ROS generated after 120 min treatment with H_2O_2.

Wound Healing Activity

In this study, the scratch assay was performed to evaluate the wound healing treatment activity in HaCaT cells. Cell regeneration and wound healing efficacy, after 24 h incubation, are illustrated in **Figure 4.31**. Results indicate that surface-functionalized THO-NPs showed greater wound healing activity than control THO. Additionally, depending on their surface composition, an increase in cell proliferation and wound closure could be observed specially in the case of THO-NP-P-C+. A lesser activity was presented by THO-NP-L-. In fact, all samples presented outstanding results in wound closure and are suitable and efficient for this type of treatment.

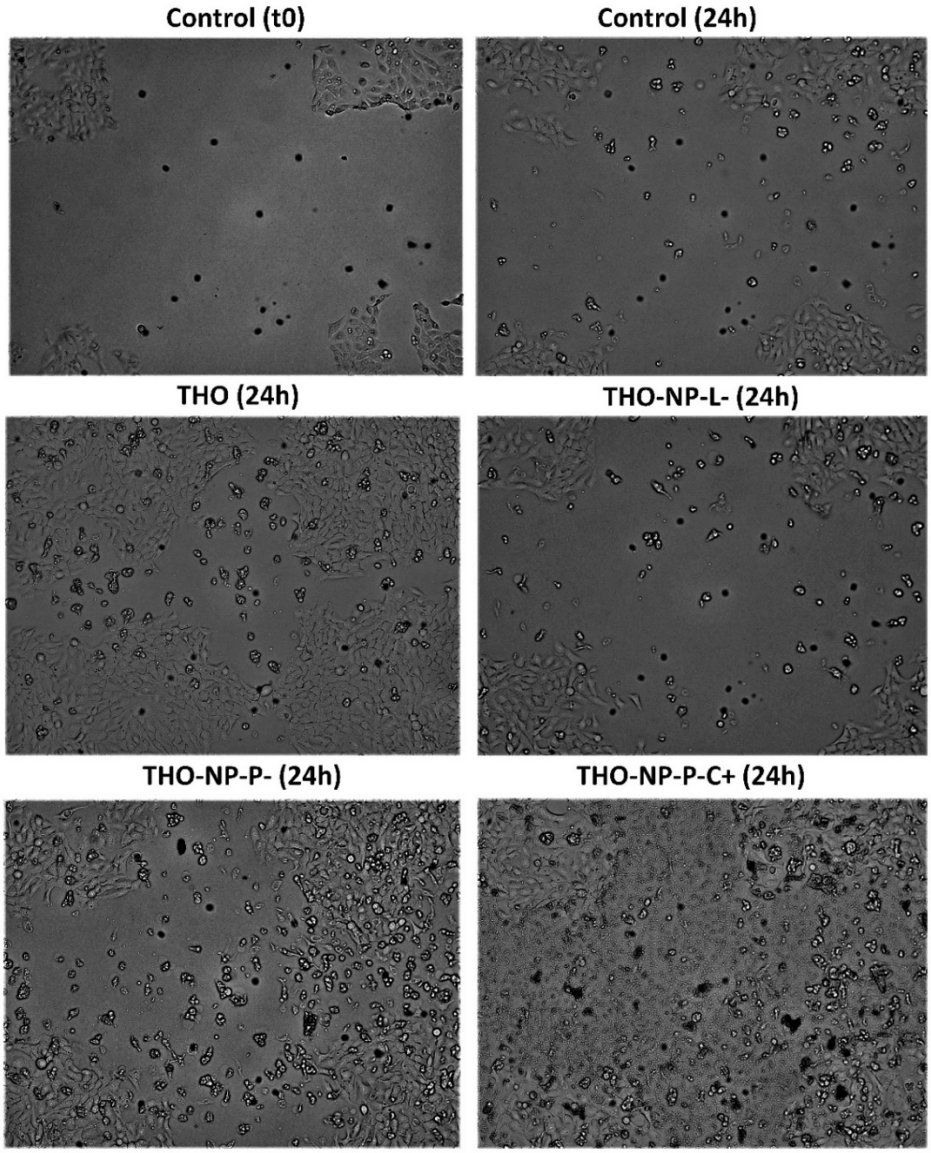

Figure 4.31. Recorded images of wound healing activity in HaCaT cells under post-scratch treatment (wound healing treatment). (**A**) Control T0, (**B**) Control after 24 h incubation, (**C**) THO, (**D**) THO-NP-L-, (**E**) THO-NP-P- and (**F**) THO-NP-P-C+

***Ex vivo* Methylene Blue Reduction**

The antioxidant efficiency of THO and surface functionalized THO-NPs was evaluated in the *ex vivo* pig skin model by measuring qualitatively the methylene blue reduction, which results in a colorless compound (**Figure 4.32**). Results showed that all tested samples showed antioxidant activity, observed by higher color reduction compared to the control. A slightly higher activity can be observed for THO-NPs compared qualitatively to THO.

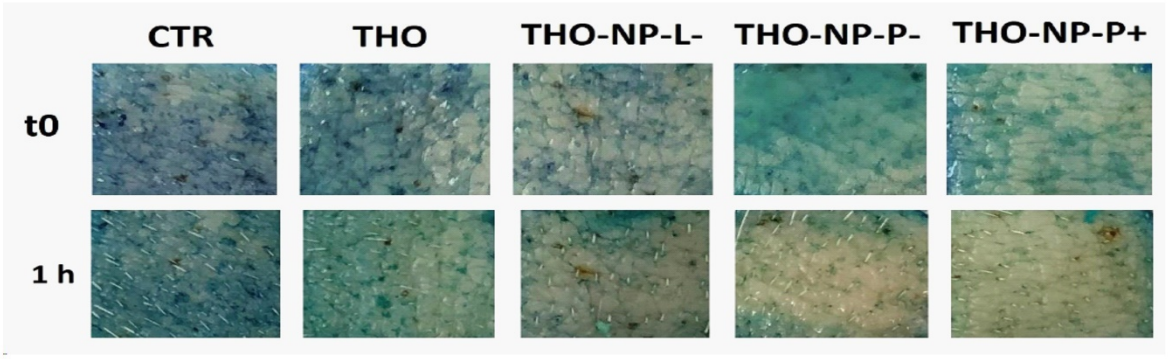

Figure 4.32. *Ex vivo* antioxidant activity by methylene blue reduction in pig skin surface. Images recorded at time 0 and after 1 h incubation at 32 °C with water (control), THO, THO-NP-L-, THO-NP-P- and THO-NP-P-C+.

4.4. Semi-Solid Formulations of Thymol and Thyme Oil PLGA NPs

4.4.1. Physicochemical and Rheological Characterization of Semi-Solid Formulations

The physicochemical characterization of surface-functionalized TH-NP was previously evaluated (data shown in Table 4.5) and it has also been examined after their incorporation into carbomer gels (**Table 4.9**). By comparing the Z_{av} of GC-TH-NP with values of TH-NPs suspensions obtained earlier in this study, the mean size has slightly increased for negatively charged TH-NPs, while for the positively charged ones this size increase was higher. Previous authors reported an electrostatic interaction between the chitosan protonated amine (NH_3^+) and the carbomer carboxylate (COO^-) (Aguilar-López and Villafuerte-Robles 2016). Therefore, this might be the reason why these particles, containing CS on the surface, presented higher Z_{av} when incorporated into the gel. In the case of the PI, data was also highly increased for all samples, due to the overall measurement includes higher sizes belonging to the gel matrix.

Table 4.9. Physicochemical characterization of TH-NPs after incorporation into carbomer gels

NP-gels	Zav (nm)	PI
GC-TH-NP-P-	232.9 ± 67.26	0.387 ± 0.098
GC-TH-NP-P-C+	551.0 ± 47.22	0.440 ± 0.067
GC-TH-NP-PP-	241.0 ± 57.2	0.293 ± 0.046
GC-TH-NP-PP-C+	478.9 ± 32.51	0.456 ± 0.102
GC-TH-NP-L-	333.3 ± 67.16	0.440 ± 0.081

Stability of TH-NP Gels

The short-term stability of GC-TH-NP-T- was predicted by examining the backscattering profile (**Figure 4.33**), showing that the macrogel matrix formed tends to stabilize TH-NPs.

The short-term accelerated stability of the surface modified TH-NP carbomer gels was studied after 1 month stored at several temperatures. The appearance of the gels stored at 4 ºC and at room temperature have maintained their semi-solid consistency. In contrast, gels stored at 30 and 40 ºC turned into fluid gels. The reason for this loss of viscosity may be due to the pH decrease as showed in **Figure 4.34**. Since carbomer gelling properties are pH dependent, when the pH decreases significantly, the gel matrix loses viscosity and becomes fluid. The reason for this could be possibly due to a partial hydrolysis of PLGA into its monomers, lactic and glycolic acids, which may have led to a slight decrease of the formulation, and therefore, destabilizing the gel matrix, since the carbomer thickness is pH dependent. Other authors previously stated that NaOH is known to catalyze the hydrolysis of PLGA co-polymer by ester cleavage (Rajapaksa et al. 2010). Being this the reason, the suitable alternative would be to increase the pH of carbomer gels using, for example, triethanolamine instead of NaOH. In the case of

the NPs covered by CS, the pH was diminished and did not present significant differences at higher temperature, therefore, this polysaccharide molecule attached to the NPs surface might help to stabilize and/or protects the PLGA.

The long-term stability of GC-TH-NP-P- and GC-THO-NP-L- were also studied for 6 months at room temperature and data of the physicochemical parameters evaluated are displayed in **Table 4.10**. It can be observed in the formulation that the TH-NPs morphometry is maintained for 4 months, but in fact, the gels lost their thickness within 4.5 month (observed by naked-eye). In contrast, formulations of TH-NP-T- incorporated into HPMC and pluronic gels have maintained stable for over 12 months stored at room temperature.

In a different study (data not shown), gels stored at 4 °C had maintained their pH and semi-solid appearance stability for 12 months, therefore, to maintain carbomer gels of PLGA NPs shelf-life, they must be stored at 4 °C. In the other hand, HPMC and pluronic gels of TH-NPs have maintained stability (pH and semi-solid appearance) stored at RT for 12 months.

The microbial preservative activity stability evaluated for GC-TH-NP-P- and GC-THO-NP-L- was found successful after 6 m storage at RT. GC-TH, GP-TH, GC-TH-NP-T- and GP-TH-NP-T- presented preservative activity stored at RT after 36 m. Therefore, TH dosage forms formulated with synthetic polymers, presented good microbial preservative activity along storage (data not shown).

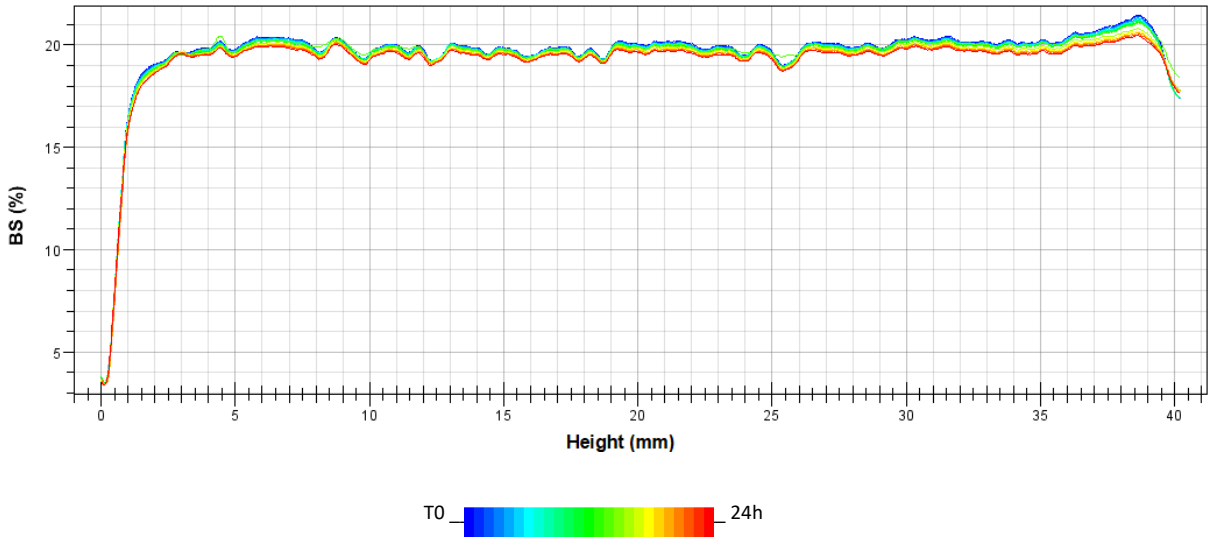

Figure 4.33. Backscattering of (A) GC-TH-NP-T- measured by TurbiscanLab®. Scans were performed from the bottom to the top of the vial, measured every hour for 24 h, represented by blue to red lines.

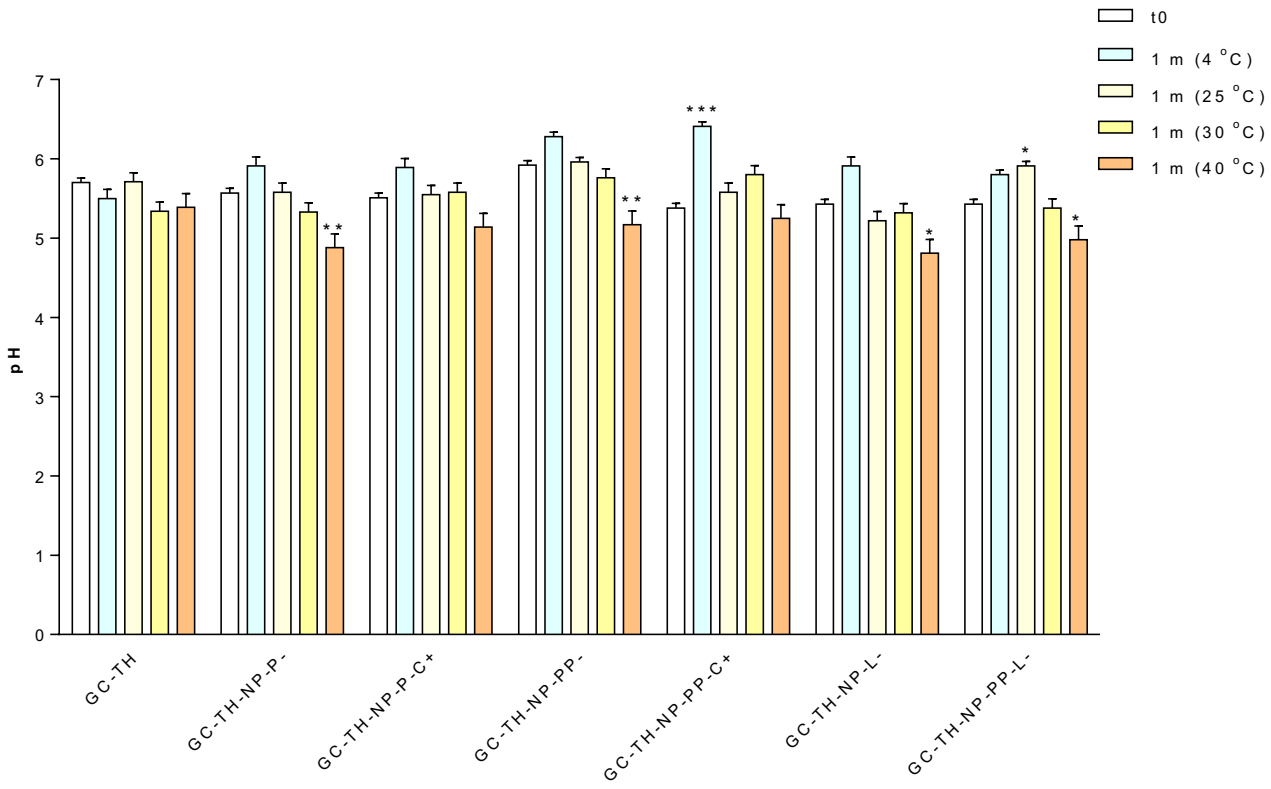

Figure 4.34. Carbomer gels of surface functionalized TH-NPs pH stability for 1 m at varied storage conditions. Data expressed as mean ± SD. Statical analysis performed as unpaired t test (*p < 0.05).

Table 4.10. Physicochemical stability of GC-TH-NP-P- and GC-THO-NP-L- stored at room temperature.

	t (month)	Appearance	pH	Zav (nm)	PI
GC-TH-NP-P-	0	semi-solid	6.15 ± 0.02	233.5 ± 6.9	0.331 ± 0.060
	1.5	semi-solid	6.12 ± 0.04	243.4 ± 17.5	0.366 ± 0.015
	3	semi-solid	6.01 ± 0.03	263.4 ± 19.5	0.376 ± 0.018
	4.5	*fluid**	*5.72 ± 0.06*	*206.5 ± 3.0*	*0.252 ± 0.047*
GC-THO-NP-L-	0	semi-solid	6.25 ± 0.04	268.0 ± 6.5	0.306 ± 0.080
	1.5	semi-solid	6.17 ± 0.03	301.9 ± 37.51	0.345 ± 0.066
	3	semi-solid	6.09 ± 0.01	303.6 ± 61.5	0.374 ± 0.112
	4.5	*fluid**	*5.79 ± 0.05*	*277.5 ± 4.8*	*0.364 ± 0.049*

Morphology of GC-TH-NP-T-

The morphology of GC-TH-NP-T- was recorded by SEM, illustrating the gel structure and the TH-NP-t- within the matrix (**Figure 4.35**). Since the gel was dried, the NPs size are seen slightly smaller than their actual size due to the dehydration process.

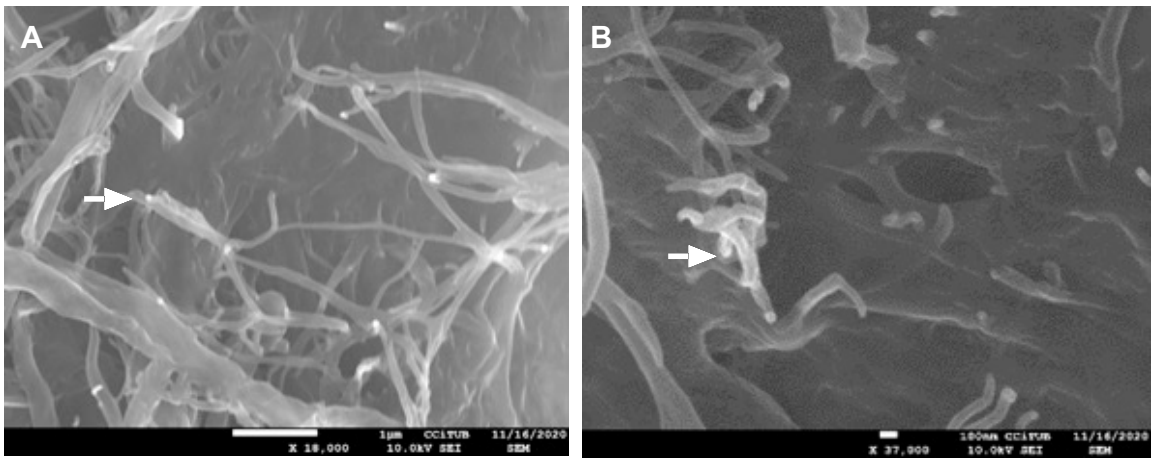

Figure 4.35. Scanning electron microscopy image of GC-TH-NP-T- scale bar (A) 1 µm (x 18.000) and (B) 100 nm (x 37.000).

Rheology Studies of TH-NP gels

The rheological results of GC-TH, GC-TH-NP-T-, GH-TH-NP-T- and GP-TH-NP-T- are illustrated in **Figure 4.36.** The rheograms revealed that all formulations showed a non-Newtonian pseudoplastic behaviour in the ascending and descending sections, with Cross's equation as the best fit model in both cases. Also, GC-TH presented slight thixotropy appearance while, in the case if gels of TH-NP-T-, it was accentuated. This can be observed in the rheograms, expressed as the hysteresis loop gap between forward and backward plots. This behaviour is commonly present in semi-solid cosmetic formulations and it makes them suitable for good spreading ability on skin. (Lee, Moturi, and Lee 2009). In terms of the viscosity, it can be observed that GC-TH-NP-T- and GP-TH-NP-T- had similar values, while GH-TH-NP-T- was considerable higher. In the case of the thixotropy appearance, the highest values can be observed for GC-TH-NP-T- and GH-TH-NP-T-, while GC-TH the lowest.

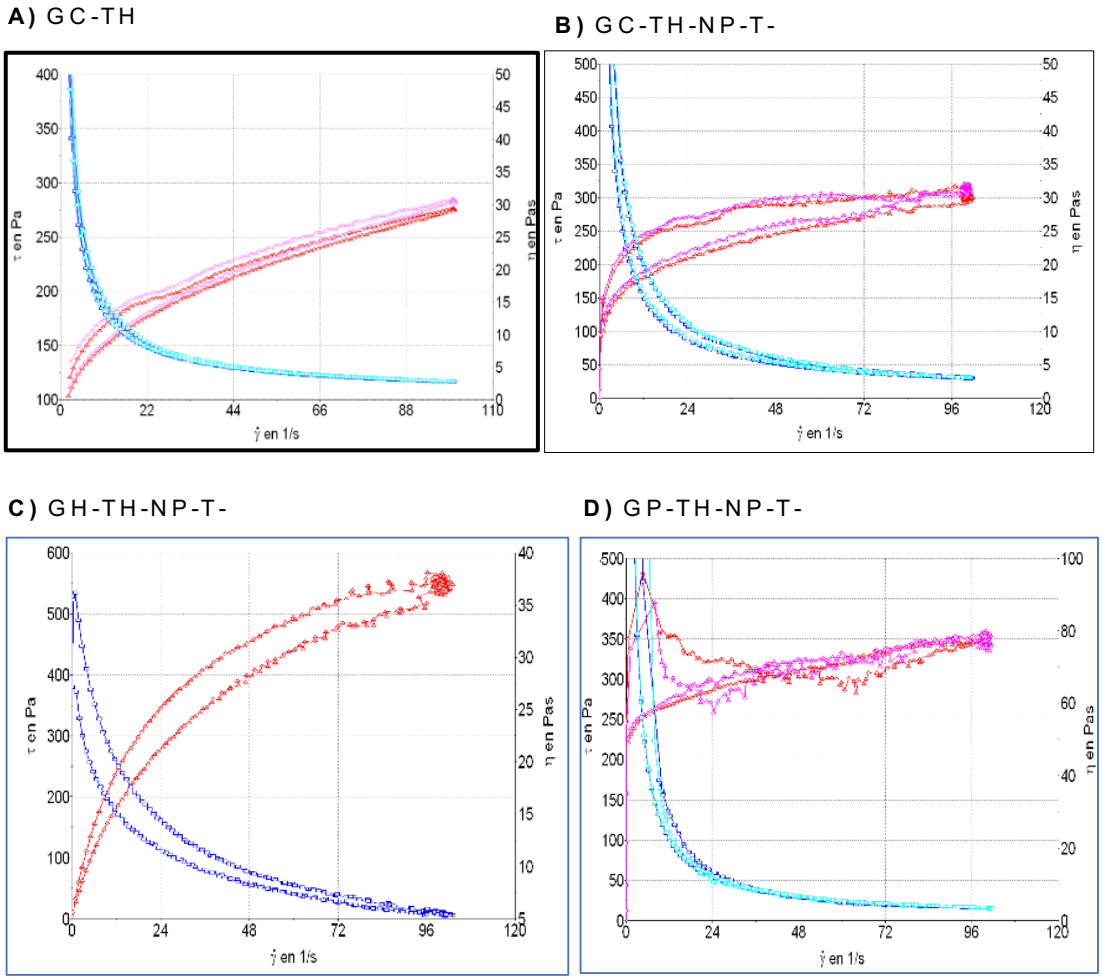

Figure 4.36. Rheograms of (A) GC-TH, (B) GC-TH-NP-T-, (C) GH-TH-NP-T- and (D) GP-TH-NT-. Data was fit to cross mathematical model corresponding to a pseudoplastic flux. All formulations presented thixotropy appearance.

Table 4.11. Rheology of TH and TH-NP-T- semi-solid formulations.

	GC-TH	GC-TH-NP-T-	GH-TH-NP-T-	GP-TH-NP-T-
pH	5.0 - 5.5	5.0 - 5.5	5.0 - 5.5	6.0 - 6.5
Viscosity (Pas)	2.831 ± 0.012	3.131 ± 0.046	5.459 ± 0.101	3.482 ± 0.024
Thixotropy (Pa/s)	-	3.28E+07	9.47E+07	1.81E+07

4.4.2. Biopharmaceutical Behaviour

In vitro Release

TH release profile was evaluated for 72 h and adjusted to hyperbole mathematic equation (best fit). In **Figure 4.37 (A-B),** for TH and TH-NP-T- as aqueous or gels, respectively, the sustained release of TH-NP-T- is found in both dosage forms compared to TH. In both cases, the steady state of non-particulate

TH was reached before 12 h, whereas TH-NP-T- formulations provided a continuous release during the entire length of the study. Statistical analysis showed significant differences of TH-NP-T- in both dosage forms at 24 h due to the retarded release from the nanocarrier (**Figure 4.37C**). In the other hand, the TH release was also studied in pluronic gels (GP-TH and GP-TH-NP-T-) for 72 h (**Figure 4.37D**). In this case, the sustained release can be observed for both formulations, adjusted to sigmoidal mathematical equation, presenting no significant differences between them (**Figure 4.37E**).

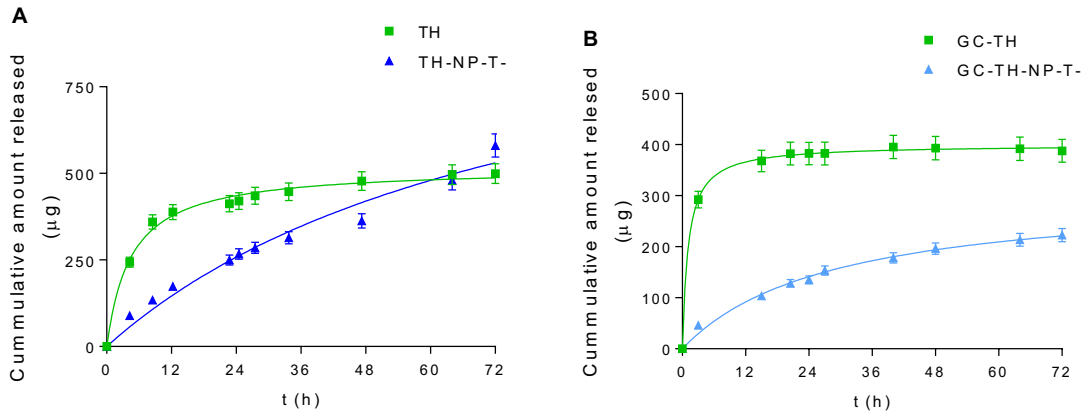

C	TH	TH-NP-T-	GC-TH	GC-TH-NP-T-
Bmax	69.06 ± 1.29	148.30 ± 27.72 *a c d*	53.29 ± 1.08	41.09 ± 2.04 *a*
Kd	4.54 ± 0.46	79.36 ± 23.41 *a c d*	1.10 ± 0.28	28.28 ± 3.33 *a c*
r^2	0.9971	0.9897	0.9997	0.9974
%r 24 h	56.01 ± 5.59	35.64 ± 3.51 *a c*	51.02 ± 6.4	18.01 ± 1.79 *a b c*
SSD ($p < 0.05$)	*a*	*b*	*c*	*D*

%r: amount of TH released, SSD: statistically significant differences

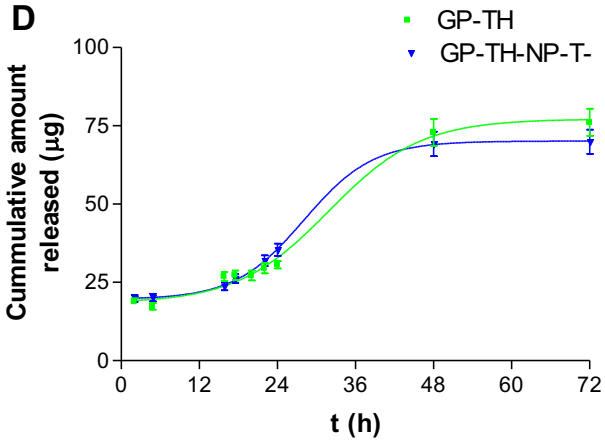

E	GP-TH	GP-TH-NP-T-
Bottom	18.35 ± 2.02	19.57 ± 1.82
Top	77.18 ± 2.48	70.12 ± 1.75
V50	31.91 ± 1.98	28.06 ± 1.72
Slope	7.06 ± 1.32	5.31 ± 1.64
r^2	0.9685	0.9717
%r 24 h	2.45 ± 0.16	2.83 ± 0.27

%r: amount of TH released

Figure 5.37. *In vitro* release profile of (A) TH and TH-NP-T- and (B) GC-TH and GC-TH-NP-T-, obtained adjusted to hyperbola equation. (C) Data of release parameters of A and B and the cumulative amount released (%) within 24 h. (D) GP-TH and GP-TH-NP-T-, obtained adjusted to sigmoidal equation and (E) Data of release parameters of D and the cumulative amount released (%) within 24 h. Data are expressed as Mean ± SD, statistical analysis performed by one-way ANOVA Tukey´s multiple comparison test.

Ex vivo Skin Permeation

The skin penetration of TH and TH-NP-T- were evaluated in *ex vivo* human skin using different types of dosage forms (aqueous and gels). In the first study (**Table 4.12**), when TH-NP-T- was compared to TH as aqueous forms, it was found that the rate of penetration was more sustained when encapsulated. Statistically significant differences were obtained for the flux (*J*), permeation constant (*Kp*) and total amount penetrated in 24 h (*Ap*).

In the case of their carbomer gel formulations, the permeation parameters obtained also presented statistically significant differences between them. Additionally, it can be observed that both gels presented significant differences compared to their aqueous forms, performing a much slower permeation rate. The cumulative amount found in the receptor fluid was also higher for the aqueous formulations than the gel being significantly higher for TH compared to TH-NPs (aqueous and gels). Moreover, the amounts retained inside the skin were found to be similar for all the formulations (**Figure 4.38A**), although, in both cases aqueous and gels, it was slightly higher for TH-NPs, and additionally, TH-NP-T- presented significant differences compared to both gels. When comparing the penetration depth of different semi-solid formulations of TH-NP-T-, it could be observed that depending on the vehicle used, the permeation parameters varied accordingly (**Table 4.13**). The highest values of all parameters were found for GP-TH-NP-T-, meanwhile GH-TH-NP-T- and GP-TH-NP-T- were similar, presenting statistically significant differences. The same was observed for the total amount retained inside the skin (**Figure 4.38B**).

A second study was performed with different skin donors than the previous experiment and the full skin layers including the fat-tissue were used to access information of the penetration depth until the hypodermis. The total amount found in the receptor fluid for GC-TH and GC-TH-T- were similar (**Table 4.14**). However, the total amount retained inside the skin (**Figure 4.38C**) was found to be significantly higher for TH, which raises the idea that GC-TH could be found retained in the fat tissue, whereas GC-TH-NP-T- could be only retained along the epidermis and dermis layers, resulting in lower total amount found inside the skin. Previous authors stated that the fat tissue may serve as a deep compartment for the drug, delaying entry into the blood (Calpena et al. 2011).

Table 4.12. *Ex vivo* skin penetration parameters of TH and TH-NP-T- dosage forms.

Parameter	**TH**	**TH-NP-T-**	**GC-TH**	**GC-TH-NP-T-**
J (μg/cm²/h)	9.36 ± 0.31 *b c d*	2.95 ± 0.15	2.53 ± 0.77	1.37 ± 0.20 *b c*
Kp (cm²/h)	2.74E-03 ± 1.240E-04 *b c d*	1.18E-03 ± 6.17E-05	1.01E-03 ± 3.08E-04	5.46E-04 ± 8.08E-05 *b c*
Ap (μg/cm²)	85.45 ± 9.63 *b c d*	71.56 ± 10.50 *c d*	38.79 ± 2.98	22.83 ± 3.78 *c*
SSD (p<0.01)	*a*	*b*	*c*	*d*

J: flux, Kp: permeability constant, Ap: total amount penetrated. Statistical analysis one-way ANOVA Tukey´s multiple comparison test.

Table 4.13. *Ex vivo* skin penetration parameters of TH-NLC incorporated in carbomer, HPMC and pluronic gels.

Parameter	**GC-TH-NP-T-**	**GH-TH-NP-T-**	**GP-TH-NP-T-**
J (μg/cm²/h)	3.85 ± 1.52 *b c*	1.34 ± 1.14	1.37 ± 0.19
Kp (cm/h)	1.54E-03 ± 6.09E-04 *b c*	5.36E-04 ± 5.65E-05	5.47E-04 ± 7.43E-05
Ap (μg/cm²)	72.11 ± 6.82 *b c*	51.73 ± 4.89	57.94 ± 2.21
SSD (p<0.05)	*a*	*b*	*c*

J: flux, Kp: permeability constant, Ap: total amount penetrated, SSD: statistically significant differences. Statistical analysis one-way ANOVA Tukey´s multiple comparison test.

Table 4.14. *Ex vivo* skin penetration of GC-TH and GC-TH-NP-T- performed with full-fat skin tissue.

Parameter	**GC-TH**	**GC-TH-NP-T-**
J (μg/cm²/h)	n.t	n.t
Kp (cm²/h)	n.t	n.t
Ap (μg/cm²)	33.56 ± 3.67	35.47 ± 10.55
n.t: not tested		

The skin penetration of GC-TH-NP-T- after 24 h was evaluated by SEM using cryo-cuts of the skin tissue. Images of untreated and treated skins are displayed in **Figure 4.39A-B**, respectively. As it can be observed, the gel matrix containing TH-NPs was found inside the skin layers.

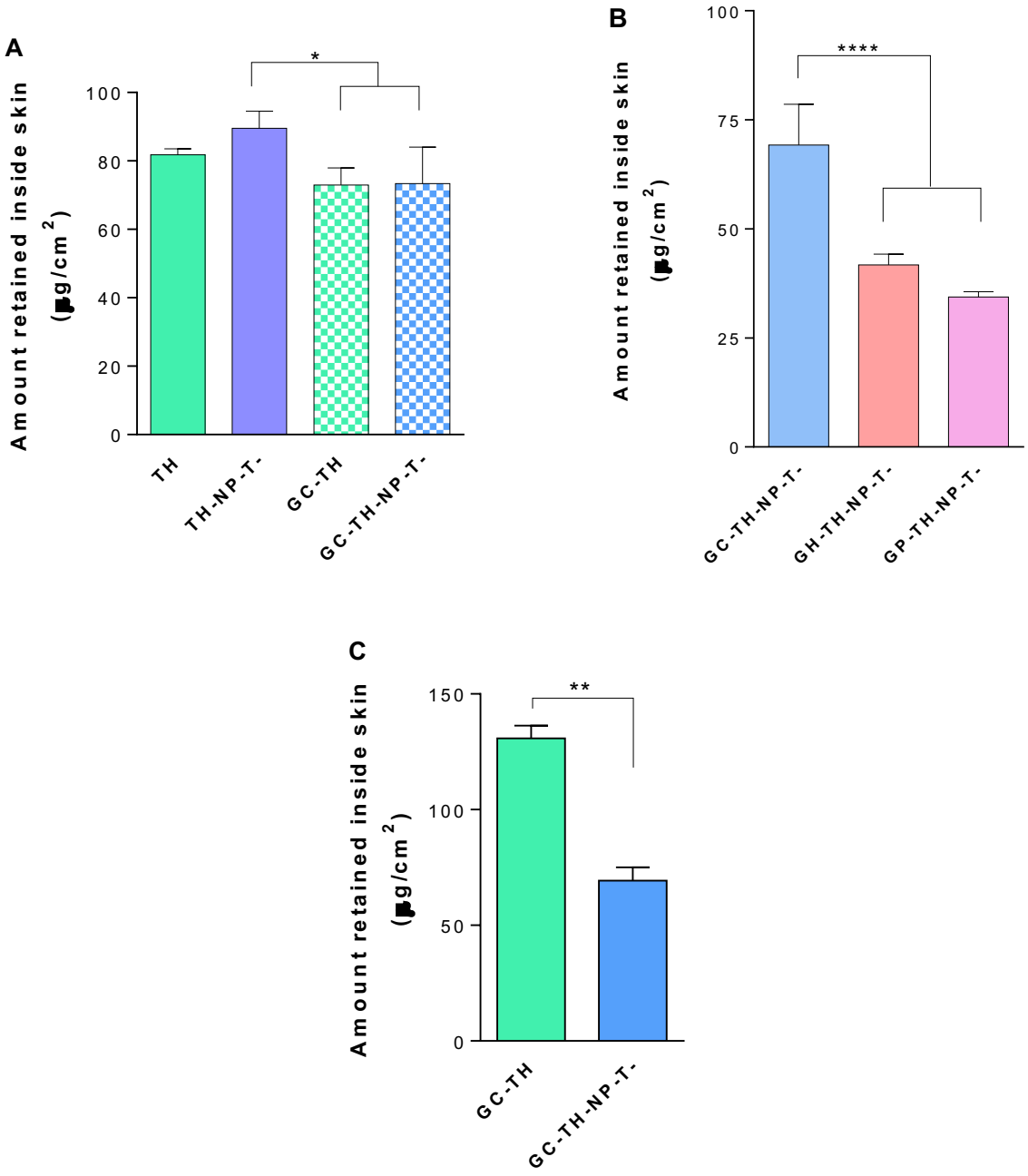

Figure 4.38. *Ex vivo* skin penetration for 24 h with the total amount retained inside the skin via extraction technique. (A) TH and TH-NP-T- aqueous and carbomer gels, (B) TH-NP-T-P carbomer, HPMC and pluronic gels and (C) GC-TH and GC-TH-NP-T- (using full skin fat tissue). Data are expressed as mean ± SD (n=3). Statistical analysis one-way ANOVA, Tukey´s multiple comparison test.

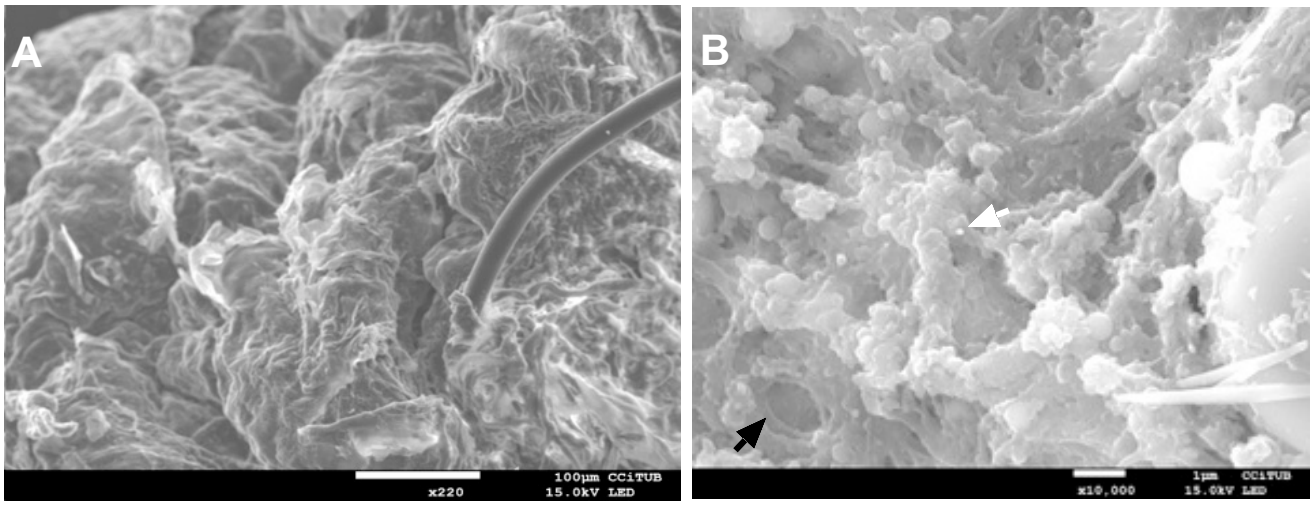

Figure 4.39. SEM images of *ex vivo* skin (A) untreated and (B) GC-TH-NP-T- permeation for 24 h. Scale bar: 10 µm (x300) and 1 µm (x10.000), respectively. The GC-TH-NP-T- matrix and the presence of the NPs are indicated by the black and white arrows, respectively.

4.4.3. Therapeutic Efficacy

In vitro Antimicrobial Efficacy

The antimicrobial activity of carbomer and pluronic gels of TH and TH-NP-T- were tested in contact with *C. acnes* for 3 h, at concentrations of 1 mg/mL. Results showed that carbomer gels (**Figure 4.40A**) detained the microbial viability of *C. acnes* within 2 h, meanwhile pluronic gels (**Figure 4.40B**) performed a sustained behaviour, since this gel formulation at 32 °C increases its initial gellification viscosity. This is in agreement with the release study. In the other hand, when carbomer gels where tested with *S. epidermidis* (**Figure 4.40C**), GC-TH abolished microbial viability within 3 h, whereas GC-TH-NP-T- still maintained a few colonies alived within 48 h contact. Therefore, nanostructured system of thymol provide fast activity against the major acne pathogen, while not affecting dramatically the healthy skin microbiota.

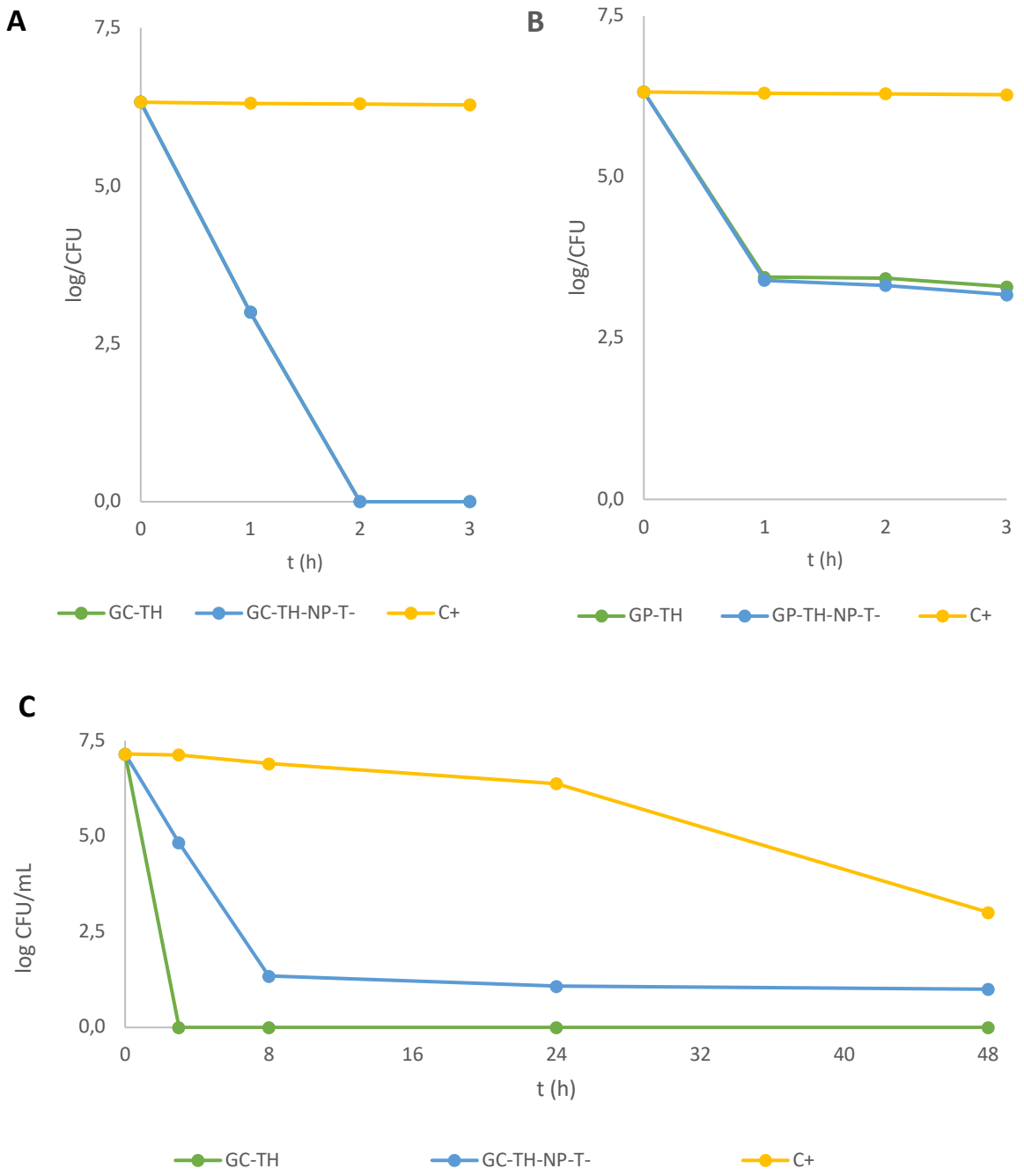

Figure 4.40. Bacterial viability assay with *C. acnes* for 3 h of (A) GC-TH and GC-TH-NP-T- and (B) GP-TH and GP-TH-NP-T-; and with *S. epidermidis* for 48 h of (C) GC-TH and GC-TH-NP-T-.

The antimicrobial activity was also assessed by SEM. The structure of untreated *C. acnes* is shown in **Figure 4.41A**, presenting a rod-shape and smooth membrane. When the bacteria were treated with GC-TH or GC-TH-NP-P- (**Figure 4.41B-C)** respectively, the cells were elongated, and the envelope thickened. In the case of GC-TH, the effect was more aggressive due to fast TH release, where the cell

membrane also presented development of blebs on the surface. **Figure 4.41D** presents the GC-TH-NP-P gel matrix entrapping the bacteria.

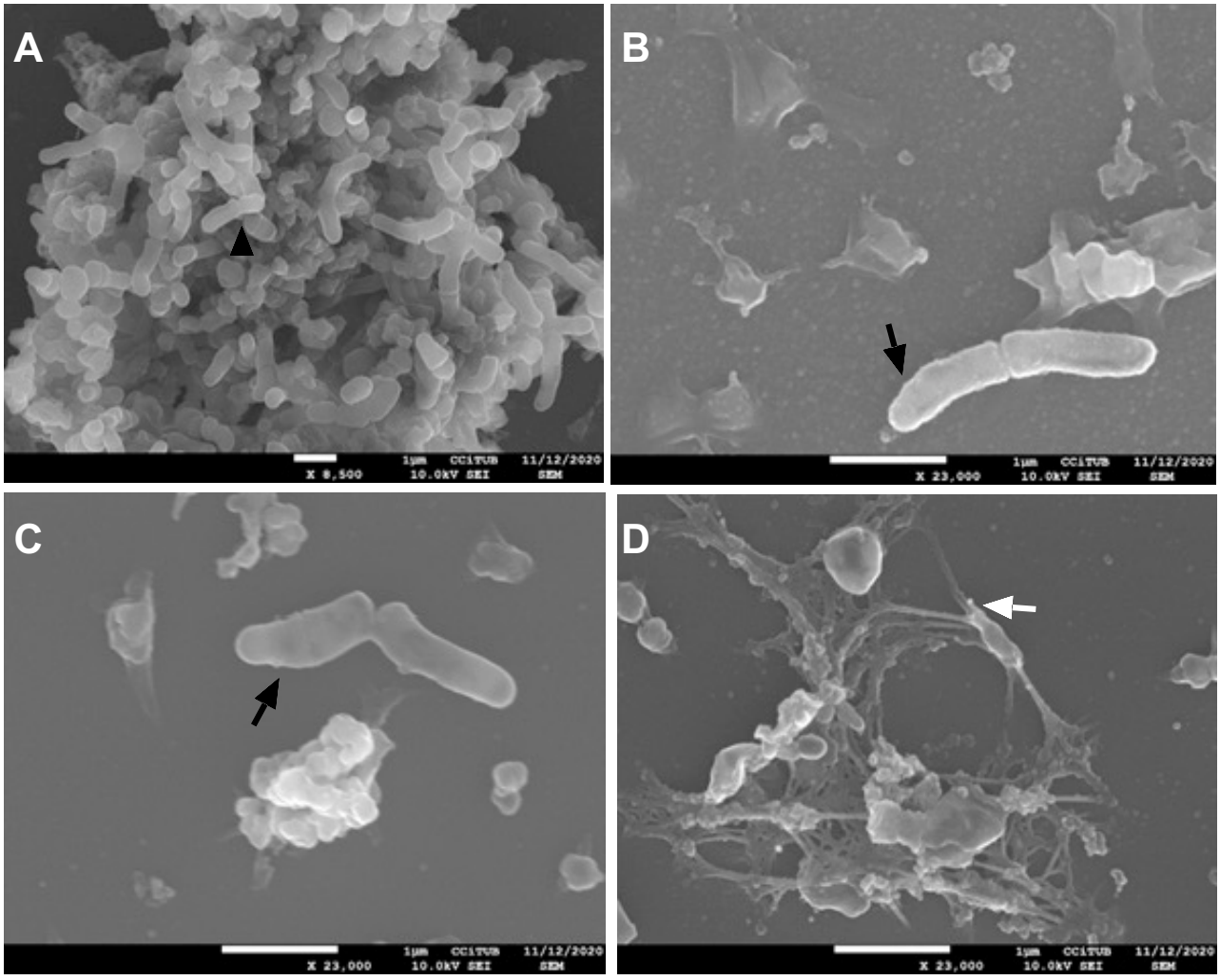

Figure 4.41. SEM micrographs of *C. acnes* (A) control and treated for 1 hour with (B) GC-TH or (C-D) GC-TH-NP. Black arrows indicate membrane disruption and white arrow points TH-NP-P-.

In vivo Biomechanical Properties

The biomechanical properties of GC-TH, GC-TH-NP-P-, GC-THO and GC-THO-NP-L- (**Figure 4.42**) (A-B, C-D, E-F, G-H, respectively) were evaluated on the forearm of 12 voluntaries, measuring the basal levels and after application during 2 h, of the SC hydration (Corneometer®) and the transepidermal water loss (TEWL®), respectively. Results provided no statistically significant differences compared to

the basal measure, in most of the cases, providing no hydration effect and do not disturbing the SC barrier function. There were only significant differences ($p < 0.05$) after 2 h application of GC-TH-NP-P- on the reduction of TEWL. This could be associated to the previous studies of the skin penetration route by confocal microscopy, where TH-NPs presented a delayed entry of particles remained on the SC, due to the slow penetration rate. Additionally, GC-TH and GC-THO-NP-L- also showed a decrease of TEWL, although not significant, while GC-THO provided no effect.

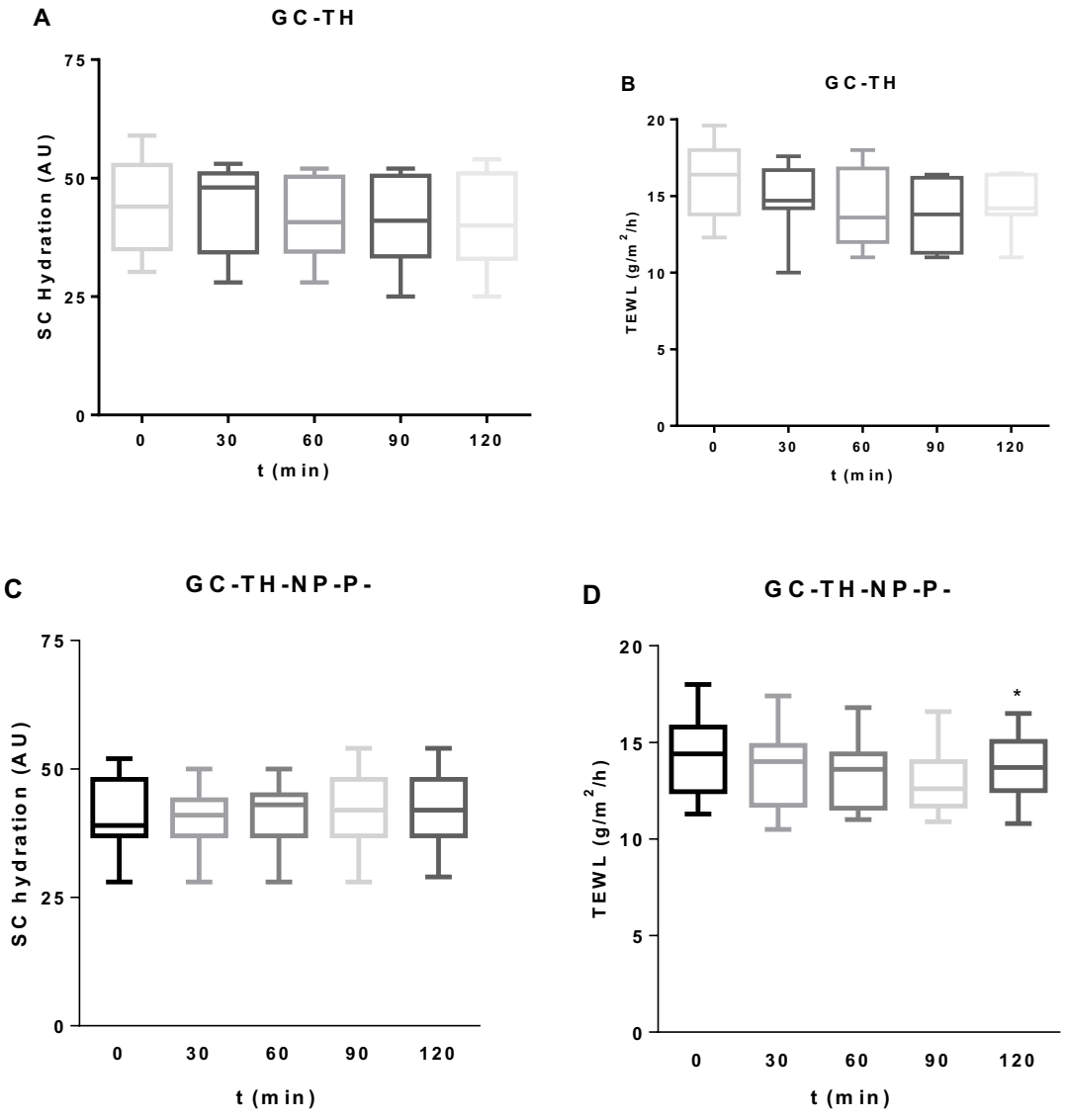

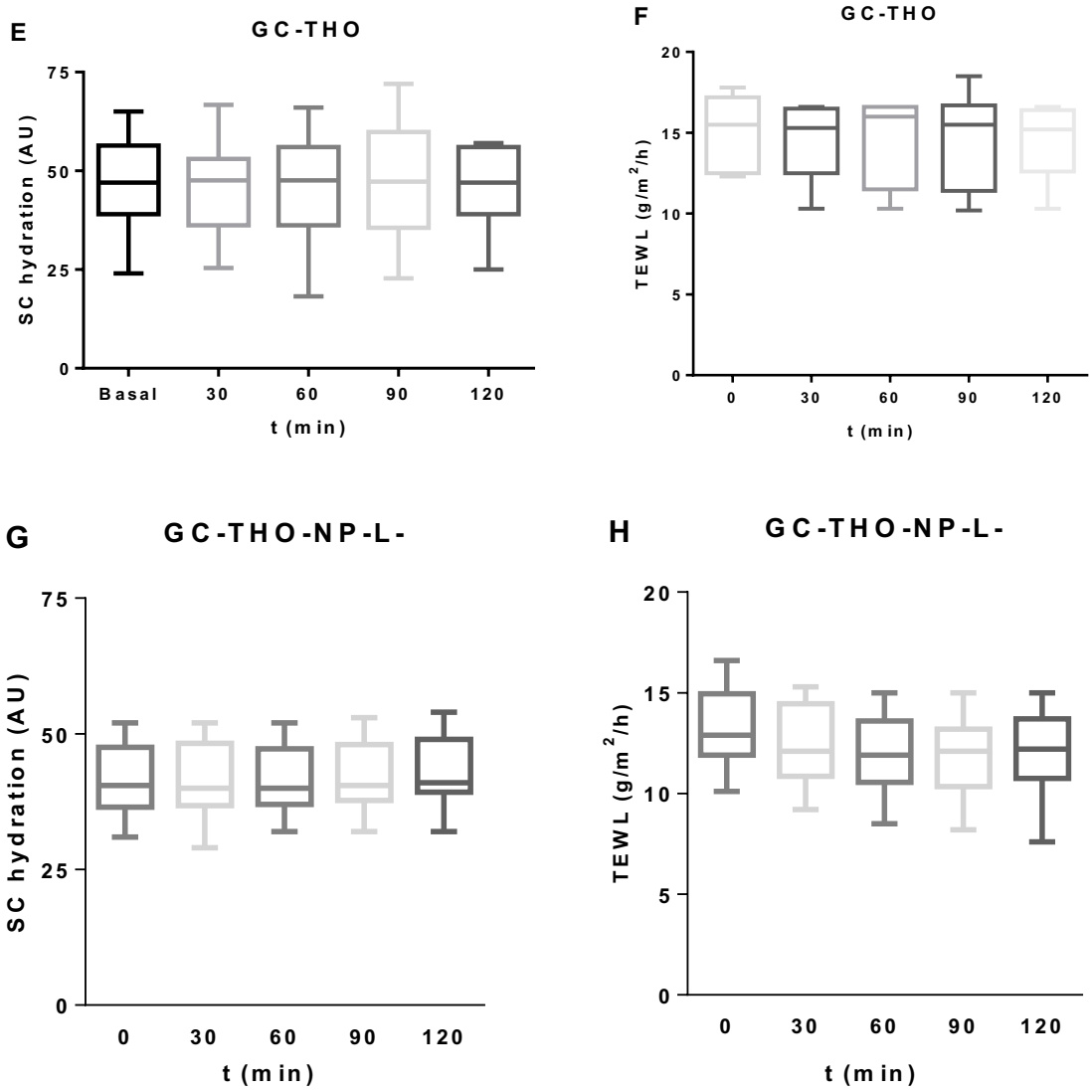

Figure 4.42. *In vivo* biomechanical properties evaluated on the forearem of vounteers (n = 12) of carbomer gel formulations for hydration of SC measured by Corneometer® and TEWL, respectively: (A-B) GC-TH, (C-D) GC-TH-NP-P- (E-F) GC-THO and (G-H) GC-THO-NP-L-. Statistical analysis performed as mean ± SD values (n = 12), non-parametric Wilcoxon paired test comparing each measure against basal level (t0).

In vivo Sebum-Regulator Efficacy

The skin sebum was measured using Sebumeter® in the forehead of 10 volunteers, before and after application of carbomer gels during 1.5 h. Results showed that the sebum reduction activity was found to be higher for GC-TH (**Figure 4.43A**) compared to GC-TH-NP-P- (**Figure 4.43B**). Statistically significant differences (*$p < 0.05$) could be observed, compared to basal level (t0), at all measured times for GC-TH while GC-TH-NP-P- was only significant at 60 min. However, GP-TH and GP-TH-NP-P- (**Figure 4.43C-D**) respectively, the effect was found similar where both presented significant differences against the basal level ($p < 0.05$). Moreover, higher activity could be observed comparing

pluronic gels against carbomer gels, which could be related to a thick and dry covering layer that this gel performs on the skin (Carvajal-Vidal et al. 2020). For all formulations, it can be observed that within 90 min, the values started to increase, meaning that the sebum levels are returning to the basal level. In contrast, when the application was continuous for 28 days, with daily application hemi-face, the activity was found much higher for GC-TH-NP-P- than GC-TH (**Figure 4.44A**), presenting statistically significant differences (**p < 0.01). Moreover, the overall sebum reduction in 28 days were by 29.8 ± 14.9 and 49.9 ± 19.1 % for GC-TH and GC-TH-NP-P-, respectively (**Figure 4.44B**). Therefore, TH has fast sebum reduction efficacy in short-term use, whereas in long-term treatment, the encapsulated dosage form increases its activity by 1.7 times.

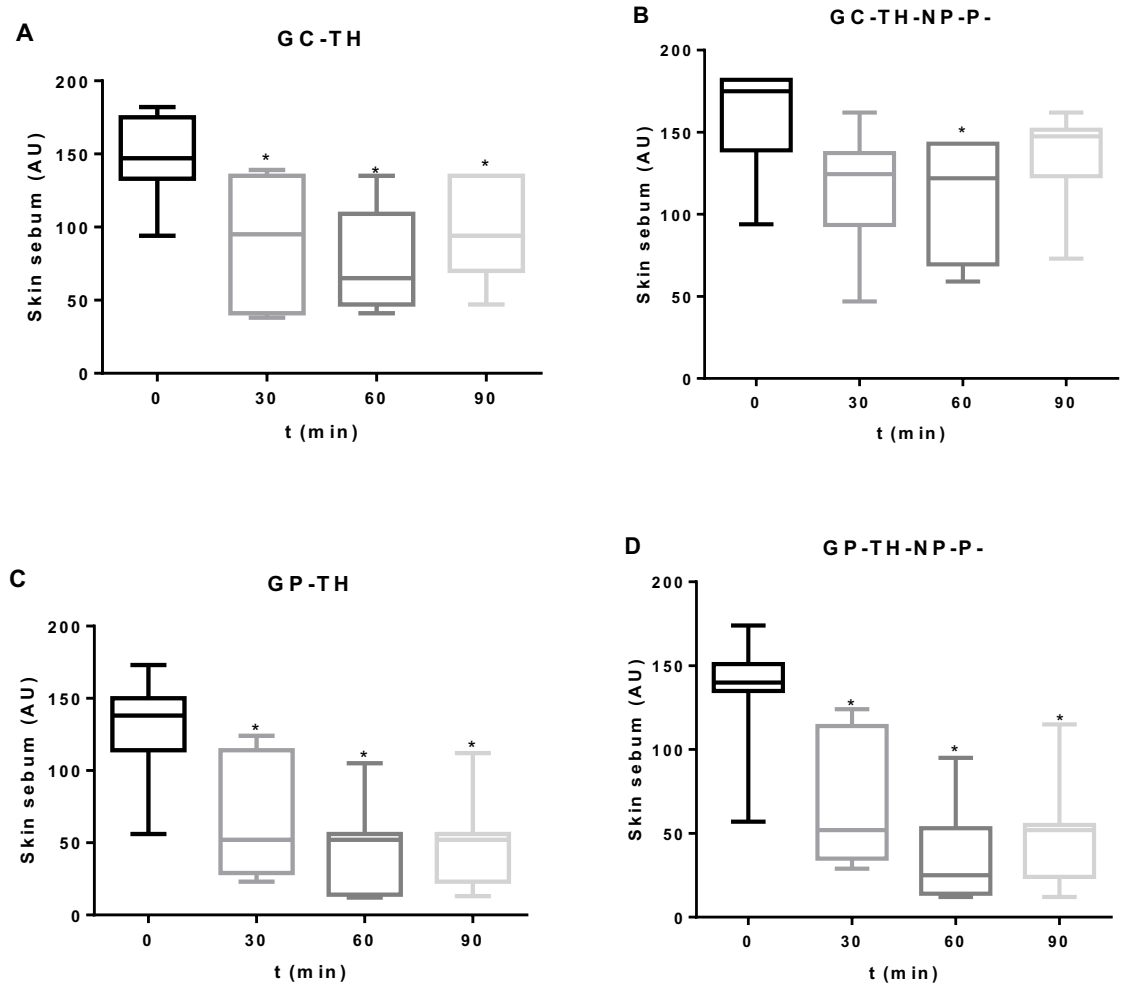

Figure 4.43. *In vivo* sebum control measured by Sebumeter® for (A) GC-TH, (B) GC-TH-NP-P-, (C) GP-TH and (D) GP-TH-NP-P- on the forehead of volunteers. Statistical analysis performed as mean ± SD values (n = 7), non-parametric Wilcoxon paired test comparing each measure against basal value (t0).

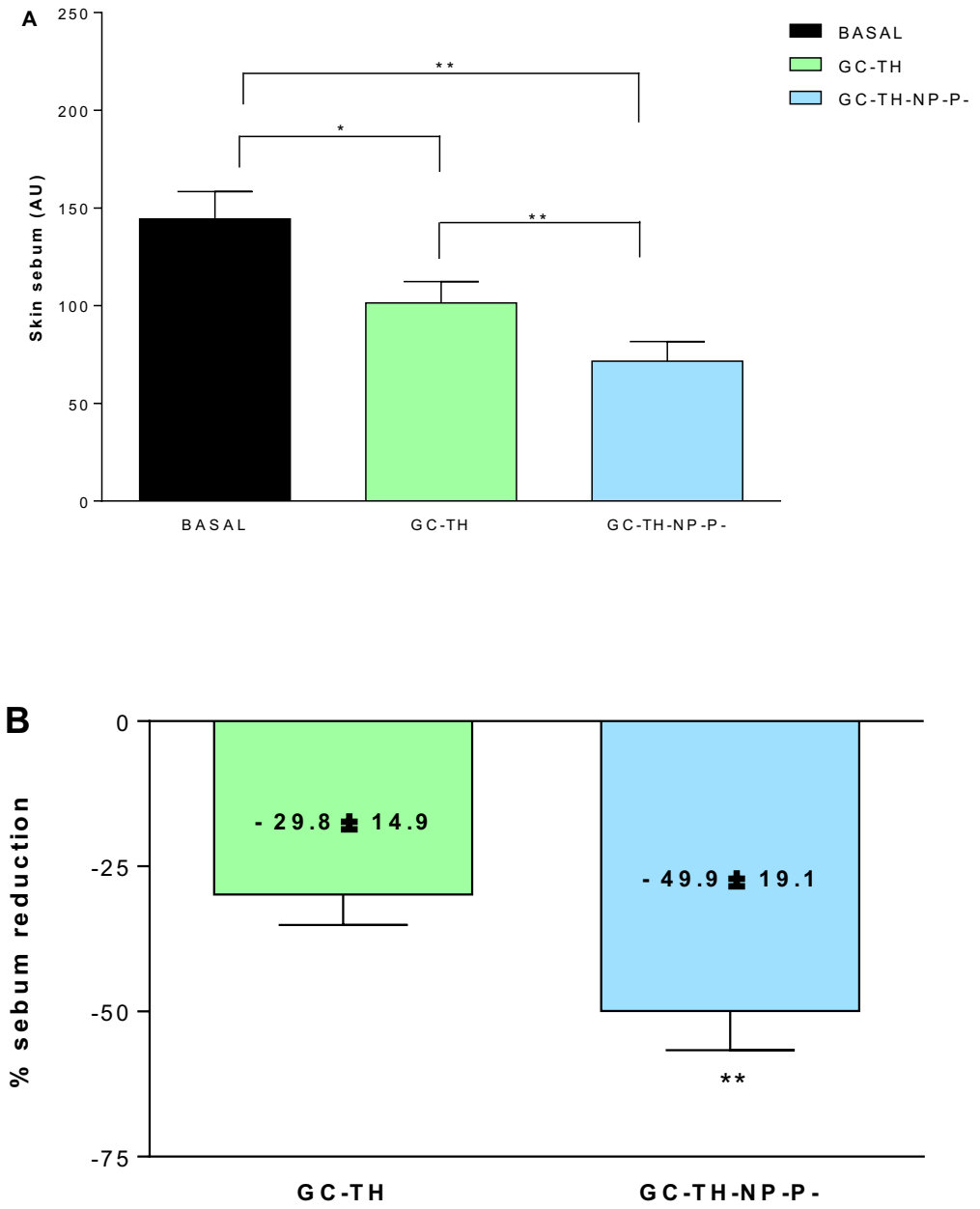

Figure 4.44. *In vivo* sebum regulator activity of GC-TH and GC-TH-NP-P- over 28 d daily application hemi-face in 10 volunteers with acne and/or oily skin measured by Sebumeter®. (A) Before and at the end of the treatment. (B) % of sebum reduction from the basal levels after each treatment. Statistical analysis performed as mean ± SD values (n = 10), non-parametric Wilcoxon paired test comparing each measure against basal value (t0).

4.5. Thymol-Loaded Nanostructured Lipid Carriers

TH was loaded to lipid nanoparticles, based on Compritol ATO888, by high energy ultrason method, , described previously (3.3.1), with the aim to atained a prolongued release of active on the site of action and protects the, improving its bioavailability on the skin.

4.5.1. Formulation, Characterization and Optimization

Pre-formulation studies

The selection of NLC lipid components and their ratios were optimized by means of DSC by analizing their thermal interactions and results are shown **in Figure 4.45**. The solid lipid (SL) was C188 but the liquid lipids (LL) were variable.

In the case of LAS (LL1), it can be observed that in the mixtures without Thymol (blank mixtures) (**Figure 4.45A**) different ratios of lipids do not alter the melting point of the lipid structure, presenting values around 70 ± 0.9 °C. However, after adding TH at 0.5 % (**Figure 4.45B**), the melting point of the mixtures was slightly decreased to 69 ± 0.5 °C In addition, no melting point modifications were observed when modifying the proportions (60:40 to 90:10).

In the case of MGL (LL2), it can be observed that the blank mixture provided melting point values ranging from 67 to 71 °C (**Figure 4.45C**) and by adding TH, these were also decreased up to 64 to 69 °C (**Figure 4.45D**). Additionally, for both combinations of lipids, the incorporation of TH was well blended since no peaks of TH were found at 51 °C in the lipid mixture thermograms. Therefore, both liquid lipids were suitable for the development of TH NLC, however, LL1 was a better option due to minimal variety of NLC melting point. Moreover, TH presented better solubility in LAS than MGL. The ratios of SL:LL showed a soft mixture (60:40), medium soft (70:30) and hard (80:20 and 90:10). The mixture of 70:30 was found the most suitable TH lipid encapsulation.

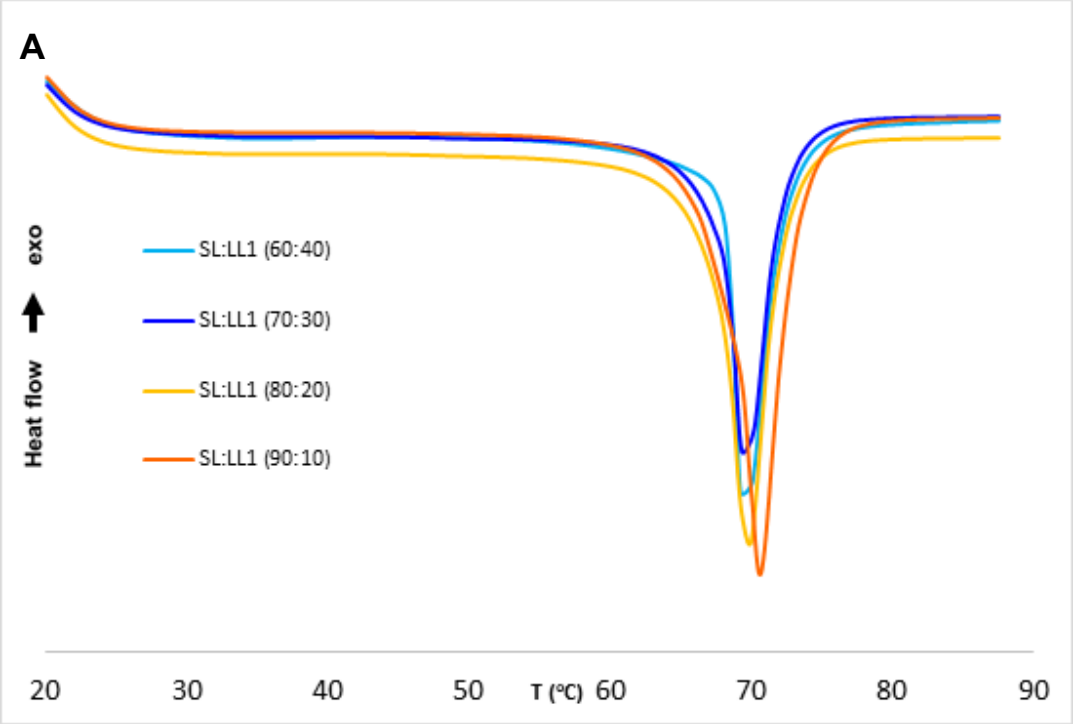
A
exo
Heat flow
SL:LL1 (60:40)
SL:LL1 (70:30)
SL:LL1 (80:20)
SL:LL1 (90:10)
20
30
40
50
T (°C)
60
70
80
90

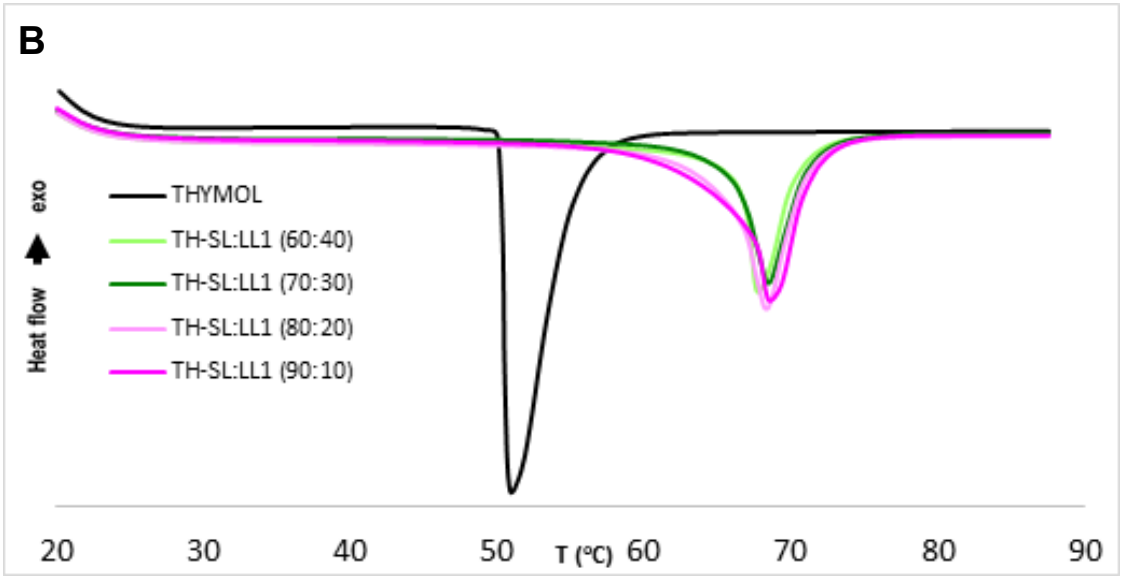
B
exo
Heat flow
THYMOL
TH-SL:LL1 (60:40)
TH-SL:LL1 (70:30)
TH-SL:LL1 (80:20)
TH-SL:LL1 (90:10)
20
30
40
50
T (°C)
60
70
80
90

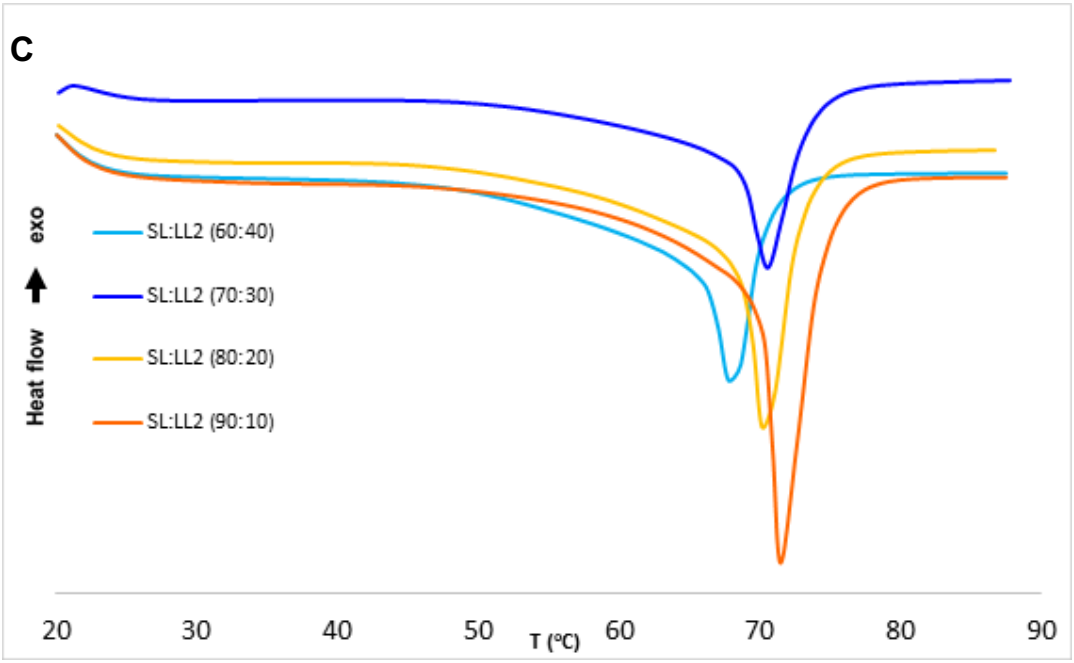

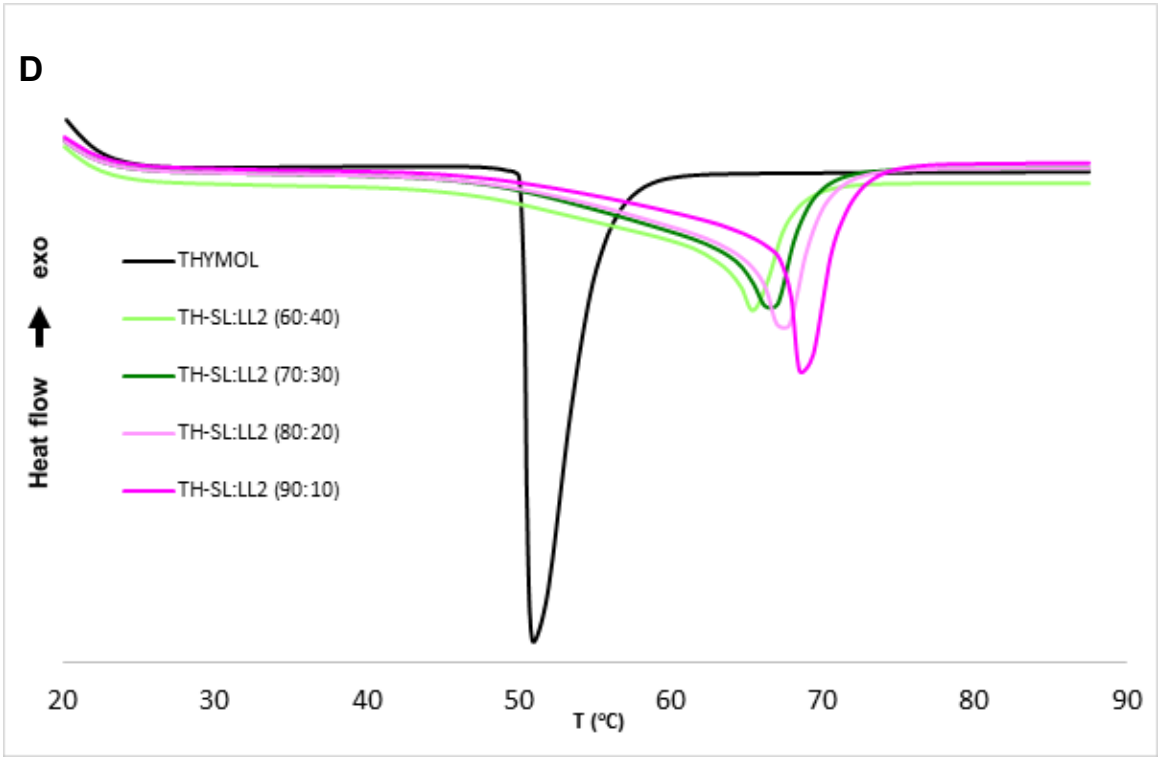

Figure 4.45. DSC thermograms of lipid mixtures using the solid lipid with 2 different liquid lipids, with or without thymol: (A) C188-LAS, (B) C188-LAS-TH, (C) C188-MGL and (D) C188-MGL-TH.

Optimization of TH-NLC

Optimization of TH-NLC was carried out by physicochemical characterization of the two preparation methods, followed by a DoE. Results obtained by TH-NLC by the two preparation methods showed minimal variations, but mostly the Z_{av} using HPH were slightly smaller (**Table 4.15**). Moreover, higher homogeneity of these systems was obtained, in both cases, with higher concentrations of surfactant (TW 1.6 %) and the best results using the lipid mixture of 70:30.

Table 4.15. Comparative physical chemical characterization of TH-NLC produced at 2 variable factors (lipid proportion and surfactant concentration) and variable preparation methods.

		High pressure homogenization		Ultrasound	
SL:LL	TW (%)	Zav	PI	Zav	PI
90:10	1	173.6 ± 2.2	0.227 ± 0.021	301.7 ± 2.1	0.259 ± 0.013
80:20	1	176.6 ± 3.3	0.280 ± 0.030	206.0 ± 4.5	0.218 ± 0.027
70:30	1	156.9 ± 3.7	0.192 ± 0.010	246.7 ± 5.5	0.189 ± 0.030
60:40	1	217.8 ± 5.1	0.175 ± 0.029	298.8 ± 32.2	0.359 ± .045
90:10	1.6	123.8 ± 3.0	0.139 ± 0.021	326.8 ± 4.9	0.271 ± 0.007
80:20	1.6	197.4 ± 3.9	0.113 ± 0.039	265.1 ± 6.4	0.181 ± 0.022
70:30	1.6	218.4 ± 3.4	0.135 ± 0.018	250.9 ± 2.9	0.139 ± 0.023
60:40	1.6	263.7 ± 0.7	0.186 ± 0.016	360.0 ± 17.9	0.223 ± 0.020

Based on the results obtained above, a DoE was carried out developing a central factorial design with two levels and two factors including a central point (SL:LL 70:30 and TW 1.6 %). Besides the Zav values were smaller using HPH method, the US was selected to carry out the DoE, due to the fact that for skin penetration, values between 200 – 400 nm are suitable and additionally, values for the central point were similar for both methods. The results of the DoE with the dependent variables of Z_{av}, PI and EE % are showed in **Table 4.16**. The value corresponding to the central point showed the lower PI and the highest EE %, and this was optimized for the following studies. The surface responses of the DoE are showed in **Figure 4.46** and no statistically significant differences between the levels applied were obtained. Results illustrate by the colour that the area of suitable values, lowest for Zav and PI and highest for EE, are broad in the combination of the variable factor. Therefore, the central point was the optimized formulation selected for further studies in this work.

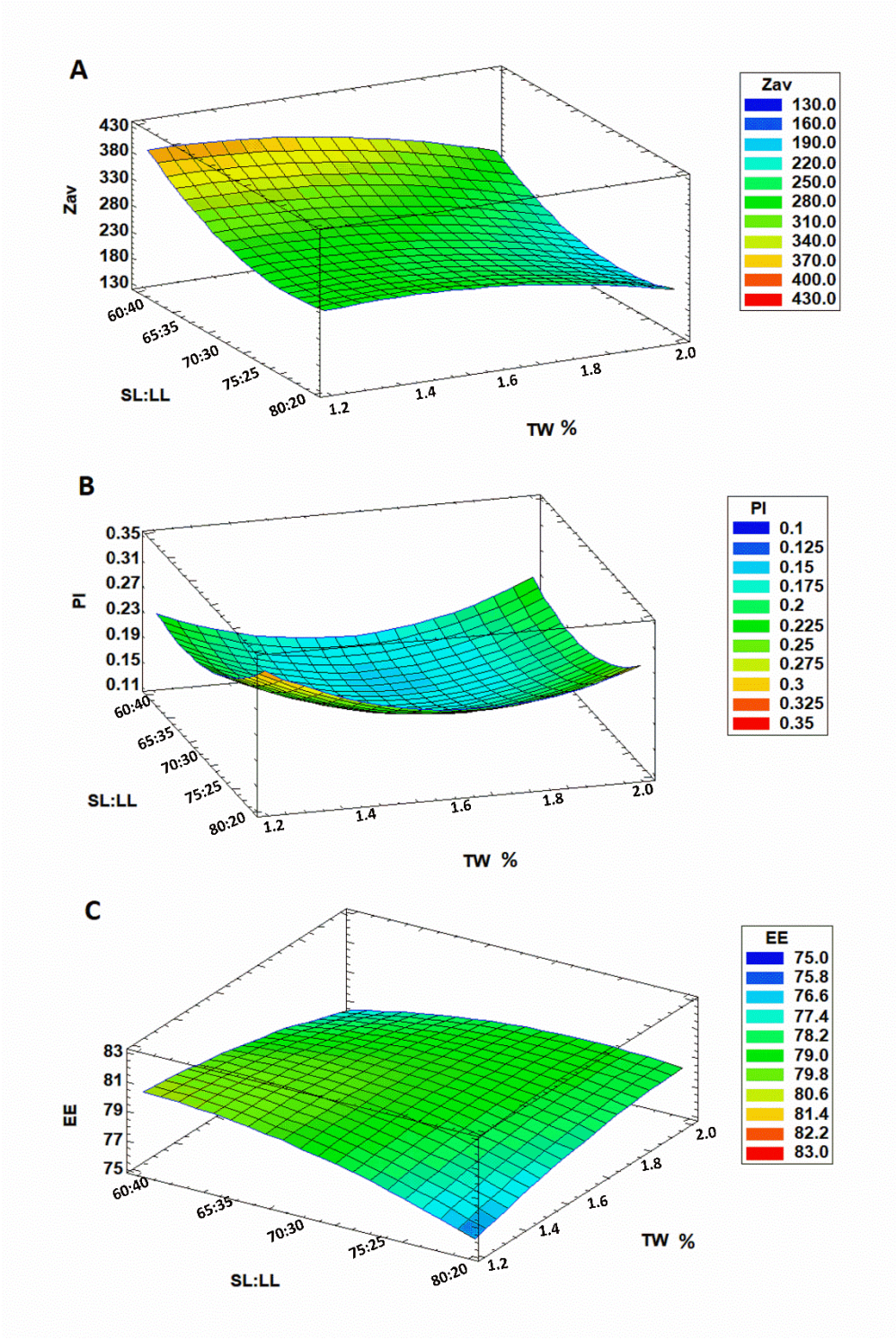

Figure 4.46. Surface response of TH-NLC-T- by DoE using TH 0.5 % of (A) Zav (nm), (B) PI and (C) EE (%).

Table 4.16. DoE performed by two levels two factors with 2 central points. Responses of physicochemical characterization of TH-NLC produced at 2 variable factors (lipid proportion and surfactant concentration) via ultrasound are shown as Zav and PI.

Levels		Independent factors		Response factors		
SL:LL	**TW**	**SL:LL (%)**	**TW (%)**	**Zav (nm)**	**PI**	**EE (%)**
-1	-1	60:40	1.2	361.3 ± 34.1	0.213 ± 0.017	81.26 ± 0.09
-1	0	60:40	1.6	350.6 ± 20.1	0.202 ± 0.003	76.98 ± 1.98
-1	+1	60:40	2.0	327.3 ± 45.1	0.215 ± 0.052	77.82 ± 1.71
+1	-1	80:20	1.2	236.5 ± 21.4	0.288 ± 0.048	76.38 ± 0.15
+1	0	80:20	1.6	286.5 ± 50.9	0.272 ± 0.035	76.53 ± 0.35
+1	+1	80:20	2.0	244.3 ± 21.1	0.216 ± 0.048	79.06 ± 1.59
0	-1	70:30	1.2	351.8 ± 29.5	0.266 ± 0.031	77.33 ± 1.21
0	+1	70:30	2.0	238.6 ± 5.3	0.218 ± 0.013	76.96 ± 1.36
0	0	70:30	1.6	259.3 ± 29.4	0.119 ± 0.031	80.42 ± 1.40
0	0	70:30	1.6	280.0 ± 23.5	0.121 ± 0.042	81.41 ± 0.62

4.5.2. Surface-Functionalization of TH-NLC and Physicochemical Characterization

Furthermore, in order to further optimize TH-NLC formulation, TH-NLC surface was functionalized using different surface functionalization approaches (using either PL, BZ and CS). The results of the obtained TH-NLCs are displayed in **Table 4.17** where it can be observed that the use of either PL or positively charged compounds (BZ and CS) increase the ZP value. Moreover, it can be observed that CS functionalization potentially increases the average particle size of TH-NLC.

Table 4.17. Physical and chemical characterization of TH-NLC surface-functionalized.

	Surface Coating (%)					Evaluated Parameters		
	TW	PL	P407	BZ	CS	Zav (nm)	PI	ZP (mV)
TH-NLC-T-	1.6					270.1 ± 9.8	0.120 ± 0.001	-18.3 ± 0.9
TH-NLC-T-L-	1.6	0.1				265.9 ± 7.4	0.293 ± 0.006	-19.3 ± 0.4
TH-NLC-L-		0.8				260.9 ± 5.2	0.296 ± 0.005	-37.5 ± 1.2
TH-NLC-PP-			0.8			130.2 ± 1.2	0.149 ± 0.014	-13.7 ± 1.8
TH-NLC-T-B+	1.6			0.1		281.3 ± 5.7	0.138 ± 0.011	+26.5 ± 1.2
TH-NLC-T-L-B+	1.6	0.1		0.1		241.3 ± 6.6	0.241 ± 0.021	+27.9 ± 1.9
TH-NLC-T-C+	1.6				0.05	452.0 ± 4.4	0.262 ± 0.035	+30.3 ± 1.1
TH-NLC-T-L-C+	1.6	0.1			0.05	527.5 ± 3.2	0.276 ± 0.019	+35.1 ± 2.3

The short-term stability was predicted by analysing the backscattering profile of the NLC in solution, measured by Turniscan®Lab (**Figure 4.47**). Results show that that the TH-NLC-T- (**Figure 4.47A**) formulations as aqueous suspension along storage will perform particle aggregation (flocculation), and this phenomenon was slightly reduced in TH-NLC-L- (**Figure 4.47B**). This indicates that the phospholipid surface attached maintains the particles more stable in solution, avoiding aggregation. The ZP values for both TH-NLC formulation are in accordance with the backscattering profile since TH-NLC-L- was twice more electronegatively charged than TH-NLC-T-. In the case of these particles modified to positively charged with BZ, it can be observed that TH-NLC-T-B+ (**Figure 4.47C**), the size fluctuation in diminished, and this might indicate particle sedimentation. Meanwhile, for TH-NLC-L-B+ (**Figure 4.47D**), the latter was improved. Even better performance could be observed for the CS-coated, TH-NLC-T-C+ and TH-NLC-L-C+ (**Figure 4.47E-F)**, respectively. In the other hand, TH-NLC-PP- formulation was obtained translucid and with low particle size, and the backscattering performance was favoured (**Figure 4.47G**).

A) TH-NLC-T-

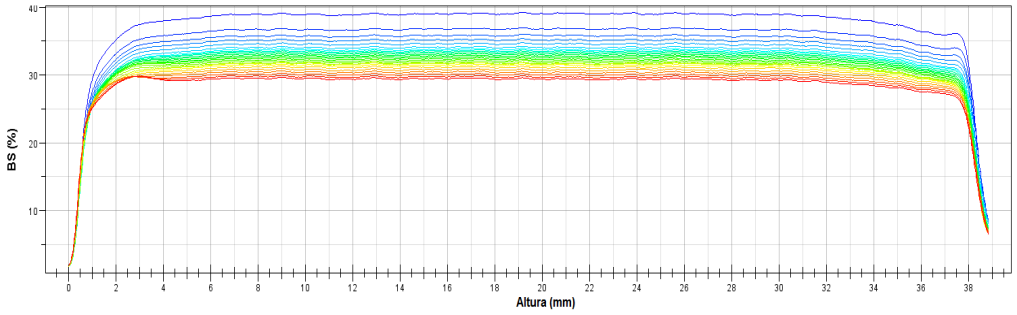

B) TH-NLC-L-

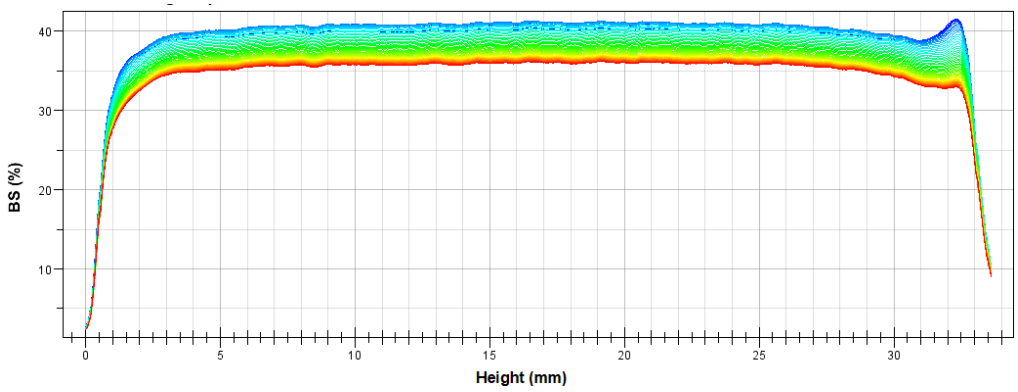

C) TH-NLC-T-B+

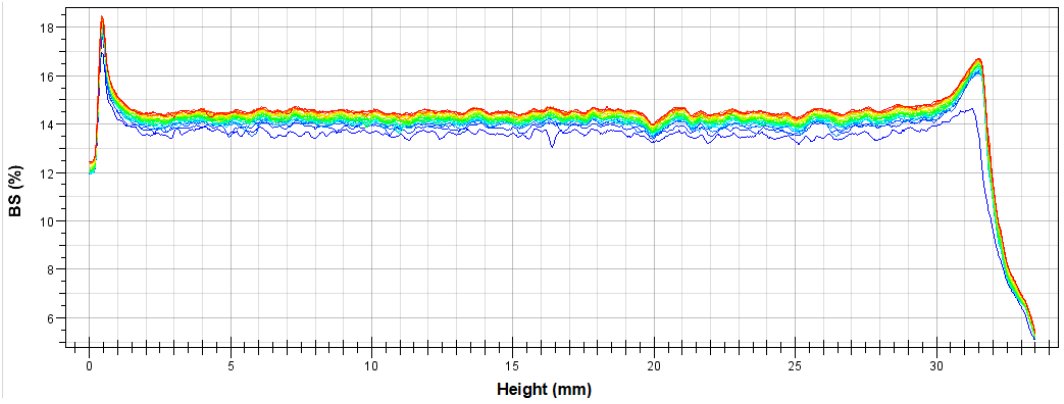

D) TH-NLC-L-B+

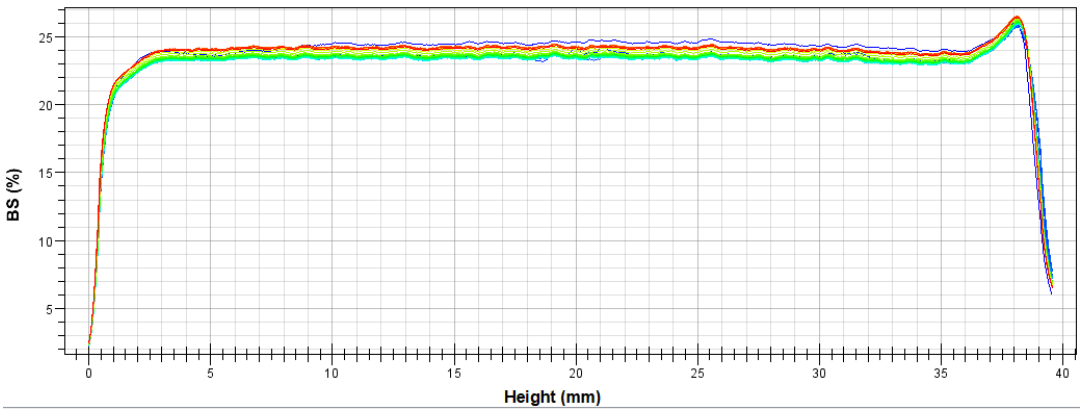

E) TH-NLC-T-C+

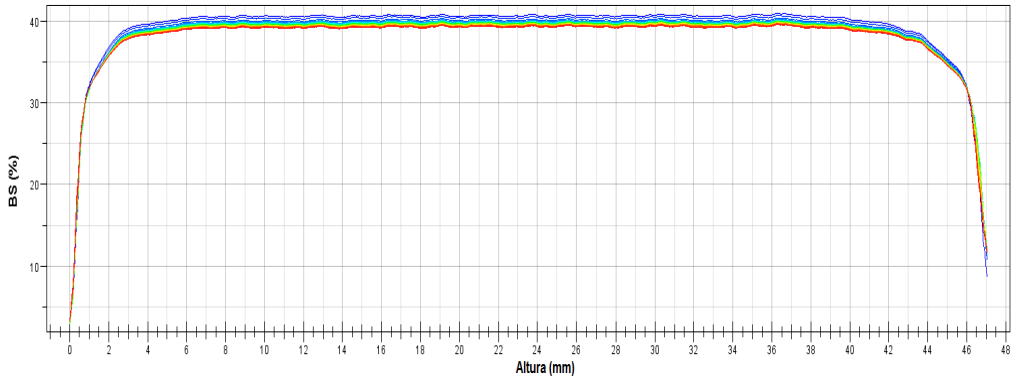

F) TH-NLC-L-C+

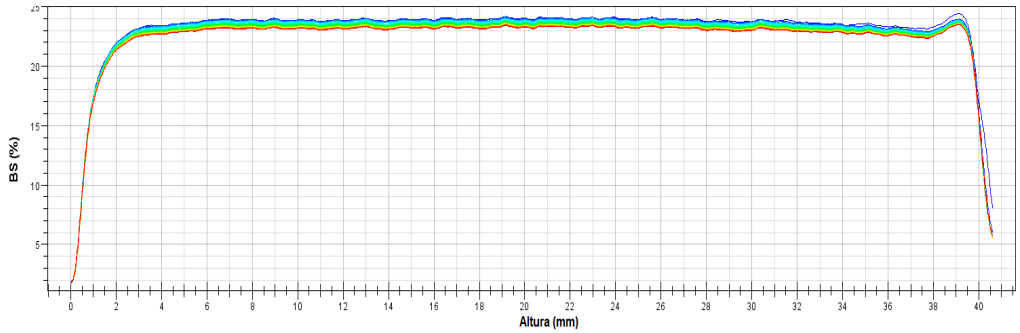

G) TH-NLC-PP-

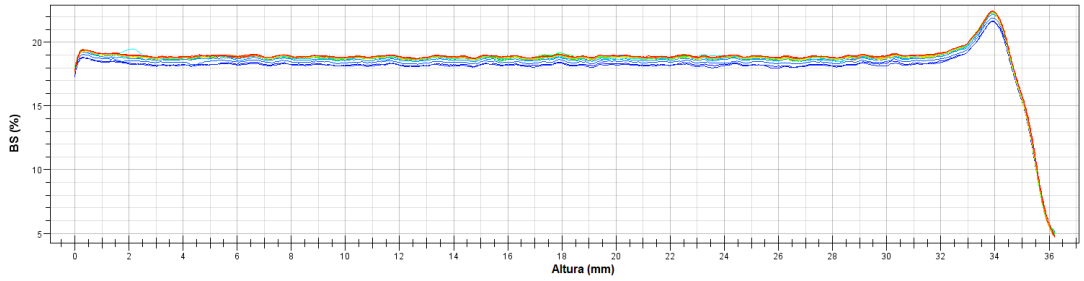

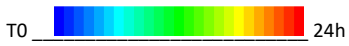

Figure 4.47. Backscattering profile of TH-NLCs, measured by Turbiscan®Lab, with different surface compositions: (A) TW, (B) PL, (C) TW and BZ, (D) PL and BZ, (E) TW and CS, (F) PL and CS, and (G) P407. Scans were performed from the bottom to the top of the vial, measured every hour for 24 h, represented from blue to red lines.

The morphology of the TH-NLC-T- was obtained using TEM images with negative staining showing NLC droplets with semi spherical soft shape (**Figure 4.48A**), characteristic of this type of nanocarrier (Carvajal-Vidal et al. 2019).

4.5.3. Physicochemical and Rheological Characterization of Semi-Solid Formulations

The aqueous formulations of TH or TH-NLC-T- were added at 50 % of final semi-solid dosage forms using carbomer (1 %) and glycerine (5 %). TH-NLC-T- was also added to gels of carbomer (1 %), HPMC (5 %) or pluronic (20%), all using glycerin (5 %).

The morphology of the carbomer gel of TH-NLC-T- was analysed by SEM, showing the gel matrix **Figure 4.48B**) and a closer image (**Figure 4.48C**).

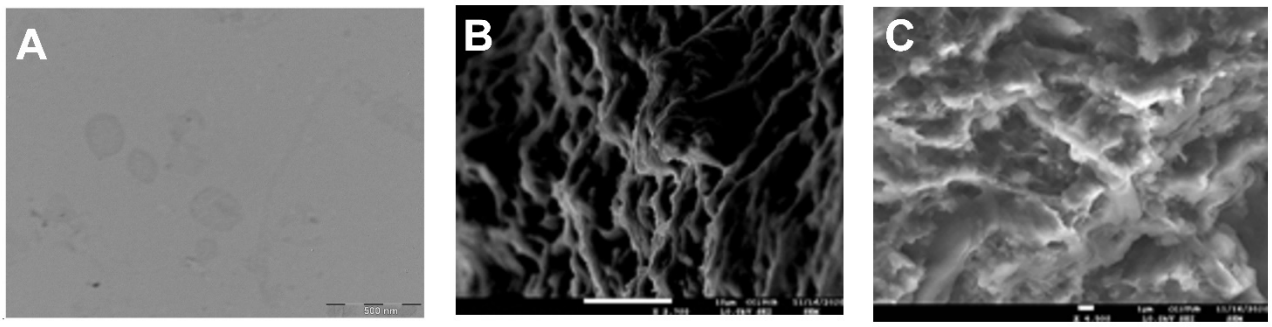

Figure 4.48. Transmission electron microscopy image of (A) TH-NLC-T- (negative staining, scale bar 500 nm). Scanning electron microscopy image of TH-NLC-T- incorporated into carbomer gel (GC-TH-NLC), scale bar (B) 10 µm (x 2.700) and (C) 1 µm (x 4.500).

Short-term Stability of GC-TH-NLC-T-

The short-term stability of TH-NLC-T-, incorporated into carbomer gel, was evaluated by Turbiscan®Lab (**Figure 4.49**). It presented a great stabilization of the initial aqueous formulation (TH-NLC-T-), where the backscattering signal was improved, confirming that no particle size increase or aggregation were predicted. This is related to the macro-gel matrix formed stabilizing the particles. Therefore, incorporation of NLC formulations into semi/solid formulations is a great approach for nanosystem stabilization. Furthermore, the pH of the gel formulations was measured for 6 m at RT, remaining stable and no colour, odour or appearance have changed.

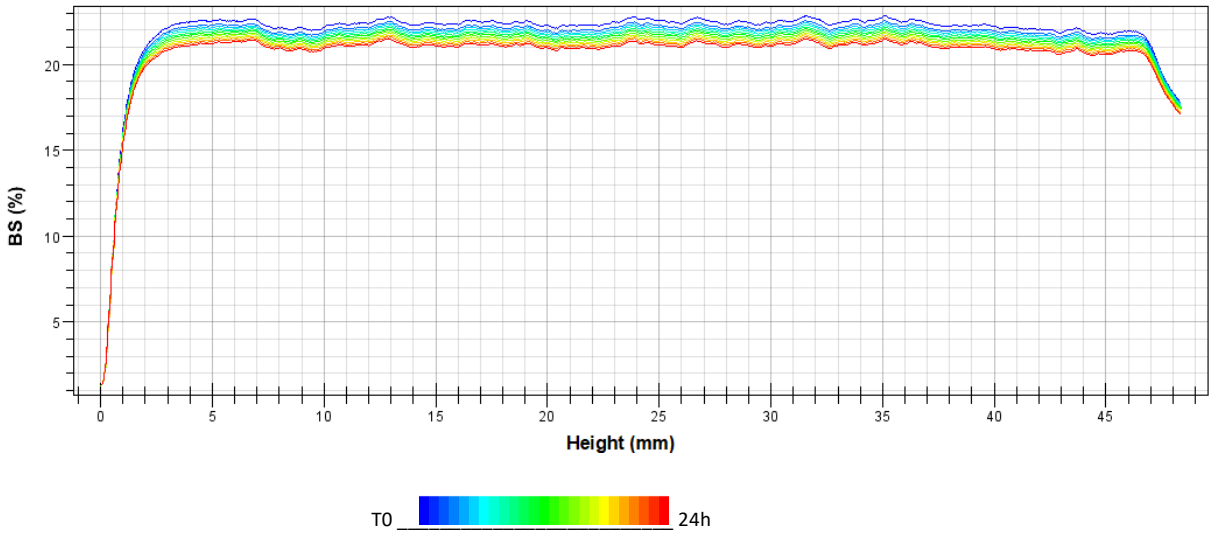

Figure 4.49. Backscattering profile of TH-NLC-T- incorporated into carbomer gel (GC-TH-NLC-T-) measured by Turbiscan®Lab, Scans were performed from the bottom to the top of the vial, measured every hour for 24 h, represented from blue to red lines.

Rheology of TH-NLC Gels

The flux and viscosity of GC-TH-NLC-T-, GH-TH-NLC-T- and GP-TH-NLC-T- were analysed and data are displayed in **Figure 4.50** and **Table 4.18**. All formulations best fitted to the cross equation, performing a non-Newtonian pseudoplastic flow and with appearance of thixotropy. This can be observed in the rheograms, expressed as a loop gap hysteresis between forward and backward plots.

Table 4.18. Rheology of TH-NLC semi-solid formulations.

	GC-TH-NLC-T-	GH-TH-NLC-T-	GP-TH-NLC-T-
pH	5.0 – 5.5	5.0 - 5.5	6.0 - 6.5
Viscosity (Pas)	2.895 ± 0.052	4.771 ± 0.206	3.042 ± 0.066
Thixotropy (Pa/s)	2.20E+07	2.24E+08	2.54E+07

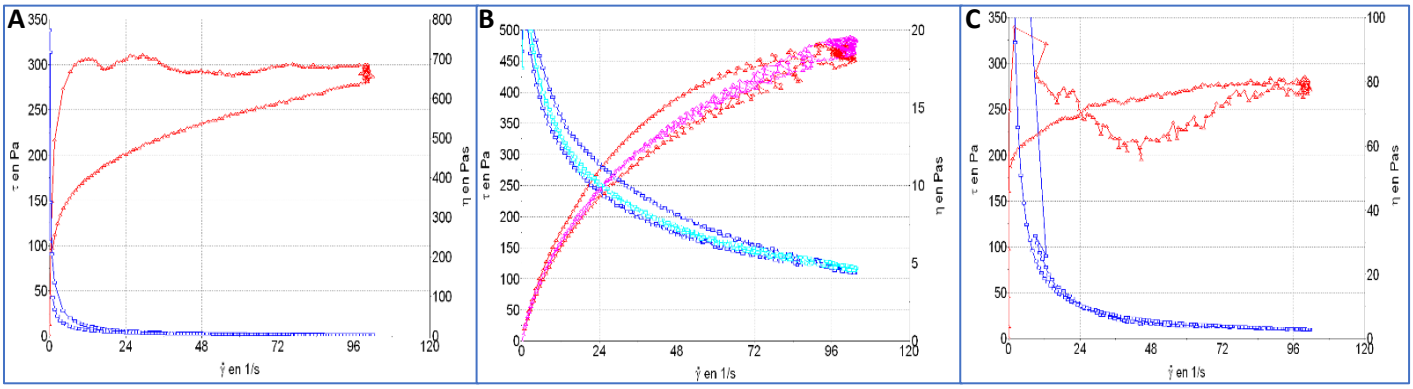

Figure 4.50. Rheograms of (A) GC-TH-NLC-T-, (B) GH-TH-NLC-T- and (C) GP-TH-NLC-T-. Data was fit to cross mathematical model corresponding to a pseudoplastic flux. All formulations presented thixotropy.

4.5.4. Biopharmaceutical Behaviour

In vitro drug release

The TH release profile was evaluated for 72 h and adjusted to hyperbole mathematic equation (best fit). In **Figure 4.51** (A-B), it can be observed for TH and TH-NLC-T- as aqueous or semi-solid forms, a sustained release of TH-NLC is found, in both formulation types, compared to TH. In both cases, the steady state of non-particulate TH was reached before 12 h, whereas TH-NLC-T- formulations provided a continuous release during the entire length of the study. Statistical analysis showed significant differences of TH-NLC-T- in both, aqueous and gels, at 24 h due to the retarded release from the nanocarrier (**Figure 4.51C**).

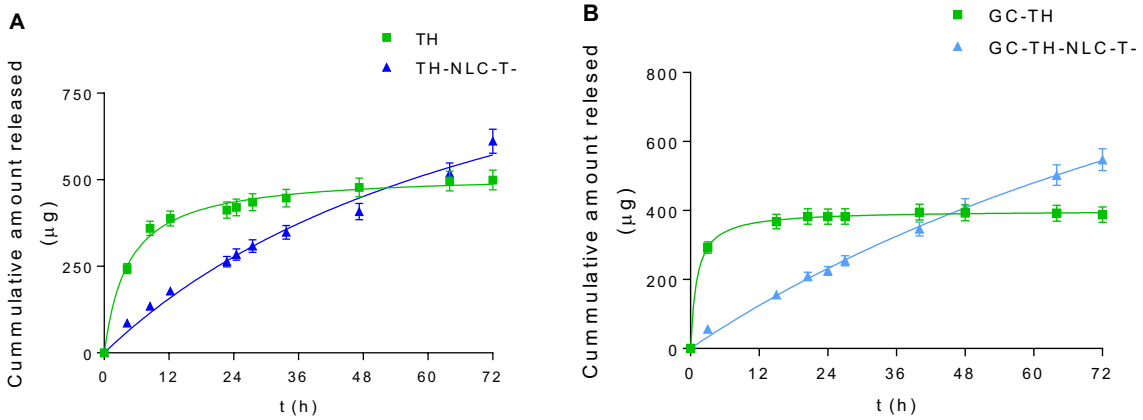

C	TH	TH-NLC-T-	GC-TH	GC-TH-NLC-T-
Bmax	69.06 ± 1.29	160.8 ± 21.8 *a c*	53.29 ± 0.23	222.6 ± 22.21 *a c*
Kd	4.543 ± 0.46	80.39 ± 17.13 *a c*	1.102 ± 0.059	148.7 ± 19.91 *a c*
r^2	0.9971	0.9948	0.9997	0.9992
%r 24 h	56.0 ± 6.4	37.9 ± 3.5 *a* c	51.0 ± 6.2	30.0 ± 2.7 *a c*
SSD (p < 0.05)	*a*	*b*	*c*	*D*

%r: amount of TH released; SSD: statistically significant differences.

Figure 4.51. *In vitro* release profile of (A) THandTH-NLC-T- and (B) GC-TH and GC-TH-NLC-T-, (C) data obtained adjusting data to hyperbola equation and amount released at 24 h. Data are expressed as Mean ± SD. Statistical analysis one-way ANOVA, Tukey´s Multiple comparison´s test.

Ex vivo Sin Permeation

The skin penetration of TH and TH-NLC-T- was evaluated in human abdominal skin explant using several dosage forms. In the first study (**Table 4.19**), TH-NLC-T- showed a more sustained penetration rate compared to TH in aqueous forms. Statistically significant differences were obtained for the flux (*J*), permeation constant (*Kp*) and total amount penetrated in 24 h (*Ap*). In the other hand, the permeation parameters obtained for the gel dosage forms were similar for GC-TH and GC-TH-NLC-T-, presenting no statistically significant differences between them. Moreover, the amount retained inside the skin was found to be higher for TH-NLC-T- (aqueous and gel) compared to TH, presenting statistically significant differences (**Figure 4.52A**).

The second study was performed with different skin donors than the previous experiment, comparing the penetration of different semi-solid formulations of TH-NLC-T-. Results showed that depending on the vehicle used, the permeation parameters were variable (**Table 4.20**). The highest penetration values were found for GH-TH-NLC-T- and the lowest for GP-TH-NLC-T-. In the other hand, HPMC provided an increase of total penetration, flux and kp compared to carbomer, although, this results were not statistically significant. Comparing the total amount retained inside the skin, GC-TH-NLC-T- and GH-TH-NLC-T- obtained higher and similar values, statistically significant compared to GP-TH-NLC-T- (**Figure 4.52B**).

Table 4.19. *Ex vivo* skin penetration parameters of TH and TH-NLC aqueous and carbomer gels.

Parameter	TH	TH-NLC	GC-TH	GC-TH-NLC
J (μg/cm²/h)	9.36 ± 0.31 *b c d*	1.66 ± 0.35 *c d*	2.53 ± 0.77	2.50 ± 0.06
Kp (cm²/h)	3.74E-03 ± 1.240E-04 *b c d*	6.66E-04 ± 1.39E-04 *c d*	1.01E-03 ± 3.08E-04	9.9E-04 ± 2.25E-05
Ap (μg/cm²)	85.45 ± 9.63 *b c d*	42.34 ± 3.20 *c d*	38.79 ± 2.98	34.50 ± 4.53
(p<0.01)	*a*	*b*	*c*	*d*

J: flux, Kp: permeability constant, Ap: total amount penetrated. Statistical analysis one-way ANOVA Tukey´s multiple comparison test.

Table 4.20. *Ex vivo* skin penetration parameters of TH-NLC incorporated in carbomer, HPMC and pluronic gels.

Parameter	**GC-TH-NLC**	**GH-TH-NLC**	**GP-TH-NLC**
J (μg/cm²/h)	2.79 ± 0.66	3.47 ± 0.14	1.25 ± 0.21 a b
Kp (cm²/h)	1.11E-03 ± 2.66E-04	1.39E-03 ± 5.50E-05	5.00E-04 ± 8.25E-05 a b
Ap (μg/cm²)	85.50 ± 3.91 b	109.45 ± 9.21	48.70 ± 3.54 a b
SSD (p<0.01)	*a*	*b*	*c*

J: flux, Kp: permeability constant, Ap: total amount penetrated. Statistical analysis one-way ANOVA Tukey´s multiple comparison test.

Table 4.21. *Ex vivo* skin penetration parameters of GC-TH versus GC-TH-NLC using full-fat skin tissue.

Parameter	**GC-TH**	**GC-TH-NLC-T-**
J (μg/cm²/h)	n.t	n.t
Kp (cm²/h)	n.t	n.t
Ap (μg/cm²)	33.56 ± 3.67	23.75 ± 1.75 *
n.t: not tested		

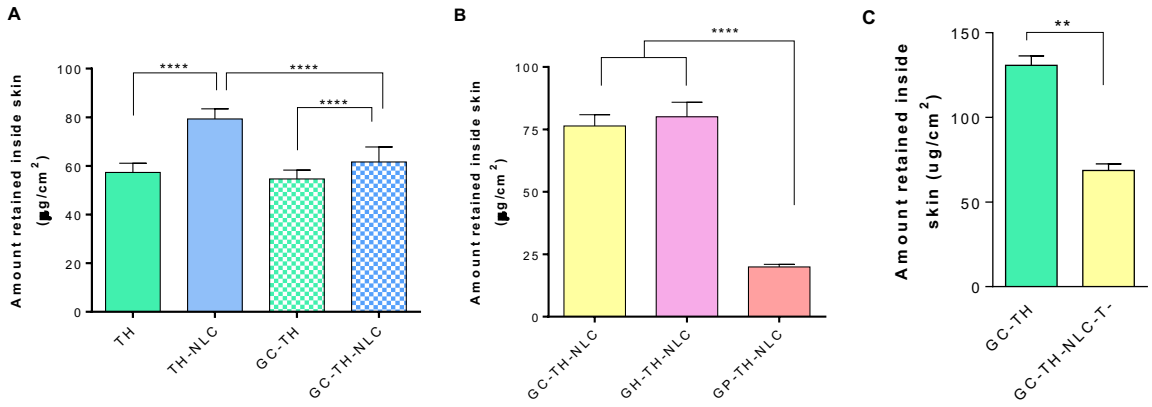

Figure 4.52. *Ex vivo* skin penetration for 24 h with the total amount retained inside the skin via extraction technique. (A) TH and TH-NLC-T- aqueous and carbomer gels, (B) GC-TH-NLC-T-, GH-TH-NLC-T- and GP-TH-NLC-T- and (C) GC-TH and GC-TH-NLC-T- (full-fat skin tissue). Data are expressed as mean ± SD (n=3). Statistical analysis one-way ANOVA, Tukey´s multiple comparison test and unpaired t test.

The skin penetration (*ex vivo*) performed in human explant for 24 h is illustrated qualitatively in **Figure 4.53**. Images were recorded by SEM cryo-cuts, and it can be observed the GC-TH-NLC-T-matrix within the skin tissue.

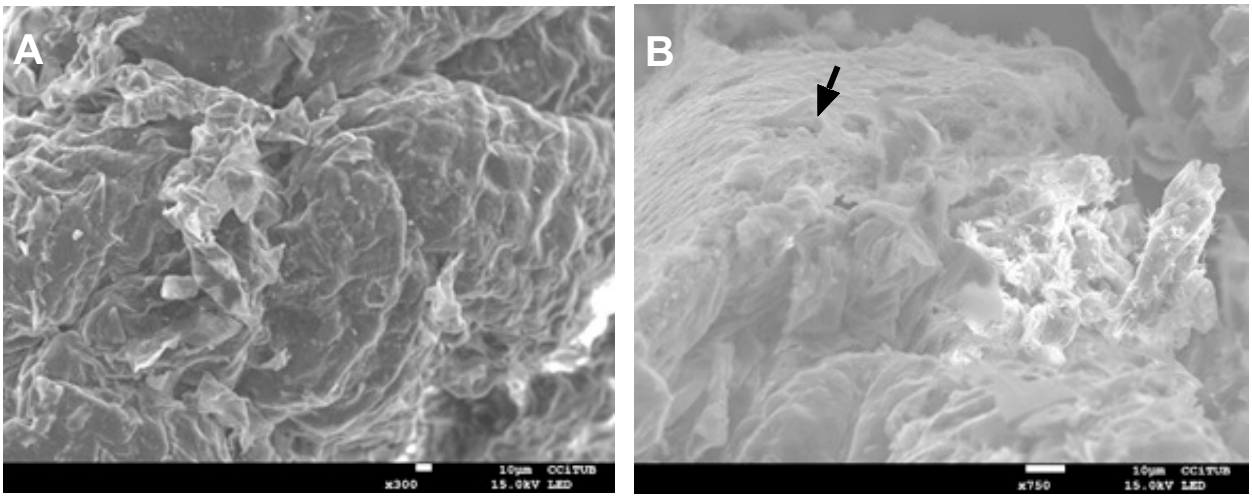

Figure 4.53. SEM images of *ex vivo* human skin (A) untreated and (B) GC-TH-NLC-T- permeation for 24 h. Scale bar: 10 µm (x300) and (x750), respectively. Black arrow indicates the gel matrix.

4.5.5. Biochemical studies

In vitro Cytotoxicity of TH-NLCs

The cell viability was assayed in HaCaT-cell line using MTT for TH-NLC-T- at varied concentrations (25 to 100 µg/mL) and also the same particles after 3 centrifugation cycles to remove excess of TW. **Figure 4.54A** shows that, at these concentrations tested, the non-washed TH-NLC-T- presented cytotoxicity. However, at lower doses, the washed particles presented significant increased cell viability, above 70 %. In the other hand, when testing those at lower dosages (2, 10 and 20 µg/mL) (**Figure 4.54B**), TH-NLC-T- presented a high increase of cell viability, although still below 60 %. However, when the surface of TH-NLCs were modified, and tested at the same lower dosages, these presented a significant increase in the cell viability (**Figure 4.54B**), although still below 80 %. Moreover, the lowest cytotoxicity can be observed at 2 µg/mL, with higher significance for the particles with PL and/or CS on the surface. The addition of CS for each nanosystem demonstrated to improve cell viability in all cases. Previous authors reported that cytotoxicity of lipid NPs in HaCaT cells are dependant on the surfactant type and concentration (Maupas et al. 2011). Additionally, other authors stated that lipid NPs cytotoxicity may be attributed to lipid peroxidation and generation of ROS, depending on the cell type and concentration used (Szwed et al. 2020).

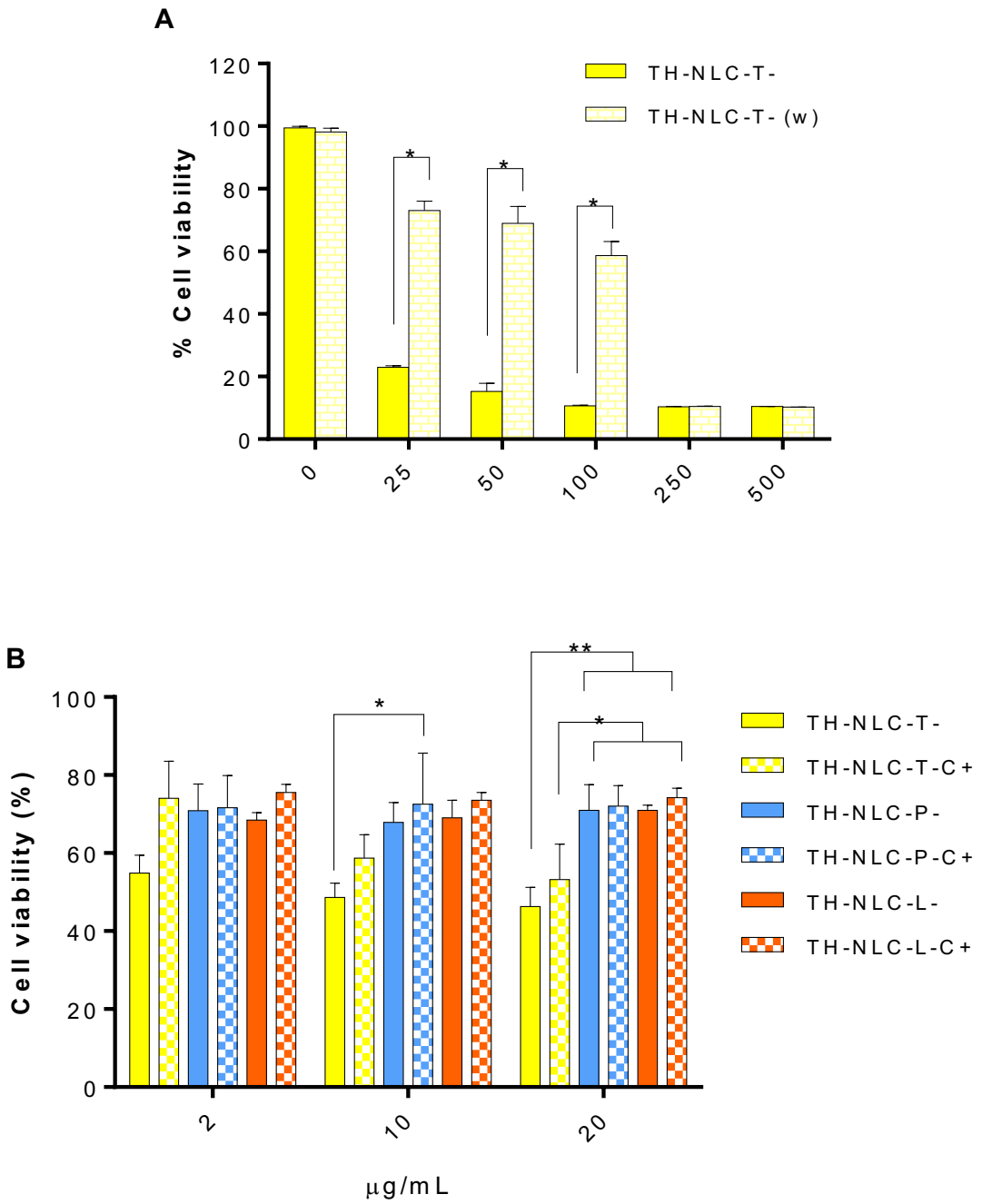

Figure 4.54. Cell viability assay performed by MTT assay in HaCaT-cell lines. (A) TH-NLC-T- and washed particles at high concentrations. (B) Surface functionalized TH-NLCs at low concentrations. Data are expressed as Mean ± SD. Statistical analysis one-way ANOVA, Tukey´s multiple comparison test analysed for each concentration tested (*$p < 0.05$, **$p < 0.01$).

4.5.6. Therapeutic Efficacy

In vitro Antimicrobial Efficacy

The antimicrobial activity was evaluated by MIC, bacterial viability, and decimal reduction time. Results of MIC against *C. acnes* presented the same value for TH or TH-NLC-T-, being 250 µg/ml. The decimal reduction time, the time taken to reduce 1/10 of the initial microbial concentration, was evaluated with values of MIC, 2X and 4X MIC (**Figure 4.55 A-C**, respectively). It can be observed that the effect of TH-NLC-T- is slightly more sustained than TH. In the other hand, when the semi-solid formulations were tested, TH formulations incorporated into carbomer gels had faster activity, whereas Pluronic gels showed a slow-rate microbial reduction, as illustrated in **Figure 4.56A-B**, respectively.

For *S. epidermidis*, the activity of TH was very fast while TH-NLC-T- **w**as highly sustained. TH achieved complete abolishment of the microorganism within 8 h, meanwhile TH-NLC-T- still presented bacteria viability after 48 h (**Figure 4.57A)**. Similar results were obtained for the carbomer gels, although the effect was slight stronger, in both cases, where bacteria viability was depleted within 3 and 24 h for GC-TH and GC-TH-NLC-T-, respectively (**Figure 4.57B**).

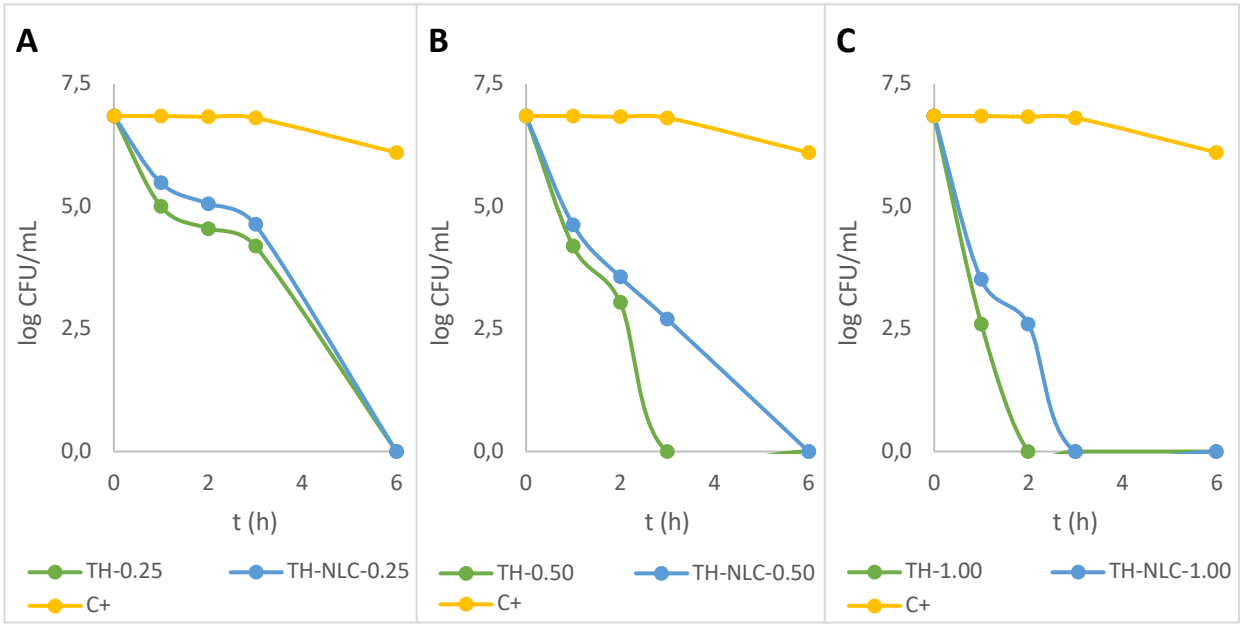

Figure 4.55. Bacterial viability assay with *C. acnes* inoculated in a timely-coarse until 6 h with TH and TH-NLC-T- at (A) 0.25 (B) 0.50 and (C) 1.00 mg/mL.

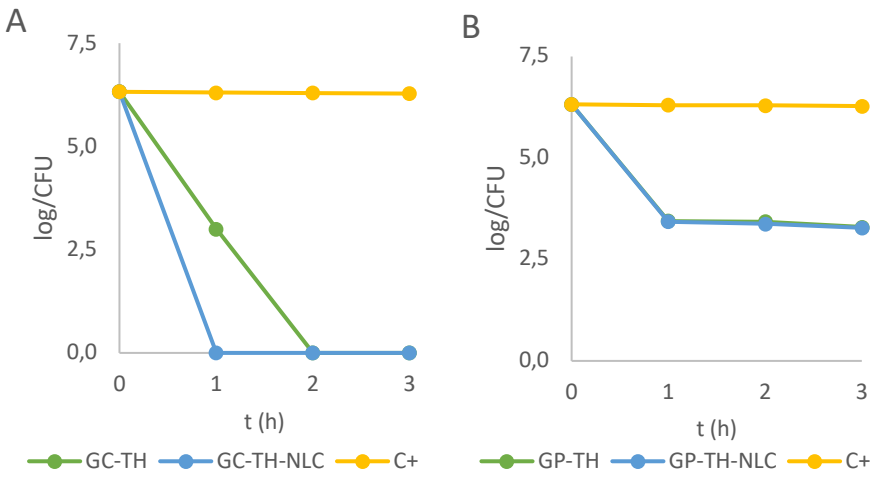

Figure 4.56. Bacterial viability assay with *C. acnes* in a timely-coarse until 48 h with carbomer gels (A) GC-TH and GC-TH-NLC and pluronic gels (B) GP-TH and GP-TH-NLC, at concentrations of 1 mg/mL.

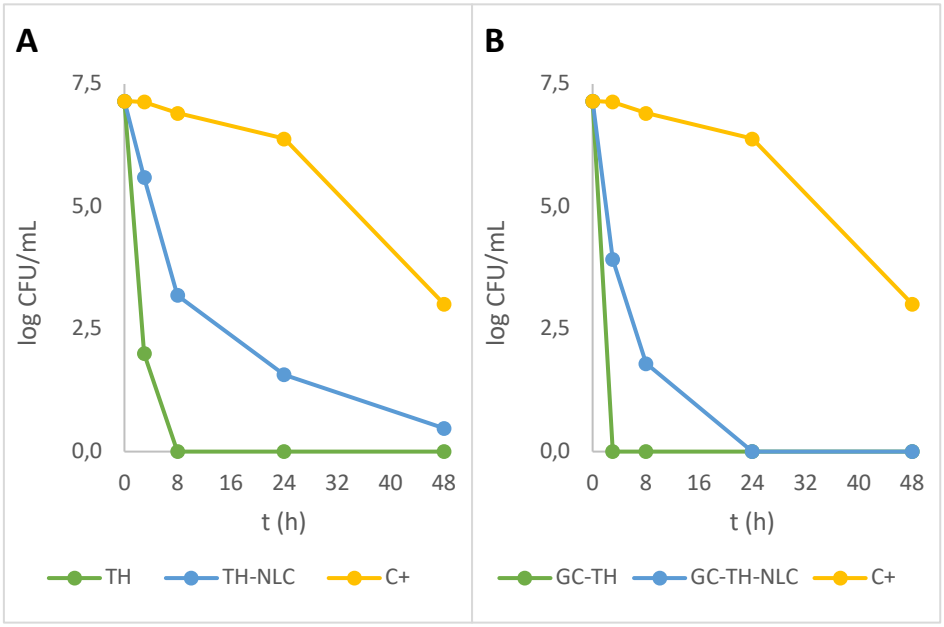

Figure 4.57. Bacterial viability assay with *S. epidermidis* inoculated in a timely-coarse until 48 h with (A) solutions TH and TH-NLC-T- and (B) carbomer gels GC-TH and GC-TH-NLC-T-, at concentrations of 1 mg/mL

Data of the decimal reduction time (D), the time taken to reduce a log10 of the initial bacteria viability, is displayed in **Table 4.22**. The kinetic data presented statistically significant differences for TH-NLC-T- against TH, on each evaluated dosages and microorganisms, ($p < 0.05$ and $p < 0.0001$) for *C. acnes* and *S. epidermidis*, respectively. Results showed that the activity of TH-NLC-T- is efficient to slowly reduce *C. acnes* viability, although, they possess a lower antimicrobial activity against *S. epidermidis,*

compared to TH. These results are favourable to maintain the healthy skin microbiota along the acne treatment.

Table 4.22. Decimal reduction time data for *C. acnes* and *S. epidermidis* treated with TH and TH-NLC.

	mg/mL	r^2	Slope	D (min)	SSD
C. acnes					
TH	0.25	0.9948	-1.645 ± 0.1184	36.47 ± 2.63	**p < 0.01
TH-NLC		0.9763	0.7629 ± 0.1188	78.65 ± 12.25	
TH	0.5	0.9960	2.256 ± 0.1435	26.60 ± 1.69	*p < 0.05
TH-NLC		0.9817	1.421 ± 0.1942	42.22 ± 5.77	
TH	1	0.9810	3.425 ± 0.4763	17.52 ± 2.44	**p < 0.01
TH-NLC		0.9973	2.261 ± 0.1175	26.54 ± 1.38	
S. epidermidis					
TH	1	0.9944	1.744 ± 0.1311	34.40 ± 2.59	****p < 0.0001
TH-NLC		0.9913	0.5130 ± 0.03395	116.96 ± 7.74	

SSD: Statistically significant differences (one-way ANOVA, t test)

Antimicrobial Activity of Surface Functionalized TH-NLCs by Suspension Test

The antimicrobial activity of different surface composition of TH-NLC were evaluated by suspension test, for 30 min incubation with *C. acnes*. Results showed that TW on the surface provide stronger activity than PL or CS (**Table 4.23**), with could be related to its detergent properties. In the other hand, TH-NLC positively charged containing BZ presented a strong bactericidal activity abolishing all bacteria colonies within 30 min. For this case, the activity was performed by BZ, and therefore, these were discarded.

Table 4.23. Antimicrobial activity by suspension test with *C. acnes* in contact with products for 30 min.

	CFU x 10^3/mL	SSD
CTR*	8800 ± 1200	
TH"	590 ± 80	* (p < 0.0001)
TH-NLC-T-	280 ± 40	*" (p < 0.0001)
TH-NLC-L-	330 ± 40	*" (p < 0.0001)
TH-NLC-T-B+	< 1	*" (p < 0.0001)
TH-NLC-L-B+	< 1	*" (p < 0.0001)

***Ex vivo* Antimicrobial Efficacy**

The antimicrobial activity of TH and TH-NLC-T- was evaluated *ex vivo* using pig skin. In every study performed, all formulations presented significant bacteria reduction compared to the control ($p < 0.0001$). The results studying prevention or treatment of the antimicrobial effects are showed in **Figure 4.58A**. In both cases, better activity was obtained for prevention than treatment of the antimicrobial capacity, statistically significant. In either protocol, the effect of TH-NLC-T- was slightly higher than TH, where statistically significant differences were presented in the prevention study. (In the other hand, when comparing dosages applied **Figure 4.58B**), it can be observed that TH-NLC-T- increases significantly the activity, by each additional dose applied, compared to a single one. Meanwhile, TH was only significant comparing 3 dosages to one. Comparing TH-NLC-T- against TH at the same dose, a single administration did not show diffenreces between them. However, after multiple applications of each formulation, their antimicrobial activity was statistically different. This can be explained by the rate of skin penetration, which in agreement to this study, TH penetrated fast through the skin layers, meanwhile TH-NLC-T- permeability is sustained. Therefore, within 24 h of total treatment period applying multiple dosages, TH can be released, from TH-NLC, inside the skin, performing prolonged and higher activity when compared to non-encapsulated TH.

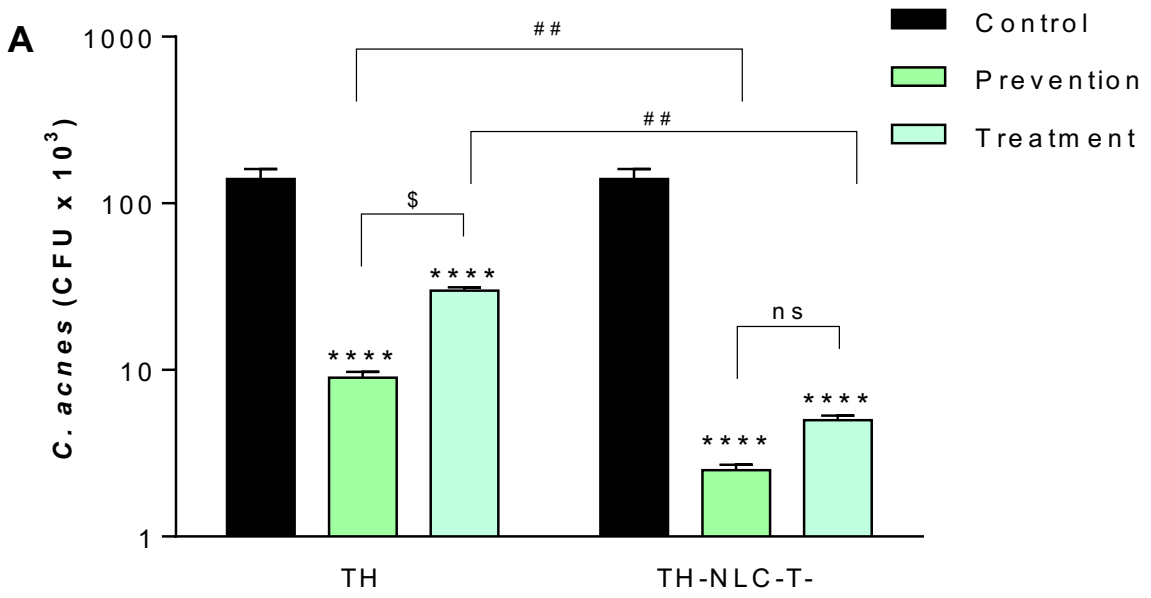

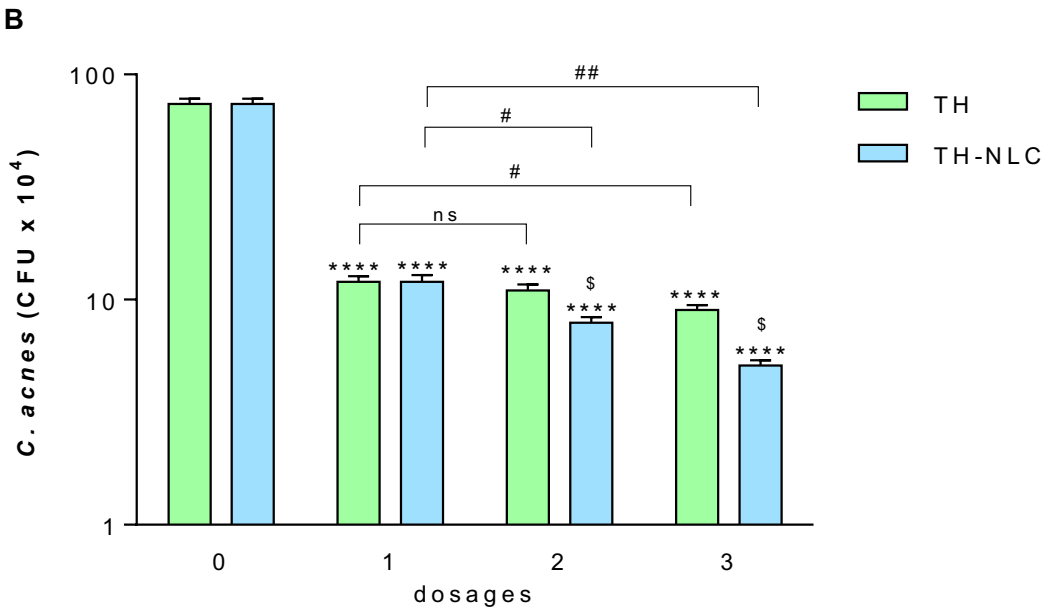

Figure 4.58. Bacteria viability on *ex vivo* treated skin with TH or TH-NLC-T- for 24 h. Values represent viable count of *C. acnes* as the Mean ± SD (n=3). (A) Prevention and treatment: Statistical analysis one-way ANOVA Tukey's Multiple Comparison Test represent ****$p < 0.0001$ compared to control; unpaired t test represents $^{\$}p < 0.05$ comparing TH and TH-NLC-T- and $^{\#\#}p < 0.01$ comparing preventions versus treatments. (B) Dose-dependent with 3 applied doses at times 0, 12 and 18 h of incubation: one-way ANOVA Tukey's Multiple Comparison Test represent ****$p < 0.0001$ compared to control and $^{\$}p < 0.05$ comparing TH and TH-NLC-T- (at the same dosage); unpaired t test represents $^{\#}p < 0.05$ or $^{\#\#}p < 0.01$ comparing multiple dosage with a single dose.

In vivo Biomechanical Properties of TH-NLC Gels

The biomechanical properties of GC-TH-NLC were evaluated on the forearm of 12 voluntaries, measuring the basal levels and after application for 2 h, the hydration of the SC (Corneometer®) and the transepidermal water loss (TEWL®). Results showed a slightly increased skin hydration, not statistically significant compared to the basal measure, with the highest value achieved within 30 min, which starts to decrease after 2 h of their application (**Figure 4.58**). Moreover, TEWL values also decreased significantly within 2 h. This result could be related to the film-forming properties of lipid nanoparticles which provided an occlusive effect, diminishing the internal water loss (Khater et al. 2021).

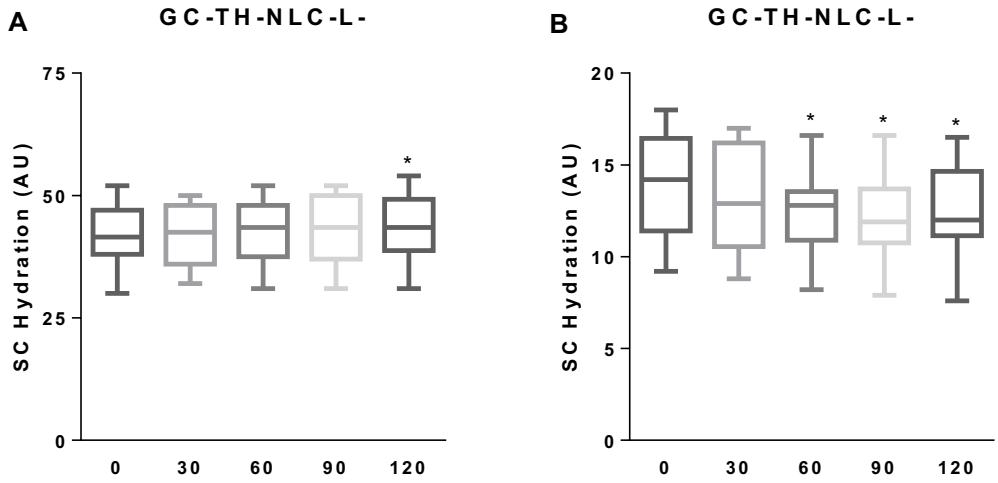

Figure 4.59. Biomechanical properties of GC-TH-NLC-T- measured in the forearm of volunteers for (A) hydration of SC by Corneometer® and (B) TEWL. Statistical analysis performed as mean ± SD values (n = 12), non-parametric Wilcoxon paired test comparing each measure against basal value (t0).

In vivo Sebum-Regulator Efficacy

The skin sebum was measured using Sebumeter® in the forehead of 7 volunteers, before and after application of the products (GC-TH and GC-TH-NLC) during 1.5 h (**Figure 4.60**). Results showed that both products achieve sebum reduction, with statistically significant differences compared to the basal levels. The activity was slightly higher for GC-TH than GC-TH-NLC, probably due to faster results since the release of GC-TH-NLC is slower. These results showed that both TH dosage forms have good sebum-regulator activity.

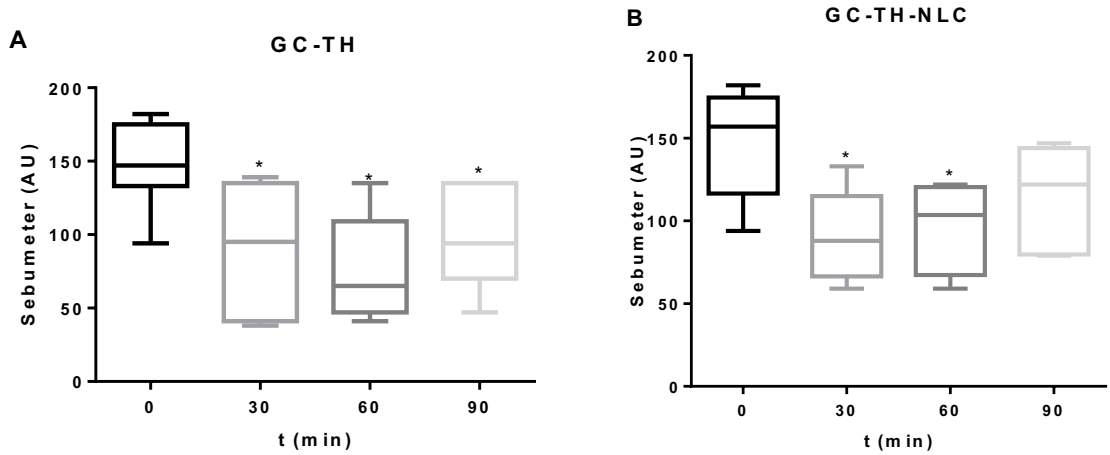

Figure 4.60. Sebum control measured by Sebumeter® for (A) GC-TH and (B) GC-TH-NCL on the forehead. Statistical analysis performed as mean ± SD values (n = 7), non-parametric Wilcoxon paired test comparing each measure against basal value (t0).

5. DISCUSION

5.1.POLYMERIC NPs

The first part of the current research was focused on the design of biodegradable polymeric nanoparticles and explore their possibilities as TH nanostructured delivery systems for dermatological and topical treatments. In this way, formulations of PLGA TH-NPs or THO-NPs were developed. These formulations were optimized and assessed for its biopharmaceutical behaviour as well as its anti-inflammatory, antimicrobial, antioxidant, and wound healing efficacy against acne.

5.1.1. Thymol-Loaded PLGA NPs

In the present study, TH was successfully loaded into PLGA NP. Developed TH-NP presented suitable physicochemical parameters with excellent stability and high EE. DoE analysis, throughout Pareto's diagram and surface responses, indicated that only the pH of the aqueous phase and the ratio of pH/TW induced statistically significant differences on Zav, being the effect of these variables not significant on the EE. The surfactant usually shows statistically significant influence on the EE and morphometry of polymeric NPs, depending on the amount applied (Vega et al. 2013). TW has good permeability profile and its amphiphilic properties may control the interactions between the active compound and the polymer carrier (Xiao et al. 2011).

Interaction studies showed that encapsulated TH was present on its amorphous form and the thermal transition was affected by TH-polymer interactions (Sánchez-López et al. 2016). Analyzing the stability of TH-NP for the first 3 months, an increase of particle size and a decrease in ZP, depending on the storage temperature, were observed. The decrease of ZP induced TH-NP-T- instability in aqueous medium, due to a decrease of electrostatic forces between surface-charged NP, generating in some cases, a slight particle aggregation. Moreover, TH-NP-T- at high temperature, presented sedimentation that was reversed by agitation, as also observed by other authors (Cano et al. 2018). TH-NP-T- stored at 4 °C have shown outstanding short-term stability in aqueous solution. However, in order to extend TH-NP stability, either incorporation in a semi-solid formulation or freeze-drying are recommended (Abrego et al. 2015; Vega et al. 2013). In addition, it has been shown that TH-NP did not present microbial contamination along storage, confirming TH antimicrobial preservative activity.

Biopharmaceutical behavior of TH-NP presented a sustained *in vitro* release profile, while TH reached the steady state very fast. The *ex vivo* skin rate of TH was higher than TH-NP by 1.6 and 1.3 times, respectively, being faster on damaged than healthy skin. As previously described (Gorzelanny et al. 2020), these results confirm that the external hydrophobic skin surface was altered, thus enabling substances to penetrate faster and easier through this barrier. The enhanced

penetration of TH and TH-NP-T- through the skin may be due to TH properties as well as the TW properties. On the one hand, TH is a terpene and these kind of compounds are known to be skin penetration enhancers, by impairing the lipids of the SC (Pham et al. 2016).

On the other hand, TW, an anionic surfactant, also provide enhanced permeability through phospholipid membranes, inducing some damage to epidermal membranes which decrease skin resistance towards the diffusion of the active. Some authors also explained that the mechanisms of TW could be attributed to an improvement of the thermodynamic activity adsorption and fusion due to micellar complexation, or decreasing the SC hindrance or modification of its intracellular lipid barriers (Akhtar et al. 2011). The amount of TH retained inside the skin was higher for TH-NP in both (healthy and damaged) skin types. The only difference between healthy and damaged skins was the highest amount in the SC and DS, respectively. The lesser amount of free TH against TH-NP retained inside the skin was probably due to its fast-rate penetration. In agreement with TH-NP-T- slow-rate penetration, confocal microscopy study confirmed that TH-NP-T- presented delayed entry, accumulating into the layers of the SC. This means that when the SC was disrupted, the flux of NPs penetration improved, and therefore, the amount inside the deeper layers of the epidermis and dermis increased. Interestingly, TH-NP skin penetration route was through the hair follicle, exactly where acne occurs. According to previous authors (Patzelt and Lademann 2020), the physicochemical properties of the active compound as well as the barrier properties of the hair follicles define the penetration route (intrafollicular or transfollicular). Polymeric NPs preferentially accumulate in the follicular entry, in a time dependent manner, where the skin penetration through the hair follicle is size dependent (Alvarez-Román et al. 2004). In this way, particles with average diameter of 200 nm are likely to penetrate faster than micro-sized particles or free molecules. Therefore, the smaller the particle size, the higher would be the accumulation into the hair follicle, and thus achieving lower permeability rates (Alvarez-Román et al. 2004),(Patzelt and Lademann 2020). Studies carried out by Yukuyama et al. (Yukuyama et al. 2020) indicated that NP stored in the hair follicle will be cleared by hair growth or sebum production. Zhu et al. (Zhu et al. 2019), developed PLGA TH microparticles as antimicrobial agents for food preservative application, containing particle size ranging for 20 to 70 μm. Due to the fact of the particle size selectivity for follicle entry, our developed TH-NP-T- would be more efficient for penetrating the hair follicle to treat acne. Furthermore, other authors stated that the reservoir of the hair follicle could store actives 10 times longer than the reservoir of the SC, and also, that hair follicle under movement (*in vivo*) would improve NP penetration (Patzelt and Lademann 2020; Yukuyama et al. 2020). Recent studies confirmed that diffusion of polymeric NPs only crossed the SC reaching the viable epidermis only after needle puncture (Patzelt and Lademann 2020). This could be also observed, by confocal microscopy in healthy skin, where TH-NP-T- were not found beyond the SC, unless inside the hair follicle. For all these reasons,

TH-NP are more efficient for acne treatment due to the prolonged penetration and release inside the hair follicle.

In the HaCaT cell line, TH-NP-T- at low concentrations did not alter cell viability, presenting no cytotoxicity. The cellular uptake images showed most of the R-TH-NP-T- in the cytosol but also some particles reached the nucleus within only 2 h. This would enable TH-NP-T- to perform its antioxidant activity inside the cells to improve the skin healing process on acne lesions (Mollarafie et al. 2015). This activity was confirmed by reducing the ROS generated, since TH-NP-T- improved significantly compared to TH. Moreover, prolonged release of TH as well as increased stability of TH-NP-T- may also favour enhanced antioxidant activity.

The antimicrobial activity of TH and TH-NP against *C. acnes* was similar and successfully demonstrated *in vitro* and *ex vivo*. The *in vitro* activity increased with high concentrations of TH-NP-T-, and they presented the decimal reduction of bacterial viability within 60, 30 and 17 minutes, for MIC, 2x MIC and 4x MIC, respectively, confirming dose-dependent activity. Additionally, the concentrations used above MBC completely reduced all CFU very fast. For the *ex vivo* experiments, simulating an acne infection inside the skin explant, samples resulted more efficient for prevention than treatment, despite, no significant differences between samples could be observed. This can be explained by the fact that part of the amount of the formulations applied were retained on the SC, and therefore, products had a direct contact with *C. acnes* when this was inoculated onto the skin. Meanwhile TH penetrates faster throughout the skin, providing only an immediate effect. For TH-NP, the effectiveness was higher when multiple dosages were applied onto the skin providing a slightly sustained effect. These results are in accordance with those observed in the biopharmaceutical studies. The same behavior was observed by electron microscopy in the *ex vivo* images, where the effect of TH on the bacterial membrane was found stronger than TH-NP-T-, for 8 h contact inside the skin. For this reason, it could predictably act in the same way on skin microbiota and therefore, TH-NP-T- would constitute a less aggressive and more efficient system for such treatment. The *in vitro* SEM images showed modified cells, with greater wall thickness and the development of blebs (Messager et al. 2004). This observation agrees with the previously mentioned mechanism of antimicrobial activity, by triggering loss of intercellular nutrients.

Concerning *S. epidermidis,* a more resistant type of microorganism, it presented very slow viability reduction in contact with TH and TH-NP-T-, compared to *C. acnes*, even tested at the highest concentration. Growth was abolished within 8 h for TH, while for TH-NP-T- this effect was observed over 24 h. Therefore, if these NP were administered *in vivo* for acne skin treatment, at the same concentrations, it would be less effective towards the entire skin microbiota, being at the same time a strong bactericidal against *C. acnes.* This favours the desirable microbiota-

friendly activity, where the antimicrobial ingredient will not alter the good functionality of the healthy skin, acting efficiently against *C. acnes* and only mediating *S. epidermidis* proliferation. Another proof of concept was previously stated by other authors (Erin Chen, Fischbach, and Belkaid 2018) providing evidence that microbiota shifts notably during puberty, increasing predominance of *Cutibacterium* species and decreasing abundance of *Staphylococcus* species. Meanwhile, in adulthood it remains unstable due to constant external environmental changes, suggesting mutual beneficial microbiome-host interactions. As a complement, the MICs showed that the concentration needed as bactericidal against *C. acnes* was lower than the minimal concentration needed to inhibit *S. epidermidis* growth. This means that for *in vivo* conditions, the desirable effect for acne treatment would maintain the skin balanced. In the case of clindamycin, the MIC for *C. acnes* and *S. epidermidis* was confirmed to be strongly efficient at a very low dose. This powerful activity is the main challenge with this type of drug, since it completely abolishes all the microbial content of the skin, therefore, treating it by unbalancing the healthy conditions for the microbiota, thus, leading to microbial resistance. For this reason, in this study we managed to confirm an effective activity of a natural active, at higher concentration, but that can maintain the microbiota function to rebalance the skin conditions, maintaining it healthy upon the treatment.

From another point of view, since the route of penetration of polymeric TH-NP-T- into the skin was through the hair follicle, the observed activity will be performed directly on the acne lesion. Therefore, TH-NP-T- perform a protective effect on the healthy skin microbiota, along with extending the retention and release of TH, directly to the site of the infection with prolonged activity. Moreover, the sebum content on the hair follicles could facilitate absorption and release of TH from TH-NP-T- by hydrophobic interactions. Nevertheless, since PLGA skin metabolism occurs by biodegradation into its monomers (lactic acid and glycolic acid), these compounds may help to modulate the skin pH, which would contribute to the sebum control.

5.1.1. Surface-Functionalized Thymol-Loaded PLGA NPs

In the present study, the surface functionalized TH-loaded PLGA NPs were successfully obtained, by the solvent displacement method. The developed NPs, TH-NP-P-, TH-NP-P-C+, TH-NP-PP-TH-NP-PP-C+ and TH-NP-L- were evaluated to compare their pharmacological activities as anti-inflammatory, antioxidant and wound healing via in vitro experiments performed in HaCaT cells. All the resulting TH-NPs presented suitable physical chemical parameters and a suitable short-term stability at 4 °C. The sedimentation phenomena observed by the backscattering signal was reversed by agitation. Confocal microscopy qualitative analysis confirmed that TH-NPs penetrated into the hair follicle, independent of their surface-coating type or charge. Some authors

stated that the reservoir of the hair follicle could store actives 10 times longer than the reservoir of the SC and that hair follicle under movement (in vivo) should improve NPs penetration (Yukuyama et al. 2020). Other authors have already described that NPs accumulate in the follicular entry, which is confirmed in the case of surface-functionalized TH-NPs (Alvarez-Román et al. 2004; Pereira et al. 2017; Santos et al. 2018). Regarding TH-NP-L, it appears that they can penetrate not only in the follicle, by also within the primary layers of the epidermis. This can be explained by the phospholipidic nature of the surface that diffuses easier through the skin. In the case of R-TH-NP-P-, their penetration was found mainly through in the entire hair follicle and a lower amount remaining in the SC. This indicated that this type of surface is favored by the follicular and not the intercellular pathway. On the other hand, concerning R-TH-NP-P-C+, which are positively charged and present slightly higher particle diameter, the penetration could be observed only inside the follicle. This is in accordance with the fact that NPs penetration into hair follicle is size and surface dependent.

Furthermore, the free-radical scavenging of TH was like endogenous control BHT and much higher than the free surface compounds themselves, which showed lower activity. The antimicrobial activity of TH and TH-NPs against C. acnes demonstrated to reduce microbial viability within only 30 min incubation. All tested samples presented similar activity, where the highest was achieved for TH-NP-P-. Moreover, since the penetration route of TH-NPs into the skin is through the hair follicle, the observed activity will presumably be performed directly on the acne lesion.

In HaCaT cell line, TH-NPs and all free compounds themselves did not alter cell viability, presenting no cytotoxicity. The cellular uptake images showed most of the NPs within only 2 h in the cytosol but also present the nucleus, especially for TH-NP-P-. The anti-inflammatory activity of TH and TH-NPs all presented significant reduction on gene expressions tested, where, in all the cases, all or most of TH-NPs performed significant reduction compared to the control and to their corresponding B-NP. Depending on the gene analyzed, the activity was enhanced for a different surface composition of the NPs. Therefore, they act as good booster of the activity. In fact, the higher antioxidant activity was mostly found for TH-NP-P-C+. Moreover, previous authors stated that PLGA-CS bilayer NPs may enhance skin penetration into the deeper layers where the inflammation is present, by opening channels of the SC (Shah et al. 2012).

The antioxidant activity in HaCaT cells was achieved for all TH-NPs, higher than TH and all other tested samples. The antioxidant activity of compounds enables cell proliferation faster, that can enhance wound healing processes to improve skin healing process on acne lesions (Mollarafie et al. 2015). For the wound healing activity, all scratched treated cells provided higher cell proliferation than control cells. Interestingly, in both prevention and treatment of wound healing

activity all surface modified TH-NPs showed suitable results. All TH-NPs provided good cell regeneration, meanwhile the B-NPs showed minimal activity. Additionally, TH-NPs showed better results than TH, confirming that surface modified TH-NPs present higher healing capacity than free antioxidant compounds. The antioxidant properties of surface compounds might have influenced on the healing activity, possibly by synergic activity with TH. Additionally, the highest wound healing activity was found for TH-NP-P-C+ and TH-NP-PP-C+. This can be attributed to CS promoting wound-healing processes due to its ability to support tissue regeneration and stimulate hemostasis (Sedlaříková et al. 2019). The antioxidant activity was also confirmed by the methylene blue reduction in ex vivo pig skin, showing that TH-NPs had greater activity than TH within 1 h incubation.

To summarize, TH was successfully encapsulated into PLGA NPs with suitable particle diameters and good stability. Moreover, other authors have developed different types of NPs for TH encapsulation such as PLA or chitosan NPs obtaining lower stability values (around 60%) (Sáez-Orviz et al. 2020). Lipid NPs containing thymol have also been developed with a negative surface charge confirming their anti-inflammatory properties but they were assessed for psoriasis treatment (Pivetta et al. 2018). In addition, Pires and colleagues studied compatibility of TH with several excipients confirming that P80 was a suitable excipient (Pires et al. 2017). Moreover, surface-functionalized TH-NPs successfully penetrated into the skin through the hair follicle, where acne occurs. Even though the antimicrobial activity of TH-NPs was similar to TH, they provided outstanding activities as anti-inflammatory, antioxidant, and wound healing, when compared to than TH and B-NPs. TH-NPs in contact with HaCaT cells showed that they were able to penetrate inside the cells, enabling greater activities than when compounds were introduced as its free form. TH and TH-NPs presented good anti-inflammatory activity by significant reduction on the gene expression tested. The efficacy of TH-NPs varied depending on their surface coating as well as genes analyzed. The antioxidant activity was proven in HaCaT and on ex vivo skin, and in all cases, TH-NPs were greater than TH. For this reason, they have also provided excellent wound closure and cell proliferation results, where the NPs positively charged, performed higher synergic activity on healing processes. Therefore, our study demonstrates that TH-NPs with surface functionalization using different approaches could constitute a potential efficient treatment for acne. However, these results would need to be assessed in in vivo experiments due to the multifactorial triggers of acne as well as the sebaceous content that can influence NPs stability (Tolentino et al. 2020).

5.1.2. Thyme-Oil-Loaded PLGA NPs

In this work, THO-loaded PLGA NPs including variable surface functionalization were successfully obtained, by the same method used for TH-NPs. These nanosystems presented

appropriate physicochemical properties and have maintained their stability during storage at 4 °C for 6 months, presenting no relevant changes. The therapeutical efficiency was evaluated for 3 developed formulations, namely THO-NP-P-, THO-NP-P-C+ and THO-NP-L-. The antimicrobial activity, performed by suspension test, provided similar results for the negatively charged THO-NPs, surface functionalized with P188 or PL. However, the positively charged THO-NP-P-C+, functionalized with CS, presented higher activity than the negatively charged ones (THO-NP-P- and THO-NP-L-). These results are different than the ones obtained with TH-NPs (on previous studies), where those provided similar activity to all types of surface functionalized NPs. In fact, other authors showed greater antimicrobial properties against varied microorganisms by the combination of THO and CS films (Sedlaříková et al. 2019). In the other hand, THO depleted the microbial viability within 30 min, which confirms that this essential oil possesses stronger antibacterial properties against *C. acnes*, compared to TH. Previous authors mentioned that the essential oils first target as antimicrobial is the bacteria cell wall and membrane, by increased membrane permeability, leading to cell leakage of proteins, genetic material, and membrane potential (Yap et al. 2021). Moreover, they also stated that essential oils with high content of TH were major drivers of cytoplasm membrane disruption.

In HaCaT cell line, THO-NPs and free THO presented no cytotoxicity as they did not alter cell viability. In fact, an increase of cell viability could be observed for THO at 2 g/mL, presenting statistically significant differences, which could be possibly considered a cell proliferation activity. The anti-inflammatory activity of THO and THO-NPs presented significant reduction of IL-6 and TNF-α the gene expressions, presenting statistically significant differences compared to the control. For the case of IL-8 and IL-1β, THO-NP-L- presented significant differences compared to the control and THO. In this case, there was no anti-inflammatory activity presented by THO. In the case of IL-1α, THO, THO-NP-P- and THO-NP-P-C+ increased the gene expression, while THO-NP-L- maintained the same value as the control. Therefore, THO had no activity to these gene expression either. Other authors confirmed that the anti-inflammatory activity of thyme oil is, apart from dose dependent, variable depending on the plant species used (Ocaña and Reglero 2012). Therefore, THO-NP-L- presented the highest activity obtained in all cases, which leads to the hypothesis that PL acted as good booster of the activity THO-NPs.

The antioxidant activity in HaCaT cells was strongly achieved for all THO-NPs, presenting higher effects than TH-NPs and TH (previously studied). However, THO performed the highest antioxidant activity, which could be due to its lipid composition that can easily diffuse into HaCaT cells. Since it is composed by several molecules that are powerful antioxidant, the activity at the cellular level is very high. In the other hand, THO-loaded PLGA would provide slow release inside the cell, and therefore, the activity during the timeframe of the experiment was lower that

free THO. Nevertheless, THO-NPs performed much higher activity than TH-NPs, which were boosted by the surface composition. Therefore, it can be expected that cellular uptake of surface functionalized PLGA-NPs (obtained for all previously tested TH-NPs), and additionally THO, are favored, whereas TH might have low affinity to the cellular membrane. Previous authors stated that essential oils may act as skin penetration booster by disrupting skin intercellular lipids and changing the cellular membrane fluidity (Çalışkan and Karakuş 2020). As a complement, the antioxidant activity performed *ex vivo* was investigated by methylene blue reduction. Results confirmed that the antioxidant activity was achieved on the skin tissue, presenting better results than THO. As expected, due to the potent antioxidant efficacy of THO and THO-NPs in HaCaT cells, the cell regeneration activity, tested for wound healing, was also stronger than those previously obtained for TH and TH-NPs. Additionally, in this experiment, the activity of the surface compounds has boosted the healing process, possibly by synergic activity, as also previously found for TH-NPs. Specifically, THO-NP-P-C+ presented the highest activity, although all THO-NPs presented higher activity than THO. This confirms that THO-loaded PLGA NPs and surface functionalized, both increased the therapeutical efficacy at the cellular level. The enhanced wound healing activity with the combination of THO and chitosan was previously reported (Barakat et al. 2018). For this reason, THO-NPs are great candidates for reducing inflammation, mostly by enhancing the skin healing process during an inflammatory skin disease. Also, the strong antimicrobial activity of THO combines the product as a good natural alternative to antibiotics.

5.1.3. Semi-Solid Formulations of Polymeric NPs

This study consisted of incorporating the previous successfully developed TH-NPs and THO-NPs, in hydrogel formulations, to test their skin properties for further in vivo applications.

The short-term stability of the surface functionalized TH-NPs carbomer gels was studied after 1 month stored at different temperatures. The results obtained showed that the pH slightly decreases, and by accelerated conditions, the gel appearance changed from semi-solid to fluid gels. This was also obtained with the short-term stability of GC-TH-NP-P- and GC-THO-NP-L- within 4.5 months maintained at RT. This physicochemical modification of the gel matrix is due to carbomer gelling properties, which is pH dependent. In fact, the gels GH-TH-NP-T- and GP-TH-NP-T- did not present viscosity changes neither pH modifications within 6 months at RT. Previous authors reported that NaOH act as a catalyst in the hydrolysis of PLGA (into lactic and glycolic acids), which is probably the reason with carbomer gels decreased the pH, destabilizing the gel matrix (Rajapaksa et al. 2010). The outcome of this issue for PLGA NPs could be possibly solved by using a different neutralizer. In another perspective, the fluidity of GC-TH-NP-P-C+

and GC-TH-NP-PP- was less affected than the other gels. Therefore, CS covered TH-NPs provided a higher protection of PLGA partial hydrolysis by NaOH. In the other hand, all gels of surface functionalized TH-NPs stored at 4 °C had maintained their semi-solid stability for 12 months. This agrees with the previous stability studies performed with the aqueous surface functionalized TH-NPs which were stable for 6 months at low temperature. This confirms that PLGA NPs stored at low temperatures maintain the polymer stability and avoid the partial hydrolysis. Moreover, the microbial preservative activity stability evaluated for the synthetic gel formulations, stored at RT, was successfully obtained, evaluated for bacteria, yeast, and fungi growth: GC-TH-NP-P- and GC-THO-NP-L- after 6 months and GC-TH, GP-TH, GP-THO, GC-TH-NP-T- and GP-TH-NP-T- after 36 months. This confirms that TH acts as a natural preservative in the formulations, maintaining their sterility. Previous authors reported the preservative activity of thymol in cosmetic formulations (Manou et al. 1998). Despite it, it is worth to mention that no challenge test was performed, in this work, to test their preservative function upon induced microorganisms. However, using natural antimicrobial in formulations, reduced the need of strong chemical preservative systems, which makes it favorable for natural products.

The rheology of the gels presented pseudoplastic flux and appearance of thixotropy, being both characteristics a key of good skin spreading ability, commonly obtained in cosmetic formulations (Lee et al. 2009).

The *in vitro* release was investigated for TH and TH-NP-T- aqueous form, carbomer and pluronic gels. The release of TH-NP-T- showed a sustained release compared to TH, both adjusted to the hyperbola equation. Similar results could be observed for both formulations when incorporated into the carbomer gels, where GC-TH-NP-T- was more sustained than GC-TH. In both studies, the total amount release in 24 h presented statistically significant differences comparing TH and TH-NP-T- as aqueous or gel forms. When comparing TH or TH-NP-T- between their formulation type (aqueous or gel), TH and GC-TH presented similar amount release in 24 h, whereas TH-NP-T- and GC-TH-NP-T- presented statistically significant differences between them, as the release of the gel formulation was even more sustained than the aqueous form. This has also been demonstrated by other authors due to the fact that TH is first released form the NPs and then contacts with the gel that also causes a delay in the release due to the higher viscous matrix (Ho et al. 2020). In the other hand, the release of GP-TH and GP-TH-NP-T-, both provided a very slow-release rate with very low cumulative amount released within 24 h, presenting no significant differences between them. Pluronic is a thermo-reversive gel, therefore, the viscosity and gel matrix properties are different at RT and at body temperature. In the experiment (32 °C), the gel matrix would increase thickness, which might be the influence of the very sustained release of

TH. Russo et al. also found similar results in drug release of diclofenac (at 2 %), comparing aqueous and pluronic gel formulations (at 17 and 20 % of P407) , where the maximum amount released in 24 h was no more 5 % of the initial dose applied (Russo et al. 2020).

The skin penetration studied parameters agree with the *in vitro* release results. They were 3 times faster for TH, when compared to TH-NP-T-, and the total amount found in the receptor medium after 24 h was also higher for TH, in all cases presenting statistically significant differences. However, in the case of the total amount retained inside the skin, the value was slightly higher for TH-NP-T-, despite not significantly. Similar results were found for the carbomer formulations. In this case, , compared to their aqueous form, GC-TH-NPs showed statistically significant differences in the permeation parameters and also in the total amount found in the receptor fluid. Moreover, carbomer and HPMC gels of TH-NPs parameters were similar, retaining inside the skin practically the same amounts of TH, although GH presented slightly faster flux and K_p than GC. Furthermore, the SEM image recorded after 24 h penetration of GC-TH-NP-T- confirmed the presence of the gel matrix and presence of the TH-NPs within the skin layers. In the other hand, the pluronic gel presented a completely different permeation parameters and total amount of TH inside the skin. In both cases, GP-TH and GP-TH-NP-T- permeation parameters were much lower compared to the other gels. This behaviour of pluronic gels may be related to the film-forming and mucoadhesive properties and the slow-rate release of active compounds. Russo et al. also found very similar results in diclofenac permeation studies, comparing aqueous free form and diclofenac incorporated into pluronic gel, where very low concentrations were found in the receptor fluid and retained inside the skin after 24 h penetration for the gel, while free-aqueous the values were much higher (Russo et al. 2020).

The antimicrobial activity, towards *C. acnes* was potent and fast, meanwhile, it was less active against *S. epidermidis*. Results coincided with the ones previously obtained in this work with the aqueous forms. However, the carbomer gel formulations provided a slightly faster activity. Other authors also found that PLGA-NPs presented higher antimicrobial activity when incorporated into a carbomer gel (Ho et al. 2020). In the other hand, Pluronic gels have shown sustained antimicrobial activity, probably due to the thickness of the gel, obtained during the experimental conditions, which mimics the *in vivo* skin conditions. In agreement, the slow-release rate of GP-TH and GP-TH-NP-T- could explain such delay on the activity *in vitro*, especially due to experimental conditions, where gels were incubated at 32 °C, where pluronic gel matrix would thicken. Previous authors also stated that the higher the polymer gelling agent concentration, influences in the gel viscosity and bio-adhesiveness, promoting a slower drug release (Ho et al. 2020). Therefore, if a very sustained effect is required in vivo, this gel vehicle would be the most appropriate, specially combined with wound healing processes (Russo et al. 2020).

The SEM images illustrated that *C. acnes*, when in contact with GC-TH or GC-TH-NP-P- for 30 min, presented the cellular membrane deteriorated and elongated. In the case of GC-TH, the cellular membrane also showed formation of blebs in the surface. These results were similar to the ones already obtained when tested with TH and TH-NP-T- in aqueous forms. In accordance with these results, the effect of GC-TH-NP-P- was slightly less aggressive than GC-TH, where the effect can be also expected to maintain the healthy skin microbiota balanced. Once again, the developed TH-NPs proven to be a potential candidate for acne treatment.

Observing the *in vivo* results obtained with TH and TH-NPs semi-solid formulations, the biomechanical properties of the skin were not altered. The skin moist values did not show significant differences for all formulations tested. However, TEWL values have shown variability, where the only significant variance was obtained for GC-TH-NP-P- after 2 h application. Therefore, the products are suitable for skin disorder treatments.

The *in vivo* sebum regulation efficacy was found slightly higher for GC-TH than GC-TH.NP-P- within a single application during 1.5 h. This could be related to the fast and direct activity of TH free, that might drain part of the sebum content during penetration, due to its highly hydrophobic affinity. In the other hand, when pluronic gels (GP-TH and GP-TH-NP-P-) were evaluated during 1.5 h, both presented equal effects on sebum reduction, which were more efficient than the carbomer gels. In fact, according to the results obtained of their release and skin penetration profiles, that were very sustained, and the fact of their thermoreversible gelling properties, that changes when it is applied onto the skin, the gel probably forms a film barrier on top of the skin layer, which may help to regulate the skin loss of water and lipids. Carvajal-vidal et al. previously stated that pluronic gel on the skin forms superficial thick and dried film adhered to the SC (Carvajal-Vidal et al. 2020). They found that this effect provided an artifact measured on the skin barrier, where skin moist could not be detected properly, as values of SC hydration were diminished by 40 %. For this reason, evaluation of TEWL and skin moisture were not performed in this work. Russo et al. confirmed that pluronic gels hardly penetrate towards damaged skin barrier, which might be related to its enhanced bioadhesive properties and this superficial film formed on the skin barrier (Russo et al. 2020).

Furthermore, when carbomer gels of TH and TH-NPs were applied *in vivo* daily, during a long-term treatment, GC-TH-NP-P- presented outstanding sebum reduction within one month compared to GC-TH. The total sebum reduction was found to be – 50 and -30 %, respectively, presenting statistically significant differences ($p < 0.001$). These results can be associated to the prolonged penetration time and slow-release kinetics, which improved the activity inside the skin.

5.2. LIPID NPs

The second part of the current research was focused on the design of biodegradable lipid nanoparticles exploring their possibilities as colloidal systems of TH for dermatological and topical treatments. The NLC developed, made by high energy methods, were optimized, and assessed for its biopharmaceutical behaviour, as well as therapeutic efficacy against acne.

5.2.1 Nanostructured Lipid Carriers of Thymol

The TH-loaded NLCs were successfully obtained using several concentrations and compositions of lipids, surfactants and two preparation methods applied. The solubility of TH in LAS was better than MGL, therefore, LAS was selected as the liquid lipid. Additionally, LAS presented less variability of lipid mixtures melting point, while MGL showed a higher temperature displacement. Observing the results obtained by HPH and US, the Zav and PI were lower using HPH. However, there were no significant differences compared to US method, in terms of proportion of the lipids and the concentration of TW. The optimization of TH-NLC-T- was based on the best solubility of TH into the liquid lipid, as well as the best values of Zav and PI by adjusting the correct concentration of TW. Moreover, the TH-NLC-T- optimized formulation presented minimal variances between the preparation methods. Additionally, observing the surface response of the DoE, the central point corresponded to the best results.

Observing the DoE, the Zav was smaller for 80:20 and 70:30, than for 60:40 proportions of SL:LL. This could be attributed due to the medium-soft structure compared to soft. The best values were found for 70:30 at level 0 and +1 of TW, and the PI increased at levels -1 and +1 compared to 0, which must be due to the correct proportion of lipids and surfactant. EE values were found in a range of 75 – 82 %, where the highest was found for the central point. This is due to the right proportion of lipids and surfactants that stabilize the system and encapsulate the active.

The short-term stability of developed TH-NLC, evaluated by TurbiscanLab®, showed a broad variability of backscattering signals measured for TH-NLC-T-. However, when this was incorporated into carbomer gel, that phenomenon was stabilized. In fact, it can be observed that by changing the surface composition of the TH-NLC, there were also relevant improvements in the stability in aqueous suspension. CS is a positively charged polysaccharide which forms a polymeric layer surrounding the lipid particle via electrostatic binding, increasing the stability (TH-NLC-T-C+). Other authors also stated that NLC surface covered CS present improved stability of the nanosystem (Choi et al. 2016). In the case of TH-NLC-PP-, although the ZP was also very low, the fact that P407 has thermo-transition properties, at high temperature this compound jellifies, and the suspension presented a translucid colour, differing from all others

TH-NLCs formulations. Previous authors also reported low ZP and small particle size for NLC covered P407, and also stated that this surfactant plays an important role in controlling the crystallization process of NLC (Zirak and Pezeshki 2015). Therefore, it could be the reason of the changes in the appearance of the formulation and the increased stability.

The morphology of TH-NLC-T- was analysed by SEM presenting a semi spherical soft shape, characteristic of this type of nanocarrier (Carvajal-Vidal et al. 2019).

The semi-solid formulations of TH-NLC-T- were developed with different gelling agents and at different viscosities. All gels presented a pseudo plastic flux with thixotropy appearance, which are ideal for cosmetic formulations to perform good spreading ability on the skin (Lee et al. 2009).

The *in vitro* release of TH-NLC-T- was sustained and similar for aqueous and gels forms, meanwhile TH presented a fast release, similar for both formulation types. There were statistically significant differences for TH-NLC-T- formulation (aqueous and gel) compared TH and GC-TH.

The skin permeation of TH-NLC-T- was also found to be much slower than TH, by 5.6 times with significant differences, whereas in the case of the gels, no differences could be observed. In the case of the carbomer gel formulations, data were similar for both gels (GC-TH and GC-TH-NLC-T-), and both presented significant differences compared to the aqueous forms. The highest amount found in the receptor fluid was for TH, presenting significant differences compared to all the other formulations. TH is also considered a penetration enhancer compound, and under *ex vivo* evaluation, differences in the penetration parameters can be observed (Pham et al. 2016). In the other hand, the total amount found retained inside the skin was highest for TH-NLC-T-, statistically significantly compared to TH Also, GC-TH-NLC-T- amount was slightly higher than GC-TH, although not statistically significant. When comparing the permeation of TH-NLC-T- in several semi-solid formulations, carbomer gel presented slower skin permeation rate than HPMC, but faster than Pluronic. In fact, GC-TH-NLC-T- and GH-TH-NLC-T- presented similar amount retained inside the skin, statistically significant different compared to GP-TH-NLC-T-. Since lipid nanoparticles are known to perform a fill-forming on the skin surface, they could also delay the entry across the entire skin depth. Other authors also confirmed that carbomer and HPMC are suitable and similar gel-forming agents for NLC formulations (Amasya, Inal, and Sengel-Turk 2020). In the other hand, Pluronic present thermo-reversive gel properties between room and body temperatures, for dermal and topical applications (Lee et al. 2009). For this reason, the gel become thicker in contact to the skin, presenting increased adhesive properties, and providing an even more sustained permeation of TH-NLC-T-, which was statistically significant compared to the other gels.

The antimicrobial activity against C. acnes, evaluated for TH-NLC-T- at MIC, 2X and 4X MIC, showed a slightly sustained effect compared to TH. It presented statistically significant differences in the decimal reduction time, being 2, 1.6 and 1.5 times slower for each dosage, respectively. When the gel formulations were applied at 1 mg/mL, the activity was similar to the aqueous forms, but slightly faster effects could be observed for their gels (GC-TH and GC-TH-NLC-T-). In contrast, GP-TH and GP-TH-NLC-T- presented a sustained antimicrobial activity. This is in accordance with the slow-rate drug release data presented before, and it could be attributed to the viscosity and appearance of the formula, since increases thickness and adhesive properties in contact to the skin, and therefore, it delays the release of TH from the NLC towards the bacterial membrane, providing a delayed activity against *C. acnes*. Further studies are needed to elucidate the differences between GP-TH and GP-TH-NLC-T- for prolonged exposure period with the microorganism.

When comparing the formulations, aqueous and carbomer gels, against *S. epidermidis* (at 2X MIC), both formulations presented prolonged time to detain the microorganism viability, compared to *C. acnes* (at 4X MIC). Moreover, the time taken to reduce a decimal of the bacteria viability was found to be 3.4 times slower for TH-NLC-T- than TH. Therefore, results obtained promoted the efficacy of TH-NLCs to efficiently decrease *C. acnes* proliferation, without affecting the healthy skin microbiota.

When the surface functionalized TH-NLCs were exposed to *C. acnes* for 30 min, there were minimal differences between the activity of TH-NLC-T-, TH-NLC-L- and TH-NLC-T-C+. Although, TW on the surface presented slightly higher activity, probably due to its detergent properties, but not statistically significant. In contrast, the positively charged TH-NLC-T-B+ and TH-NLC-L-B+ resulted on complete depletion of *C. acnes*, confirming that the bactericidal effect of BZ is highly strong, and therefore, not suitable for this purpose. The good balance of the skin microbiota is the key role on treating skin infections, since the healthy skin conditions need the appropriate function of the host microorganism.

The *ex vivo* antimicrobial activity was successfully investigated in human skin explants as prevention and treatment. The activity was found higher for TH-NLC-T- than TH in both cases, presenting statistically significant differences. In the study of multiple doses applied, there were only significant differences for TH comparing three doses against a single one. However, for TH-NLC-T-, there were statistically significant differences at each multiple doses applied compared to a single one. These results agree with the skin permeation parameters, where the TH-NLC-T- are able to be maintained for longer time inside the skin, while TH penetrates across the entire layers in a fast manner. Therefore, a long-term treatment would be expected to provide more efficient results using TH- NLC than TH alone.

The biomechanical properties of carbomer gels of TH and TH-NLC-T- provided no skin hydration of the SC. However, both products reduced the TEWL, presenting statistically significant differences compared to the basal levels. This effect can be stronger observed for GC-TH-NLC-T- and this can be explained by the film-forming properties that lipid NPs perform on the skin surface, due to their high affinity with the intercellular lipids of the skin barrier. Previous authors also stated that NLC formulation present a film-forming behaviour in the skin due to their affinity to the SC lipids reordering it and that their incorporation into C934 or HPMC revealed promoting results in decreasing the TEWL values (Amasya et al. 2020).

The sebum reduction activity was also successfully obtained by both formulation, GC-TH and GC-TH-NLC-T-, after a single application, compared to the basal measurement. In this case, GC-TH performed stronger activity and that could be expected due to the fast activity of free TH to reduce the sebum content, while TH-NLC would need a longer timeframe to achieve the same efficacy. Nevertheless, since NLCs develop a film-forming and long-term release, they could be expected to perform higher efficacy in long-term treatments.

6. CONCLUSIONS

In this work, biodegradable nanoparticles for sustained delivery of natural products, TH and THO, have been successfully developed, characterized physicochemically and evaluated for their biopharmaceutical behaviour and therapeutical efficacy, demonstrating excellent properties for acne topical treatment.

6.1 TH polymeric nanoparticles, based on PLGA, were prepared by solvent displacement method, and optimized by DoE, confirming to be suitable for dermal administration, with particle size below 200 nm, high EE and adequate stability.

6.2 Polymeric nanoparticles were characterised by spectroscopic (X-Ray) and thermal (DSC) methods confirming that the drug was encapsulated into the polymeric matrix, on its amorphous (molecular) form.

6.3 PLGA TH-NPs presented a sustained release and slow-rate penetration on skin, through the hair follicle, with higher amounts retained inside the skin, especially on the deeper layers, compared to free TH.

6.4 PLGA TH-NPs showed outstanding antimicrobial activity *in vitro* and *ex vivo* against *C. acnes*, with minor effects towards *S. epidermidis*, which promises to be a great microbiota-friendly candidate for acne treatment. They do not present microbial growth under a storage period of 12 months, due to antimicrobial properties of TH, which acts act as natural preservative system.

6.5 The incorporation of TH-NPs into semi-solid formulations increased their stability and shelf-live improving, in some cases, TH release and permeation. The rheological and the biomechanical properties of the gel formulations presented suitable characteristics for skin delivery, increasing antimicrobial activity.

6.6 Studies of cellular uptake elucidated that TH-NP improved the antioxidant activity in keratinocyte cells, which would be promising on cell regeneration and the healing process of the acne lesion

6.7 Surface-functionalized TH-NPs demonstrated increased anti-inflammatory, antioxidant and wound healing properties and route of penetration through the hair follicle, being suitable for the treatment of severe acne disease.

6.8 Surface-functionalized THO-NPs improved the strong wound healing activity of THO at the cellular level. The antioxidant effect was lower than THO when tested *in vitro*, however, it was increased when tested *ex vivo*, for all THO-NPs. Only THO-NP-L- proven successful anti-inflammatory activity, against THO or other THO-NPs tested.

6.9 Optimization of TH loaded NLC, by DOE, showed that the better proportion of SL:LL (Compritol ATO888:LAS) was 70:30 to obtained particles of smaller size, with an EE ranging between 75 from 82 %.

6.10 The incorporation of TH-NLC into semi-solid formulations increased their stability, avoiding aggregation. The release of TH from TH-NLC was similar as aqueous and gel formulations, improving skin permeation of TH-NLC by incorporation in HPMC gels. The rheological behaviour and the biomechanical properties of the TH-NLC gel formulations were suitable for skin delivery, with improved antimicrobial activity when using the gels formulations.

6.11 The developed gels for skin administration containing nanostructured systems of thymol, which allows to reduce the frequency of applications, could constitute, after adequate clinical development, a new strategy for acne treatment.

7. REFERENCES

A

Abrego, Guadalupe, Helen Alvarado, Eliana B. Souto, Bessy Guevara, Lyda Halbaut Bellowa, Alexander Parra, Ana Calpena, and María Luisa Garcia. 2015. "Biopharmaceutical Profile of Pranoprofen-Loaded PLGA Nanoparticles Containing Hydrogels for Ocular Administration." *European Journal of Pharmaceutics and Biopharmaceutics* 95 (February): 261–70. https://doi.org/10.1016/j.ejpb.2015.01.026.

Aguilar-López, Yuritze Alejandra, and Leopoldo Villafuerte-Robles. 2016. "Functional Performance of Chitosan/Carbopol 974P NF Matrices in Captopril Tablets." *Journal of Pharmaceutics* 2016: 1–9. https://doi.org/10.1155/2016/3240290.

Ajay Bhatia, Jean-Francoise Maisonneuve, and David H. Persing. 2004. "Propinobacterium Acnes and Chronic Diseases." In *The Infectious Etiology of Chronic Diseases: Defining the Relationship, Enhancing the Research, and Mitigating the Effects: Workshop Summary*.

Akhtar, N., M. U. Rehman, H. M.S. Khan, F. Rasool, T. Saeed, and G. Murtaza. 2011. "Penetration Enhancing Effect of Polysorbate 20 and 80 on the in Vitro Percutaneous Absorption of L-Ascorbic Acid." *Tropical Journal of Pharmaceutical Research* 10 (3): 281–88. https://doi.org/10.4314/tjpr.v10i3.1.

Alvarado, H. L., G. Abrego, E. B. Souto, M. L. Garduño-Ramirez, B. Clares, M. L. García, and A. C. Calpena. 2015. "Nanoemulsions for Dermal Controlled Release of Oleanolic and Ursolic Acids: In Vitro, Ex Vivo and in Vivo Characterization." *Colloids and Surfaces B: Biointerfaces* 130: 40–47. https://doi.org/10.1016/j.colsurfb.2015.03.062.

Alvarez-Román, R., A. Naik, Y. N. Kalia, R. H. Guy, and H. Fessi. 2004. "Skin Penetration and Distribution of Polymeric Nanoparticles." *Journal of Controlled Release* 99 (1): 53–62. https://doi.org/10.1016/j.jconrel.2004.06.015.

Aly, R, Howard I. Maibach, and H R Shinefield. 1977. "Microbial Flora of Atopic Dermatitis." *Archives of Dermatology* 113: 780–82.

Aman, Shazia, Shagufta Moin, M. Owais, and M. U. Siddiqui. 2013. "Antioxidant Activity of Thymol: Protective Role in AAPH-Induced Hemolysis in Diabetic Erythrocytes." *International Journal of Pharmaceutical Science Invention* 2 (3): 55–60.

Amasya, Gulin, Ozge Inal, and Ceyda Tuba Sengel-Turk. 2020. "SLN Enriched Hydrogels for Dermal Application: Full Factorial Design Study to Estimate the Relationship between Composition and Mechanical Properties." *Chemistry and Physics of Lipids* 228 (November 2019). https://doi.org/10.1016/j.chemphyslip.2020.104889.

Amiri, Hamzeh. 2012. "Essential Oils Composition and Antioxidant Properties of Three Thymus Species." *Evidence-Based Complementary and Alternative Medicine* 2012. https://doi.org/10.1155/2012/728065.

Anderson, James M., and Matthew S. Shive. 2012. "Biodegradation and Biocompatibility of PLA and PLGA Microspheres." *Advanced Drug Delivery Reviews* 64 (SUPPL.): 72–82. https://doi.org/10.1016/j.addr.2012.09.004.

Armstrong, Jeffrey S. 2006. "Mitochondrial Membrane Permeabilization: The Sine qua Non for Cell Death." *BioEssays* 28 (3): 253–60. https://doi.org/10.1002/bies.20370.

Atanasov, A G, S B Zotchev, V M Dirsch, and C T Supuran. 2021. "Natural Products in Drug Discovery: Impacts and Opportunities - Google Search." *Nature Review* 20 (March): 200–216. https://www.google.com/search?sourceid=chrome-psyapi2&ion=1&espv=2&ie=UTF-8&q=natural products in drug discovery%3A impacts and opportunities&oq=natural products in drug discovery%3A impacts and opportunities&aqs=chrome..69i57.15718j0j7.

B

Bagatin, Edileia, Thais Helena Proença De Freitas, Maria Cecilia Rivitti Machado, Beatriz Medeiros Ribeiro, Samanta Nunes, and Marco Alexandre Dias Da Rocha. 2019. "Adult Female Acne: A Guide to Clinical Practice." *Anais Brasileiros de Dermatologia* 94 (1): 62–75. https://doi.org/10.1590/abd1806-4841.20198203.

Bakkali, F., S. Averbeck, D. Averbeck, and M. Idaomar. 2008. "Biological Effects of Essential Oils - A Review." *Food and Chemical Toxicology* 46 (2): 446–75. https://doi.org/10.1016/j.fct.2007.09.106.

Balk, Ludwig Josef. 1988. "Scanning Electron Acoustic Microscopy." *Advances in Electronics and Electron Physics* 71: 1–73. https://doi.org/https://doi.org/10.1016/S0065-2539(08)60900-2.

Barakat, Hassan, Hamad S Aljabeili, and Hassan A Abdel Rahman. 2018. "Synergistic Effect of Thymus Vulgaris Essential Oil Oral Administration on Topically Treated Wound with Chitosan, Thyme Essential Oil and Their Combination in Rats." *Journal of Nutrition & Food Sciences* 08 (03). https://doi.org/10.4172/2155-9600.1000695.

Barros, Maria Elisabete Da Silva, Daniel De Assis Santos, and Júnia Soares Hamdan. 2007. "Evaluation of Susceptibility of Trichophyton Mentagrophytes and Trichophyton Rubrum Clinical Isolates to Antifungal Drugs Using a Modified CLSI Microdilution Method (M38-A)." *Journal of Medical Microbiology* 56 (4): 514–18. https://doi.org/10.1099/jmm.0.46542-0.

Becker Peres, Luana, Laize Becker Peres, Pedro Henrique Hermes de Araújo, and Claudia Sayer. 2016. "Solid Lipid Nanoparticles for Encapsulation of Hydrophilic Drugs by an Organic Solvent Free Double Emulsion Technique." *Colloids and Surfaces B: Biointerfaces* 140: 317–23. https://doi.org/10.1016/j.colsurfb.2015.12.033.

Bharti, Sneha, and Harini Chowdary Vadlamudi. 2021. "A Strategic Review on the Involvement of Receptors, Transcription Factors and Hormones in Acne Pathogenesis." *Journal of Receptors and Signal Transduction* 41 (2): 105–16. https://doi.org/10.1080/10799893.2020.1805626.

Bilia, Anna Rita, Clizia Guccione, Benedetta Isacchi, Chiara Righeschi, Fabio Firenzuoli, and Maria Camilla Bergonzi. 2014. "Essential Oils Loaded in Nanosystems: A Developing Strategy for a Successful Therapeutic Approach." *Evidence-Based Complementary and Alternative Medicine* 2014. https://doi.org/10.1155/2014/651593.

Bos, Jan D., and Marcus M.H.M. Meinardi. 2000. "The 500 Dalton Rule for the Skin Penetration of Chemical Compounds and Drugs." *Experimental Dermatology* 9 (3): 165–69. https://doi.org/10.1034/j.1600-0625.2000.009003165.x.

Boukraâ, Laïd, Fatiha Abdellah, and Leïla Ait-Abderrahim. 2013. "Antimicrobial Properties of Bee Products and Medicinal Plants." *Formatex*, no. Microbial pathogens and strategies for combating them: science, technology and education: 960–70. http://www.formatex.info/microbiology4/vol2/960-970.pdf.

Boxberger, Manon, Valérie Cenizo, Nadim Cassir, and Bernard La Scola. 2021. "Challenges in Exploring and Manipulating the Human Skin Microbiome." *Microbiome* 9 (1): 1–14. https://doi.org/10.1186/s40168-021-01062-5.

Briganti, S., and M. Picardo. 2003. "Antioxidant Activity, Lipid Peroxidation and Skin Diseases. What's New." *Journal of the European Academy of Dermatology and Venereology* 17 (6): 663–69. https://doi.org/10.1046/j.1468-3083.2003.00751.x.

Buck Louis, Germaine M, and Rajeshwari Sundaram. 2012. "Exposome: Time for Transformative Research." *Stat Med* 31 (22): 1–9. https://doi.org/10.1002/sim.5496.Exposome.

C

Çalışkan, Ufuk Koca, and Methiye Mancak Karakuş. 2020. "Essential Oils as Skin Permeation Boosters and Their Predicted Effect Mechanisms" 2 (3): 24–30.

Calpena, Ana C, Beatriz Clares, and Francisco Fernández. 2011. "Technological, Biopharmaceutical and Pharmacokinetic Advances: New Formulations of Application on the Skin and Oral Mucosa." In *Recent Advances in Pharmaceutical Sciences*, edited by Diego Muñoz-Torrero, 661:175–98. Kerala, India: Transworld Research Network.

Cano, Amanda, Miren Ettcheto, Marta Espina, Carmen Auladell, Ana Cristina Calpena, Jaume Folch, Marta Barenys, Elena Sánchez-López, Antoni Camins, and Maria Luisa García. 2018. "Epigallocatechin-3-Gallate Loaded PEGylated-PLGA Nanoparticles: A New Anti-Seizure Strategy for Temporal Lobe Epilepsy." *Nanomedicine: Nanotechnology, Biology, and Medicine* 14 (4): 1073–85. https://doi.org/10.1016/j.nano.2018.01.019.

Carvajal-Vidal, Paulina, María José Fábrega, M. Espina, Ana Cristina Calpena, and M. Luisa García. 2019. "Development of Halobetasol-Loaded Nanostructured Lipid Carrier for Dermal Administration: Optimization, Physicochemical and Biopharmaceutical Behavior, and Therapeutic Efficacy." *Nanomedicine: Nanotechnology, Biology, and Medicine* 20: 1–10. https://doi.org/10.1016/j.nano.2019.102026.

Carvajal-Vidal, Paulina, Roberto González-Pizarro, Carolina Araya, Marta Espina, Lyda Halbaut, Immaculada Gómez de Aranda, M. Luisa García, and Ana C. Calpena. 2020. "Nanostructured Lipid Carriers Loaded with Halobetasol Propionate for Topical Treatment of Inflammation: Development, Characterization, Biopharmaceutical Behavior and Therapeutic Efficacy of Gel Dosage Forms." *International Journal of Pharmaceutics*. https://doi.org/10.1016/j.ijpharm.2020.119480.

Choi, Kyeong Ok, Jaehyeog Choe, Seokjin Suh, and Sanghoon Ko. 2016. "Positively Charged Nanostructured Lipid Carriers and Their Effect on the Dissolution of Poorly Soluble Drugs." *Molecules* 21 (5). https://doi.org/10.3390/molecules21050672.

Claudel, Jean Paul, Nicole Auffret, Marie Thérèse Leccia, Florence Poli, Stéphane Corvec, and Brigitte Dréno. 2019. "Staphylococcus Epidermidis: A Potential New Player in the Physiopathology of Acne?" *Dermatology* 235 (4): 287–94. https://doi.org/10.1159/000499858.

Coates, Margaret, Min Jin Lee, Diana Norton, and Amanda S. MacLeod. 2019. "The Skin and Intestinal Microbiota and Their Specific Innate Immune Systems." *Frontiers in Immunology* 10 (December): 1–11. https://doi.org/10.3389/fimmu.2019.02950.

Coenye, Tom, Elke Peeters, and Hans J. Nelis. 2007. "Biofilm Formation by Propionibacterium Acnes Is Associated with Increased Resistance to Antimicrobial Agents and Increased Production of Putative Virulence Factors." *Research in Microbiology* 158 (4): 386–92. https://doi.org/10.1016/j.resmic.2007.02.001.

Couto, Ana, Rúben Fernandes, M Natália S Cordeiro, Sara S Reis, Rogério T Ribeiro, and Ana M Pessoa. 2014. "Dermic Diffusion and Stratum Corneum : A State of the Art Review of Mathematical Models" 177: 74–83.

D

Diaz-Garrido, Natalia, María José Fábrega, Rodrigo Vera, Rosa Giménez, Josefa Badia, and Laura Baldomà. 2019. "Membrane Vesicles from the Probiotic Nissle 1917 and Gut Resident Escherichia Coli Strains Distinctly Modulate Human Dendritic Cells and Subsequent T Cell Responses." *Journal of Functional Foods* 61 (May). https://doi.org/10.1016/j.jff.2019.103495.

Dréno, B., V. Bettoli, E. Araviiskaia, M. Sanchez Viera, and A. Bouloc. 2018. "The Influence of

Exposome on Acne." *Journal of the European Academy of Dermatology and Venereology* 32 (5): 812–19. https://doi.org/10.1111/jdv.14820.

Dreno, B., H. P.M. Gollnick, S. Kang, D. Thiboutot, V. Bettoli, V. Torres, and J. Leyden. 2015. "Understanding Innate Immunity and Inflammation in Acne: Implications for Management." *Journal of the European Academy of Dermatology and Venereology* 29 (S4): 3–11. https://doi.org/10.1111/jdv.13190.

E

Erin Chen, Y., Michael A. Fischbach, and Yasmine Belkaid. 2018. "Skin Microbiota-Host Interactions." *Nature* 553 (7689): 427–36. https://doi.org/10.1038/nature25177.

F

Fernández-García, Elisabet, Hayat Heluani-Gahete, and Ralf E. Wellinger. 2016. "A New Colorimetric Assay for Antioxidant Capacity and Photostability." *Coloration Technology* 132 (3): 195–200. https://doi.org/10.1111/cote.12210.

Fessi, H., F. Puisieux, J. Ph Devissaguet, N. Ammoury, and S. Benita. 1989. "Nanocapsule Formation by Interfacial Polymer Deposition Following Solvent Displacement." *International Journal of Pharmaceutics* 55 (1): R1–4. https://doi.org/10.1016/0378-5173(89)90281-0.

Flowers, Laurice, and Elizabeth A. Grice. 2020. "The Skin Microbiota: Balancing Risk and Reward." *Cell Host and Microbe* 28 (2): 190–200. https://doi.org/10.1016/j.chom.2020.06.017.

Frans Weber. 1995. *Toluene: Biological Waste-Gas Treatment Toxicitz and Microbial Adaptation*.

G

Ghasemi Pirbalouti, A., M. Rahimmalek, F. Malekpoor, and A. Karimi. 2011. "Variation in Antibacterial Activity, Thymol and Carvacrol Contents of Wild Populations of Thymus Daenensis Subsp. Daenensis Celak." *Plant OMICS* 4 (4): 209–14.

Gill, Pooria, Tahereh Tohidi Moghadam, and Bijan Ranjbar. 2010. "Differential Scanning Calorimetry Techniques: Applications in Biology and Nanoscience." *Journal of Biomolecular Techniques* 21 (4): 167–93.

Gómez-Segura, Lídia, Alexander Parra, Ana Cristina Calpena-Campmany, Álvaro Gimeno, Immaculada Gómez de Aranda, and Antonio Boix-Montañes. 2020. "Ex Vivo Permeation of Carprofen Vehiculated by PLGA Nanoparticles through Porcine Mucous Membranes and Ophthalmic Tissues." *Nanomaterials* 10 (2). https://doi.org/10.3390/nano10020355.

Gonzalez-Pizarro, Roberto, Graziella Parrotta, Rodrigo Vera, Elena Sánchez-López, Ruth Galindo, Frank Kjeldsen, Josefa Badia, Laura Baldoma, Marta Espina, and María L. García. 2019. "Ocular Penetration of Fluorometholone-Loaded PEG-PLGA Nanoparticles Functionalized with Cell-Penetrating Peptides." *Nanomedicine* 14 (23): 3089–3104. https://doi.org/10.2217/nnm-2019-0201.

Gorzelanny, Christian, Christian Mess, Stefan W. Schneider, Volker Huck, and Johanna M. Brandner. 2020. "Skin Barriers in Dermal Drug Delivery: Which Barriers Have to Be Overcome and How Can We Measure Them?" *Pharmaceutics* 12 (7): 1–31. https://doi.org/10.3390/pharmaceutics12070684.

Governa, Paolo, Gabriele Carullo, Marco Biagi, Vittoria Rago, and Francesca Aiello. 2019. "Evaluation of the in Vitro Wound-Healing Activity of Calabrian Honeys." *Antioxidants* 8 (2): 1–16. https://doi.org/10.3390/antiox8020036.

Graham-Brown, R, and J Bourke. 2006. "Mosby's Color Atlas and Text of Dermatology." london.

Grice, Elizabeth A., and Julia A. Segre. 2011. “The Skin Microbiome.” *Nature Reviews Microbiology* 9 (4): 244–53. https://doi.org/10.1038/nrmicro2537.

Grigore, A., Ina Paraschiv, S. Colceru-Mihul, C. Bubueanu, E. Draghici, and M. Ichim. 2010. “Chemical Composition and Antioxidant Activity of Thymus Vulgaris L. Volatile Oil Obtained by Two Different Methods.” *Romanian Biotechnological Letters* 15 (4): 5436–43.

Gu, Yongwei, Meng Yang, Xiaomeng Tang, Ting Wang, Dishun Yang, Guangxi Zhai, and Jiyong Liu. 2018. “Lipid Nanoparticles Loading Triptolide for Transdermal Delivery: Mechanisms of Penetration Enhancement and Transport Properties.” *Journal of Nanobiotechnology* 16 (1): 1–14. https://doi.org/10.1186/s12951-018-0389-3.

H

Ho, Hoang Nhan, Thien Giap Le, Thi Thanh Tuyen Dao, Thi Ha Le, Thi Thanh Hai Dinh, Dang Hoa Nguyen, Trinh Cong Tran, and Chien Ngoc Nguyen. 2020. “Development of Itraconazole-Loaded Polymeric Nanoparticle Dermal Gel for Enhanced Antifungal Efficacy.” *Journal of Nanomaterials* 2020. https://doi.org/10.1155/2020/8894541.

Honary, Soheyla, and Foruhe Zahir. 2013. “Effect of Zeta Potential on the Properties of Nano-Drug Delivery Systems - A Review (Part 1).” *Tropical Journal of Pharmaceutical Research* 12 (2): 255–64. https://doi.org/10.4314/tjpr.v12i2.19.

I

Inaoki, Makoto, Chihiro Nishijima, Miho Miyake, Toshiyuki Asaka, Youichi Hasegawa, Kazushi Anzawa, and Takashi Mochizuki. 2015. “Case of Dermatophyte Abscess Caused by Trichophyton Rubrum: A Case Report and Review of the Literature.” *Mycoses* 58 (5): 318–23. https://doi.org/10.1111/myc.12317.

Ingham, E., E A Eady, C E Goodwin, J H Cove, and WJ Cunliffe. 1992. “Pro-Inflammatory Levels of Interleukin-1 Alpha-like Bioactivity Are Present in the Majority of Open Comedones in Acne Vulgaris.” *J Invest Dermatol* . 98 (6): 895–901. https://doi.org/doi: 10.1111/1523-1747.ep12460324.

J

Jangpromma, Nisachon, Sutthidech Preecharram, Thanawan Srilert, Surachai Maijaroen, Pramote Mahakunakorn, Natsajee Nualkaew, Sakda Daduang, and Sompong Klaynongsruang. 2016. “In Vitro and in Vivo Wound Healing Properties of Plasma and Serum from Crocodylus Siamensis Blood.” *Journal of Microbiology and Biotechnology* 26 (6): 1140–47. https://doi.org/10.4014/jmb.1601.01054.

Jeremy, Anthony H.T., Diana B. Holland, Susan G. Roberts, Kathryn F. Thomson, and William J. Cunliffe. 2003. “Inflammatory Events Are Involved in Acne Lesion Initiation.” *Journal of Investigative Dermatology* 121 (1): 20–27. https://doi.org/10.1046/j.1523-1747.2003.12321.x.

K

Kampf G, and Karamer A. 2004. “Epidemiologic Background of Hand Hygiene and Evaluation of the Most Important Agents for Scrubs and Rubs.” *Clinical Microbiology Reviews* 17 (4): 863–93. https://doi.org/10.1128/CMR.17.4.863.

Kapuścińska, Alicja, and Izabela Nowak. 2015. “Use of Organic Acids in Acne and Skin Discolorations Therapy.” *Postepy Higieny i Medycyny Doswiadczalnej* 69: 374–83. https://doi.org/10.5604/17322693.1145825.

Katsuta, Y., T. Iida, K. Hasegawa, S. Inomata, and M. Denda. 2009. “Function of Oleic Acid on Epidermal Barrier and Calcium Influx into Keratinocytes Is Associated with N-Methyl d-Aspartate-Type Glutamate Receptors.” *British Journal of Dermatology* 160 (1): 69–74.

https://doi.org/10.1111/j.1365-2133.2008.08860.x.

Khater, Dima, Hamdi Nsairat, Fadwa Odeh, Mais Saleh, Areej Jaber, Walhan Alshaer, Abeer Al Bawab, and Mohammad S Mubarak. 2021. "And Transdermal Lipid Nanoparticles : A Review," 1–43.

Khmaladze, Ia, Michele Leonardi, Susanne Fabre, Cyril Messaraa, and Alain Mavon. 2020. "The Skin Interactome: A Holistic 'Genome-Microbiome-Exposome' Approach to Understand and Modulate Skin Health and Aging." *Clinical, Cosmetic and Investigational Dermatology* 13: 1021–40. https://doi.org/10.2147/CCID.S239367.

Kim, D, H El-Shall, D Dennis, and T Morey. 2005. "Interaction of PLGA Nanoparticles with Human Blood Constituents." *Colloids and Surfaces. B, Biointerfaces* 40 (2): 83–91. https://doi.org/10.1016/j.colsurfb.2004.05.007.

Kim, Byel, Hang-Eui Cho, Sun He Moon, Hyun-Jung Ahn, Seunghee Bae, Hyun-Dae Cho, and Sungkwan An. 2020. "Transdermal Delivery Systems in Cosmetics." Biomedical Dermatology 4(1):1–12.

Kim, Jenny. 2005. "Review of the Innate Immune Response in Acne Vulgaris: Activation of Toll-like Receptor 2 in Acne Triggers Inflammatory Cytokine Responses." *Dermatology* 211 (3): 193–98. https://doi.org/10.1159/000087011.

Kim, Ji Young, Sumi Oh, Bora Yi, Mi Ja Kim, and Jae Hwan Lee. 2015. "Synergism of Phosphatidylcholine on the Antioxidant Properties of α-Tocopherol in Corn Oils under Different Relative Humidity." *International Journal of Food Science and Technology* 50 (6): 1421–28. https://doi.org/10.1111/ijfs.12793.

Koeth, L.M., and L.A. Miller. 2019. "Antimicrobial Susceptibility Test Methods: Dilution and Disk Diffusion Methods." In *Manual of Clinical Microbiology, 12th Ed*, edited by K.C. Carroll, M.A. Pfaller, M.L. Landy, R. Patel, A.J. McAdam, and S.S Richter, 12th ed., 1284–99. ASM Press. Washington D. C. https://doi.org/10.1128/9781683670438.MCM.ch73.

Kostyuk, Vladimir, Alla Potapovich, Andrea Stancato, Chiara de Luca, Daniela Lulli, Saveria Pastore, and Liudmila Korkina. 2012. "Photo-Oxidation Products of Skin Surface Squalene Mediate Metabolic and Inflammatory Responses to Solar UV in Human Keratinocytes." *PLoS ONE* 7 (8): 1–11. https://doi.org/10.1371/journal.pone.0044472.

Kühbacher, Andreas, Anke Burger-Kentischer, and Steffen Rupp. 2017. "Interaction of Candida Species with the Skin." *Microorganisms* 5 (4): 32. https://doi.org/10.3390/microorganisms5020032.

L

Lampe, M. A., A. L. Burlingame, J. A. Whitney, M. L. Williams, B. E. Brown, E. Roitman, and P. M. Elias. 1983. "Human Stratum Corneum Lipids: Characterization and Regional Variations." *Journal of Lipid Research*. https://doi.org/10.1016/s0022-2275(20)38005-6.

Lauterbach, Andreas, and Christel C. Müller-Goymann. 2015. "Applications and Limitations of Lipid Nanoparticles in Dermal and Transdermal Drug Delivery via the Follicular Route." *European Journal of Pharmaceutics and Biopharmaceutics* 97: 152–63. https://doi.org/10.1016/j.ejpb.2015.06.020.

Lee, Byun, and Kim. 2019. "Potential Role of the Microbiome in Acne: A Comprehensive Review." *Journal of Clinical Medicine* 8 (7): 987. https://doi.org/10.3390/jcm8070987.

Lee, Chi H., Venkat Moturi, and Yugyung Lee. 2009. "Thixotropic Property in Pharmaceutical Formulations." *Journal of Controlled Release* 136 (2): 88–98. https://doi.org/10.1016/j.jconrel.2009.02.013.

Lemarchand, Caroline, Patrick Couvreur, Christine Vauthier, Dominique Costantini, and Ruxandra Gref. 2003. "Study of Emulsion Stabilization by Graft Copolymers Using the

Optical Analyzer Turbiscan." *International Journal of Pharmaceutics* 254 (1): 77–82. https://doi.org/10.1016/S0378-5173(02)00687-7.

Li, Zheng Jun, Dae Kyoung Choi, Kyung Cheol Sohn, Min Seok Seo, Hae Eul Lee, Young Lee, Young Joon Seo, et al. 2014. "Propionibacterium Acnes Activates the NLRP3 Inflammasome in Human Sebocytes." *Journal of Investigative Dermatology* 134 (11): 2747–56. https://doi.org/10.1038/jid.2014.221.

Lira Mota, Kelly Samara De, Fillipe De Oliveira Pereira, Wylly Araújo De Oliveira, Igara Oiveira Lima, and Edeltrudes De Oliveira Lima. 2012. "Antifungal Activity of Thymus Vulgaris l. Essential Oil and Its Constituent Phytochemicals against Rhizopus Oryzae: Interaction with Ergosterol." *Molecules* 17 (12): 14418–33. https://doi.org/10.3390/molecules171214418.

Liu, Lihong, Kun Guo, Jia Lu, Subbu S. Venkatraman, Dan Luo, Kian Chye Ng, Eng Ang Ling, Shabbir Moochhala, and Yi Yan Yang. 2008. "Biologically Active Core/Shell Nanoparticles Self-Assembled from Cholesterol-Terminated PEG-TAT for Drug Delivery across the Blood-Brain Barrier." *Biomaterials* 29 (10): 1509–17. https://doi.org/10.1016/j.biomaterials.2007.11.014.

Liu, Yuh Hwa, Yin Shiou Lin, Yu Wei Huang, Sheng Uei Fang, Shyr Yi Lin, and Wen Chi Hou. 2016. "Protective Effects of Minor Components of Curcuminoids on Hydrogen Peroxide-Treated Human HaCaT Keratinocytes." *Journal of Agricultural and Food Chemistry* 64 (18): 3598–3608. https://doi.org/10.1021/acs.jafc.6b01196.

Luelmo-aguilar, Jesús, and Mireia Sàbat Santandreu. 2004. "Folliculitis Recognition and Management." *Am J Clin Dermatol* 5 (5): 301–10.

M

MacGowan, A. P., M. Wootton, A. J. Hedges, K. E. Bowker, H. A. Holt, and D. S. Reeves. 1996. "A New Time-Kill Method of Assessing the Relative Efficacy of Antimicrobial Agents Alone and in Combination Developed Using a Representative β-Lactam, Aminoglycoside and Fluoroquinolone." *Journal of Antimicrobial Chemotherapy* 38 (2): 193–203. https://doi.org/10.1093/jac/38.2.193.

Mandal, Shyamapada, and Manisha Debmandal. 2016. "Thyme (Thymus Vulgaris L .) Oils," no. 1998: 825–34.

Manou, I., L. Bouillard, M. J. Devleeschouwer, and A. O. Barel. 1998. "Evaluation of the

Preservative Properties of Thymus Vulgaris Essential Oil in Topically Applied

Formulations under a Challenge Test." *Journal of Applied Microbiology* 84(3):368–76.

Maupas, Caroline, Brice Moulari, Arnaud Béduneau, Alf Lamprecht, and Yann Pellequer. 2011. "Surfactant Dependent Toxicity of Lipid Nanocapsules in HaCaT Cells." *International Journal of Pharmaceutics* 411 (1–2): 136–41. https://doi.org/10.1016/j.ijpharm.2011.03.056.

Mazia, Daniel, Gerald Schatten, and Winfield Sale. 1975. "Adhesion of Cells to Surfaces Coated with Polylysine: Applications to Electron Microscopy." *Journal of Cell Biology* 66 (1): 198–200. https://doi.org/10.1083/jcb.66.1.198.

McConnell, Michael L. 1981. "Particle Size Determination by Quasielastic Light Scattering." *Analytical Chemistry* 53 (8): 1–5. https://doi.org/10.1021/ac00231a799.

Melnik, Bodo C. 2018. "Acne Vulgaris: The Metabolic Syndrome of the Pilosebaceous Follicle." *Clinics in Dermatology* 36 (1): 29–40. https://doi.org/10.1016/j.clindermatol.2017.09.006.

Mengoni, Tamara, Manuela Adrian, Susana Pereira, Beatriz Santos-Carballal, Mathias Kaiser, and Francisco M. Goycoolea. 2017. "A Chitosan-Based Liposome Formulation Enhances

the in Vitro Wound Healing Efficacy of Substance P Neuropeptide." *Pharmaceutics* 9 (4). https://doi.org/10.3390/pharmaceutics9040056.

Messager, S., P. A. Goddard, P. W. Dettmar, and J. Y. Maillard. 2001. "Determination of the Antibacterial Efficacy of Several Antiseptics Tested on Skin by an 'ex-Vivo' Test." *Journal of Medical Microbiology* 50 (3): 284–92. https://doi.org/10.1099/0022-1317-50-3-284.

Messager, S., A. C. Hann, P. A. Goddard, P. W. Dettmar, and J. Y. Maillard. 2004. "Use of the 'ex Vivo' Test to Study Long-Term Bacterial Survival on Human Skin and Their Sensitivity to Antisepsis." *Journal of Applied Microbiology* 97 (6): 1149–60. https://doi.org/10.1111/j.1365-2672.2004.02403.x.

Miller, Gary W., and Dean P. Jones. 2014. "The Nature of Nurture: Refining the Definition of the Exposome." *Toxicological Sciences* 137 (1): 1–2. https://doi.org/10.1093/toxsci/kft251.

Mollarafie, P., P. Khadiv Parsi, R. Zarghami, M. Amini Fazl, and R. Ghafarzadegan. 2015. "Antibacterial and Wound Healing Properties of Thymol (Thymus Vulgaris Oil) and Its Application in a Novel Wound Dressing." *Journal of Medicinal Plants* 14 (53): 69–81.

Müller, R. H., M. Radtke, and S. A. Wissing. 2002. "Nanostructured Lipid Matrices for Improved Microencapsulation of Drugs." *International Journal of Pharmaceutics* 242 (1–2): 121–28. https://doi.org/10.1016/S0378-5173(02)00180-1.

N

Nagle PS, Pawar YA, Sonawane AE, Nikum AP, Patil UD and More DH. 2013. "Thymol: Synthesis, Reactions & Its Spectrum of Pharmacological and Chemical Applications." *Indo American Journal of Pharmaceutical Research* 3 (9): 387–420. https://doi.org/10.1016/B978-1-4557-2550-2.00010-9.

Nagoor Meeran, M. F., G. S. Jagadeesh, and P. Selvaraj. 2016. "Thymol, a Dietary Monoterpene Phenol Abrogates Mitochondrial Dysfunction in β-Adrenergic Agonist Induced Myocardial Infarcted Rats by Inhibiting Oxidative Stress." *Chemico-Biological Interactions* 244: 159–68. https://doi.org/10.1016/j.cbi.2015.12.006.

Nagoor Meeran, Mohamed Fizur, Hayate Javed, Hasan Al Taee, Sheikh Azimullah, and Shreesh K. Ojha. 2017. "Pharmacological Properties and Molecular Mechanisms of Thymol: Prospects for Its Therapeutic Potential and Pharmaceutical Development." *Frontiers in Pharmacology* 8 (JUN): 1–34. https://doi.org/10.3389/fphar.2017.00380.

Nagy, István, Andor Pivarcsi, Andrea Koreck, Márta Széll, Edit Urbán, and Lajos Kemény. 2005. "Distinct Strains of Propionibacterium Acnes Induce Selective Human β-Defensin-2 and Interleukin-8 Expression in Human Keratinocytes through Toll-like Receptors." *Journal of Investigative Dermatology*. https://doi.org/10.1111/j.0022-202X.2005.23705.x.

Najafloo, Raziyeh, Mahla Behyari, Rana Imani, and Shirin Nour. 2020. "A Mini-Review of Thymol Incorporated Materials: Applications in Antibacterial Wound Dressing." *Journal of Drug Delivery Science and Technology* 60 (March). https://doi.org/10.1016/j.jddst.2020.101904.

Nanang, M., N. Fuad, R. Didik, S. Topo, and J. Panuwun. 2018. "Effect of Alkaline Fluids to Blood PH and Lactic Acid Changes on Sub Maximal Physical Exercise." *IOP Conference Series: Earth and Environmental Science* 197 (1). https://doi.org/10.1088/1755-1315/197/1/012049.

Noble, W. C. 1993. *The Skin Microflora and Microbial Skin Disease*. Edited by W.C. Noble. cambridge: University Press.

Nostro, Antonia, Andrea Sudano Roccaro, Giuseppe Bisignano, Andreana Marino, Maria A. Cannatelli, Francesco C. Pizzimenti, Pier Luigi Cioni, Francesca Procopio, and Anna Rita Blanco. 2007. "Effects of Oregano, Carvacrol and Thymol on Staphylococcus Aureus and

Staphylococcus Epidermidis Biofilms." *Journal of Medical Microbiology* 56 (4): 519–23. https://doi.org/10.1099/jmm.0.46804-0.

Nowak, Agnieska, Danuta Kalemba, Malgorzata Piotrowska, and Agata Czyzowska. 2013. "Effects of Thyme (Thymus Vulgaris L.) and Rosemary (Rosmarinus Officinalis L.) Essential Oils on Growth of Brochothrix." *African Journal of Microbiology Research* 7 (26): 3396–3404. https://doi.org/DOI: 10.5897/AJMR12.1618 ISSN.

O

Ocaña, A., and G. Reglero. 2012. "Effects of Thyme Extract Oils (from Thymus Vulgaris, Thymus Zygis, and Thymus Hyemalis) on Cytokine Production and Gene Expression of OxLDL-Stimulated THP-1-Macrophages." *Journal of Obesity* 2012. https://doi.org/10.1155/2012/104706.

Otto, Michael. 2009. "Staphylococcus Epidermidis – the 'Accidental' Pathogen." *Nat Rev Microbiol* 7 (8): 557–67. https://doi.org/10.1038/nrmicro2182.

Özcan, Musa, and Jean-claude Chalchat. 2004. "Aroma Profile of Thymus Vulgaris L. Growing Wild in Turkey." *Bulgarian Journal of Plant Physiology* 30: 68–73.

Özgüven, Menşure, and Sezen Tansi. 1998. "Drug Yield and Essential Oil of Thymus Vulgaris L. as in Influenced by Ecological and Ontogenetical Variation." *Turkish Journal of Agriculture and Forestry* 22 (6): 537–42. https://doi.org/10.3906/tar-96123.

P

Palmer, Brian C., and Lisa A. DeLouise. 2016. "Nanoparticle-Enabled Transdermal Drug Delivery Systems for Enhanced Dose Control and Tissue Targeting." *Molecules* 21 (12): 7–9. https://doi.org/10.3390/molecules21121719.

Pappas, Apostolos. 2009. "Epidermal Surface Lipids." *Dermato-Endocrinology* 1 (2): 72–76. https://doi.org/10.4161/derm.1.2.7811.

Patel, D, R Kesharwani, and P S Gupta. 2013. "Development & Screening Approach for Lipid Nano Particle: A Review." Innovations in Pharmaceutical Sciences 2 (5): 27–32.

Patzelt, Alexa, and Juergen Lademann. 2020. "Recent Advances in Follicular Drug Delivery of Nanoparticles." *Expert Opinion on Drug Delivery* 17 (1): 49–60. https://doi.org/10.1080/17425247.2020.1700226.

Pereira, Maíra N., Heidi L. Schulte, Natane Duarte, Eliana M. Lima, Livia L. Sá-Barreto, Tais Gratieri, Guilherme M. Gelfuso, and Marcilio S.S. Cunha-Filho. 2017. "Solid Effervescent Formulations as New Approach for Topical Minoxidil Delivery." *European Journal of Pharmaceutical Sciences* 96: 411–19. https://doi.org/10.1016/j.ejps.2016.10.016.

Petkovšek, Živa, Kristina Eleršič, Marija Gubina, Darja Žgur-Bertok, and Marjanca Starčič Erjavec. 2009. "Virulence Potential of Escherichia Coli Isolates from Skin and Soft Tissue Infections." *Journal of Clinical Microbiology* 47 (6): 1811–17. https://doi.org/10.1128/JCM.01421-08.

Pham, Quoc Dat, Sebastian Björklund, Johan Engblom, Daniel Topgaard, and Emma Sparr. 2016. "Chemical Penetration Enhancers in Stratum Corneum - Relation between Molecular Effects and Barrier Function." *Journal of Controlled Release* 232: 175–87. https://doi.org/10.1016/j.jconrel.2016.04.030.

Pinto Reis, Catarina, Ronald J. Neufeld, António J. Ribeiro, and Francisco Veiga. 2006. "Nanoencapsulation I. Methods for Preparation of Drug-Loaded Polymeric Nanoparticles." *Nanomedicine: Nanotechnology, Biology, and Medicine* 2 (1): 8–21. https://doi.org/10.1016/j.nano.2005.12.003.

Pires, Felipe Q., Tamara Angelo, Joyce K.R. Silva, Lívia C.L. Sá-Barreto, Eliana M. Lima,

Guilherme M. Gelfuso, Tais Gratieri, and Marcílio S.S. Cunha-Filho. 2017. "Use of Mixture Design in Drug-Excipient Compatibility Determinations: Thymol Nanoparticles Case Study." *Journal of Pharmaceutical and Biomedical Analysis* 137: 196–203. https://doi.org/10.1016/j.jpba.2017.01.037.

Pivetta, Thais P., Sandra Simões, Margarete M. Araújo, Tânia Carvalho, Caroline Arruda, and Priscyla D. Marcato. 2018. "Development of Nanoparticles from Natural Lipids for Topical Delivery of Thymol: Investigation of Its Anti-Inflammatory Properties." *Colloids and Surfaces B: Biointerfaces* 164: 281–90. https://doi.org/10.1016/j.colsurfb.2018.01.053.

Platsidaki, Eftychia, and Clio Dessinioti. 2018. "Recent Advances in Understanding Propionibacterium Acnes (Cutibacterium Acnes) in Acne [Version 1; Referees: 2 Approved]." *F1000Research* 7 (0). https://doi.org/10.12688/f1000research.15659.1.

Porte, Alexandre, and Ronoel L.O. Godoy. 2008. "Chemical Composition of Thymus Vulgaris L. (Thyme) Essential Oil from the Rio de Janeiro State (Brazil)." *Journal of the Serbian Chemical Society* 73 (3): 307–10. https://doi.org/10.2298/JSC0803307P.

Poulose, A J, and R Croteau. 1978. "Biosynthesis of Aromatic Monoterpenes: Conversion of γ-Terpinene to p-Cymene and Thymol in Thymus Vulgaris L." *Archives of Biochemistry and Biophysics* 187 (2): 307–14. https://doi.org/https://doi.org/10.1016/0003-9861(78)90039-5.

R

Rajapaksa, Thejani E., Mary Stover-Hamer, Xiomara Fernandez, Holly A. Eckelhoefer, and David D. Lo. 2010. "Claudin 4-Targeted Protein Incorporated into PLGA Nanoparticles Can Mediate M Cell Targeted Delivery." *J. Control Release* 142 (2): 196.205. https://doi.org/doi:10.1016/j.jconrel.2009.10.033.

Rappaport, Stephen M. 2011. "Implications of the Exposome for Exposure Science." *Journal of Exposure Science and Environmental Epidemiology* 21 (1): 5–9. https://doi.org/10.1038/jes.2010.50.

Rehman, Khurram, Mohd Fadhlizil Fasihi Mohd Aluwi, Kamal Rullah, Lam Kok Wai, Mohd Cairul Iqbal Mohd Amin, and Mohd Hanif Zulfakar. 2015. "Probing the Effects of Fish Oil on the Delivery and Inflammation-Inducing Potential of Imiquimod." *International Journal of Pharmaceutics* 490 (1–2): 131–41. https://doi.org/10.1016/j.ijpharm.2015.05.045.

Roldan, Lina P, Gonzalo J Díaz, and Jennifer M Duringer. 2010. "Composition and Antibacterial Activity of Essential Oils Obtained from Plants of the Lamiaceae Family against Pathogenic and Beneficial Bacteria." *Revista Colombiana de Ciencias Pecuarias* 23 (2): 451–61.

Rosen, Jamie, and Adam J Friedman. 2014. "Guest Editorial Editorial TI o No t c Op y O."

Rozas, Miquel, Astrid Hart de Ruijter, Maria Jose Fabrega, Amine Zorgani, Marc Guell, Bernhard Paetzold, and Francois Brillet. 2021. "From Dysbiosis to Healthy Skin: Major Contributions of Cutibacterium Acnes to Skin Homeostasis." *Microorganisms* 9 (3): 1–18. https://doi.org/10.3390/microorganisms9030628.

Russo, Jackson, Jennifer Fiegel, and Nicole K. Brogden. 2020. "Rheological and Drug Delivery Characteristics of Poloxamer-Based Diclofenac Sodium Formulations for Chronic Wound Site Analgesia." *Pharmaceutics* 12 (12): 1–18. https://doi.org/10.3390/pharmaceutics12121214.

S

Sachdeva, Muskaan, Josephine Tan, Jacqueline Lim, Matilda Kim, Ibrahim Nadeem, and Ramprasad Bismil. 2021. "The Prevalence, Risk Factors, and Psychosocial Impacts of Acne Vulgaris in Medical Students: A Literature Review." *International Journal of Dermatology*

60 (7): 792–98. https://doi.org/10.1111/ijd.15280.

Sáez-Orviz, Sara, Ismael Marcet, Shihan Weng, Manuel Rendueles, and Mario Díaz. 2020. "PLA Nanoparticles Loaded with Thymol to Improve Its Incorporation into Gelatine Films." *Journal of Food Engineering* 269 (September 2019): 1–7. https://doi.org/10.1016/j.jfoodeng.2019.109751.

Salsberg, Jennifer, Anneke Andriessen, Sonya Abdulla, Renita Ahluwalia, Jennifer Beecker, Megan Sander, and Jordana Schachter. 2019. "A Review of Protection against Exposome Factors Impacting Facial Skin Barrier Function with 89% Mineralizing Thermal Water." *Journal of Cosmetic Dermatology* 18 (3): 815–20. https://doi.org/10.1111/jocd.12927.

Sánchez-López, E., M. A. Egea, A. Cano, M. Espina, A. C. Calpena, M. Ettcheto, A. Camins, E. B. Souto, A. M. Silva, and M. L. García. 2016. "PEGylated PLGA Nanospheres Optimized by Design of Experiments for Ocular Administration of Dexibuprofen-in Vitro, Ex Vivo and in Vivo Characterization." *Colloids and Surfaces B: Biointerfaces* 145 (September): 241–50. https://doi.org/10.1016/j.colsurfb.2016.04.054.

Sánchez-López, E., M. Espina, S. Doktorovova, E. B. Souto, and M. L. García. 2017. "Lipid Nanoparticles (SLN, NLC): Overcoming the Anatomical and Physiological Barriers of the Eye – Part II - Ocular Drug-Loaded Lipid Nanoparticles." *European Journal of Pharmaceutics and Biopharmaceutics* 110: 58–69. https://doi.org/10.1016/j.ejpb.2016.10.013.

Sánchez-López, Elena, Maria Antonia Egea, Benjamin Michael Davis, Li Guo, Marta Espina, Amelia Maria Silva, Ana Cristina Calpena, et al. 2017. "Memantine-Loaded PEGylated Biodegradable Nanoparticles for the Treatment of Glaucoma." *Small* 1701808: 1701808.

Sánchez-López, Elena, Miren Ettcheto, Maria Antonia Egea, Marta Espina, Ana Cristina Calpena, Jaume Folch, Antoni Camins, and Maria Luisa García. 2017. "New Potential Strategies for Alzheimer's Disease Prevention: Pegylated Biodegradable Dexibuprofen Nanospheres Administration to APPswe/PS1dE9." *Nanomedicine: Nanotechnology, Biology, and Medicine* 13 (3): 1171–82.

Sánchez-López, Elena, Miren Ettcheto, Maria Antonia Egea, Marta Espina, Amanda Cano, Ana Cristina Calpena, Antoni Camins, et al. 2018. "Memantine Loaded PLGA PEGylated Nanoparticles for Alzheimer's Disease: In Vitro and in Vivo Characterization." *Journal of Nanobiotechnology* 16 (1): 1–16. https://doi.org/10.1186/s12951-018-0356-z.

Santos, G. A., T. Angelo, L. M. Andrade, S. M.M. Silva, P. O. Magalhães, M. Cunha-Filho, G. M. Gelfuso, S. F. Taveira, and T. Gratieri. 2018. "The Role of Formulation and Follicular Pathway in Voriconazole Cutaneous Delivery from Liposomes and Nanostructured Lipid Carriers." *Colloids and Surfaces B: Biointerfaces* 170 (April): 341–46. https://doi.org/10.1016/j.colsurfb.2018.06.037.

Satyal, Prabodh, Brittney L. Murray, Robert L. McFeeters, and William N. Setzer. 2016. "Essential Oil Characterization of Thymus Vulgaris from Various Geographical Locations." *Foods* 5 (4): 1–12. https://doi.org/10.3390/foods5040070.

Schneider, Marc, Frank Stracke, Steffi Hansen, and Ulrich F. Schaefer. 2009. "Nanoparticles and Their Interactions with the Dermal Barrier." *Dermato-Endocrinology* 1 (4): 197–206. https://doi.org/10.4161/derm.1.4.9501.

Sedlaříková, Jana, Magda Janalíková, Ondřej Rudolf, Jana Pavlačková, Pavlína Egner, Petra Peer, Vendula Varad'ová, and Jiří Krejčí. 2019. "Chitosan/Thyme Oil Systems as Affected by Stabilizing Agent: Physical and Antimicrobial Properties." *Coatings* 9 (3). https://doi.org/10.3390/coatings9030165.

Selwyn, S. 1980. "Microbiology and Ecology of Human Skin." *Practioner* 224: 1059–62.

Shah, Punit P., Pinaki R. Desai, Apurva R. Patel, and Mandip S. Singh. 2012. "Skin Permeating Nanogel for the Cutaneous Co-Delivery of Two Anti-Inflammatory Drugs." *Biomaterials* 33 (5): 1607–17. https://doi.org/10.1016/j.biomaterials.2011.11.011.

Shim, Jongwon, Hyung Seok Kang, Won Seok Park, Sang Hun Han, Junoh Kim, and Ih Seop Chang. 2004. "Transdermal Delivery of Mixnoxidil with Block Copolymer Nanoparticles." *Journal of Controlled Release* 97 (3): 477–84. https://doi.org/10.1016/j.jconrel.2004.03.028.

Siljander, T., M. Karppelin, S. Vahakuopus, J. Syrjanen, M. Toropainen, J. Kere, R. Vuento, T. Jussila, and J. Vuopio-Varkila. 2008. "Acute Bacterial, Nonnecrotizing Cellulitis in Finland: Microbiological Findings." *Clinical Infectious Diseases* 46 (6): 855–61. https://doi.org/10.1086/527388.

Silva-Abreu, Marcelle, Ana Cristina Calpena, Marta Espina, Amelia M. Silva, Alvaro Gimeno, María Antonia Egea, and María Luisa García. 2018. "Optimization, Biopharmaceutical Profile and Therapeutic Efficacy of Pioglitazone-Loaded PLGA-PEG Nanospheres as a Novel Strategy for Ocular Inflammatory Disorders." *Pharmaceutical Research* 35 (1): 11. https://doi.org/10.1007/s11095-017-2319-8.

Singh, Rakesh Kumar. 2019. "Uses of Medicinal Plants In Traditional and Modern Medicine" 8 (08): 578–81.

Smijs, Threes G.M., and Stan Pavel. 2011. "The Susceptibility of Dermatophytes to Photodynamic Treatment with Special Focus on Trichophyton Rubrum." *Photochemistry and Photobiology* 87 (1): 2–13. https://doi.org/10.1111/j.1751-1097.2010.00848.x.

Sosa, Lilian, Ana Cristina Calpena, Marcelle Silva-Abreu, Lupe Carolina Espinoza, María Rincón, Nuria Bozal, Oscar Domenech, María José Rodríguez-Lagunas, and Beatriz Clares. 2019. "Thermoreversible Gel-Loaded Amphotericin B for the Treatment of Dermal and Vaginal Candidiasis." *Pharmaceutics* 11 (7): 1–18. https://doi.org/10.3390/pharmaceutics11070312.

Souto, E. B., W. Mehnert, and R. H. Müller. 2006. "Polymorphic Behaviour of Compritol®888 ATO as Bulk Lipid and as SLN and NLC." *Journal of Microencapsulation* 23 (4): 417–33. https://doi.org/10.1080/02652040600612439.

Souto, Eliana B., Iara Baldim, Wanderley P. Oliveira, Rekha Rao, Nitesh Yadav, Francisco M. Gama, and Sheefali Mahant. 2020. "SLN and NLC for Topical, Dermal, and Transdermal Drug Delivery." *Expert Opinion on Drug Delivery* 17 (3): 357–77. https://doi.org/10.1080/17425247.2020.1727883.

Suñer-Carbó, Joaquim, Antonio Boix-Montañés, Lyda Halbaut-Bellowa, Nelvis Velázquez-Carralero, Joanna Zamarbide-Ledesma, Nuria Bozal-de-Febrer, and Ana Cristina Calpena-Campmany. 2017. "Skin Permeation of Econazole Nitrate Formulated in an Enhanced Hydrophilic Multiple Emulsion." *Mycoses* 60 (3): 166–77. https://doi.org/10.1111/myc.12575.

Szwed, Marzena, Maria Lyngaas Torgersen, Remya Valsala Kumari, Sunil Kumar Yadava, Sascha Pust, Tore Geir Iversen, Tore Skotland, Jyotsnendu Giri, and Kirsten Sandvig. 2020. "Biological Response and Cytotoxicity Induced by Lipid Nanocapsules." *Journal of Nanobiotechnology* 18 (1): 1–19. https://doi.org/10.1186/s12951-019-0567-y.

T

Taborda, Esteban A., Camilo A. Franco, Vladimir Alvarado, and Farid B. Cortés. 2017. "A New Model for Describing the Rheological Behavior of Heavy and Extra Heavy Crude Oils in the Presence of Nanoparticles." *Energies*. https://doi.org/10.3390/en10122064.

Tanghetti, Emil A. 2013. "The Role of Inflammation in the Pathology of Acne." *Journal of*

Clinical and Aesthetic Dermatology 6 (9): 27–35.

Tanner, Trevor, and R. Marks. 2008. "Delivering Drugs by the Transdermal Route: Review and Comment." *Skin Research and Technology* 14 (3): 249–60. https://doi.org/10.1111/j.1600-0846.2008.00316.x.

Tolentino, Seila, Maira N. Pereira, Mikaella C. de Sousa, Marcilio Cunha-Filho, Guilherme M. Gelfuso, and Tais Gratieri. 2020. "The Influence of Sebaceous Content on the Performance of Nanosystems Designed for the Treatment of Follicular Diseases." *Journal of Drug Delivery Science and Technology* 59 (October): 101895. https://doi.org/10.1016/j.jddst.2020.101895.

Trombetta, Domenico, Francesco Castelli, Maria Grazia Sarpietro, Vincenza Venuti, Mariateresa Cristani, Claudia Daniele, Antonella Saija, Gabriela Mazzanti, and Giuseppe Bisignano. 2005. "Mechanisms of Antibacterial Action of Three Monoterpenes." *Antimicrobial Agents and Chemotherapy* 49 (6): 2474–78. https://doi.org/10.1128/AAC.49.6.2474-2478.2005.

U

Uchechi, Okoro, John D. N. Ogbonna, and Anthony A. Attama. 2014. "Nanoparticles for Dermal and Transdermal Drug Delivery." In *Intech*, 193–235. https://doi.org/http://dx.doi.org/10.5772/58672.

Ultee, A., M. H.J. Bennik, and R. Moezelaar. 2002. "The Phenolic Hydroxyl Group of Carvacrol Is Essential for Action against the Food-Borne Pathogen Bacillus Cereus." *Applied and Environmental Microbiology* 68 (4): 1561–68. https://doi.org/10.1128/AEM.68.4.1561-1568.2002.

V

Vaara, M. 1992. "Agents That Increase the Permeability of the Outer Membrane." *Microbiological Reviews* 56 (3): 395–411. https://doi.org/10.1128/mmbr.56.3.395-411.1992.

Veeresham, Ciddi. 2012. "Natural Products Derived from Plants as a Source of Drugs." *Journal of Advanced Pharmaceutical Technology and Research* 3 (4): 200–201. https://doi.org/10.4103/2231-4040.104709.

Vega, Estefanía, M. Antònia Egea, M. Luisa Garduño-Ramírez, M. Luisa García, Elena Sánchez, Marta Espina, and Ana Cristina Calpena. 2013. "Flurbiprofen PLGA-PEG Nanospheres: Role of Hydroxy-β-Cyclodextrin on Ex Vivo Human Skin Permeation and in Vivo Topical Anti-Inflammatory Efficacy." *Colloids and Surfaces B: Biointerfaces* 110: 339–46. https://doi.org/10.1016/j.colsurfb.2013.04.045.

Vega, Estefanía, María Antonia Egea, O Valls, Marta Espina, and María Luisa Garcia. 2006. "Flurbiprofen Loaded Biodegradable Nanoparticles for Ophtalmic Administration." *Journal of Pharmaceutical Sciences* 95 (11): 2393–2405. https://doi.org/https://doi.org/10.1002/jps.20685.

W

Wattanasatcha, Anna, Sirirat Rengpipat, and Supason Wanichwecharungruang. 2012. "Thymol Nanospheres as an Effective Anti-Bacterial Agent." *International Journal of Pharmaceutics* 434 (1–2): 360–65. https://doi.org/10.1016/j.ijpharm.2012.06.017.

Wertz, Philip W. 1996. "Drug Deliiry Barrier : Biochemical Aspects," no. 95.

Wild, Christopher Paul. 2005. "Complementing the Genome with an 'Exposome': The Outstanding Challenge of Environmental Exposure Measurement in Molecular Epidemiology." *Cancer Epidemiology Biomarkers and Prevention* 14 (8): 1847–50. https://doi.org/10.1158/1055-9965.EPI-05-0456.

Wilkes, G, I Brown, and R Wildnauer. 1973. “The Biomechanical Properties of Skin.” *Critical Reviews in Bioengineering*, 453–95.

Williams, Hywel C., Robert P. Dellavalle, and Sarah Garner. 2012. “Acne Vulgaris.” *The Lancet* 379 (9813): 361–72. https://doi.org/10.1016/S0140-6736(11)60321-8.

X

Xiao, Dan, Christina Gömmel, P. Michael Davidson, and Qixin Zhong. 2011. “Intrinsic Tween 20 Improves Release and Antilisterial Properties of Co-Encapsulated Nisin and Thymol.” *Journal of Agricultural and Food Chemistry* 59 (17): 9572–80. https://doi.org/10.1021/jf201864v.

Xue, Xiang, and Daniel M. Falcon. 2019. “The Role of Immune Cells and Cytokines in Intestinal Wound Healing.” *International Journal of Molecular Sciences* 20 (23): 1–19. https://doi.org/10.3390/ijms20236097.

Y

Yap, Polly Soo Xi, Khatijah Yusoff, Swee Hua Erin Lim, Chou Min Chong, and Kok Song Lai. 2021. “Membrane Disruption Properties of Essential Oils-a Double-Edged Sword?” *Processes* 9 (4): 1–11. https://doi.org/10.3390/pr9040595.

Yin Win, Khin, and Si Shen Feng. 2005. “Effects of Particle Size and Surface Coating on Cellular Uptake of Polymeric Nanoparticles for Oral Delivery of Anticancer Drugs.” *Biomaterials* 26 (15): 2713–22. https://doi.org/10.1016/j.biomaterials.2004.07.050.

Yukuyama, Megumi Nishitani, Gabriel Lima Barros De Araújo, and Nádia Araci Bou-Chacra. 2020. “Nanomaterials for Hair Care Applications.” *Nanocosmetics*, 205–25. https://doi.org/10.1016/b978-0-12-822286-7.00010-3.

Z

Zhang, Xiaoyan, Muzhen Sun, Aiping Zheng, Deying Cao, Yunqi Bi, and Jianxu Sun. 2012. “Preparation and Characterization of Insulin-Loaded Bioadhesive PLGA Nanoparticles for Oral Administration.” *European Journal of Pharmaceutical Sciences* 45 (5): 632–38. https://doi.org/10.1016/j.ejps.2012.01.002.

Zhang, Zheng, Pei Chin Tsai, Tannaz Ramezanli, and Bozena B. Michniak-Kohn. 2013. “Polymeric Nanoparticles-Based Topical Delivery Systems for the Treatment of Dermatological Diseases.” *Wiley Interdisciplinary Reviews: Nanomedicine and Nanobiotechnology* 5 (3): 205–18. https://doi.org/10.1002/wnan.1211.

Zhu, Tingting, Wenjuan Wu, Shuyun Yang, Donglin Li, Dongjie Sun, and Li He. 2019. “Polyphyllin I Inhibits Propionibacterium Acnes-Induced Inflammation In Vitro.” *Inflammation* 42 (1): 35–44. https://doi.org/10.1007/s10753-018-0870-z.

Zhu, Zhu, Tiantian Min, Xueji Zhang, and Yongqiang Wen. 2019. “Microencapsulation of Thymol in Poly(Lactide-Co-Glycolide) (PLGA): Physical and Antibacterial Properties.” *Materials* 12 (7). https://doi.org/10.3390/ma12071133.

Zirak, Maryam Banay, and Akram Pezeshki. 2015. “Effect of Surfactant Concentration on the Particle Size, Stability and Potential Zeta of Beta Carotene Nano Lipid Carrier.” *International Journal of Current Microbiology and Applied Sciences* 4 (9): 924–32. http://www.ijcmas.com.

Zouboulis, C. C., E. Jourdan, and M. Picardo. 2014. “Acne Is an Inflammatory Disease and Alterations of Sebum Composition Initiate Acne Lesions.” *Journal of the European Academy of Dermatology and Venereology* 28 (5): 527–32. https://doi.org/10.1111/jdv.12298.

9. APPENDIX

pharmaceutics

MDPI

Article

Surface-Modified Multifunctional Thymol-Loaded Biodegradable Nanoparticles for Topical Acne Treatment

Camila Folle [1], Natalia Díaz-Garrido [2,3,4], Elena Sánchez-López [1,5,*], Ana Maria Marqués [6], Josefa Badia [2,3,4], Laura Baldomà [2,3,4], Marta Espina [1,5], Ana Cristina Calpena [1,5] and María Luisa García [1,5]

1 Department of Pharmacy and Pharmaceutical Technology and Physical Chemistry, Faculty of Pharmacy and Food Sciences, University of Barcelona, 08028 Barcelona, Spain; cfollefo7@alumnes.ub.edu (C.F.); m.espina@ub.edu (M.E.); anacalpena@ub.edu (A.C.C.); marisagarcia@ub.edu (M.L.G.)
2 Department of Biochemistry and Physiology, Faculty of Pharmacy and Food Sciences, University of Barcelona, 08028 Barcelona, Spain; ndiazgarrido@ub.edu (N.D.-G.); josefabadia@ub.edu (J.B.); lbaldoma@ub.edu (L.B.)
3 Institute of Biomedicine, University of Barcelona, 08028 Barcelona, Spain
4 Sant Joan de Déu Research Institute (IR-SJD), 08950 Barcelona, Spain
5 Institute of Nanoscience and Nanotechnology (IN2UB), University of Barcelona, 08028 Barcelona, Spain
6 Department of Biology, Healthcare and Environment, Faculty of Pharmacy and Food Sciences, University of Barcelona, 08028 Barcelona, Spain; ammarques@ub.edu
* Correspondence: esanchezlopez@ub.edu

Abstract: The present work is focused on the development of novel surface-functionalized poly(lactic-co-glycolic acid) nanoparticles loaded with thymol (TH-NPs) for topical administration enhancing thymol anti-inflammatory, antioxidant and wound healing activities against acne. TH-NPs were prepared by solvent evaporation method using different surface functionalization strategies and obtaining suitable physicochemical parameters and a good short-term stability at 4 °C. Moreover, TH-NPs skin penetration and antioxidant activity were assessed in ex vivo pig skin models. Skin penetration of TH-NPs followed the follicular route, independently of the surface charge and they were able to enhance antioxidant capacity. Furthermore, antimicrobial activity against *Cutibacterium acnes* was evaluated in vitro by the suspension test showing improved antibacterial performance. Using human keratinocyte cells (HaCat), cytotoxicity, cellular uptake, antioxidant, anti-inflammatory and wound healing activities were studied. TH-NPs were non-toxic and efficiently internalized inside the cells. In addition, TH-NPs displayed significant anti-inflammatory, antioxidant and wound healing activities, which were highly influenced by TH-NPs surface modifications. Moreover, a synergic activity between TH-NPs and their surface functionalization was demonstrated. To conclude, surface-modified TH-NPs had proven to be suitable to be used as anti-inflammatory, antioxidant and wound healing agents, constituting a promising therapy for treating acne infection and associated inflammation.

Keywords: PLGA; thymol; nanoparticles; skin; HaCaT cells; anti-inflammatory; chitosan; phosphatidylcholine; poloxamer

Citation: Folle, C.; Díaz-Garrido, N.; Sánchez-López, E.; Marqués, A.M.; Badia, J.; Baldomà, L.; Espina, M.; Calpena, A.C.; García, M.L. Surface-Modified Multifunctional Thymol-Loaded Biodegradable Nanoparticles for Topical Acne Treatment. *Pharmaceutics* **2021**, *13*, 1501. https://doi.org/10.3390/pharmaceutics13091501

Academic Editor: Bozena B. Michniak-Kohn

Received: 15 August 2021
Accepted: 10 September 2021
Published: 18 September 2021

1. Introduction

Acne vulgaris is one of the most prevalent skin inflammatory disorders affecting 9.4% of the population worldwide [1,2]. It is a multifactorial disease. Their pathophysiology is complex, with both internal and external triggers [3]. This disease is induced by several factors such as irregular keratinocyte proliferation and differentiation, increased sebum production by active sebaceous glands and imbalances in the skin microbiota. This imbalance is particularly related to certain *Cutibacterium* strains, among them *Cutibacterium acnes*, a normal skin commensal previously known as *Propionibacterium acnes* [4]. In addition, exogenous factors such as hormones, drugs, nutrition, stress or smoke habits, can also trigger acne development [5,6]. This combination of factors leads to skin lesions such as whiteheads, blackheads, pustules and cysts developing into swelling and inflammation [7].

C. acnes is a normal resident of healthy skin, mainly located surrounding the hair follicle, which is likely to proliferate under unbalanced function of the sebaceous glands, contributing to inflammation and acne development [8]. Hence, *C. acnes* has a dual activity. This skin commensal strain is essential for sebum control and maintenance of the acidic pH of the pilosebaceous follicle by hydrolysing sebum triglycerides and via propionic acid secretion [4,9]. However, it can act as a pathogen under dysbiosis conditions that help its overgrowth in active sebaceous glands [10].

Imbalanced skin microbiome, including *C. acnes* overgrowth, trigger innate immune system activation, leading to cutaneous inflammation. Consequently, the great array of induced immune-regulatory and pro-inflammatory mediators amplify direct damaging effects on molecules and cells, including DNA, proteins and lipids, causing immunosuppression [11].

Skin inflammation is an innate and non-specific skin immunological response towards external and internal environment modifications or aggressions. The skin immunological activity includes microbial ligands for toll-like receptors (TLR). Host responses to gram-positive bacteria peptidoglycan and gram-negative bacterial lipopolysaccharide are mediated by TLR-2 and TLR-4, respectively [12]. The skin anti-inflammatory mechanism of action consists in modulating the expression of certain genes in order to produce an increase in anti-inflammatory proteins and inhibit pro-inflammatory cytokines release. Cytokines are small proteins which modulate immune responses, regulate cell activation and proliferation. They are produced by epithelial cells, macrophages, CD4 and CD8 T cells. On keratinocytes, *C. acnes* activates TLR-2 and TLR-4 leading to the activation of MAPK and NF-kB pathways. Moreover, they produce interleukins such as (IL)-1, IL-6, IL-8 and TNF-α. Then, ROS production is stimulated, when CD-36 recognizes *C. acnes*, clearing away the bacteria and inducing the inflammation [13]. In acute inflammation, these mediators are present for short periods of time, whereas in chronic inflammation, there is an imbalanced production. Chemokines are cytokine subtypes that take on monocytes/macrophages, neutrophils and T cells from the circulation to the areas of infection. Moreover, neutrophils promote wound healing due to secretion of cytokines, chemokines and growth factors to abolish bacteria and adjust wound microenvironment through oxygen metabolism [14].

Furthermore, sebum composition is severely altered in acne, the ROS produced by neutrophils are involved in the irritation and disruption of the follicular wall, leading to a progressive inflammatory response. ROS overflow might be associated to the lipids present in the sebum. A mediated production of monounsaturated oleic acid is a crucial step in virulence factor of biofilm formation, playing a critical role for bacterial adherence, since it has been found to be an essential nutrient for resident *C. acnes* microbiota [15]. It is also known to enhance epidermal calcium influx in keratinocytes, inducing abnormal keratinization and barrier function associated with increased release of IL-1α in comedones [16]. Furthermore, uric acid increases IL-1β expression through a TLR4-mediated pathway. Thus, increased sebum in acne may activate uric acid–mediated inflammasome. Hyper-keratinization might be initiated via IL-1, suggesting keratinocyte activation cycles, and hence, hyper-proliferation [17]. Hyper-keratinization leads to sebaceous gland obstruction clogging the follicle in function of lipids, bacteria and induced cytokines. In addition to *C. acnes* being a gram-positive bacterium, it possesses a featured cell wall and outer envelope that synthesizes phosphatidylinositol. Its surrounding peptidoglycan containing a cross-linkage peptide chain may allow recognition of receptors contributing to inflammation, secreting TNF-α, IL-1α and IL-8 [12]. In particular, IL-8 together with other factors, may attract neutrophils to the pilosebaceous unit.

Superoxide or hydroxyl ions, and hydrogen peroxide are highly reactive molecules generated in normal cell metabolism. Moreover, acne-related strains generate ROS and raise inflammation in keratinocytes. Then, it can cause oxidative damage to proteins, lipids, enzymes and DNA [18,19]. These factors reflect on impaired skin function, thus an inflammatory response and cell death. Therefore, the skin is constantly exposed to induced oxidative stress. However, intrinsic antioxidant defence mechanisms contribute to barrier

integrity, which is essential for a healthy skin. The cellular redox environment plays a key role in skin homeostasis, preventing oxidative damage of lipids and proteins, and avoiding an imbalanced pro-oxidant/antioxidant stimulus. The oxidation of phenolic compounds normally takes place in the cytosol, in contact with peroxidase/H_2O_2. This would produce phenoxyl radical and may co-oxidize glutathione [20]. Consecutive inflammation may affect the skin internal components and their functions. Moreover, cicatrisation processes rely on cell regeneration while healing the infection and the inflammatory responses.

Natural anti-inflammatory, antioxidants and antimicrobial agents could be the key for preventing or ameliorating acne associated symptoms [21]. In this area, natural compounds are gaining increased importance. Among them, Thymol (TH) is a monoterpene with a phenolic structure associated with several activities such as antioxidant, antimicrobial, antifungal, antiseptic as well as anti-inflammatory [22–24]. Despite its multifunctional properties, TH present a low penetration trough skin which could decrease its potential effects against acne. Moreover, TH commercial use is still underexplored, probably because its low water solubility, high volatility and high light sensibility and its low solubility in water [25,26].

In order to overcome TH physicochemical drawbacks, several authors have attempted to encapsulate it into several delivery platforms such as cyclodextrins [26,27], and lipid nanoparticles [25] among others [28]. Moreover, in order to improve active compounds bioavailability after topical administration, polymeric nanoparticles (NPs) constitute excellent potential candidates. Specially for acne treatment due to their small particle diameter, able to penetrate the skin inside the follicle. Additionally, NPs enable the encapsulated active compounds for long-term release inside the lesions. Among the most widely used polymers, poly(lactic-co-glycolic acid) (PLGA) has been approved by the Food and Drug Administration and is one of the most successful biodegradable polymers [29]. Despite their great potential, to our knowledge, to date no other group have developed TH loaded PLGA nanoparticles. In addition, PLGA negative surface is highly versatile and can be modified using several compounds in order to improve NPs performance after topical skin delivery. In this area, Chitosan is a natural polysaccharide, positively charged, that has known anti-inflammatory and wound healing activities [30]. Chitosan can be used either as polymer carrier or be adhered on the surface of other types of negatively charged NPs [31]. In addition, some types of natural phospholipids such as phosphatidylcholine that are normally used to produce liposomes, also have demonstrated to possess antioxidant or anti-inflammatory activities enhancing the efficacy of some encapsulated drugs [32]. Moreover, some synthetic types of surfactants such as Poloxamers, have antioxidant and anti-inflammatory activities [33,34].

Therefore, this study was developed to designed thymol-loaded polymeric NPs (TH-NPs) assessing several surface functionalization compounds and comparing their activity in vitro and ex vivo for the treatment of acne. TH-NPs were functionalized either with phosphatidylcholine, Poloxamer 188 or Poloxamer 407. Additionally, combination of chitosan and Poloxamer surface functionalization was also carried out. Bacterial infection inflammation was induced by *C. acnes* inoculation in keratinocyte cells (HaCaT). Moreover, the antioxidant properties, cell regeneration and wound healing activities were also assayed comparing the different formulations developed.

2. Materials and Methods

2.1. Materials

PLGA Resomer® RG 504H (consisting of a carboxylic terminal group, molecular weight 38,000–54,000 Da and molar ratio lactide:glycolide 50:50) was purchased from Boehringer Ingelheim (Ingelheim am Rhein, Germany). Thymol (TH), Poloxamer 188 (P) and Poloxamer 407 (PP) were purchased from Sigma Aldrich (Madrid, Spain). Chitosan (C) was supplied by HMC+ (GmbH, Saale, Germany), and phosphatidylcholine (L) was acquired from Lipoid® (GmbH, Ludwigshafen am Rhein, Germany). Double distilled

water was used after filtration in a Millipore system. All other chemicals and reagents used in the study were of analytical grade.

2.2. Methods

2.2.1. Preparation of Thymol Loaded Nanoparticles

Thymol-loaded PLGA NPs (TH-NPs) containing a matrix structure (nanospheres) were obtained by solvent displacement evaporation, as described by Fessi et al. [35]. In the current study, a previously optimized formulation based on TH-PLGA-NPs was modified by functionalizing TH-NPs surface using several compounds. In order to prepare the NPs, the organic phase composed by PLGA and 2.5 mg/mL of TH was dissolved in acetone and the aqueous phase consisted on either phosphatidylcholine (TH-NP-L-) or Poloxamer 188 (TH-NP-P-) or Poloxamer 407 (TH-NP-PP-), for negatively charged particles. Additionally, positively charged particles were also produced containing chitosan (TH-NP-P-C+, TH-NP-PP-C+), where the aqueous solution contained 1% acetic acid. The organic phase was added dropwise into the aqueous phase, under continuous stirring. A rotatory evaporator (Buchi, Flawil, Switzerland) under constant pressure was used to evaporate the organic phase, obtaining the nanoparticles. Empty NPs (B-NPs) were prepared using the same procedure but without the addition of TH.

2.2.2. Nanoparticles Physicochemical Characterization

The average particle size (Z_{av}) and polydispersity index (PI) were determined by photon correlation spectroscopy, using a ZetaSizer Nano ZS (Malvern Instruments; Malvern, UK). The surface charge, measured as zeta-potential (ZP), was determined by electrophoretic mobility using the same instrument.

Encapsulation of TH was measured indirectly by quantification of unloaded amount. Samples were diluted 1:10 in Milli-Q water:ethanol (90:10) and centrifuged (Centrifuge 5415C, Geratebau Eppendorf GmbH, Engelsdorf, Germany) for 10 min at 14,000 rpm, using Millipore filter device (Amicon® Ultra, 0.5 mL 100 K, Merck Millipore Ltd., Carrigtwohill Co. Cork IRL, Darmstadt, Germany). The filtered fractions were quantified by HPLC, and the EE was determined by the Equation (1):

$$EE = (Ci - Cs)/Ci \cdot 100 \quad (1)$$

where Ci is the initial concentration of the active and Cs is the concentration of the unloaded amount found in the filtered fraction.

HPLC quantitative analysis was performed by reverse-phase high-performance liquid chromatography (HPLC) by a modification of the method described previously [36]. Studies were carried out in Acquity Waters System with UV detector, using a Kromasil® column (C18, 5 µm, 150 mm × 4.6 mm), (Teknokroma, Barcelona, Spain). The mobile phase consisted of acetonitrile:water under gradient conditions of 30:70/58:42/30:70 during 20 min. TH was determined at wavelength of 275 nm.

2.2.3. Stability of Thymol Loaded Nanoparticles

Short-term stability of TH NPs was evaluated after one month of storage at 4, 25, 30 and 40 °C by measuring Z_{av}, PI, ZP and pH. Additional long-term studies were carried out during 6 months by measuring the physicochemical parameters monthly at 4 °C. Moreover, backscattering profiles of TH-NPs stored at 4 °C, were also recorded using TurbiscanLab® (Formulation, Toulousse, France) [37].

2.2.4. Ex Vivo Skin Penetration Route of Thymol Loaded Nanoparticles

Ex vivo pig skin was obtained from the animal house (Bellvitge, University of Barcelona), used in accordance with the protocol approved by the Ethics Committee of the University of Barcelona.

Prior to the experiment, rhodamine-labelled PLGA (R-PLGA) was synthesized as described by Gonzalez-Pizarro et al. [38] and used at 0.01% obtaining rhodamine labelled

nanoparticles (R-TH-NPs). Skin penetration assay was executed using vertical diffusion Franz cells (FDC-400, Vidra-Foc, Barcelona, Spain) with a thermal bath set to 32 °C to mimic skin in vivo conditions, under constant stirring. R-TH-NPs were applied onto ex vivo pig skin 0.64 cm^2 (donor compartment) and penetration was allowed for 24 h. Skin samples were washed, fixed in PBS containing 4% paraformaldehyde (PFA) for 4 h, followed by cryoprotection into PBS with 30% sucrose for 24 h, snap-frozen in isopentane at −50 °C and then kept overnight at −80 °C. Samples were mounted in O.C.T. ® Compound (Tissue-Tek®, Sakura Finetek, Torrance, CA, USA) and sliced with cryostat microtome (LEICA CM3050 S) at −20 °C onto glass-slides Superfrost® Plus (Menzel-Glaser, Thermo Scientific, USA), covered with Fluoromount G® (Invitrogen, Thermo Fisher Scientific, Rockford, IL, USA). Samples were visualized by confocal laser scanning microscopy (Zeiss LSM 880). Images were acquired using Zen Black 2.3 software performing z-stack sections and thus processed with ImageJ software v1.53k.

2.2.5. Ex Vivo Skin Antioxidant Activity by Methylene Blue Reduction

A colorimetric assay was performed using methylene blue dye to test the ex vivo antioxidant activity of TH and surface functionalized TH-NPs. Methylene blue, in combination with an antioxidant molecule, reduces into a colorless lecomethylene blue [39].

Pig skin samples were cut into 2 cm^2 and placed into a 6-well plate containing 0.5 mL of PBS, with the stratum corneum (SC) facing up. Then, a methylene blue solution at 0.01% was applied on the surface of each skin sample and incubated for 4 h at 32 °C, in the presence of humidity. Skin fragments were washed with PBS and the SC was dried with filter paper. TH-NPs were applied onto the skin (30 µL) and further incubated for 1 h. The control sample was treated with distilled water. Images were recorded at initial and 1 h post-treatment to assess differences in methylene blue reduction.

2.2.6. Free-Radical Scavenging by DPPH

The scavenging capacity of TH, surface functionalized TH-NPs and surface functionalization components was evaluated using DPPH (2,2-diphenyl-1-picrylhydrazyl) assay, based on other authors with some modifications [40]. Samples were dissolved and diluted in methanol at concentrations ranging from 0.1 to 10 mg/mL, and DPPH, a free radical compound, was prepared in 80% methanol at 0.1 mM. Sample dilutions were transferred into a 96-well plate (200 µL/well) and 20 µL of the DPPH stock solution was added into each well. BHT (butyl-hydroxytoluene), a known antioxidant compound was used as endogenous control.

Samples without DPPH were used as blank. Samples were incubated in the dark for 45 min on a mechanical shaker. The UV-VIS absorbance was measured at 517 nm and data were calculated using the Equation (2):

$$Free\ Radical\ Scavening(\%) = \frac{Ac - (As - Ab)}{Ac} \cdot 100 \quad (2)$$

where *Ac, As* and *Ab are* the absorbances of the control, sample and blank, respectively.

2.2.7. Antimicrobial Efficacy of Thymol Loaded Nanoparticles

A fresh inoculum of *C. acnes* was prepared in PBS adjusted to an optical density of 0.72 at 550 nm, using a UV-visible spectrophotometer (Shimadzu Corp., Kyoto, Japan). The assay was carried out in a total volume of 1 mL containing TH or TH-NPs (900 µL) at a final concentration of 250 µg/mL and fresh bacterial inoculum (100 µL). Samples were kept at 37 °C in a shaker incubator (Innova 4080, New Brunswick Scientific, Edison, NJ, USA) for 30 min. Then, 100 µL of each test tube was neutralized in 900 µL of Berens cosmetic diluent (Scharlab, Barcelona, Spain) for 15 min [41]. Ten-fold dilutions in PBS (10 µL) were added to clostridium reinforced medium agar dishes for enumerating bacteria by the drop count method. Microbial count was performed after incubation for 48 h under anaerobic conditions at 37 °C. Bacterial viability was expressed as CFU/mL against time (h).

2.2.8. Cytotoxicity and Cellular Uptake of Thymol Loaded Nanoparticles

Human keratinocytes (HaCaT) cells were cultured in high glucose Dulbecco's Modified Eagle's Medium (DMEM) from Thermofisher, supplemented with 10% fetal bovine serum (FBS), 2 mM L-glutamine, 100 units/mL penicillin G and 100 µg/mL streptomycin. Cells were incubated at 37 °C and 5% CO_2 and experiments were performed when cells reached 80–90% of confluence.

Cytotoxicity of TH-NPs was evaluated by the MTT (3-(4,5-Dimethylthiazol-2-yl)-2,5-diphenyl tetrazolium bromide) assay that is based on the mitochondrial reduction of tetrazolium salt by intracellular dehydrogenases of viable cells. Samples were tested at concentrations up to 2, 10 and 20 µg/mL. Briefly, HaCaT cells were seeded in 96-well plates (100 µL) at a density of 2×10^5 cells/well, adjusted in an automated cell counter (Countess, Invitrogen, Thermofisher) and grown for 24 h at 37 °C. Then, TH-NPs were added at the indicated concentrations and cells were further incubated for 24 h. Finally, the medium was removed and MTT (Sigma-Aldrich Chemical Co, St. Louis, MO, USA) was added at 0.25% in PBS. After 2 h incubation, the medium was replaced by 100 µL DMSO (99% dimethyl sulfoxide, Sigma-Aldrich, Madrid, Spain) [42]. Cell viability was then measured at 570 nm in a Modulus® Microplate Photometer (Turner BioSystems Inc., Sunnyvale, CA, USA). Results were expressed as percentage of cell survival relative to untreated cells.

HaCaT cells were seeded in an 8-well µ-slide (Ibidi®). Cells were incubated in FBS/phenol red-free medium in the presence or absence of TH-NPs for 2 h at the indicated concentration. Cell membrane was stained with wheat germ agglutinin (WGA) Alexa-488 (Molecular Probes) at 1 µg/mL for 15 min followed by fixation with 3% paraformaldehyde for 25 min. Cell nuclei were stained with 4′,6-diamidino-2-phenylindole (DAPI, Sigma Aldrich, Madrid, Spain) at 0.5 µg/mL for 15 min. Internalization of NPs in HaCaT cells was assessed by confocal microscopy (Leica TCS SPII), using the 63X oil immersion objective lens [38]. Images were processed using Fiji image software [38].

2.2.9. Anti-Inflammatory Activity in TNF-α-Induced Inflammation Model

HaCaT cells were seeded in 12-well plates at a density of 2×10^5 cells/well and grown until 80–90% confluence. Cells were then treated with TH-NPs for 2 h, followed by stimulation with 50 µM TNF-α for 2 h to induce inflammation [43]. The medium was replaced by fresh FSB-free medium and cells were incubated overnight. Supernatants were collected, and quantification of secreted interleukin-6 (IL-6) was carried out by using ELISA Human kit (BD OptEIA® Set Human IL-6, BD Biosciences, Franklin Lakes, NJ, USA) following manufacturer instructions. Absorbance was measured at 450 and 560 nm using a plate reader (Varioskan, Thermo Fisher Scientific, Rockford, IL, USA). Data were processed and analyzed using version 5 GraphPad® Prism software.

2.2.10. Anti-Inflammatory Activity in *C. acnes*-Induced Inflammation Model

This experiment was performed as described in the previous section, but *C. acnes* fresh inoculum was added instead of TNF-α. *C. acnes* was grown until the stationary phase (5 days incubation under anaerobiosis in BHI culture medium). Then bacterial cells were harvested and diluted in FSB-free DMEM medium, adjusted to OD 1.2 at 550 nm. Different dilutions of this inoculum were added to HaCaT cells and incubated overnight. Quantification of IL-6 in cell culture supernatants was assayed by using ELISA Human kit (BD OptEIA® Set Human IL-6, BD Biosciences, Franklin Lakes, NJ, USA) following manufacturer instructions [44].

2.2.11. Real-Time Quantitative Polymerase Chain Reaction (RT-qPCR)

HaCaT cells were adjusted to a density of 2×10^5 cells/well and seeded in 12-well plates. After 48 h, cells were treated with TH or TH-NPs or blank NPs (B-NPs) for 2 h. Next, cells were stimulated for 4 h with *C. acnes* prepared in FBS-free DMEM medium, adjusted to OD 1.2 at 550 nm. HaCaT cells without any treatment were used as a negative control and cells incubated only with *C. acnes* as a positive control. Total RNA was isolated from

cells using an RNA extraction kit (Qiagen RNeasy, Germantown, MD, USA) following the manufacturer's guide (Qiagen, Crawley, UK) and quantified by the ratio of absorbance values at 260 and 280 nm using a NanoDrop TM-2000 spectrophotometer (Thermo Fisher Scientific, Waltham, MA, USA). cDNA was synthesized from RNA (1 µg) by using the High-Capacity cDNA Reverse Transcription kit (Applied Biosystems, Foster City, CA, USA) in a final volume of 20 µL. Quantitative PCR reactions were performed in a StepOne Plus PCR cycler (Applied Biosystems, Foster City, CA, USA) by using SYBR® Green PCR Master Mix (Applied Biosystems, Foster City, CA, USA) and specific human oligonucleotide primers for IL-1α, IL-1β, IL-6, IL-8, TNF-α and β-actin (endogenous control, primers specified in Table S1 of Supplementary Materials). Control reactions were performed in the absence of RNA. The standard PCR program was conducted by one denaturation cycle for 10 min at 95 °C followed by 40 cycles of 15 s at 95 °C and 1 min at 60 °C. Relative gene expression was calculated as fold change compared to sample control by means of $2-\Delta\Delta Ct$ formula [42].

2.2.12. Antioxidant Activity Assessed by ROS Quantification

HaCaT cells were seeded in 96-well plates at 2×10^5 cells/well (100 µL) for 72 h. Cells were loaded with the fluorogenic dye H_2DCFDA (2′,7′-dichlorodihydrofluorescein diacetate) at 25 µM diluted in phenol red/FBS-free DMEM medium, for 45 min in the dark. This fluorogenic dye passively diffuses into the cells, is deacetylated by intracellular esterase and emits fluorescence upon oxidation by reactive oxygen species (ROS) [45]. Then, cells were washed with PBS and incubated for 2 h with TH, surface-functionalization compounds, functionalized TH-NPs or B-NPs. At this time, 10 µL of 20 mM H_2O_2 were added to the wells. Fluorescence was measured at excitation and emission wavelengths of 485 and 530 nm, respectively. Data were acquired at 0, 30, 60 and 120 min. The data of the positive control (H_2O_2) after 2 h was used to normalize values (%). Background fluorescence of control cells were subtracted from all measurements.

2.2.13. Wound Healing Activity in HaCaT Cells by the Scratch Assay

In order to study wound healing activity of the developed TH-NPs, prevention and treatment were assessed. In order to study wound healing prevention, HaCaT cells were seeded in 12-well plates at a density of 5×10^4 cells/well and grown for 24 h until 70–80% confluence. Cells were treated for 2 h with free TH, surface-functionalized TH-NPs or functionalization compounds, washed with PBS and further incubated for 24 h. Then, scratches were performed in the middle of each well using a 200 µL pipette tip, washed with PBS, refilled with FBS-free culture medium and incubated for 24 h [46,47]. Contrast phase images of the scratches were obtained at the beginning of the experiment (T0) and after 24 h using a fluorescent microscope, and the wound area was measured using ImageJ software.

In the previous assay, the capacity to prevent wound healing was assessed, whereas in a second assay, wound healing treatment was examined by applying the formulations after the lesion was caused. For this second experiment, HaCaT cells were seeded and grown for 24 h. After creating the scratches as previously mentioned, cells were washed with PBS and refilled with DMEM containing 1% FBS. Images at this timepoint were recorded by using fluorescent microscope at 10X (LEICA DFC300FX). Cells were then treated with either TH, surface functionalized TH-NP or surface functionalization compounds for 2 h and further incubated for 24 h in 1% FBS—culture medium [30]. Images at 24 h were recorded and processed using ImageJ software.

3. Results and Discussion

3.1. Thymol Loaded Nanoparticles Physicochemical Characterization

TH-NPs were prepared using the solvent displacement method and surface functionalized with different compounds (TH-NP-L-, TH-NP-P-; TH-NP-PP-, TH-NP-P-C+, TH-NP-PP-C+). Their physical-chemistry characterization is shown in Table 1. All formulations presented good homogeneity below 0.2 indicating monodisperse systems and high

entrapment efficacy values around 80% leading to 2 mg/mL of TH encapsulated inside the NP [48]. Moreover, Z_{av} was adequate for skin topical administration and pH was slightly acidic in all the cases. Regarding ZP, TH-NP-L-, TH-NP-P-; TH-NP-PP- show negative surface charges but the formulations functionalized with chitosan showed highly positive surface charge which may be able to favor interaction with negatively charged skin tissues.

Table 1. Surface functionalized formulations of Thymol loaded PLGA NPs (TH-NP-L-: TH-NPs functionalized with phosphatidylcholine; TH-NP-P-: TH-NPs functionalized with Poloxamer 188; TH-NP-PP-: TH-NPs functionalized with Poloxamer 407; TH-NP-P-C+: TH-NPs functionalized with Poloxamer 188 and Chitosan; TH-NP-PP-C+: TH-NPs functionalized with Poloxamer 407 and Chitosan).

	$Z_{av} \pm$ SD (nm)	PI $\pm$ SD	ZP $\pm$ SD (mV)	pH $\pm$ SD
NPP-P-	180.2 $\pm$ 6.5	0.066 $\pm$ 0.037	−28.9 $\pm$ 1.0	4.15 $\pm$ 0.10
NPP-P-C+	316.5 $\pm$ 3.8	0.123 $\pm$ 0.035	43.4 $\pm$ 0.6	3.15 $\pm$ 0.10
NPP-PP-	206.9 $\pm$ 9.9	0.101 $\pm$ 0.041	−17.8 $\pm$ 0.7	4.29 $\pm$ 0.10
NPP-PP-C+	297.3 $\pm$ 22.9	0.150 $\pm$ 0.068	19.6 $\pm$ 0.8	3.16 $\pm$ 0.10
NPP-L-	235.8 $\pm$ 29.7	0.063 $\pm$ 0.018	−32.1 $\pm$ 0.2	4.08 $\pm$ 0.10

3.2. Stability of Thymol Loaded Nanoparticles

TH-NPs stability with different surface functionalization compounds (TH-NP-L-, TH-NP-P-; TH-NP-PP-, TH-NP-P-C+, TH-NP-PP-C+) were measured in order to assess their short-term stability. Physical-chemical properties were measured after one-month of storage at 4, 25, 30 and 40 °C. As can be observed in Figure 1, after 1 month it was corroborated that the most suitable storage temperature was 4 °C since no statistically significant differences were observed regarding the average size of TH-NPs. Even though ZP and pH of chitosan functionalized TH-NPs show significant differences after one month, its values are still adequate for topical administration. In addition, it can be observed that at higher temperatures such as 30 or 40 °C, all the parameters vary significantly as it has been previously reported by other authors developing PLGA NPs [49,50].

Since the most suitable temperature for surface functionalized TH-NPs storage was found to be 4 °C, 6-month stability was studied at this temperature. Results obtained in Table 2 show differences in the stability of the different functionalized NPs. It can be observed that after 6 months, NPP-P- vary its parameters. Even though NPP-P- Z_{av} remains below 200 nm and PI below 0.1, ZP decreases significantly after 6 months of storage. A similar behavior is observed when chitosan was added to the formulation (NPP-P-C+) observing stability until 3-months of storage. NPP-PP- also show a ZP decrease after 3 months although their chitosan functionalized formulations (NPP-PP-C+) not vary their properties until 6 months. In the case of NPP-L-, NPs modified their physicochemical properties prior to 3 months after their preparation.

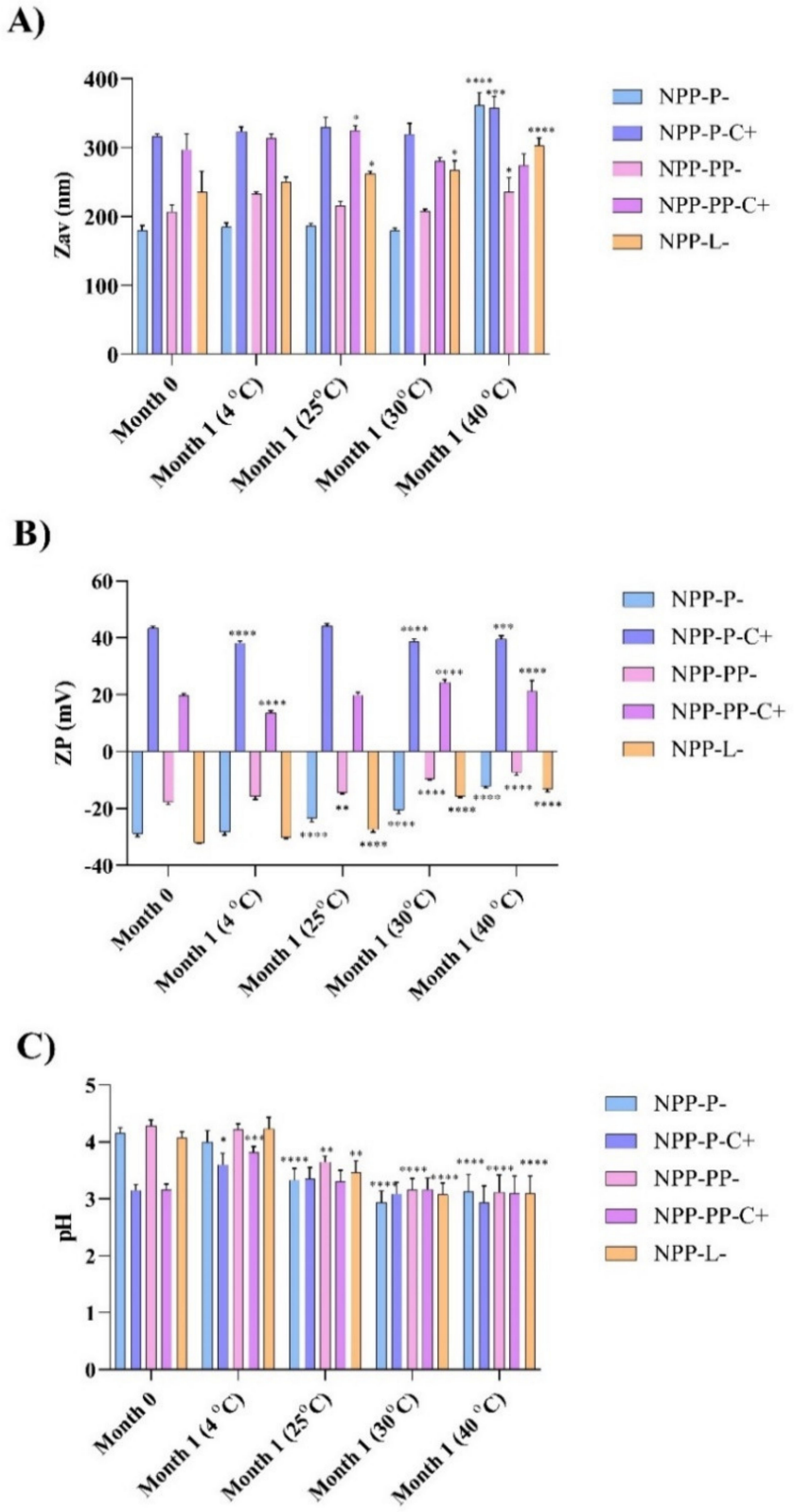

Figure 1. One-month stability of TH NPs with different surface functionalization strategies at 4, 25, 30 and 40 °C. (**A**) Average size, (**B**) Zeta potential (ZP), (**C**) pH values. Statistical significance was analyzed against freshly prepared formulations (one month), * $p < 0.5$; ** $p < 0.01$; *** $p < 0.001$; **** $p < 0.0001$.

Table 2. Physicochemical values of TH-NPs with different surface functionalization stored at 4 °C.

	Month	Z_{av} (nm) ± SD	PI ± SD	ZP ± SD (mV)
NPP-P-	0	172.9 ± 1.9	0.066 ± 0.037	−24.5 ± 0.9
	1	177.7 ± 2.2	0.071 ± 0.015	−20.9 ± 0.5
	3	183.8 ± 3.6	0.082 ± 0.005	−18.3 ± 0.7
	6	191.5 ± 1.5	0.091 ± 0.015	−14.3 ± 0.6
NPP-P-C+	0	337.3 ± 7.4	0.123 ± 0.035	23.6 ± 0.3
	1	365.4 ± 3.2	0.141 ± 0.011	23.2 ± 0.9
	3	392.9 ± 8.0	0.158 ± 0.037	21.0 ± 0.3
	6	419.6 ± 11.5	0.197 ± 0.066	17.2 ± 0.2
NPP-PP-	0	184.0 ± 0.9	0.101 ± 0.041	−22.2 ± 0.6
	1	191.2 ± 0.7	0.098 ± 0.022	−18.2 ± 0.6
	3	189.1 ± 10.1	0.099 ± 0.015	−12.1 ± 0.4
	6	220.0 ± 10.8	0.123 ± 0.33	−8.4 ± 0.7
NPP-PP-C+	0	221.1 ± 3.3	0.149 ± 0.036	10.5 ± 0.6
	1	224.1 ± 5.3	0.150 ± 0.068	9.8 ± 0.6
	3	256.1 ± 5.3	0.152 ± 0.077	7.3 ± 0.7
	6	348.5 ± 17.2	0.189 ± 0.023	6.1 ± 0.5
NPP-L-	0	178.5 ± 0.6	0.063 ± 0.018	−41.2 ± 1.8
	1	180.9 ± 1.4	0.076 ± 0.019	−39.7 ± 0.5
	3	214.7 ± 2.7	0.114 ± 0.032	−29.7 ± 0.5
	6	201.9 ± 3.4	0.132 ± 0.027	−23.9 ± 0.8

In addition, backscattering profile of surface-functionalized TH-NPs was analyzed by Turbiscan® and results are shown in Figure 2. All optimized TH-NPs underwent a slight sedimentation that was reversible by agitation. This sedimentation might be the cause of the physicochemical modifications previously observed (Table 2). Moreover, since the difference between the obtained profiles was below 10%, this indicates a suitable stability of all the functionalized TH-NPs. However, in order to ensure long-term stability, TH-NPs lyophilization and incorporation into semi-solid formulations would be contemplated in further studies.

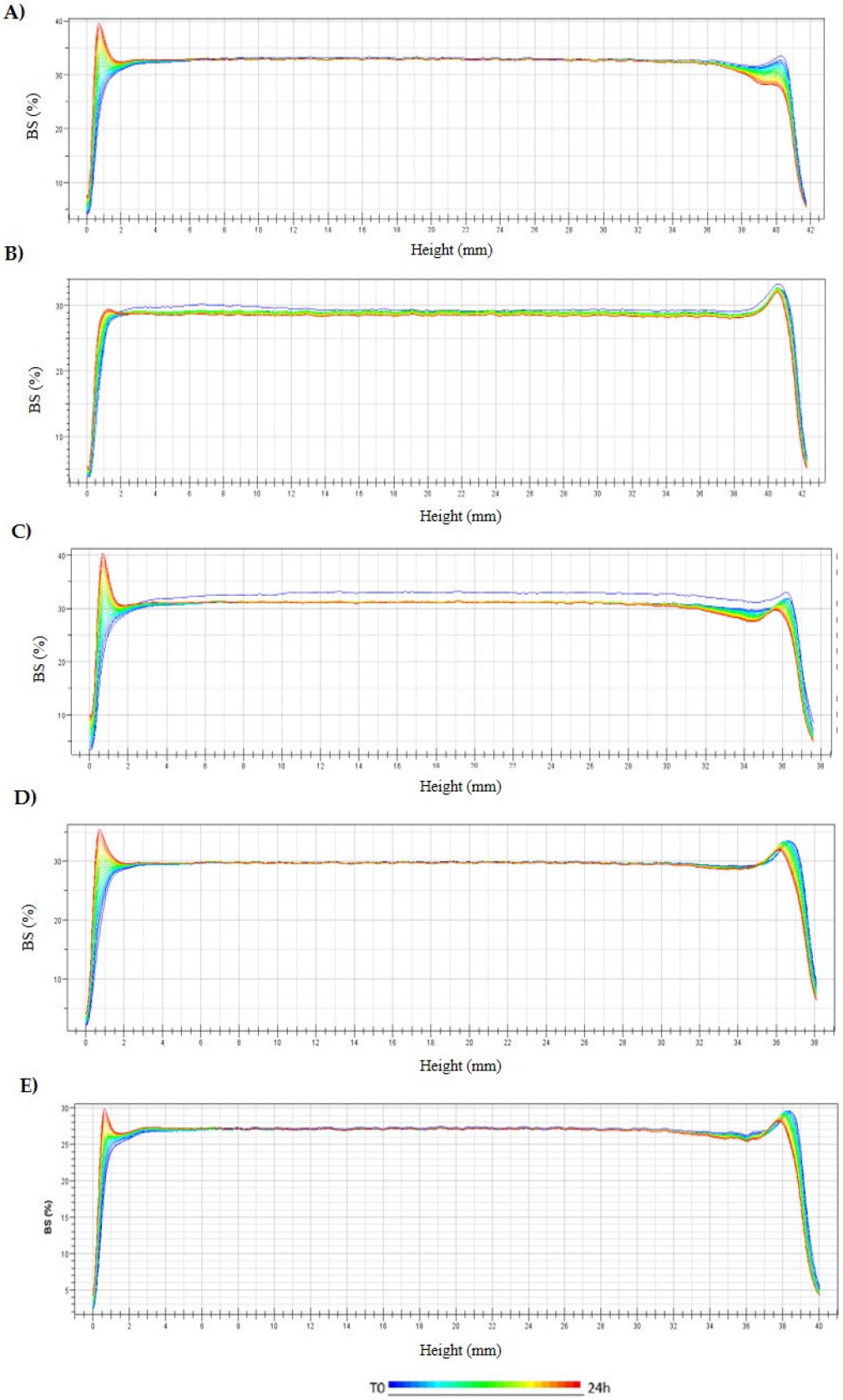

Figure 2. Backscattering profile of NPs measured monthly for 6 months after storage at 4 °C. (**A**) TH-NP-L-, (**B**) TH-NP-P-, (**C**) TH-NP-P-C+, (**D**) TH-NP-PP- and (**E**) TH-NP-PP-C+.

3.3. Ex Vivo Skin Penetration of Thymol Loaded Nanoparticles

As can be observed in Figure 3, R-TH-NPs successfully penetrated into the skin hair follicle within 24 h. This is of extreme relevance since it is the main site where acne associated infection and inflammation occurs. Moreover, it can be observed that penetration was not influenced by the surface charge carried out since both negatively and positively charge TH NPs were able to penetrate through the skin follicle ex vivo.

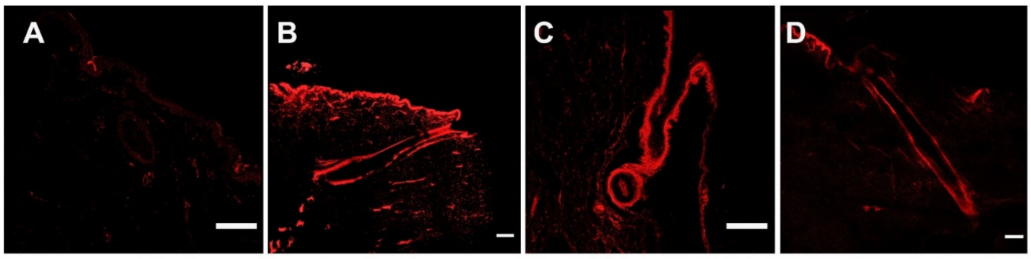

Figure 3. Pig skin hair follicle penetration of R-TH-NPs in 24 h by confocal microscopy. (**A**) untreated (control), (**B**) R-TH-NP-L-, (**C**) R-TH-NP-P- and (**D**) R-TH-NP-P+. Scale bar: 200 μm.

3.4. Ex Vivo Methylene Blue Reduction

The antioxidant efficiency of TH and surface functionalized TH-NPs was evaluated in the ex vivo pig skin model by measuring methylene blue reduction, which results in a colorless compound (Figure 4). Results showed that all the assessed TH-NPs showed antioxidant activity, greater than that of free TH. No qualitative differences between TH-NPs were observed.

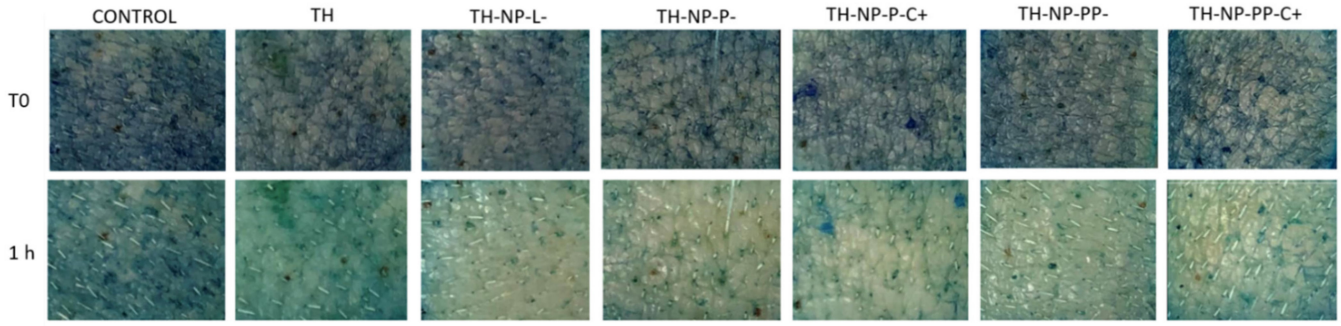

Figure 4. Ex vivo antioxidant activity by methylene blue reduction in pig skin. Images recorded at time 0 and 1 h of the studied compounds (control, free TH, TH-NP-L-, TH-NP-P-, TH-NP-P-C+, TH-NP-PP- and TH-NP-PP-C+).

3.5. In Vitro Antioxidant Activity

The in vitro antioxidant activity of the different compounds used to prepare the formulations was evaluated individually by the DPPH assay (Figure 5). Results expressed as free radical scavenging capacity (%) showed that TH has similar antioxidant activity as the control BHT, although slightly higher. When tested separately, the surface compounds P, PP and L displayed slightly in vitro free radical scavenging activity, although it was lower than the activity of TH and BHT in all dosages tested.

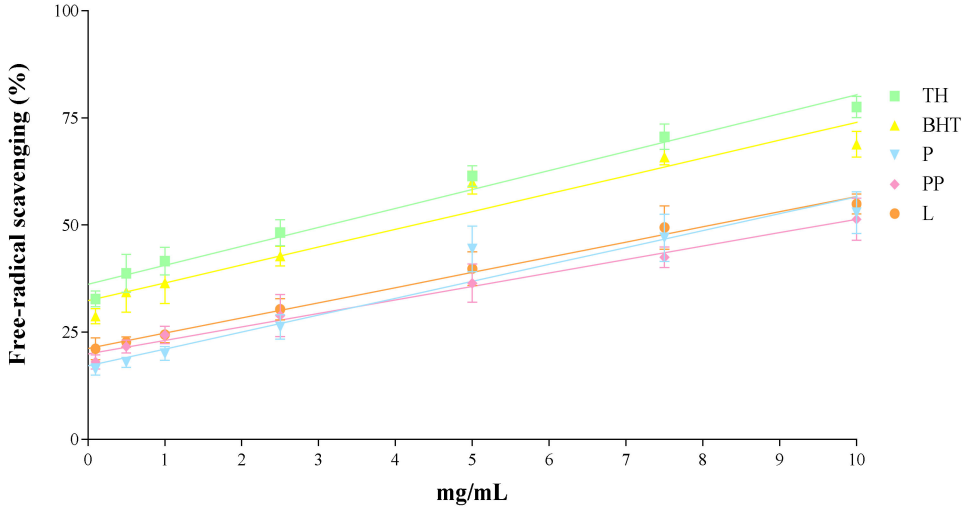

Figure 5. Antioxidant activity of TH, BHT and surface compounds alone (P, PP and L) assessed by the DPPH free-radical scavenging assay. The 100% ROS was obtained by the value of the control (H_2O_2) in 2 h.

3.6. In Vitro Antimicrobial Efficacy

The in vitro antimicrobial activity of optimized surface functionalized TH-NPs against *C. acnes* was similar to that of TH and in all the cases, statistical signifcant differences were obtained against the positive control (Figure 6). The higher antimicrobial activity was obtained with TH-NP-P-, although no statistically significant differences were observed between the different formulations.

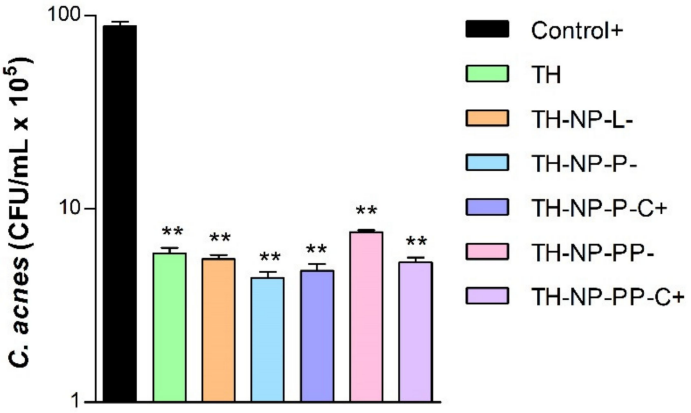

Figure 6. Antimicrobial activity of NPs against *C. acnes* measured by the suspension test. Values represent microbial counts in CFU/mL after 30 min incubation and are expressed as Mean ± SD (n = 3). Statistical analysis was carried out via one-way ANOVA, with Tukey's Multiple Comparison Test: **, $p < 0.001$ against control (*C. acnes* without any treatment).

3.7. Cytotoxicity and Cellular Uptake of Thymol Loaded NPs in HaCaT Cells

Cytotoxicity of TH-NPs was evaluated on HaCaT cells using the MTT assay. Cells were incubated for 24 h with TH or each TH-NP at concentrations of 2, 10 or 20 µg/mL. The surface compounds alone (P, PP, L) were tested at concentrations equivalent to those present in each formulation. Results showed that none of the samples were cytotoxic as cell viability was kept close to the untreated control cells, above 90% (data not shown).

Cellular uptake was evaluated for R-TH-NP-L-, R-TH-NP-P- and R-TH-NP-P-C+ (20 µg/mL) in HaCaT cells in order to evaluate composition and surface charge influence on cellular uptake. After 2 h incubation, TH-NPs-associated fluorescence was detected by confocal microscopy in cells treated with any of the R-TH-NPs tested (Figure 7). The cell

membrane was stained with WGA (green) and the nucleus (blue) with DAPI. In the merged images the internalized TH-NPs were mainly localized in the cytoplasm in all the cases.

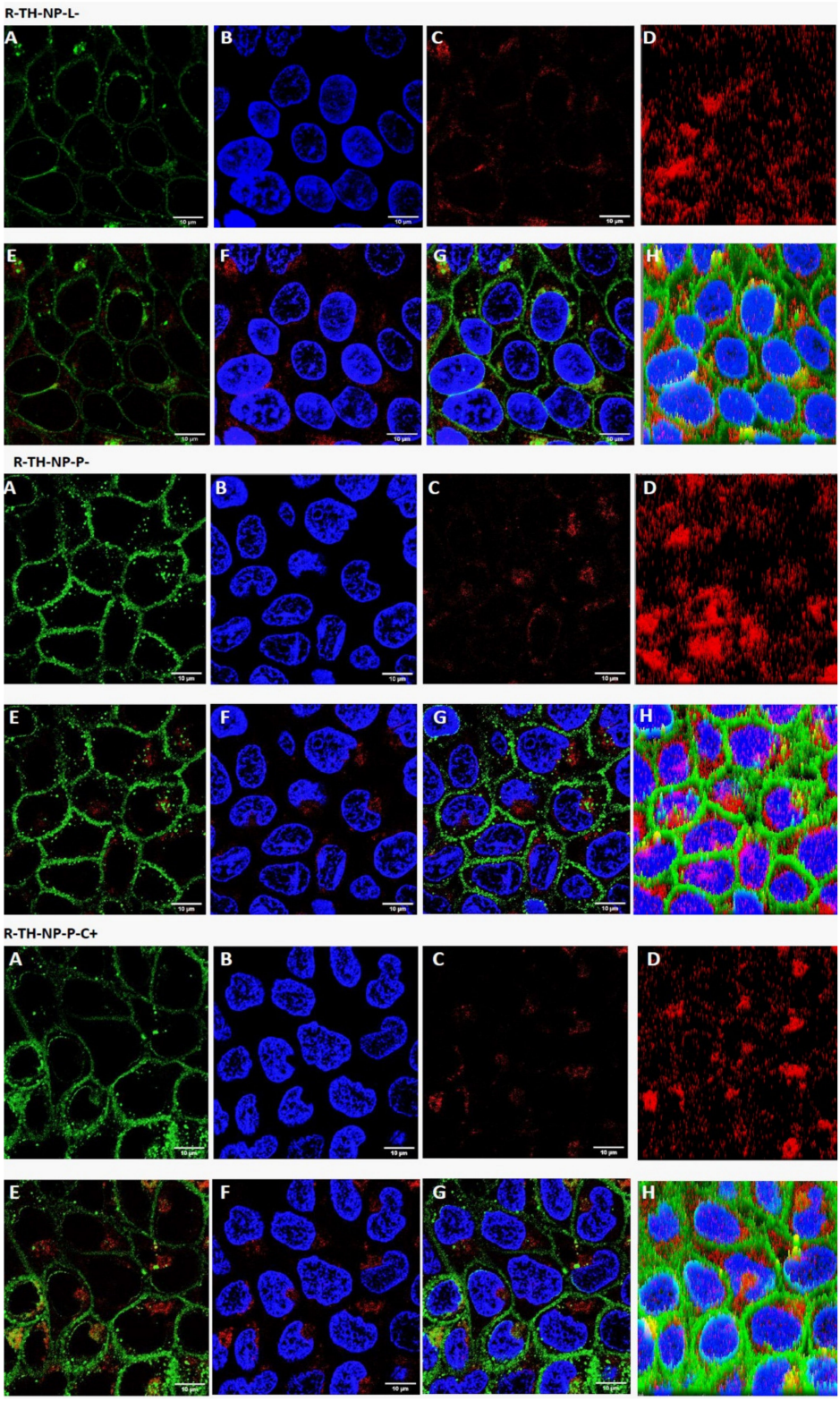

Figure 7. Cellular uptake by confocal microscopy analysis of HaCaT cells incubated with the indicated rhodamine-labelled NPs. (**A**) membrane staining with WGA, (**B**) nuclei staining with DAPI; (**C**) fluorescence of internalized R-TH-NPs, (**D**) 3D-plot of C, (**E**) merged A and C, (**F**) merged B and C, (**G**) merged A, B and C, (**H**) 3D-plot of G. Figure scale bar corresponds to 10 μm.

3.8. Anti-Inflammatory Activity of Thymol Loaded NPs in HaCaT Cells Treated with TNF-α

The anti-inflammatory activity of the formulated NPs was evaluated in the TNF-α-induced inflammation model using HaCaT cells. Secretion of IL-6 was quantified by ELISA in cell supernatants of untreated control HaCaT cells (basal IL-6 expression), TNFα-treated HaCaT cells in the absence (positive control of inflammation) or in the presence of the different NPs. Free TH and surface compounds (C, L, P, PP) were also tested in parallel (Figure 8). Results showed that TH significantly reduced TNF-α-induced secretion of IL-6. All surface compounds analyzed individually, except PP, have similar anti-inflammatory activity as TH. Additionally, all TH-NPs, except TH-NP-PP-, presented higher anti-inflammatory activity than free compounds. The most effective NPs were the positively charged formulations, containing C. However, only TH-NP-P-C+ displayed a significant difference compared to TH.

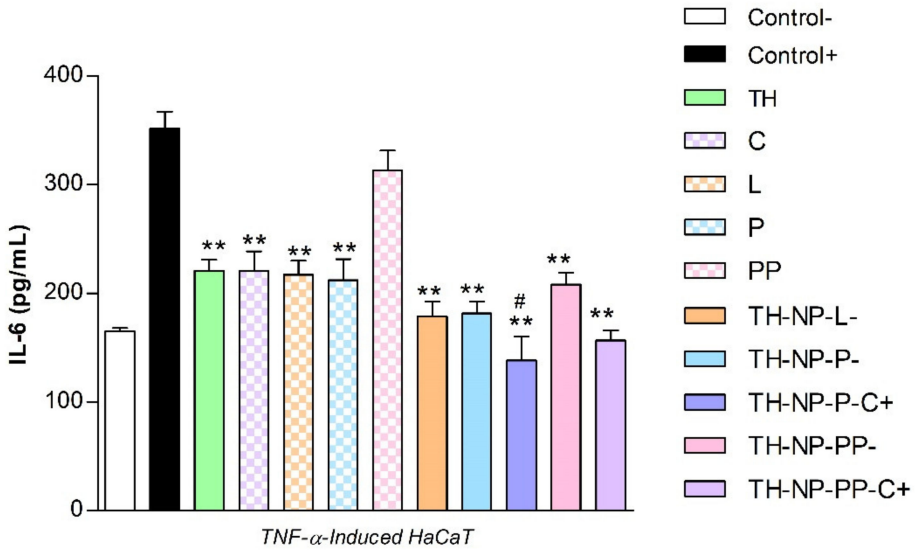

Figure 8. Quantification of secreted IL-6 by ELISA in TNF-α-stimulated HaCaT cells pre-incubated with formulated NPs and free compounds. Values of IL-6 (pg/mL) are the Mean ± SD, n = 3. Negative control: HaCaT cells without any treatment; Positive control: HaCaT cells treated only with TNF-α. Statistical analysis was performed by via one-way ANOVA, followed by Tukey's Multiple Comparison Test. ** $p < 0.001$ compared to positive control, and # $p < 0.01$ compared to TH.

3.9. Anti-Inflammatory Activity of Thymol Loaded NPs in HaCaT Cells Treated with C. acnes

The inflammatory activity of *C. acnes* was assessed in HaCaT cells treated with different dilutions of a *C. acnes* stock inoculum prepared in DMEM medium (OD 1.2 at 550 nm). Inflammation was evaluated by quantification of secreted IL-8 by ELISA. Results showed that *C. acnes* triggered IL-8 secretion in a dose- dependent manner (Figure S1 of Supplementary Materials).

From these results, the undiluted *C. acnes* stock inoculum prepared in DMEM medium (OD 1.2 at 550 nm) was optimized to be added directly to HaCaT cells to induce inflammation in further experiments aimed at evaluating the anti-inflammatory potential of TH-NPs. In this context, expression of genes encoding the inflammatory cytokines TNF-α, IL-1α, IL-1β, IL-6 and IL-8 was analyzed by RT-qPCR after *C. acnes* infection in HaCaT cells pre-treated with TH, TH-NPs or B-NPs (NPs without TH). Cells challenged only with *C. acnes* were used as a positive control of the inflammatory response. Results are illustrated in Figure 9. Infection by *C. acnes* strongly induced the expression of all pro-inflammatory cytokines tested. According to its anti-inflammatory properties, TH significantly decreased the expression of all of them.

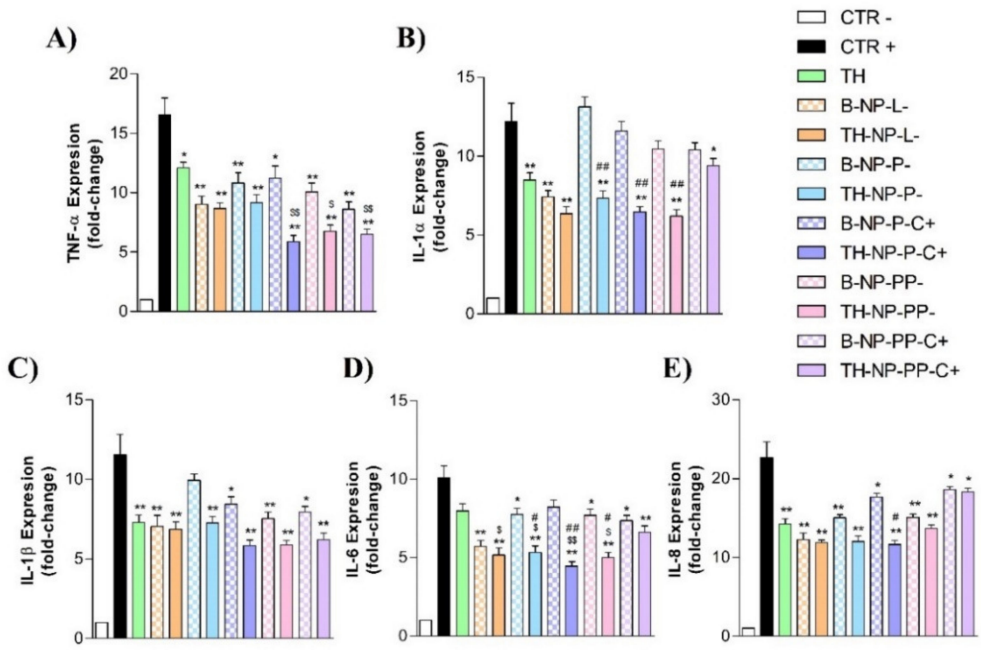

Figure 9. Gene expression levels of inflammatory cytokines in *C. acnes*-infected HaCaT cells. Before the addition of undiluted *C. acnes* inoculum (adjusted to OD 1.2 at 550 nm), HaCaT cells were pre-incubated with TH or the indicated NPs. Relative mRNA levels of (**A**) IL-6, (**B**) IL-8, (**C**) IL-1α, (**D**) IL-1β and (**E**) TNF-α were measured by RT-qPCR, using β-actin as the reference gene. Values (Mean ± SEM, $n = 3$) are expressed as fold-change compared to untreated HaCaT cells (control-). Statistical analysis was performed via one-way ANOVA, followed by Tukey's Multiple Comparison Test ($p < 0.05$* or $p < 0.001$**): versus positive control (control+); ($p < 0.05^{\$}$ or $p < 0.001^{\$\$}$): versus TH and ($p < 0.05^{\#}$ or $p < 0.001^{\#\#}$): versus the respective B-NP.

Infection by *C. acnes* strongly induced the expression of all pro-inflammatory cytokines tested (positive control). According to its anti-inflammatory properties, TH significantly decreased the expression of all of them. In general, all TH-NPs have anti-inflammatory activity, being able to reduce the mRNA levels of the different cytokines to a greater or lesser degree depending on the type of TH-NPs and the cytokine analyzed. Some TH-NPs have an anti-inflammatory activity greater than that of free TH. Statistically significant differences with respect the reduction caused by TH were apparent when analyzing the expression of IL-1α and IL-6. In the case of the TH-NP-P-C + formulation, statistical differences with respect to TH were also significant for TNF-α and IL-8. The results showed that B-NPS can also reduce significantly the expression of all cytokines except IL-1α. However, the anti-inflammatory activity was less than that exhibited by the equivalent TH-NP. The only TH-NP that did not show significant differences with respect the equivalent B-NP is the TH-NP-L formulation.

3.10. Antioxidant Activity via ROS Quantification in H_2O_2-Induce H2DCFDALabelled HaCaT

The antioxidant activity of TH-NPs was evaluated by ROS quantification in HaCaT cells stressed with hydrogen peroxide. Treatment with any of the surface funtionalized TH-NPs significantly reduced intracellular ROS to a greater extent than TH (Figure 10). TH displayed antioxidant activity at all assay times (Figure 10A). Moreover, the surface compounds tested individually did not show significant antioxidant activity (Figure 10A), indicating their inability to act as free radical scavengers at the cellular level. In the case of the B-NPs (Figure 10B), they showed a ROS scavenging activity similar to TH up to 60 min after H_2O_2 challenge. Even though no significant differences were found, TH-NP-L- showed an increased antioxidant activity that may be due to phosphaditilcholine coating potentiation of TH antioxidant effects [51].

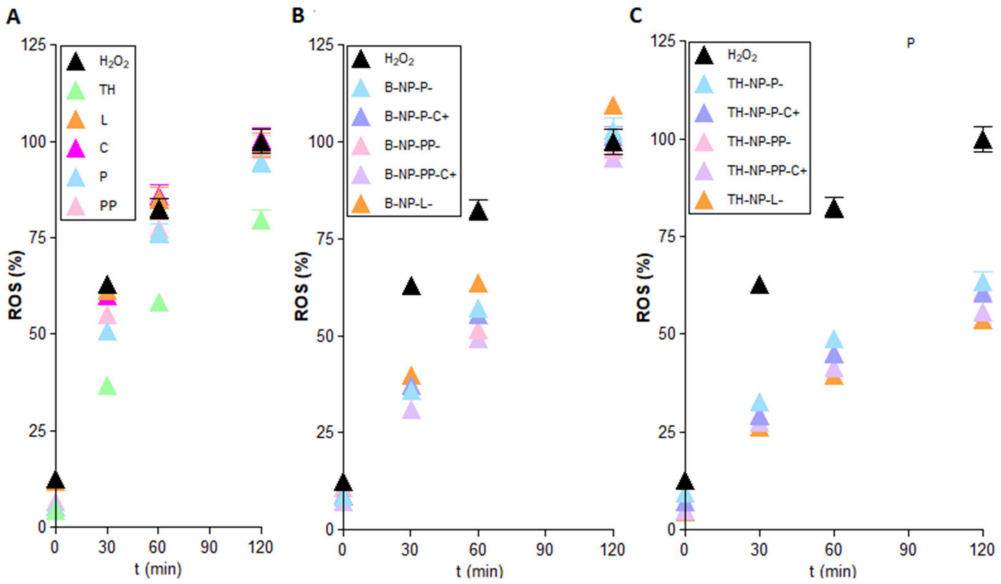

Figure 10. Antioxidant activity of (**A**) TH and free surface compounds, (**B**) B-NPs (blank NPs) and (**C**) TH-NPs evaluated in HaCaT cells challenged with H_2O_2. ROS were quantified using the fluorescent probe H2DCFDA. Data are expressed as the Mean ± SD (n = 8) of the amount of quantified ROS (%), assigning the value of 100 to the amount of ROS generated after 120 min treatment with H_2O_2.

However, this activity was lost at 120 min of incubation since ROS values were similar to that of H_2O_2-treated cells. Therefore, surface functionalization compounds could increase TH-NPs antioxidant activity at the cellular level potentiating their effects. In the other hand, all TH-NPs displayed greater antioxidant activity than TH and B-NPs, with minimal variances between them (Figure 10C).

3.11. Wound Healing Activity

In this study, the wound healing activity of the samples was analyzed in HaCaT cells following two different protocols. The first study was focused on studying prevention wound healing capacity. In this experiment, a 2 h-treatment with TH-NPs and the coating compounds was applied 24 h prior to the scratch (Figure 11). Images were recorded at the time of the scratch (T0) and after 24 h incubation. Results showed that all samples increased cell regeneration and possess wound healing activity compared to control. TH-NPs (Figure 11E–I) presented higher activity than TH (Figure 11B), specially un the case of TH-NP-PP-C+. The surface compounds alone had minor effects. Therefore, using this assay, wound healing prevention of surface modified TH-NPs has been demonstrated.

The second protocol was performed in order to study wound healing treatment. Figure 12 illustrates cell regeneration and wound healing efficacy after 24 h incubation. Results indicate that surface-functionalized TH-NPs showed greater wound healing activity than control TH and all other individually tested compounds. Additionally, depending on their surface composition, an increase in cell proliferation and wound closure could be observed specially in the case of Chitosan coated TH-NPs. Therefore, this test confirms that TH-NPs could also be used for wound healing treatment. Meanwhile, B-NPs and surface compounds alone presented minimal activity thus indicating synergic effect between TH and surface functionalization compounds.

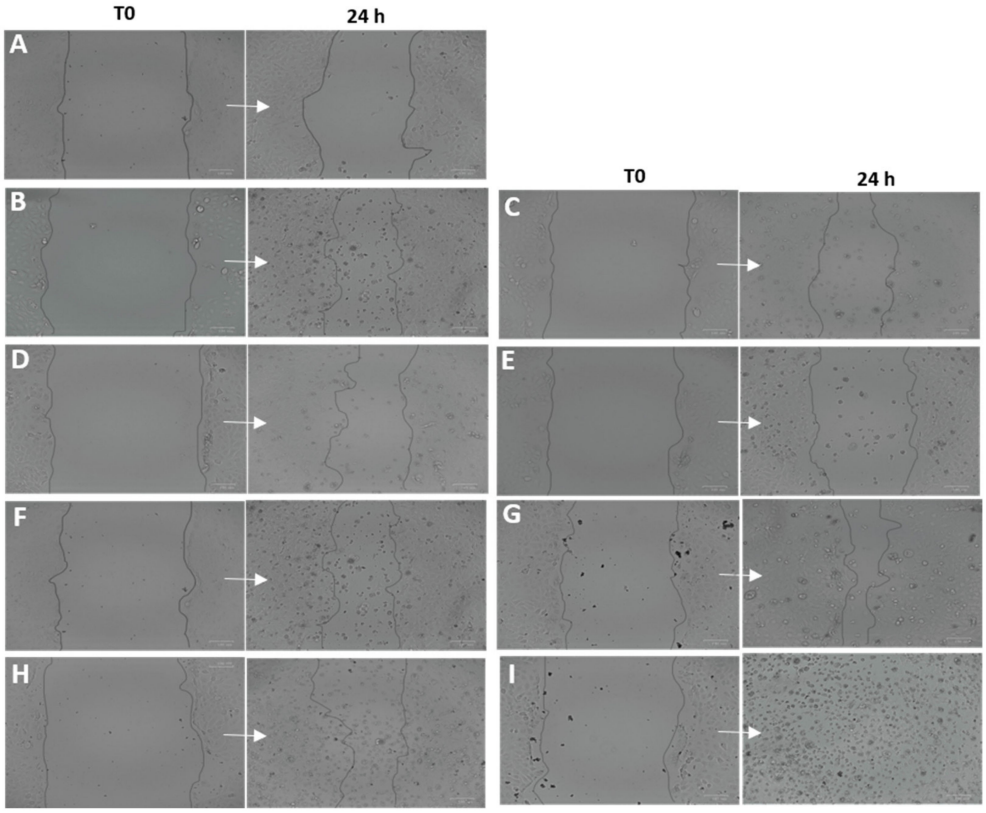

Figure 11. Wound healing activity in HaCaT pre-scratch treatment (wound healing prevention). Scratches were monitored at T0 and after 24 h incubation. (**A**) control, (**B**) Free TH, (**C**) chitosan, (**D**) phosphatidylcholine, (**E**) TH-NP-L-, (**F**) TH-NP-P-, (**G**) TH-NP-P-C+, (**H**) TH-NP-PP- and (**I**) TH-NP-PP-C+.

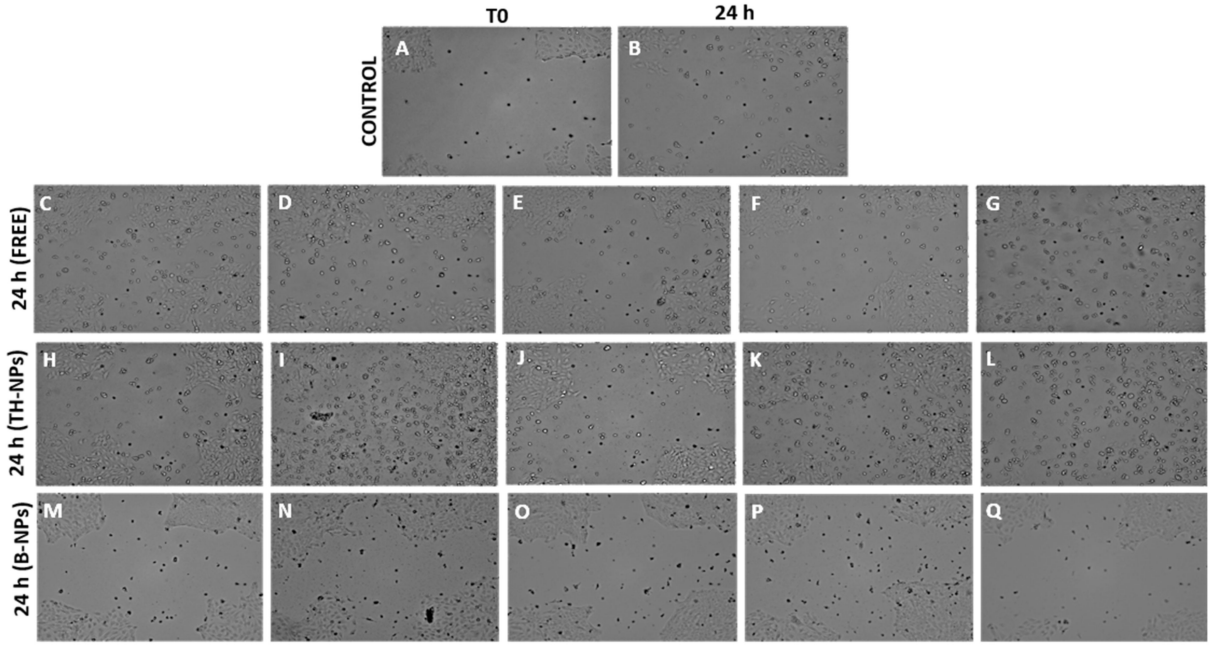

Figure 12. Recorded images of wound healing activity in HaCaT cells under post-scratch treatment (wound healing treatment). (**A**) Control T0, (**B**) Control after 24 h incubation, (**C**) Free TH, (**D**) Poloxamer 188, (**E**) poloxamer 407, (**F**) chitosan, (**G**) phosphatidylcholine, (**H**) TH-NP-P-, (**I**) TH-NP-P-C+, (**J**) TH-NP-PP-, (**K**) TH-NP-PP-C+, (**L**) TH-NP-L-, (**M**) B-TH-NP-P-, (**N**) B-NP-P-C+, (**O**) B-NP-PP-, (**P**) B-NP-PP-C+, (**Q**) TH-NP-L-.

4. Discussion

In the present study, surface-functionalized PLGA NPs were successfully loaded with thymol by the solvent displacement method in order to avoid TH instability and high volatility. To compare their pharmacological activities against acne, 5 formulations were developed, namely TH-NP-P-, TH-NP-P-C+, TH-NP-PP-, TH-NP-PP-C+ and TH-NP-L-. All the resulting TH-NPs presented suitable physical chemical parameters and a suitable short-term stability at 4 °C. The sedimentation phenomena observed by the backscattering signal was reversed by agitation. Confocal microscopy qualitative analysis confirmed that TH-NPs penetrated into the hair follicle, independent of their surface-coating type or charge. Some authors stated that the reservoir of the hair follicle could store actives 10 times longer than the reservoir of the SC and that hair follicle under movement (in vivo) should improve NPs penetration [52]. Other authors have already described that NPs accumulate in the follicular entry, which is confirmed in the case of surface-functionalized TH-NPs [53–55]. Regarding TH-NP-L, it appears that they can penetrate not only in the follicle, by also within the primary layers of the epidermis. This can be explained by the phospholipidic nature of the surface that diffuses easier through the skin. In the case of R-TH-NP-P-, their penetration was found mainly through in the entire hair follicle and a lower amount remaining in the SC. This indicated that this type of surface is favored by the follicular and not the intercellular pathway. On the other hand, concerning R-TH-NP-P-C+, which are positively charged and present slightly higher particle diameter, the penetration could be observed only inside the follicle. This is in accordance with the fact that NPs penetration into hair follicle is size and surface dependent.

Furthermore, the free-radical scavenging of TH was similar to endogenous control BHT and much higher than the free surface compounds themselves, which showed lower activity. The antimicrobial activity of TH and TH-NPs against *C. acnes* demonstrated to reduce microbial viability within only 30 min incubation. All tested samples presented similar activity, where the highest was achieved for TH-NP-P-. Moreover, since the penetration route of TH-NPs into the skin is through the hair follicle, the observed activity will presumably be performed directly on the acne lesion.

In HaCaT cell line, TH-NPs and all free compounds themselves did not alter cell viability, presenting no cytotoxicity. The cellular uptake images showed most of the NPs within only 2 h in the cytosol but also present the nucleus, especially for TH-NP-P-. The anti-inflammatory activity of TH and TH-NPs all presented significant reduction on gene expressions tested, where, in all the cases, all or most of TH-NPs performed significant reduction compared to the control and to their corresponding B-NP. Depending on the gene analyzed, the activity was enhanced for a different surface composition of the NPs. Therefore, they act as good booster of the activity. The antioxidant activity in HaCaT cells was achieved for all TH-NPs, higher than TH and all other tested samples. The antioxidant activity of compounds enables cell proliferation faster, that can enhance wound healing processes to improve skin healing process on acne lesions [56]. For the wound healing activity, all scratched treated cells provided higher cell proliferation than control cells. Interestingly, in both prevention and treatment of wound healing activity all surface modified TH-NPs showed suitable results. All TH-NPs provided good cell regeneration, meanwhile the B-NPs showed minimal activity. The antioxidant properties of surface compounds might have influenced on the healing activity, possibly by synergic activity with TH. All TH-NPs showed better results than TH, confirming that surface modified TH-NPs present higher healing capacity than free antioxidant compounds. The antioxidant activity was also confirmed by the methylene blue reduction in ex vivo pig skin, showing that TH-NPs had greater activity than TH within 1 h incubation.

To summarize, TH was successfully encapsulated into PLGA NPs with suitable particle diameters and good stability. Moreover, other authors have developed different types of NPs for TH encapsulation such as PLA or chitosan NPs obtaining lower stability values (around 60%) [28]. Lipid NPs containing thymol have also been developed with a negative surface charge confirming their anti-inflammatory properties but they were assessed for

psoriasis treatment [25]. In addition, Pires and colleagues studied compatibility of TH with several excipients confirming that P80 was a suitable excipient [57]. Moreover, surface-functionalized TH-NPs successfully penetrated into the skin through the hair follicle, where acne occurs. Even though the antimicrobial activity of TH-NPs was similar to TH, they provided outstanding activities as anti-inflammatory, antioxidant and wound healing, when compared to than TH and B-NPs. TH-NPs in contact with HaCaT cells showed that they were able to penetrate inside the cells, enabling greater activities than when compounds were introduced as its free form. TH and TH-NPs presented good anti-inflammatory activity by significant reduction on the gene expression tested. The efficacy of TH-NPs varied depending on their surface coating as well as genes analyzed. The antioxidant activity was proven in HaCaT and on ex vivo skin, and in all cases, TH-NPs were greater than TH. For this reason, they have also provided excellent wound closure and cell proliferation results, where the NPs positively charged, performed higher synergic activity on healing processes. Therefore, our study demonstrates that TH-NPs with surface functionalization using different approaches could constitute a potential efficient treatment for acne. However, these results would need to be assessed in in vivo experiments due to the multifactorial triggers of acne as well as the sebaceous content that can influence NPs stability [58].

5. Conclusions

Surface-modified TH-NPs demonstrated to possess antimicrobial, anti-inflammatory, antioxidant and wound healing properties. In addition to TH-NPs multifunctional therapeutic benefits, they penetrate through the hair follicle and, therefore, they could be suitable for the treatment of severe acne disease.

Supplementary Materials: The following are available online at https://www.mdpi.com/article/10.3390/pharmaceutics13091501/s1, Table S1: Oligonucleotinde primers used for RT-qPCR, Figure S1: Dose-dependent inflammatory capacity of *C. acnes*. HaCaT cells were incubated for 24 with the indicated dilutions of the *C. acnes* stock inoculum (adjusted to OD 1.2 at 550 nm). Value 1 indicates no dilution. Secreted IL-8 was quantified in the cell culture supernatant by ELISA. Values of IL-8 (pg/mL) are the Mean ± SD, n = 3.

Author Contributions: Conceptualization, C.F., A.C.C., J.B., L.B. and M.L.G.; methodology, C.F., N.D.-G., A.M.M., M.E. and A.C.C.; formal analysis, C.F., E.S.-L. and A.C.C.; investigation, C.F., N.D.-G. and M.E.; resources, A.M.M., J.B. and L.B.; writing—original draft preparation, C.F., M.E. and E.S.-L.; writing—review and editing, E.S.-L., A.M.M., J.B., L.B. and M.L.G., funding acquisition, J.B., L.B. and M.L.G. All authors have read and agreed to the published version of the manuscript.

Funding: This research received no external funding.

Institutional Review Board Statement: The study was conducted according to the guidelines of the Declaration of Helsinki, and approved by the Ethics Committee of the University of Barcelona.

Acknowledgments: The authors ESL, MLG and ME would like to acknowledge 2017SGR1477.

Conflicts of Interest: The authors declare no conflict of interest.

References

1. Williams, H.C.; Dellavalle, R.P.; Garner, S. Acne vulgaris. *Lancet* **2012**, *379*, 361–372. [CrossRef]
2. Sachdeva, M.; Tan, J.; Lim, J.; Kim, M.; Nadeem, I.; Bismil, R. The prevalence, risk factors, and psychosocial impacts of acne vulgaris in medical students: A literature review. *Int. J. Dermatol.* **2021**, *60*, 792–798. [CrossRef]
3. Well, D.; Levine, S.R. Acne vulgaris: A review of causes and treatment options. *J. Dermatol. Nurses. Assoc.* **2014**, *6*, 302–309. [CrossRef]
4. Flowers, L.; Grice, E.A. The Skin Microbiota: Balancing Risk and Reward. *Cell Host Microbe* **2020**, *28*, 190–200. [CrossRef] [PubMed]
5. Chlebus, E.; Chlebus, M. Factors affecting the course and severity of adult acne. Observational cohort study. *J. Dermatolog. Treat.* **2017**, *28*, 737–744. [CrossRef]
6. Bansal, P.; Sardana, K.; Vats, G.; Sharma, L.; Garga, U.C.; Khurana, A. A Prospective Study Examining Trigger Factors and Hormonal Abnormalities in Adult Female Acne. *Indian Derm. Online J.* **2020**, *11*, 544–550. [CrossRef]

7. Tanghetti, E.A. The Role of Inflammation in the Pathology of Acne. *J. Clin. Aesthetic Dermatol.* **2013**, *6*, 27–35.
8. Bhatia, A.; Maisonneuve, J.F.; Persing, D.H. Propionibacterium acnes and chronic diseases. In *The Infectious Etiology of Chronic Diseases: Defining the Relationship, Enhancing the Research, and Mitigating the Effects: Workshop Summary*; Knobler, S.L., O'Connor, S., Lemon, S.M., Eds.; National Academies Press: Washington, DC, USA, 2004.
9. Platsidaki, E.; Dessinioti, C. Recent advances in understanding Propionibacterium acnes (*Cutibacterium acnes*) in acne. *F1000Research* **2018**, *7*, 1953. [CrossRef]
10. Rozas, M.; de Ruijter, A.H.; Fabrega, M.J.; Zorgani, A.; Guell, M.; Paetzold, B.; Brillet, F. From dysbiosis to healthy skin: Major contributions of cutibacterium acnes to skin homeostasis. *Microorganisms* **2021**, *9*, 628. [CrossRef]
11. Bharti, S.; Vadlamudi, H.C. A strategic review on the involvement of receptors, transcription factors and hormones in acne pathogenesis. *J. Recept. Signal Transduct.* **2021**, *41*, 105–116. [CrossRef]
12. Kim, J. Review of the innate immune response in acne vulgaris: Activation of toll-like receptor 2 in acne triggers inflammatory cytokine responses. *Dermatology* **2005**, *211*, 193–198. [CrossRef] [PubMed]
13. Lee, Y.B.; Byun, E.J.; Kim, H.S. Potential Role of the Microbiome in Acne: A Comprehensive Review. *J. Clin. Med.* **2019**, *8*, 987. [CrossRef]
14. Xue, X.; Falcon, D.M. The role of immune cells and cytokines in intestinal wound healing. *Int. J. Mol. Sci.* **2019**, *20*, 6097. [CrossRef]
15. Melnik, B.C. Acne vulgaris: The metabolic syndrome of the pilosebaceous follicle. *Clin. Dermatol.* **2018**, *36*, 29–40. [CrossRef] [PubMed]
16. Katsuta, Y.; Iida, T.; Hasegawa, K.; Inomata, S.; Denda, M. Function of oleic acid on epidermal barrier and calcium influx into keratinocytes is associated with N-methyl d-aspartate-type glutamate receptors. *Br. J. Dermatol.* **2009**, *160*, 69–74. [CrossRef]
17. Dreno, B.; Gollnick, H.P.M.; Kang, S.; Thiboutot, D.; Bettoli, V.; Torres, V.; Leyden, J. Understanding innate immunity and inflammation in acne: Implications for management. *J. Eur. Acad. Dermatol. Venereol.* **2015**, *29*, 3–11. [CrossRef]
18. Amiri, H. Essential oils composition and antioxidant properties of three thymus species. *Evid.-Based Complement Altern. Med.* **2012**, *2012*, 728065. [CrossRef] [PubMed]
19. Briganti, S.; Picardo, M. Antioxidant activity, lipid peroxidation and skin diseases. What's new. *J. Eur. Acad. Dermatol. Venereol.* **2003**, *17*, 663–669. [CrossRef]
20. Bakkali, F.; Averbeck, S.; Averbeck, D.; Idaomar, M. Biological effects of essential oils—A review. *Food Chem. Toxicol.* **2008**, *46*, 446–475. [CrossRef]
21. Zouboulis, C.C.; Jourdan, E.; Picardo, M. Acne is an inflammatory disease and alterations of sebum composition initiate acne lesions. *J. Eur. Acad. Dermatol. Venereol.* **2014**, *28*, 527–532. [CrossRef]
22. Trombetta, D.; Castelli, F.; Sarpietro, M.G.; Venuti, V.; Cristani, M.; Daniele, C.; Saija, A.; Mazzanti, G.; Bisignano, G. Mechanisms of antibacterial action of three monoterpenes. *Antimicrob. Agents Chemother.* **2005**, *49*, 2474–2478. [CrossRef] [PubMed]
23. Nagoor Meeran, M.F.; Javed, H.; Al Taee, H.; Azimullah, S.; Ojha, S.K. Pharmacological properties and molecular mechanisms of thymol: Prospects for its therapeutic potential and pharmaceutical development. *Front. Pharmacol.* **2017**, *8*, 1–34. [CrossRef] [PubMed]
24. Najafloo, R.; Behyari, M.; Imani, R.; Nour, S. A mini-review of Thymol incorporated materials: Applications in antibacterial wound dressing. *J. Drug Deliv. Sci. Technol.* **2020**, *60*, 101904. [CrossRef]
25. Pivetta, T.P.; Simões, S.; Araújo, M.M.; Carvalho, T.; Arruda, C.; Marcato, P.D. Development of nanoparticles from natural lipids for topical delivery of thymol: Investigation of its anti-inflammatory properties. *Colloids Surf. B Biointerfaces* **2018**, *164*, 281–290. [CrossRef]
26. Pires, F.Q.; Pinho, L.A.; Freire, D.O.; Silva, I.C.R.; Sa-Barreto, L.L.; Cardozo-Filho, L.; Gratieri, T.; Gelfuso, G.M.; Cunha-Filho, M. Thermal analysis used to guide the production of thymol and Lippia origanoides essential oil inclusion complexes with cyclodextrin. *J. Therm. Anal. Calorim.* **2019**, *137*, 543–553. [CrossRef]
27. Tao, F.; Hill, L.E.; Peng, Y.; Gomes, C.L. Synthesis and characterization of β-cyclodextrin inclusion complexes of thymol and thyme oil for antimicrobial delivery applications. *LWT-Food Sci. Technol.* **2014**, *59*, 247–255. [CrossRef]
28. Sáez-Orviz, S.; Marcet, I.; Weng, S.; Rendueles, M.; Díaz, M. PLA nanoparticles loaded with thymol to improve its incorporation into gelatine films. *J. Food Eng.* **2020**, *269*, 1–7. [CrossRef]
29. Sánchez-López, E.; Esteruelas, G.; Ortiz, A.; Espina, M.; Prat, J.; Muñoz, M.; Cano, A.; Calpena, A.C.; Ettcheto, M.; Camins, A.; et al. Dexibuprofen biodegradable nanoparticles: One step closer towards a better ocular interaction study. *Nanomaterials* **2020**, *10*, 720. [CrossRef]
30. Mengoni, T.; Adrian, M.; Pereira, S.; Santos-Carballal, B.; Kaiser, M.; Goycoolea, F.M. A chitosan-based liposome formulation enhances the in vitro wound healing efficacy of substance P neuropeptide. *Pharmaceutics* **2017**, *9*, 56. [CrossRef] [PubMed]
31. Chronopoulou, L.; Massimi, M.; Giardi, M.F.; Cametti, C.; Devirgiliis, L.C.; Dentini, M.; Palocci, C. Chitosan-coated PLGA nanoparticles: A sustained drug release strategy for cell cultures. *Colloids Surf. B Biointerfaces* **2013**, *103*, 310–317. [CrossRef]
32. Erös, G.; Ibrahim, S.; Siebert, N.; Boros, M.; Vollmar, B. Oral phosphatidylcholine pretreatment alleviates the signs of experimental rheumatoid arthritis. *Arthritis Res. Ther.* **2009**, *11*, 1–10. [CrossRef]
33. Hunter, R.L.; Luo, A.Z.; Zhang, R.; Kozar, R.A.; Moore, F.A. Poloxamer 188 inhibition of ischemia/reperfusion injury: Evidence for a novel anti-adhesive mechanism. *Ann. Clin. Lab. Sci.* **2010**, *40*, 115–125. [PubMed]

34. Moghimi, S.M.; Hunter, A.C. Poloxamers and poloxamines in nanoparticle engineering and experimental medicine. *Trends Biotechnol.* **2000**, *18*, 412–420. [CrossRef]
35. Fessi, H.; Puisieux, F.; Devissaguet, J.P.; Ammoury, N.; Benita, S. Nanocapsule formation by interfacial polymer deposition following solvent displacement. *Int. J. Pharm.* **1989**, *55*, R1–R4. [CrossRef]
36. Ghasemi Pirbalouti, A.; Rahimmalek, M.; Malekpoor, F.; Karimi, A. Variation in antibacterial activity, thymol and carvacrol contents of wild populations of Thymus daenensis subsp. daenensis Celak. *Plant Omics* **2011**, *4*, 209–214.
37. Sánchez-López, E.; Egea, M.A.; Cano, A.; Espina, M.; Calpena, A.C.; Ettcheto, M.; Camins, A.; Souto, E.B.; Silva, A.M.; García, M.L. PEGylated PLGA nanospheres optimized by design of experiments for ocular administration of dexibuprofen-in vitro, ex vivo and in vivo characterization. *Colloids Surf. B Biointerfaces* **2016**, *145*, 241–250. [CrossRef]
38. Gonzalez-Pizarro, R.; Parrotta, G.; Vera, R.; Sánchez-López, E.; Galindo, R.; Kjeldsen, F.; Badia, J.; Baldoma, L.; Espina, M.; García, M.L. Ocular penetration of fluorometholone-loaded PEG-PLGA nanoparticles functionalized with cell-penetrating peptides. *Nanomedicine* **2019**, *14*, 3089–3104. [CrossRef]
39. Fernández-García, E.; Heluani-Gahete, H.; Wellinger, R.E. A new colorimetric assay for antioxidant capacity and photostability. *Color. Technol.* **2016**, *132*, 195–200. [CrossRef]
40. Aman, S.; Moin, S.; Owais, M.; Siddiqui, M.U. Antioxidant activity of thymol: Protective role in AAPH-induced hemolysis in diabetic erythrocytes. *Int. J. Pharm. Sci. Invent.* **2013**, *2*, 55–60.
41. Messager, S.; Goddard, P.A.; Dettmar, P.W.; Maillard, J.Y. Determination of the antibacterial efficacy of several antiseptics tested on skin by an "ex-vivo" test. *J. Med. Microbiol.* **2001**, *50*, 284–292. [CrossRef]
42. Diaz-Garrido, N.; Fábrega, M.J.; Vera, R.; Giménez, R.; Badia, J.; Baldomà, L. Membrane vesicles from the probiotic Nissle 1917 and gut resident Escherichia coli strains distinctly modulate human dendritic cells and subsequent T cell responses. *J. Funct. Foods* **2019**, *61*, 103495. [CrossRef]
43. Carvajal-Vidal, P.; Fábrega, M.J.; Espina, M.; Calpena, A.C.; García, M.L. Development of Halobetasol-loaded nanostructured lipid carrier for dermal administration: Optimization, physicochemical and biopharmaceutical behavior, and therapeutic efficacy. *Nanomed. Nanotechnol. Biol. Med.* **2019**, *20*, 102026. [CrossRef] [PubMed]
44. Zhu, T.; Wu, W.; Yang, S.; Li, D.; Sun, D.; He, L. Polyphyllin I Inhibits Propionibacterium acnes-Induced Inflammation In Vitro. *Inflammation* **2019**, *42*, 35–44. [CrossRef]
45. Liu, Y.H.; Lin, Y.S.; Huang, Y.W.; Fang, S.U.; Lin, S.Y.; Hou, W.C. Protective Effects of Minor Components of Curcuminoids on Hydrogen Peroxide-Treated Human HaCaT Keratinocytes. *J. Agric. Food Chem.* **2016**, *64*, 3598–3608. [CrossRef]
46. Governa, P.; Carullo, G.; Biagi, M.; Rago, V.; Aiello, F. Evaluation of the in vitro wound-healing activity of calabrian honeys. *Antioxidants* **2019**, *8*, 36. [CrossRef]
47. Jangpromma, N.; Preecharram, S.; Srilert, T.; Maijaroen, S.; Mahakunakorn, P.; Nualkaew, N.; Daduang, S.; Klaynongsruang, S. In vitro and in vivo wound healing properties of plasma and serum from Crocodylus siamensis blood. *J. Microbiol. Biotechnol.* **2016**, *26*, 1140–1147. [CrossRef]
48. Vega, E.; Egea, M.A.; Garduño-Ramírez, M.L.; García, M.L.; Sánchez, E.; Espina, M.; Calpena, A.C. Flurbiprofen PLGA-PEG nanospheres: Role of hydroxy-β-cyclodextrin on ex vivo human skin permeation and in vivo topical anti-inflammatory efficacy. *Colloids Surf. B Biointerfaces* **2013**, *110*, 339–346. [CrossRef] [PubMed]
49. Sánchez-López, E.; Ettcheto, M.; Egea, M.A.; Espina, M.; Cano, A.; Calpena, A.C.; Camins, A.; Carmona, N.; Silva, A.M.; Souto, E.B.; et al. Memantine loaded PLGA PEGylated nanoparticles for Alzheimer's disease: In vitro and in vivo characterization. *J. Nanobiotechnol.* **2018**, *16*, 1–16. [CrossRef] [PubMed]
50. Sánchez-López, E.; Ettcheto, M.; Egea, M.A.; Espina, M.; Calpena, A.C.; Folch, J.; Camins, A.; García, M.L. New potential strategies for Alzheimer's disease prevention: Pegylated biodegradable dexibuprofen nanospheres administration to APPswe/PS1dE9. *Nanomed. Nanotechnol. Biol. Med.* **2017**, *13*, 1171–1182. [CrossRef]
51. Kim, J.Y.; Oh, S.; Yi, B.; Kim, M.J.; Lee, J.H. Synergism of phosphatidylcholine on the antioxidant properties of α-tocopherol in corn oils under different relative humidity. *Int. J. Food Sci. Technol.* **2015**, *50*, 1421–1428. [CrossRef]
52. Yukuyama, M.N.; De Araújo, G.L.B.; Bou-Chacra, N.A. Nanomaterials for hair care applications. *Nanocosmetics* **2020**, 205–225. [CrossRef]
53. Santos, G.A.; Angelo, T.; Andrade, L.M.; Silva, S.M.M.; Magalhães, P.O.; Cunha-Filho, M.; Gelfuso, G.M.; Taveira, S.F.; Gratieri, T. The role of formulation and follicular pathway in voriconazole cutaneous delivery from liposomes and nanostructured lipid carriers. *Colloids Sur. B Biointerfaces* **2018**, *170*, 341–346. [CrossRef]
54. Pereira, M.N.; Schulte, H.L.; Duarte, N.; Lima, E.M.; Sá-Barreto, L.L.; Gratieri, T.; Gelfuso, G.M.; Cunha-Filho, M.S.S. Solid effervescent formulations as new approach for topical minoxidil delivery. *Eur. J. Pharm. Sci.* **2017**, *96*, 411–419. [CrossRef] [PubMed]
55. Alvarez-Román, R.; Naik, A.; Kalia, Y.N.; Guy, R.H.; Fessi, H. Skin penetration and distribution of polymeric nanoparticles. *J. Control. Release* **2004**, *99*, 53–62. [CrossRef] [PubMed]
56. Mollarafie, P.; Khadiv Parsi, P.; Zarghami, R.; Amini Fazl, M.; Ghafarzadegan, R. Antibacterial and wound healing properties of thymol (*Thymus vulgaris* Oil) and its application in a novel wound dressing. *J. Med. Plants* **2015**, *14*, 69–81.

57. Pires, F.Q.; Angelo, T.; Silva, J.K.R.; Sá-Barreto, L.C.L.; Lima, E.M.; Gelfuso, G.M.; Gratieri, T.; Cunha-Filho, M.S.S. Use of mixture design in drug-excipient compatibility determinations: Thymol nanoparticles case study. *J. Pharm. Biomed. Anal.* **2017**, *137*, 196–203. [CrossRef] [PubMed]
58. Tolentino, S.; Pereira, M.N.; de Sousa, M.C.; Cunha-Filho, M.; Gelfuso, G.M.; Gratieri, T. The influence of sebaceous content on the performance of nanosystems designed for the treatment of follicular diseases. *J. Drug Deliv. Sci. Technol.* **2020**, *59*, 101895. [CrossRef]

ORIGINAL RESEARCH

C. Folle et al.

Thymol-loaded PLGA nanoparticles: An efficient approach for acne treatment

Camila Folle[1], Ana M. Marqués[2], Natalia Díaz-Garrido[3], Marta Espina[1,4], Elena Sánchez-López[1,4*], Josefa Badia[3], Laura Baldoma[3], Ana Cristina Calpena [1,4], Maria Luisa García[1,4*]

[1]Department of Pharmacy and Pharmaceutical Technology and Physical Chemistry, Faculty of Pharmacy and Food Sciences, University of Barcelona, 08028, Barcelona, Spain

[2]Department of Biology, Healthcare and Environment, Faculty of Pharmacy and Food Sciences, University of Barcelona, 08028, Barcelona, Spain

[3]Department of Biochemistry and Physiology, Biochemistry and Biomolecular Science, University of Barcelona, 08028, Barcelona, Spain; Institute of Biomedicine of the University of Barcelona (IBUB), 08028 Barcelona, Spain; Research Institute Sant Joan De Déu (IR-SJD), 08950 Barcelona, Spain.

[4]Institute of Nanoscience and Nanotechnology (IN2UB), University of Barcelona, 08028, Barcelona, Spain

*Correspondence:

Dr. Maria Luisa García López, marisagarcia@ub.edu

Dr. Elena Sánchez López, esanchezlopez@ub.edu

Department of Pharmacy and Pharmaceutical Technology and Physical Chemistry, Faculty of Pharmacy and Food Sciences, University of Barcelona.

Abstract

Background: Acne is a common skin disorder that involves an infection inside the hair follicle, which is usually treated with antibiotics, resulting in unbalanced skin microbiota and microbial resistance. For this reason, we developed polymeric nanoparticles encapsulating thymol, a natural active compound with antimicrobial and antioxidant properties. In this work, optimization physicochemical characterization, biopharmaceutical behavior and therapeutic efficacy of this novel nanostructured system were assessed.

Results: Thymol NPs (TH-NP) resulted on suitable average particle size below 200 nm with a surface charge around -28 mV and high encapsulation efficiency (80%). TH-NP released TH in a sustained manner and provide a slow-rate penetration into the hair follicle, being highly retained inside the skin. TH-NP possess a potent antimicrobial activity against *Cutibacterium acnes* and minor effect towards *Staphylococcus epidermis*, the major resident of the healthy skin microbiota. Additionally, the stability and sterility of developed NPs were maintained along storage.

Conclusion: TH-NP showed a promising and efficient alternative for the treatment of skin acne infection, avoiding antibiotic administration, reducing side effects, and preventing microbial drug resistance, without altering the healthy skin microbiota. Additionally, TH-NP enhanced TH antioxidant activity, constituting a natural, preservative-free, approach for acne treatment.

Keywords: Acne, Thymol, PLGA nanoparticles, skin delivery system, *Cutibacterium acnes*, skin microbiota, antimicrobial, antioxidant

Background

Acne is a common skin disorder, known as *acne vulgaris*, that affects a large number of the population. Several factors, such as hormones, diet, stress and environmental pollution, among others, may contribute to acne development. These factors trigger hyperactivity of sebaceous glands that produce elevated levels of sebum, hyperkeratosis by blockage of the hair follicle and, additionally, contribute to the excessive microbiota reproduction [1].

The skin is divided into three functional layers that surround the hair follicle. The base is found on the dermis-hypodermis junction, just above the fat tissue. Production of sebum occurs in the sebaceous gland, which is located inside the dermis. The upper layers of the epidermis are composed by keratinocyte cells surrounding the hair top-to-bottom. The external skin layer, stratum corneum (SC), protects the skin from the external environment, being considered the main challenge for several topical drugs penetration.

Several microorganisms reside in the skin and can be classified as resident or transient microbiota. They are normally gram-positive bacteria, not regarded as pathogens, which survive longer on intact skin than gram-negative transient species. The protective microbiota functions are believed to confer microbial antagonism activity and nutrient competition for the stability of the dermal ecosystem, preventing the adherence of pathogens and maintaining the skin health balanced [2]. *Staphylococcus epidermidis* is the most abundant colonizer of human skin and, despite considered a benign microorganism, it is highly present in acne lesions [3]. It is ubiquitously found mainly concentrated on the upper layers of the skin and may have a probiotic function by preventing colonization of pathogenic bacteria such as *Staphylococcus aureus* [4]. Concerning *Cutibacterium acnes*, previously known as *Propionibacterium acnes*, it is a resident bacteria, mainly located surrounding the hair follicle, which is likely to proliferate under unbalanced function of the sebaceous glands, leading to acne development, swelling and inflammation [5]. Hence, *C. acnes* has a dual activity on the skin microbiota, being a non-pathogen essential for sebum control, as well as an active pathogen on acne infection and inflammation. Additionally, it maintains the acidic pH of the pilosebaceous follicle by hydrolyzing sebum triglycerides and via propionic acid secretion.

Moreover, it has been previously stated that acne might be the result of an unbalanced equilibrium between *C. acnes* and *S. epidermidis* [6]. Therefore, a suitable treatment for acne should provide good antimicrobial activity but acquiring mild effect to the healthy microbiota.

Nanoparticles (NP) are a good approach to enter the hair follicle and release the antimicrobial agent directly in the acne lesion [7], [8]. The fat deposit on the subcutaneous tissue may behave as a deep compartment for the drug, delaying its entry in the blood circulation [9]. Polymeric nanospheres of poly(lactic-co-glycolic) acid (PLGA), form a matrix structure containing the entrapped active compound. PLGA, approved by the Food and Drug Administration (FDA), is known to be safe for dermal applications due to its bioavailability and biodegradable profile. One of the advantages of PLGA NPs entrapping highly volatile compounds is that their production can be performed at room temperature. Moreover, nanotechnology also has several advantages in dermal drug delivery since small particle diameters tend to penetrate into the deep skin (DS), withdraw the drug in a controlled manner and be mainly retained in the deeper layers [8], [10]. The size and flexibility of PLGA NPs enable entry into host cells via endocytosis, thus allowing intracellular release. In addition, they are easily phagocytosed by host phagocytes [11].

In this area, several clinical assays highlight the successful combination of nutraceuticals/cosmetic compounds and their encapsulation in nanostructured systems for topical acne treatment. In this area, Abd-Allah and colleagues showed successful reduction of acne inflammatory lesions with nicotinamide loaded chitosan nanoparticles [12]. Furthermore, quercetin has also been encapsulated into nanovesicles and proven to be effective both as antibacterial and anti-inflammatory [13].

Among the wide range of nutraceutical compounds, thymol (TH), is a multifunctional monoterpene of aromatic phenolic structure, with a volatile compound with a strong and characteristic odor. It can be found naturally occurring in plant extracts or on its white crystalline synthetic form. It is found in *Lamiaceae* plant species, especially oreganos and thymes, which present antimicrobial, antioxidant and antiseptic properties [14]–[17]. It is considered safe in cosmetic formulations up to 0.5 %, according to the Cosmetic Ingredients Review (CIR) and it is used as preservative in cosmetics and foods [18]. Moreover, TH antioxidant and antimicrobial properties allow cosmetic

products to avoid the use of other chemical compounds as preservatives. The effects of TH are largely attributed to its antioxidant properties, via free radical scavenging thus enhancing endogenous antioxidant activities and chelation of metal ions [19]. The antioxidant activity provides an interesting therapeutic approach to restore skin homeostasis, maintaining its internal conditions relatively constant and stable, modulates the stratum corneum SC barrier function and prevents skin irritation [20].

Bacterial survival depends on membrane lipid homeostasis and the ability to adjust the lipid composition of bacterial cells in different environments. There are biochemical processes that underlie adjustments and are responsible for membrane phospholipid homeostasis in bacteria, controlling the movement of substances across the cell membrane [21]. These processes depend on proteins embedded in a lipid matrix that closely approximates a phospholipid bilayer.

The hydrophobic nature of TH facilitates its interaction with the lipidic bacterial membrane via direct binding with biomolecules, such as proteins, providing strong antimicrobial effect by altering its morphology and leading to bacterial death [22], [23]. Disruption of bacterial membrane will lead to cell disfunction and apoptosis, resulting in loss of intracellular contents. Some authors suggested that TH antibacterial action is due to the increased permeability of bacterial cell membranes [24]. However, other studies suggest that TH is responsible for the inactivation of enzymes implicated in synthesis of structural constituents [14]. The extent of bacteria membrane damage induced by a compound could be related to its intrinsic hydrophobicity. In the other hand, the slight hydrophilicity could enhance diffusion through the extracellular polysaccharide matrix and cause destabilization of bacterial biofilms [16].

With the aim to increase and prolong skin penetration into the hair follicle, without affecting the entire microbiota, PLGA NP containing TH (TH-NP) have been developed and optimized using the design of experiments (DoE) approach. Physicochemical characterization and biopharmaceutical behavior of optimized TH-NPs have been determined. Cytotoxicity, cellular uptake and antioxidant activity of TH-NP have also been assessed in human keratinocytes cell-line (HaCaT). In addition, antimicrobial therapeutic efficacy of this colloidal system was evaluated *in vitro* and *ex vivo*.

Results

Formulation characterization and optimization

The optimization of TH-NP was obtained by developing a full composite factorial design of five levels and three factors. Studied independent variables were the amount of TW and TH as well as pH formulation. The latter was chosen due both to Thymol pKa (pKa 10.6) which, as previously reported in other studies, can influence in the EE [25], [26].

The results of the DoE physicochemical characterization and the entrapment efficiency of TH-NPs are shown in Table 1. The average particle size (*Zav)* values ranged from 162 to 235 nm, being the polydispersity index (PI) comprised between 0.06 and 0.12. Based on the criteria for monodispersed systems (PI < 0.1), all the formulations presented homogeneity [27]. The surface charge of TH-NP, measured as Z-potential (ZP), ranged from -22 to -31 mV. This negative ZP is associated with negative surface charge associated with PLGA, the main NPs compound [25], [28], [29], [30]. Moreover, ZP is related to the stability of colloidal dispersions, for this reason, the developed formulations with values closest to -30 mV, were considered the most stable. The encapsulation efficiency (EE) of designed formulations ranged from 71 to 83 %.

Table 1. Values of the 2^3 + star central composite factorial design, parameters, and responses

Independent Variables				Dependent Variables/Responses			
	TH	**TW**	**pH**	**Z_{av}** (nm)	**PI**	**ZP** (mV)	**EE** (%)
Factorial Points							
F1	-1	-1	-1	217.9 ± 1.2	0.112 ± 0.001	-30.7 ± 0.9	76.35 ± 1.53
F2	1	-1	-1	234.9 ± 2.1	0.093 ± 0.004	-29.9 ± 0.4	79.16 ± 0.18
F3	-1	1	-1	176.2 ± 1.0	0.075 ± 0.023	-27.7 ± 1.3	76.67 ± 2.17
F4	**1**	**1**	**-1**	**174.0 ± 0.6**	**0.081 ± 0.012**	**-28.3 ± 0.8**	**80.07 ± 3.65**
F5	-1	-1	1	162.0 ± 0.4	0.072 ± 0.011	-26.2 ± 0.3	79.64 ± 3.79
F6	1	-1	1	163.5 ± 1.4	0.071 ± 0.009	-23.6 ± 0.5	73.52 ± 1.83
F7	-1	1	1	183.9 ± 0.4	0.087 ± 0.020	-29.5 ± 0.1	78.41 ± 2.51

F8	1	1	1	172.4 ± 1.1	0.094 ± 0.009	-26.6 ± 0.3	76.60 ± 5.60
Axial Points							
F9	*1.68*	*0*	0	174.2 ± 0.6	0.061 ± 0.018	-25.2 ± 0.4	77.01 ± 3.07
F10	*-1.68*	*0*	0	176.7 ± 1.1	0.083 ± 0.033	-23.6 ± 0.3	73.55 ± 2.93
F11	*0*	*1.68*	0	187.1 ± 0.8	0.024 ± 0.006	-23.1 ± 0.6	71.38 ± 0.62
F12	*0*	*-1.68*	0	167.4 ± 2.1	0.046 ± 0.021	-26.1 ± 0.4	76.92 ± 2.47
F13	*0*	*0*	1.68	164.6 ± 1.1	0.057 ± 0.010	-23.1 ± 0.8	72.44 ± 1.66
F14	*0*	*0*	-1.68	202.6 ± 3.5	0.063 ± 0.045	-22.5 ± 1.1	82.89 ± 6.01
Central Points							
F15	0	0	0	175.4 ± 2.1	0.053 ± 0.013	-24.5 ± 0.6	74.94 ± 1.77
F16	0	0	0	176.3 ± 1.9	0.072 ± 0.016	-25.3 ± 0.7	78.14 ± 0.49

Surface response charts of the DoE, performed by Statgraphics® software, are shown in Figure 1. The statistical analysis (ANOVA) only presented significant differences for the particle size ($p < 0.01$), influenced by both, pH of the aqueous phase and ratio of surfactant/pH (Figure 1A). The responses at a fixed TH concentration (2.5 mg/mL) are illustrated for *Zav*, ZP and EE (Figure 1B, 1C, 1D), respectively. Results show that the highest EE was achieved at the lowest pH, while for ZP, the absolute high values were reached when the pH and surfactant were simultaneously low or high. Considering all the evaluated parameters, formulation F4, containing 0.25 % of TH and 0.4 % tween 20 (TW) has been optimized to carry out further experiments.

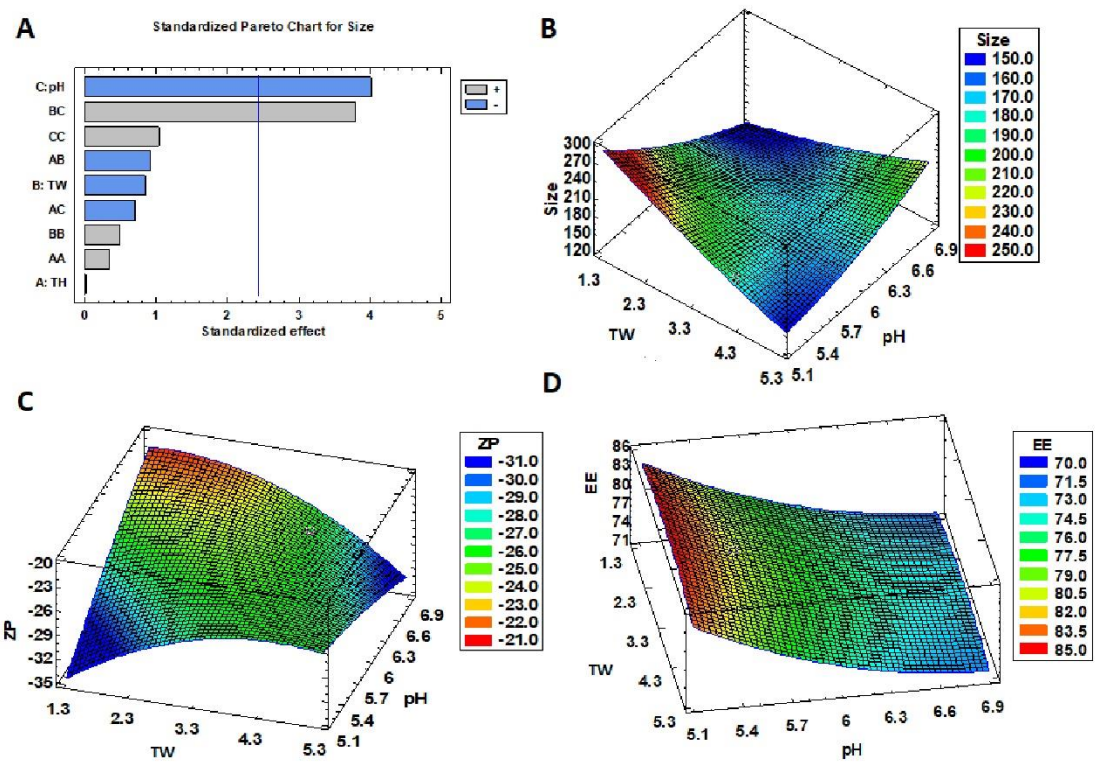

Figure 1. Factorial design with TH-NP fixed at 2.5 mg/mL TH: **(A)** Pareto's chart for particle size (ANOVA) and surface response for **(B)** Z*av* particle size (nm), **(C)** ZP (mV) and (D) EE (%).

Morphology and stability of TH-NP

The morphology of TH-NP was evaluated by transmission electron microscopy (TEM) and it is shown in Figure 2A. Moreover, TH-NP maintained their structure for 1 month at 4 and 25 °C and additionally, for 12 months at 4 °C (Figure 1 of SM). A small particle aggregation takes place after 12 months, which was confirmed by a slightly increased particle size, as indicated in Table 2.

This slight aggregation is also related with the decrease of ZP, since electrostatic forces between surface-charged NPs decrease when stored in aqueous media. Temperature showed to accelerate particle destabilization by decreased ZP. A slight decrease of the pH value was also observed, probably due to a partial hydrolysis of the polymer.

Table 2: Physicochemical stability of TH-NP stored at different temperatures (4, 25 and 37 ºC) measured at 0, 1, 3, 6 and 12 months.

	t (months)	Z_{av} (nm)	PI	ZP (mV)	pH
4 °C	**0**	**158.8 ± 1.7**	**0.068 ± 0.027**	**-24.7 ± 1.0**	**4.20**
	1	158.6 ± 1.8	0.108 ± 0.046	-20.1 ± 0.6	4.07
	3	159.0 ± 2.1	0.101 ± 0.034	-17.1 ± 0.1	3.90
	6	168.6 ± 1.7	0.152 ± 0.033	-15.3 ± 0.1	3.68
	12	204.5 ± 1.3	0.231 ± 0.015	-11.1 ± 0.7	3.61
25 °C	1	162.3 ± 0.4	0.119 ± 0.015	-19.1 ± 0.1	3.91
	3	182.3 ± 1.4	0.145 ± 0.020	-10.3 ± 0.2	3.64
37 °C	1	177.4 ± 1.2	0.128 ± 0.012	-15.3 ± 0.6	3.32
	3	216.4 ± 2.8	0.205 ± 0.001	-8.56 ± 0.3	2.95

All these phenomena are in accordance with the predicted backscattering profile shown in Figure 2 of SM, where TH-NP sedimentation was observed by the first left peak at the bottom of the vial, being reversible by agitation. Moreover, it can be observed that at 37 °C the signal greatly decreases, presenting TH-NP destabilization at higher temperatures. Additionally, EE was maintained at 4 and 25 °C for 6 months, whereas at 37 °C, decreased by 2.5-fold from the initial value. The parameters of all storage conditions were within stable criteria, presenting better short-term stability when stored at 4 °C. Moreover, samples presented no microbial growth within storage, confirming the preservative effect of TH.

Interaction studies

The interactions between TH and PLGA, carried out by differential scanning calorimetry (DSC) and X-ray diffraction (XRD), are shown in Figure 2. DSC thermograms of TH showed an endothermic peak at 52 °C, which corresponds to its melting transition (Figure 2**B**). A minimal displacement of endotherm was presented by polymer alone and blank NPs (B-NP). However, TH-NP presented an onset peak displaced at 40 °C, due to TH-PLGA interaction. The XRD diffractograms (Figure 2C) show TH on its crystalline form, expressed by the sharp diffraction peaks. TH-NP could be

observed as non-sharp peaks, confirming that TH was dispersed in the polymer matrix in its amorphous form (molecular dispersion) and also showing a similar profile to B-NP.

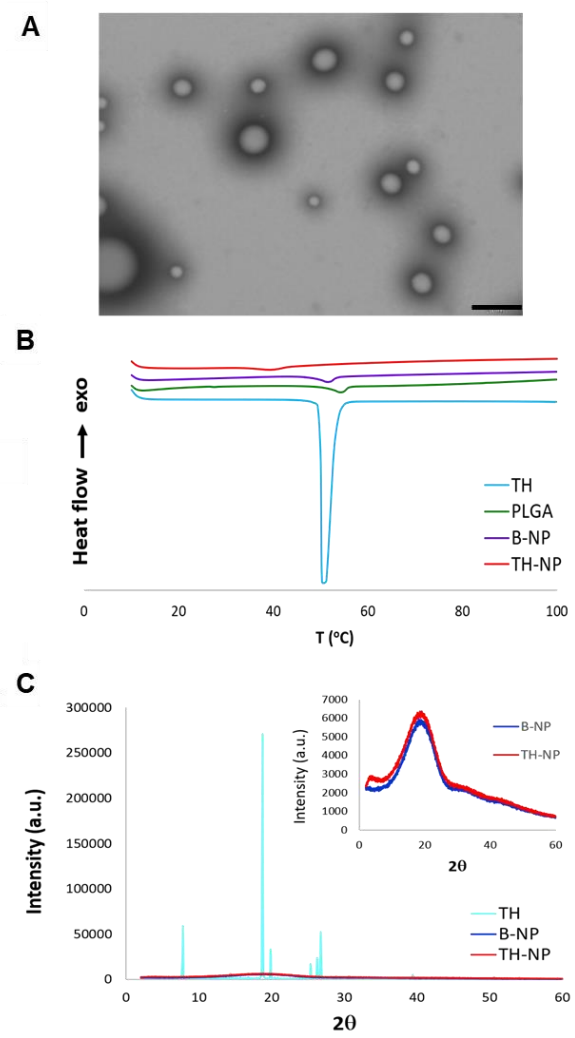

Figure 2. **(A)** Transmission electron microscopy image of TH-NP. Scale bar: 200 nm, **(B)** DSC thermograms of TH-NP, B-NP, and compounds separately, **(C)** X-ray diffraction patterns of TH-NP, B-NP, and compounds separately.

In vitro drug release

The *in vitro* release profile of TH from TH-NP against free TH, carried out in Franz diffusion cells, is shown in Figure 3A. As can be observed, the release of free TH through the dialysis membrane was faster, while TH-NP provided a slow-rate prolonged release. Kinetic data was adjusted to

Boltzmann Sigmoidal equation showing that TH reached 50 % (V50) of total amount released within a short period of time (1.5 h), while TH-NP only achieved the same within 23 h. The total amount of TH released in 24 h was 55 % and 35 % for TH and TH-NP, respectively, presenting statistically significant differences ($p < 0.01$).

Ex vivo skin permeation

The *ex vivo* skin permeation of TH and TH-NP were performed in healthy skin and, additionally, in damaged skin, where the SC was previously scratched to mimic skin barrier disorders. The corresponding kinetics of both skin types are shown in Table 3. The permeation flux (*J*) of TH and TH-NP were increased by 2.1 and 2.6-fold, respectively, on damaged compared to healthy skin, where all samples presented significant statistical differences ($p < 0.001$) between them. In both cases, damaged and healthy skins, TH presented significantly ($p < 0.001$) faster penetration rate compared to TH-NP, increased by 1.6 and 1.3-fold, respectively. The total amount penetrated (*Ap*) was significantly higher ($p < 0.001$) in damaged skin. In the other hand, the total amount retained inside the skin (*As*) was similar for both samples comparing healthy to damaged skins and there were significant differences ($p < 0.001$) comparing TH-NP with TH.

Table 3. *Ex vivo* skin permeation parameters

	Healthy Skin		Damaged Skin	
	TH	**TH-NP**	**TH**	**TH-NP**
J (μg/cm²/h)	12.68 ± 1.73	8.03 ± 0.55 *a*	26.43 ± 2.13 *a b d*	21.03 ± 0.92 *a b*
Kp (cm/h)	5.07E-03 ± 6.91E-03	3.21E-03 ± 2.19E-04 *a*	1.06E-02 ± 3.51E-04 *a b d*	8.41E-03 ± 3.69E-04 *a b*
Ap (μg/cm²)	106.43 ± 9.96	96.39 ± 12.68	272.36 ± 14.02 *a b d*	202.58 ± 11.65 *a b*
As (μg/cm²)	6.19 ± 1.45	10.85 ± 1.12 *a c*	5.92 ± 0.92	10.83 ± 2.13 *a c*
At (μg/cm²)	**112.61 ± 11.41**	**107.24 ± 13.80**	**278.28 ± 14.93 *a b d***	**213.78 ± 13.78 *a b***
SSD (p < 0.01)	*a*	*b*	*c*	*d*

J: flux, Kp: permeability constant, Ap: total amount penetrated, As: total amount retained inside the skin, At: total amount penetrated and retained inside the skin

The total amount of thymol penetrated within 24 h (Figure 3B), was split into stratum corneum (SC) and deep skin (DS). The amount found in the SC was the same for TH on both skin types and

similarly to TH-NP on damaged skin. However, for TH-NP, the retained amount was significantly higher ($p < 0.01$) on normal skin, in agreement with the slow-rate penetration, presenting delayed entry of the particles. In the other hand, it can be observed that TH-NP presented significantly ($p < 0.001$) higher amounts retained in DS on both skin types, compared to TH. Meanwhile, TH-NP on damaged skin was significantly higher than normal skin ($p < 0.01$).

Ex vivo skin permeation route was studied by confocal microscopy using rhodamine-labelled TH-NP (R-TH-NP) after 24 h of permeation (Figure 3C). The results obtained showed that R-TH-NP successfully penetrated inside the skin hair follicle, where acne pathogen infection and inflammation occur. The image (Figure 3C_II) illustrates that R-TH-NP were found concentrated in the hair follicle and presented delayed entry accumulation in the SC.

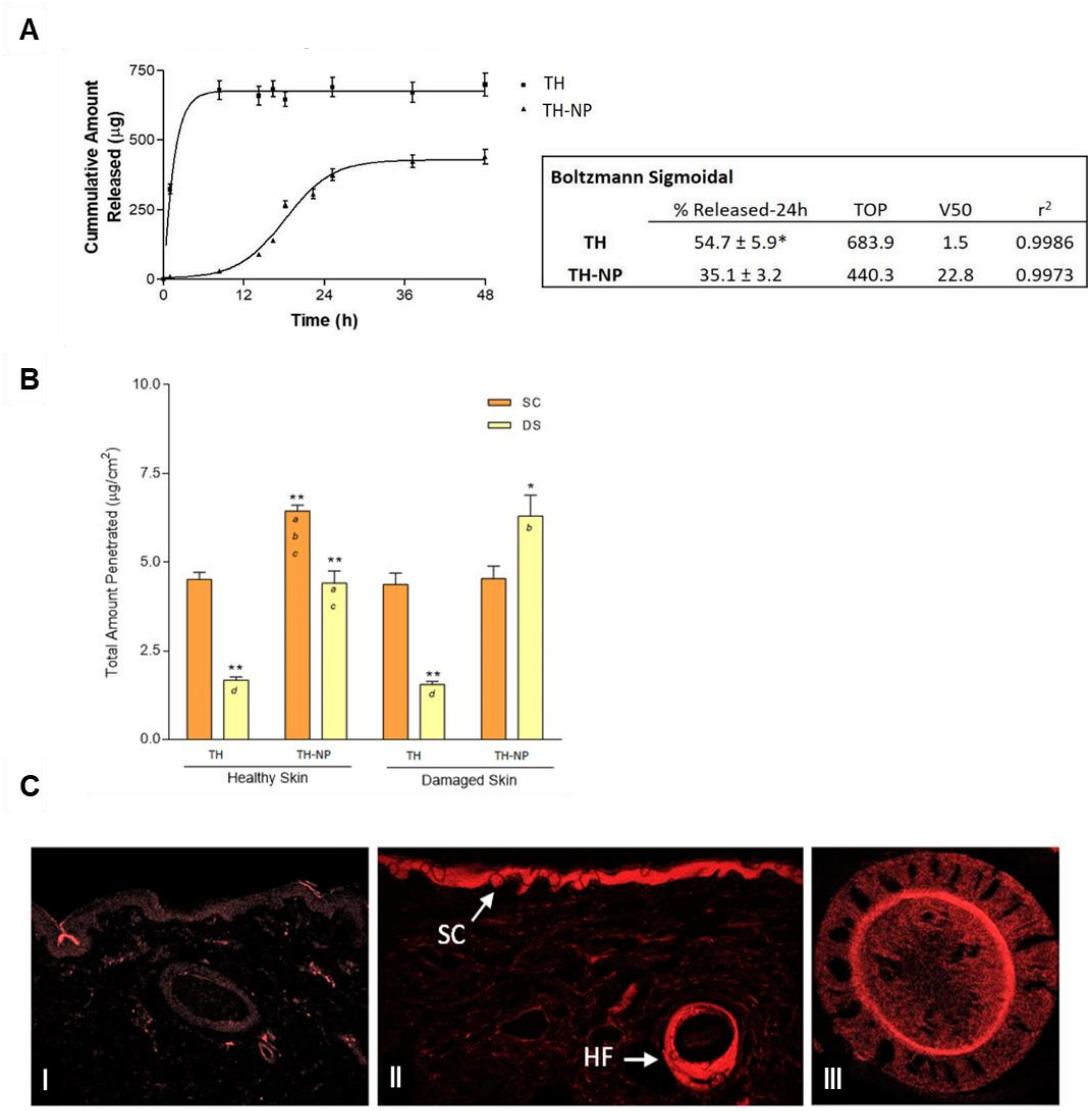

Boltzmann Sigmoidal

	% Released-24h	TOP	V50	r^2
TH	54.7 ± 5.9*	683.9	1.5	0.9986
TH-NP	35.1 ± 3.2	440.3	22.8	0.9973

Figure 3. (A) Release profile of TH and TH-NP adjusted to Boltzmann Sigmoidal equation. Total amount released in 24 h expressed as % Mean ± SD (n = 3). Statistical analysis one-way ANOVA t-student test *p < 0.01, **(B)** Total amount of TH and TH-NP penetrated in 24 hours in healthy and damage skin. SC: stratum corneum (tape stripping), DS: deep skin (extraction). Values represent the Mean ± SD (n=3). Statistical analysis for each localization via one-way ANOVA Tukey´s Multiple Comparison Test. Different letters inside the bars indicates significant differences between groups (*p < 0.01 and **p < 0.001), **(C)** Confocal microscopy images of pig skin R-TH-NP penetration after 24 h: (I) untreated skin control, (II) SC and hair follicle, (III) hair follicle cross-section.

Cytotoxicity in HaCaT cells

The cytotoxicity of TH-NP was evaluated on HaCaT cells, incubated for 24 h with concentrations up to 1 mg/mL (Figure 4A). Results showed that TH-NP was not cytotoxic at concentrations up to 50 µg/mL, as cell viability was kept close to the untreated control cells. A 20 % reduction in cell viability was observed at 100 µg/mL and close to 90 % reduction at concentrations ≥ 250 µg/mL. Different results were obtained with washed nanoparticles (TH-NP-w), which were not cytotoxic at 100 µg/mL and caused only a 25 % reduction in cell viability at 250 µg/mL. Differences between TH-NP and TH-NP-w indicate that the presence of free TW in the samples could cause toxicity to HaCaT cells.

Cellular uptake of TH-NP

The cellular uptake of R-TH-NP (20 µg/mL) was analyzed in HaCaT cells. At this nanoparticle concentration, cell viability was over 90 %. After 2 hours incubation, fluorescence was detected by confocal microscopy in cells treated with R-TH-NP but not in untreated control cells (Figure 4B). The cell membrane and the nucleus are represented as green and blue, respectively. In the merged images, it can be observed that the internalized nanoparticles were mainly localized in the cytoplasm.

In vitro antioxidant efficacy in HaCaT cells

The antioxidant activity of TH and TH-NP, performed in HaCaT cells, was successfully achieved by reducing the amount of reactive oxygen species (ROS) generated. While B-NP did not present activity, TH and TH-NP showed a 20 % and 32 % of ROS reduction, respectively, within 2 h treated with H_2O_2 (Figure 4C). Moreover, TH-NP was statistically significant compared to TH.

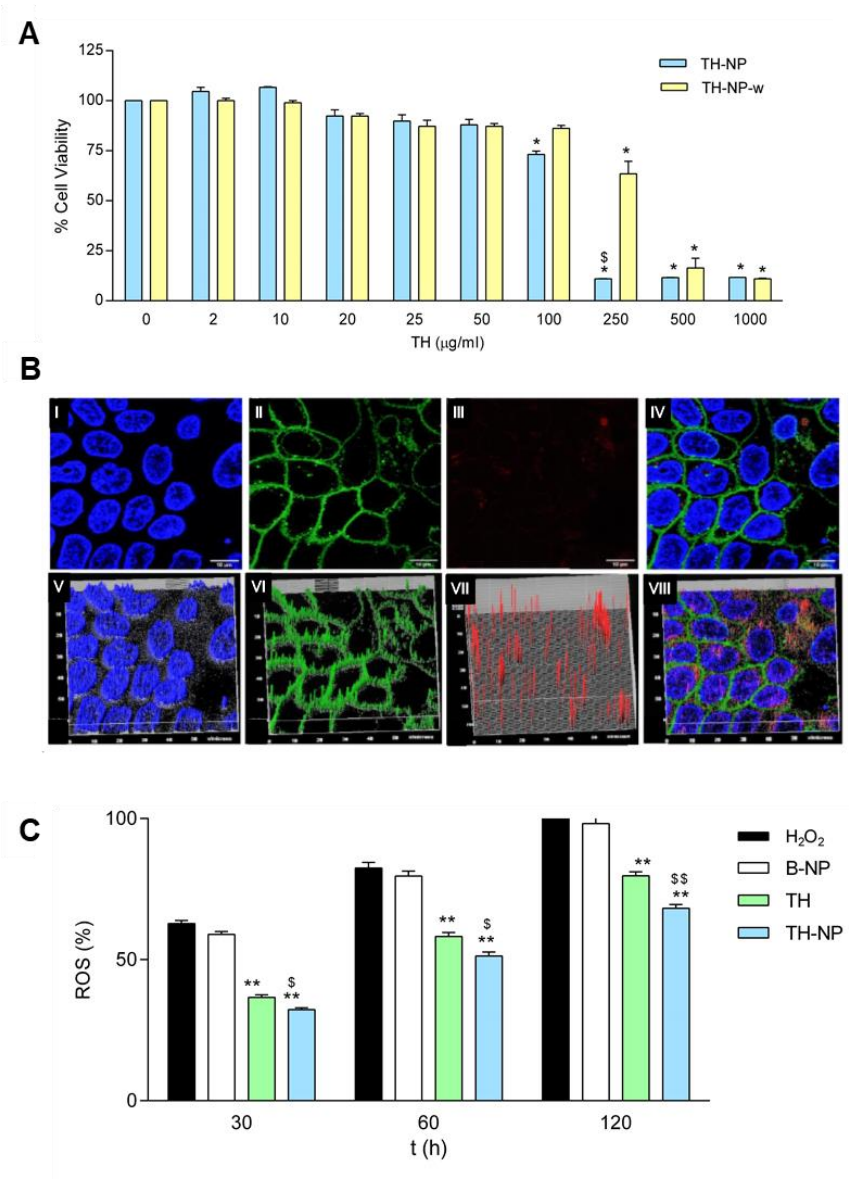

Figure 4. (A) Cell viability of HaCaT keratinocytes after incubation for 24 h with TH-NP and the washed NPs (TH-NP-w) at different concentrations. Cell viability was assayed by the MTT reduction method; 100 % viability was set with the values obtained with the untreated control cells. Values represent the Mean ± SD (n = 3). Statistical analysis one-way ANOVA Tukey 's Multiple Comparison Test, *$p < 0.01$ versus control and $^{\$}p < 0.01$ versus TH-NP-w, **(B)** Confocal microscopy analysis of HaCaT cells incubated with R-TH-NP: (I) nuclei; (II) membranes; (III) R-TH-NP; (IV) merged (I), (II), and (III), respectively; (V-VIII-h) 3D-plot of (I)-(IV), respectively, **(C)** Time course analysis of ROS production induced by H_2O_2 (2 mM) in HaCaT cells treated with TH or TH-NP. The ROS production (100 %) was set with the values obtained with cells challenged with H_2O_2 for 2 h.

Data were expressed (%) as the Mean ± SD (n = 8). Statistical analysis was performed by one-way ANOVA Tukey's Multiple Comparison Test, **$p < 0.001$ versus controls at 2 h; $^{\$}p < 0.05$ and $^{\$\$}p < 0.001$ between TH and TH-NP treated cells

In vitro antimicrobial efficacy

The minimal inhibitory concentration (MIC) was determined for TH and TH-NP on *S. epidermidis* being both 512 µg/mL. For *C. acnes,* TH and TH-NP displayed the same MIC and minimal bactericidal concentration (MBC) values, being 250 µg/mL and 400 µg/mL, respectively. Therefore, no differences were observed in the concentrations between samples. However, there were relevant differences between different bacterial strains. In the other hand, clindamycin, a strong antibiotic commonly used to treat severe acne, presented MIC < 2 µg/mL for both microorganisms. For this reason, clindamycin is able to treat acne. However, it also affects the healthy resident bacteria of the skin.

The bacterial viability reduction, evaluated by determination of decimal reduction time (D), treated with TH or TH-NP in a timely manner, is illustrated in Figure 5A. In the case of *C. acnes,* the decrease of viable bacteria correlated with the applied dose. Although the effect of TH and TH-NP were similar, the activity of TH-NP was slightly sustained at lower dosages. At the MIC concentrations, they present minimal reduction activity, whereas, at concentrations higher than MBC, the reduction was boosted for all tested samples. Meanwhile, *S. epidermidis* presented very slow viability reduction when incubated with TH and TH-NP at twice the MIC (Figure 5B), the same highest concentration tested for *C. acnes*. It can be observed that TH completely reduced *S. epidermidis* viability within 8 h, whereas TH-NP treated cultures still presented living colonies within 24 h.

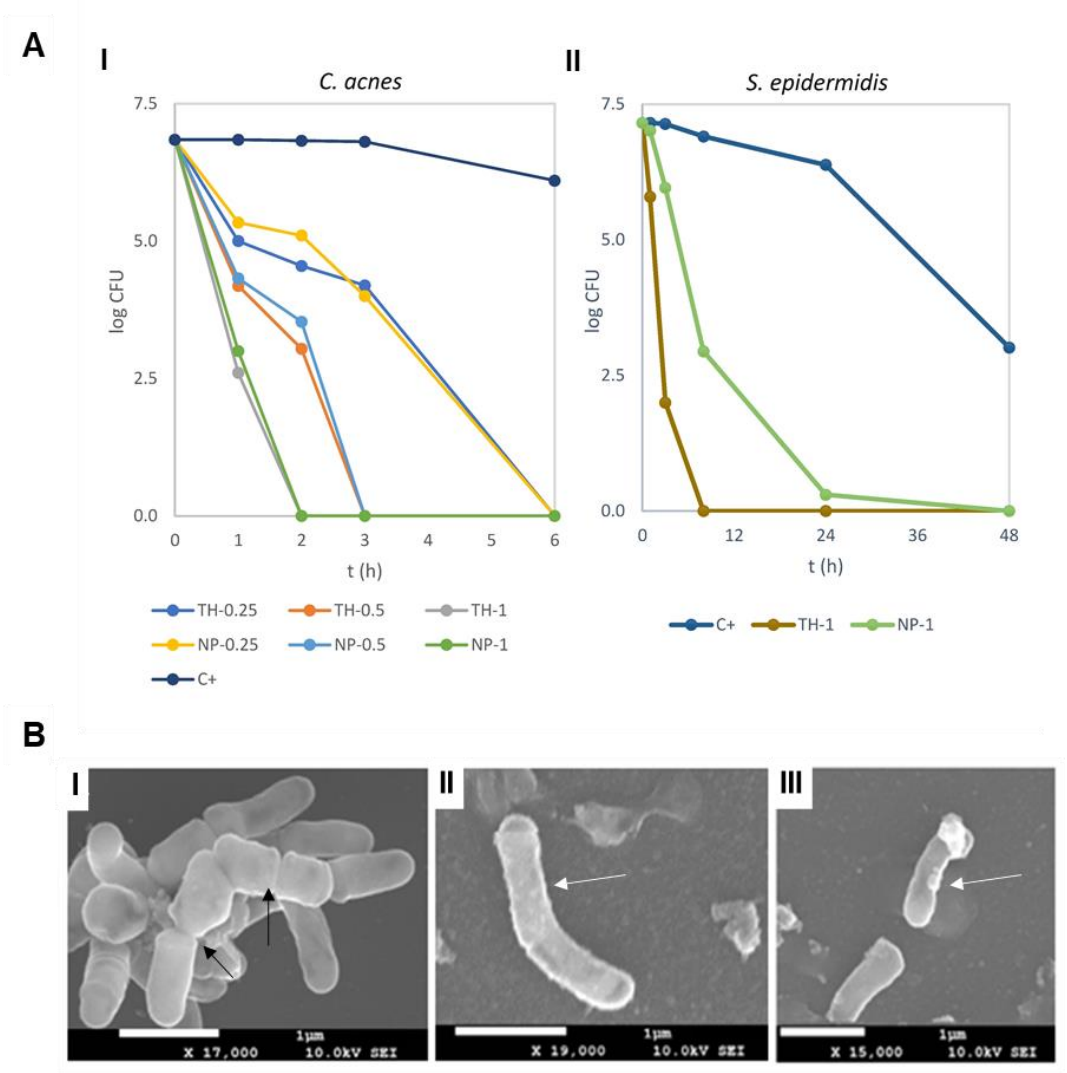

307

308 **Figure 5. (A)** Bacterial viability reduction of (I) *C. acnes* 6 hours contact with TH or TH-NP (dose
309 dependent) at 0.25, 0.5 and 1 mg/ml, (II) *S. epidermidis* 48 hours contact with THF or TH-NP at 1
310 mg/ml. Data is expressed as $\log_{10}$CFU of mean values, **(B)** SEM micrographs of *C. acnes* (I) control
311 and treated for 1 hour with (II) TH or (III) TH-NP. Black arrows indicate bacteria division and white
312 arrows membrane disruption.

313

314 Data of decimal reduction time (D), the time taken to reduce a decimal part of the of bacterial
315 viability, is shown in Table 4. In the case of *C. acnes,* differences could be observed comparing the
316 variable dosages applied. However, variations between TH and TH-NP were not detected. In the

case of *S. epidermidis*, TH-NP presented statistically significant differences compared to TH. Moreover, comparing the activity between both microorganisms, at the same dosage, only TH-NP presented statistically significant differences for *S. epidermidis* against *C. acnes*.

Table 4. Decimal reduction time(D) for *C. acnes* and *S. epidermidis* viability

	TH (mg/mL)			**TH-NP** (mg/mL)		
	0.25	**0.50**	**1.00**	**0.25**	**0.50**	**1.00**
C. acnes						
r^2	0.9654	0.9743	0.9812	0.9964	0.9984	0.9949
k (logCFU/h)	1.00 ± 0.11	2.03 ± 0.19	3.48 ± 0.08	1.02 ± 0.12	1.96 ± 0.43	3.44 ± 0.03
D (min)	**60.5 ± 6.5**	**29.6 ± 2.7**	**17.3 ± 0.4**	**59.0 ± 7.0**	**31.4 ± 6.9**	**17.4 ± 0.1**
S. epidermidis						
r^2			0.9944			0.9886
k (logCFU/h)			1.75 ± 0.02			0.54 ± 0.01
D (min)			**34.2 ± 0.4**			**111.1 ± 2.9*$**

*CFU: colony forming units. One-way ANOVA (t test): statistically significant differences *p > 0.001 versus TH, $p > 0.0001 against C. acnes, same dosages.*

Moreover, the structure of *C. acnes* (Figure 5B), evaluated by scanning electron microscopy (SEM), presents a rod-shape and smooth membrane. Treatment with TH or TH-NP resulted on elongated cells, thickened cell envelope, and blebs formed on the surface.

Ex vivo antimicrobial efficacy

The *ex vivo* antimicrobial efficacy of TH and TH-NP on *C. acnes* skin inoculated, as prevention or treatment for 24 h, were successfully determined. In both studies, all samples presented significant differences against the control (**p < 0.001). The activity was found greater as prevention than treatment (Figure 6A), where TH-NP presented higher activity than TH, but no statistically significant differences were observed. In the other hand, for the dose-dependent treatment (Figure 6B), administration of a single dose showed significant differences between TH and TH-NP ($^{\#}p < 0.05$).

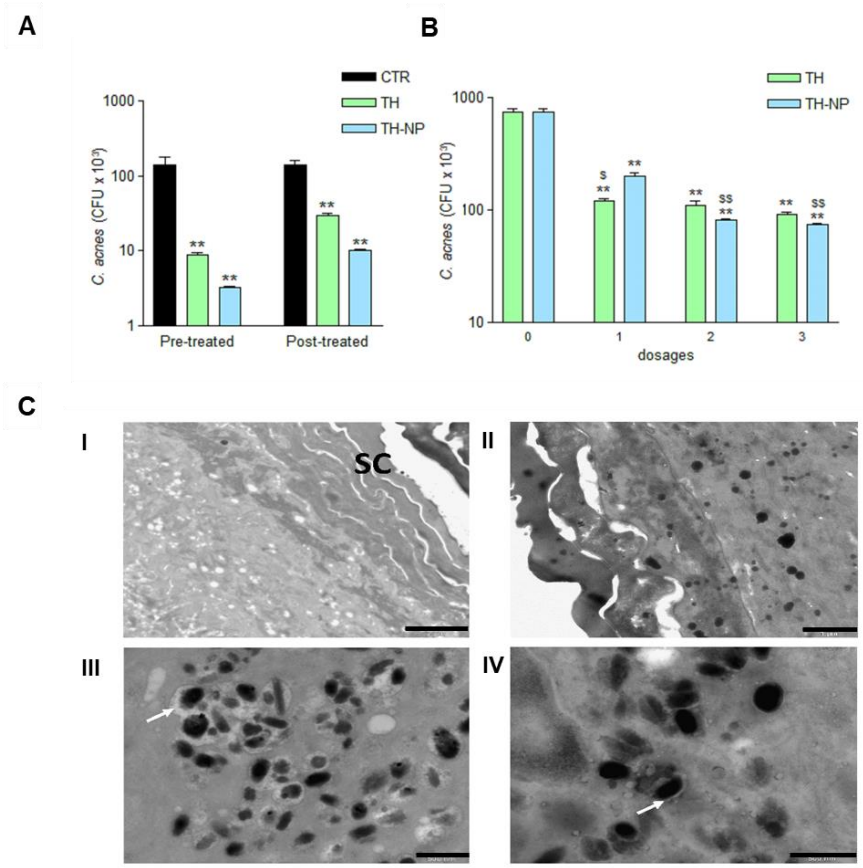

Figure 6. **(A)** Bacterial viability on *ex vivo* treated skin with TH or TH-NP prevention, **(B)** Bacterial viability on *ex vivo* treated skin with TH or TH-NP dose-dependent treatment with 3 applied doses at times 0, 12 and 18 h of incubation. Values represent viable count of *C. acnes* as the Mean ± SD (n=3), (**C)** TEM images of normal human *ex vivo* skin: (I) untreated, (II) inoculated with *C. acnes (black)*, treated with (III) TH and (IV) TH-NP. White arrows indicate the loss of bacterial intracellular material. Scale bars: 2 µm (I), 1 µm (II) and 500 nm (III and IV). Statistical analysis one-way ANOVA Tukey's Multiple Comparison Test represent **$p < 0.001$ compared to control and $^{\$}p < 0.01$ / $^{\$\$}p < 0.001$ comparing TH and TH-NP.

Although TH-NP had lower effectiveness within one dose, they performed greater activity than TH when 2 or 3 doses were applied ($^{\$\$}p < 0.001$). Meanwhile, TH did not show statistical differences comparing the 3 dosage protocols. Moreover, the highest efficiency of the experiment was achieved by 3 doses of TH-NP.

The simulation of skin infection and treatment was carried out on *ex vivo* fresh human skin explants, by inoculating *C. acnes* for 16 h, followed by 8 h treatment with TH or TH-NP. Figure 6C illustrates the untreated skin and the *C. acnes* inoculated and penetrated within the skin layers. The treatment with TH demonstrated a fast and strong activity towards the bacteria membrane, presenting surrounding it, a great loss of intercellular material which may indicate damaged membrane. In the case of TH-NP, a slower effect with less amount of cellular leakage could be observed. The minor effects of TH-NP within 8 h of treatment might be related to the slow-rate release and penetration.

Discussion

In the present study, TH was successfully loaded into PLGA NP. Developed TH-NP presented suitable physicochemical parameters with excellent stability and high EE. DoE analysis showed that Pareto's diagram and surface responses indicated that only the pH of the aqueous phase and the ratio of pH/TW induced statistically significant differences on Z_{av}, being the effect of these variables not significant on the EE. The surfactant usually shows statistically significant influence on the EE and morphometry of polymeric NP, depending on the amount applied [27]. TW has good permeability profile and its amphiphilic properties may control the interactions between the active compound and the biopolymer carrier [31]. Interaction studies showed that encapsulated TH was present on its amorphous form and the thermal transition was affected by TH-polymer interactions [32]. Analyzing the stability of TH-NP for the first 3 months, an increase of particle size and a decrease in ZP, depending on the storage temperature, were observed. The decrease of ZP induced TH-NP instability in aqueous medium, due to a decrease of electrostatic forces between surface-charged NP, generating in some cases, a slight particle aggregation. Moreover, TH-NP at high temperature, presented sedimentation that was reversed by agitation, as also observed by other authors [33]. TH-NP stored at 4 °C have shown outstanding short-term stability in aqueous solution. However, in order to extend TH-NP stability, either incorporation in a semi-solid formulation or freeze-drying are recommended [27], [34]. In addition, it has been shown that TH-

NP did not present microbial contamination along storage, confirming TH antimicrobial preservative activity.

Biopharmaceutical behavior of TH-NP presented a sustained *in vitro* release profile, while TH reached the steady state very fast. The *ex vivo* skin rate of TH was higher than TH-NP by 1.6 and 1.3-fold, respectively, being faster on damaged than healthy skin. As previously described [35], these results confirm that the external hydrophobic skin surface was altered, thus enabling substances to penetrate faster and easier through this barrier. The enhanced penetration of TH and TH-NP through the skin may be due to TH properties as well as the TW properties. On the one hand, TH is a terpene and these kind of compounds are known to be skin penetration enhancers, by impairing the lipids of the SC [36]. On the other hand, TW, an anionic surfactant, also provide enhanced permeability through phospholipid membranes, inducing some damage to epidermal membranes which decrease skin resistance towards the diffusion of the active. Some authors also explained that the mechanisms of TW could be attributed to an improvement of the thermodynamic activity adsorption and fusion due to micellar complexation, or decreasing the SC hindrance or modification of its intracellular lipid barriers [37]. The amount of TH retained inside the skin was higher for TH-NP in both (healthy and damaged) skin types. The only difference between healthy and damaged skins was the highest amount in the SC and DS, respectively. The lesser amount of free TH against TH-NP retained inside the skin was probably due to its fast-rate penetration. In agreement with TH-NP slow-rate penetration, confocal microscopy study confirmed that TH-NP presented delayed entry, accumulating into the layers of the SC. This means that when the SC was disrupted, the flux of NPs penetration improved, and therefore, the amount inside the deeper layers of the epidermis and dermis increased. Interestingly, TH-NP skin penetration route was through the hair follicle, exactly where acne occurs. According to previous authors [38], the physicochemical properties of the active compound as well as the barrier properties of the hair follicles define the penetration route (intrafollicular or transfollicular). Polymeric NPs preferentially accumulate in the follicular entry, in a time dependent manner, where the skin penetration through the hair follicle is size dependent [8]. In this way, particles with average diameter of 200 nm are likely to penetrate faster than micro-sized particles or free molecules. Therefore, the smaller the particle size, the

higher would be the accumulation into the hair follicle, and thus achieving lower permeability rates [8],[38]. Studies carried out by Yukuyama et al. [39], indicated that NP stored in the hair follicle will be cleared by hair growth or sebum production. Zhu et al.[40], developed PLGA TH microparticles as antimicrobial agents for food preservative application, containing particle size ranging for 20 to 70 µm. Due to the fact of the particle size selectivity for follicle entry, our developed TH-NP would be more efficient for penetrating the hair follicle to treat acne. Furthermore, other authors stated that the reservoir of the hair follicle could store actives 10 times longer than the reservoir of the SC, and also, that hair follicle under movement (*in vivo*) would improve NP penetration [38], [39]. Recent studies confirmed that diffusion of polymeric NPs only crossed the SC reaching the viable epidermis only after needle puncture [38]. This could be also observed, by confocal microscopy in healthy skin, where TH-NP were not found beyond the SC, unless inside the hair follicle. For all these reasons, TH-NP are more efficient for acne treatment due to the prolonged penetration and release inside the hair follicle.

In the HaCaT cell line, TH-NP at low concentrations did not alter cell viability, presenting no cytotoxicity. The cellular uptake images showed most of the NPs in the cytosol but also some particles reached the nucleus within only 2 h. This would enable TH-NP to perform its antioxidant activity inside the cells to improve the skin healing process on acne lesions [20]. This activity was confirmed by reducing the ROS generated, since TH-NP improved significantly compared to TH. Moreover, prolonged release of TH as well as increased stability of TH-NP may also favor enhanced antioxidant activity.

The antimicrobial activity of TH and TH-NP against *C. acnes* was similar and successfully demonstrated *in vitro* and *ex vivo*. The *in vitro* activity increased with high concentrations of TH-NP, and they presented the decimal reduction of bacterial viability within 60, 30 and 17 minutes, for MIC, 2x MIC and 4x MIC, respectively, confirming dose-dependent activity. Additionally, the concentrations used above MBC completely reduced all CFU very fast. For the *ex vivo* experiments, simulating an acne infection inside the skin explant, samples resulted more efficient for prevention than treatment, despite, no significant differences between samples could be observed. This can be explained by the fact that part of the amount of the formulations applied

were retained on the SC, and therefore, products had a direct contact with *C. acnes* when this was inoculated onto the skin. Meanwhile TH penetrates faster throughout the skin, providing only an immediate effect. For TH-NP, the effectiveness was higher when multiple dosages were applied onto the skin providing a slightly sustained effect. These results are in accordance with those observed in the biopharmaceutical studies. The same behavior was observed by electron microscopy in the *ex vivo* images, where the effect of TH on the bacterial membrane was found stronger than TH-NP, for 8 h contact inside the skin. For this reason, it could predictably act in the same way on skin microbiota and therefore, TH-NP would constitute a less aggressive and more efficient system for such treatment. The *in vitro* SEM images showed modified cells, with greater wall thickness and the development of blebs [41]. This observation agrees with the previously mentioned mechanism of antimicrobial activity, by triggering loss of intercellular nutrients.

Concerning *S. epidermidis,* a more resistant type of microorganism, it presented very slow viability reduction in contact with TH and TH-NP, compared to *C. acnes*, even tested at the highest concentration. Growth was abolished within 8 h for TH, while for TH-NP this effect was observed over 24 h. Therefore, if these NP were administered *in vivo* for acne skin treatment, at the same concentrations, it would be less effective towards the entire skin microbiota, being at the same time a strong bactericidal against *C. acnes.* This favors the desirable microbiota-friendly activity, where the antimicrobial ingredient will not alter the good functionality of the healthy skin, acting efficiently against *C. acnes* and only mediating *S. epidermidis* proliferation. Another proof of concept was previously stated by other authors [42] providing evidence that microbiota shifts notably during puberty, increasing predominance of *Cutibacterium* species and decreasing abundance of *Staphylococcus* species. Meanwhile, in adulthood it remains unstable due to constant external environmental changes, suggesting mutual beneficial microbiome-host interactions. As a complement, the MICs showed that the concentration needed as bactericidal against *C. acnes* was lower than the minimal concentration needed to inhibit *S. epidermidis* growth. This means that for *in vivo* conditions, the desirable effect for acne treatment would maintain the skin balanced. In the case of clindamycin, the MIC for *C. acnes* and *S. epidermidis* was confirmed to be strongly efficient at a very low dose. This powerful activity is the main challenge with this type of drug, since it

completely abolishes all the microbial content of the skin, therefore, treating it by unbalancing the healthy conditions for the microbiota, thus, leading to microbial resistance. For this reason, in this study we managed to confirm an effective activity of a natural active, at higher concentration, but that can maintain the microbiota function to rebalance the skin conditions, maintaining it healthy upon the treatment.

From another point of view, since the route of penetration of polymeric TH-NP into the skin was through the hair follicle, the observed activity will be performed directly on the acne lesion. Therefore, TH-NP perform a protective effect on the healthy skin microbiota, along with extending the retention and release of TH, directly to the site of the infection with prolonged activity. Moreover, the sebum content on the hair follicles could facilitate absorption and release of TH from TH-NP by hydrophobic interactions. Nevertheless, since PLGA skin metabolism occurs by biodegradation into its monomers (lactic acid and glycolic acid), these compounds may help to modulate the skin pH, which would contribute to the sebum control.

Conclusions

TH was successfully encapsulated into PLGA NPs with particle size below 200 nm and high EE with suitable stability. Moreover, TH-NP solution did not present microbial growth under a storage period of 12 months, due to antimicrobial properties of TH. Therefore, they can act as natural preservative system. TH-NP presented a sustained release and slow-rate penetration on skin, through the hair follicle, with higher amounts retained inside the skin, compared to TH free. Moreover, TH-NP showed outstanding antimicrobial activity *in vitro* and *ex vivo* against *C. acnes*, with minor effects towards *S. epidermidis*, which promises to be a great microbiota-friendly candidate for acne treatment. Additionally, TH-NP adhered into the SC layers would provide good protection on the acne lesions against external microbial aggressors. Moreover, the cellular uptake of TH-NP has also improved the antioxidant activity in keratinocyte cells, which would be promising on cell regeneration on the healing process of the acne lesion. Therefore, TH loaded

nanostructured system has been successfully developed and physicochemically characterized demonstrating excellent properties for acne topical treatment.

Methods

Materials

PLGA Resomer® RG 504H (consisting of a carboxylic terminal group, molecular weight 38000 - 54000 Da and molar ratio lactide:glycolide 50:50) was purchased from Boehringer Ingelheim (Ingelheim, Germany). Thymol (TH), Tween 20 (TW) and acetone were purchased from Sigma-Aldrich (Spain). Milli-Q water was obtained from a double distilled Millipore system. All chemicals and reagents used were analytical grade (HPLC).

Preparation of TH-NP

TH-NP containing a matrix structure (nanospheres) were obtained by solvent displacement evaporation, described by Fessi et al. [43]. Briefly, an aqueous phase containing TW and an organic phase were prepared. The organic phase was made by dissolving PLGA and TH in acetone, and it was added dropwise into the aqueous phase under continuous stirring. Finally, in order to evaporate the organic solvent, a rotatory evaporator (Buchi, Switzerland) was used at 30 ^{o}C under constant pressure, obtaining TH-NP dispersed in water [44], [45], [46].

Optimization of TH-NP

TH-NP were optimized using the design of experiments approach (DoE). A full factorial central design of five levels and three factors was applied in order to reduce the number of experiments [47]. This experimental design consisted of 16 formulations with variable factorial points (-1/+1), axial points (-1.68/+1.68) and central points (0), each involving 8, 6 and 2 formulations, respectively. The concentration of active (TH), surfactant (TW) and the pH of the aqueous phase were selected

as the independent variables (Table 5). PLGA was fixed to 9 mg/mL for the entire experiment. The effect of the independent on the dependent variables (morphology, z-potential and encapsulation efficiency) has been analyzed [48].

Table 5. Factors and levels of DoE independent variables

	Levels				
Factors	*-1.68*	*-1*	*0*	*1*	*1.68*
TH (mg/mL)	1.16	1.5	2.0	2.5	2.84
TW (mg/mL)	1.32	2.0	3.0	4.0	4.68
pH	4.32	5.5	6.0	6.5	7.68

Physicochemical characterization of TH-NP

Z_{av} and PI were determined by photon correlation spectroscopy, using a ZetaSizer Nano ZS (Malvern Instruments; Malvern, UK). The surface charge, measured as ZP, was determined by electrophoretic mobility using the same instrument. The morphology of the particles was accessed by TEM (transmission electron microscopy, JEOL JEM1010, Tokyo, Japan), using Megaview III (Soft Imaging Systems, GmbH, Münster, Germany). The negative staining was carried out with 2 % uranyl acetate.

Quantitative analysis was performed by reverse-phase high-performance liquid chromatography (HPLC) by a modification of the method described previously [49]. Studies were carried out in Acquity Waters System with UV detector, using a Kromasil® column (C18, 5 µm, 150x4.6 mm). The mobile phase consisted of acetonitrile:water under gradient conditions of 30:70 / 58:42 / 30:70 during 20 min. TH was determined at wavelength of 275 nm.

The encapsulation of TH was measured indirectly by quantification of unloaded amount. Samples were diluted 1:10 in Milli-Q water:ethanol (90:10) and centrifuged (Centrifuge 5415C, Geratebau Eppendorf GmbH, Engelsdorf, Germany) for 10 min at 14000 rpm, using Millipore filter device (Amicon® Ultra, 0.5 mL 100K, Merck Millipore Ltd., Carrigtwohill Co. Cork IRL). The filtered fractions were quantified by HPLC, and the EE was determined by the equation (1):

$$EE = \frac{Ci - Cs}{Ci} \cdot 100 \qquad (1)$$

where *Ci* is the initial concentration of the active and *Cs* is the concentration of the unloaded amount found in the filtered fraction.

Interaction studies

Interaction studied were carried out by previous ultracentrifugation of the samples at 15.000 rpm during 30 min of TH-NPs (Beckmann-Coulter ultracentrifuge). The possible interactions between TH and PLGA were assessed by differential scanning calorimetry (DSC). Thermograms were obtained on a DSC823e System (Mettler-Toledo, Barcelona, Spain). A pan with indium (purity ≥ 99.95 %; Fluka, Switzerland) was used to check the calibration of the calorimetric system and an empty pan was used as a reference [32]. Samples were heated from 10 °C to 100 °C at 5 °C/min under a nitrogen atmosphere. Data were evaluated from the peak areas with Mettler STARe V 9.01 DB software (Mettler-Toledo). The physical state (amorphous or crystalline) of TH and TH-NP was analyzed by X-ray diffraction (XRD). Samples were sandwiched between 3.6 µm films of polyester and exposed to Cu K α radiation (λ = 1.5418 Å) with work power (45 kV, 40 mA). Diffractograms were recorded on a PANalytical X'Pert PRO MPD θ/θ, powder diffractometer of 240 mm of radius, using PIXcel detector (active length = 3.347 º). The measure time was defined 200 s per step, $2\theta/\theta$ scans from 2 to 60 º2θ with a step size of 0.026 º2θ [50].

Stability of TH-NP

The physicochemical stability of the optimized formulation was followed during storage at different conditions: 25 and 37 °C for 3 months and 4 °C for 12 months. The stability was studied by measuring backscattering of near-infrared pulsed light (λ = 880 nm), bottom-to-top of the turbiscan cell containing TH-NP, using optical analyzer Turbiscan®Lab expert (Formulaction, L'Union, France), to predict the behavior of the NPs in solution. Additionally, measurements of Z_{av}, PI, ZP and TEM images were also monitored at selected times. The EE stability was also measured at 6 months of storage.

To analyze the microbial preservative activity of TH during storage, samples stored for 6 months at room temperature and 12 months at 4 °C where used. For direct measurement, 0.1 mL of each sample was transferred into the plates or, additionally, samples where diluted 1:10 in neutralizing solution (Berens Cosmetic Diluent, Scharlab, UK), then 1 mL was transferred into the plates. The total viable count was carried out by inclusion on TSA (Tryptone Soy Agar, Oxoid, UK) for bacteria or Sabouraud Dextrose Agar (Oxoid, UK) for fungi and yeasts. Plates were incubated at 35 ± 2 °C for 3 days or at 28 ± 2 °C for 7 days, respectively. This methodology was designed based on specifications of the European Pharmacopeia monographs (2.6.12. Microbiological examination of non-sterile products: total viable aerobic count).

In vitro release

The *in vitro* release of TH from TH-NP against free TH was carried out using vertical diffusion Franz cells (FDC-400, Vidra-Foc, Barcelona, Spain) with a thermal bath set to 32 °C, to mimic skin *in vivo* conditions, under constant stirring. For this study, methylcellulose membranes (Dialysis Tubing – ViskingCode DTV12000.03.000, Size 3, Inf Day 20/32"– 15.9 mm, MWCO– 12–14.000 Da, Liverpool Road, London, UK) were placed between donor/receptor compartments (2.54 cm^2). Samples of TH or TH-NP were added to the donor phase (0.5 mL) and the receptor phase was filled with Transcutol P®:water (50:50), maintaining sink conditions. Aliquots of 300 µL were collected at selected times, replaced with the same amount of receptor medium [34]. Data were analyzed by HPLC and processed with the Boltzmann Sigmoidal mathematical model, equation (2), using GraphPad®.

$$Y = \frac{Bottom+(Top-Bottom)}{(1+\exp\left(\frac{(V50-X)}{Slope}\right)} \qquad (2)$$

Ex vivo skin permeation

Ex vivo human skin permeation was carried out by vertical diffusion Franz Cells, using the same methodology as described above. Human skin was obtained from abdominal plastic surgery

589 (Hospital de Barcelona, SCIAS, Barcelona, Spain), following a protocol approved by the Bioethics
590 Committee of the Barcelona-SCIAS Hospital. Skin samples (2.54 cm², 0.4 mm thick) were clamped
591 into the Franz cells with the SC facing up [51]. Previously, some of the skin samples were scratched
592 with sandpaper to mimic damaged skin SC. The donor compartment was filled (0.5 mL) with TH or
593 TH-NP (0.25 %). Data were analyzed by HPLC and processed using GraphPad®. The skin
594 permeation parameters were calculated by the equation (3):

595 $$J = Kp \,.\, C_0 \qquad (3)$$

596 where *J* is the flux, *Kp* is the permeability coefficient and C_0 is the initial concentration of the active
597 [52].
598
599 The amount retained inside the skin was assessed by tape striping and skin extraction techniques.
600 Firstly, skin samples were washed with sodium lauryl sulphate (0.02 %) and rinsed with distilled
601 water, dried, cut, and weighted. For determination of the amount retained in the SC, tape stripping
602 assay was developed based on previous authors with minimal modifications [53]. The first layers
603 of the skin were removed by 7 strips of the same region of the SC using a transparent label dressing
604 (3M Tegaderm®, 6x7cm, 10u, Spain, S.A.). The strips were added into 4 mL of ethanol and placed
605 into an ultrasonic bath (JP, Selecta) for 20 min for compound extraction. For determination of the
606 total amount retained inside the deeper layers, the rest of the skin was perforated, added into 2 mL
607 of ethanol:water (50:50) and then kept in the ultrasonic bath for 20 min [52]. The amount of thymol
608 extracted was determined by HPLC and calculated using the recovery factor previously obtained.
609 To determine the permeation route of TH-NP, vertical diffusion Franz cells were used as described
610 before. *Ex vivo* pig skin penetration was obtained from the animal house (Bellvitge, University of
611 Barcelona), used in accordance with the protocol approved by the Ethics Committee of the
612 University of Barcelona. For this study, rhodamine-labelled PLGA (R-PLGA) was synthesized as
613 previously described [44]. R-PLGA was used at 0.01 % into TH-NP, added in the organic phase
614 with PLGA. R-TH-NP were applied onto the *ex vivo* pig skin 0.64 cm² (donor compartment) and
615 allowed penetration for 24 h. Skin samples were washed, fixed in PBS containing 4 %
616 paraformaldehyde (PFA) for 4 h, followed by cryoprotection into PBS with 30 % sucrose for 24 h,

snap-frozen in isopentane at – 50 °C, then kept overnight at - 80 °C. Samples were mounted in O.C.T.® Compound (Tissue-Tek®, Sakura) and sliced with cryostat microtome (LEICA CM3050 S) at -20 °C onto glass-slides Superfrost® Plus (Menzel-Glaser, Thermo Scientific, USA), covered with Fluoromount G® (Invitrogen, Thermo Fisher Scientific, USA). Samples were visualized by confocal laser scanning microscopy (Zeiss LSM 880), using objective lens 10X 0.45. Images were acquired using Zen Black 2.3 software performing z-stack sections and thus processed with ImageJ software.

Cytotoxicity studies in HaCaT cells

Human keratinocytes (HaCaT) cells were cultured in high glucose DMEM (Dulbecco's Modified Eagle's Medium (Thermofisher), supplemented with 10 % fetal bovine serum (FBS), 2 mM L-glutamine, 100 units/mL penicillin G and 100 µg/mL streptomycin. Cells were incubated at 37 °C and 5 % CO_2 and experiments were performed when cells reached 80 – 90 % of confluence.

Cytotoxicity of TH-NP was determined by MTT (3-(4,5-Dimethylthiazol-2-yl)-2,5-diphenyl tetrazolium bromide) assay, by reduction of tetrazolium salt by intracellular dehydrogenases of viable living cells. TH-NP were tested at concentrations up to 1 mg/ml. The assay was also performed with TH-NP previously washed thrice (TH-NP-w) to remove excess of free TW (centrifugation at 14000 rpm for 15 min). Briefly, HaCaT cells were seeded in 96-well plates with 100 µL of culture medium (DMEM) at a density of 2×10^5 cells/well, adjusted in automated cell counter (Countess, Invitrogen, Thermofisher). Cells were incubated with samples for 24 h. Then, the medium was removed and MTT (Sigma-Aldrich Chemical Co, St. Louis, MO, USA) was added at 0.25 % in PBS. After 2 h incubation, the medium was replaced by 100 µL DMSO (99 % dimethyl sulfoxide, Sigma-Aldrich) [54]. Cell viability was then measured at wavelength of 570 nm in a Modulus® Microplate Photometer (Turner BioSystems Inc., Sunnyvale, CA, USA). Results were expressed as percentage of cell survival relative to untreated cells.

Cellular uptake of TH-NP

Cellular uptake of TH-NPs was assayed in HaCaT cells seeded in an 8-well µ-slide (Ibidi®) following the same methodology as described before. Cells were incubated with or without R-TH-NP for 2 h at the indicated concentration, using FBS/phenol red free medium. Cell membranes were stained with wheat germ agglutinin (WGA) Alexa-488 (Molecular Probes) at 1 µg/mL for 15 min followed by fixation with paraformaldehyde 3 % for 25 min. Cell nuclei were stained with 4',6-diamidino-2-phenylindole (DAPI, Sigma Aldrich, Spain) at 0.5 µg/mL for 15 min. Internalization of NPs in HaCaT cells was assessed by confocal microscopy (Leica TCS SPII), 63X oil immersion objective lens [44]. Images were processed using Fiji image software.

In vitro antioxidant efficacy in HaCaT cells

The antioxidant activity of TH, TH-NP, and B-NP (blank NPs) was assayed in HaCaT cells by quantification of ROS using the fluorogenic probe H2DCFDA. Cells were seeded in 96-well plates at 2×10^5 cells/well (100 µL) for 72 h. Cells were loaded with the fluorogenic dye H_2DCFDA (2',7'-dichlorodihydrofluorescein diacetate) at 25 µM diluted in DMEM medium absent of phenol red and FBS, for 45 min in the dark. This fluorogenic dye passively diffuses into the cells, being deacetylated by intracellular esterase and emits fluorescence upon oxidation by reactive oxygen species (ROS) [55]. Then, cells were washed with PBS and incubated for 2 h with TH, TH-NP or B-NP. After this period, 10 µL of H_2O_2 20 mM was added to each well. Untreated cells with or without H_2O_2 were used as positive and negative controls, respectively. Fluorescence was measured at excitation and emission wavelengths of 485 and 530 nm, respectively. Data were acquired at times t0 up to 120 min. Data of the positive control (H_2O_2) at 2 h, were used to normalize values (%). Background fluorescence of the negative control was subtracted from all measurements.

In vitro antimicrobial efficacy

S. epidermidis was grown overnight 37 °C in Mueller Hinton Broth (MHB) culture medium (Oxoid, Basingstoke, UK). Prior to each experiment, the inoculum was prepared in PBS adjusted to 0.5 MacFarland (McF) standard, to obtain a suspension with a cell density at the range of 1.5×10^8

colony forming units/mL (CFU/mL). Microbial count of *S. epidermis* was performed in TSA plates, incubated at 37 °C. The *C. acnes* was cultured in Brain Heart Infusion (BHI) medium (Oxoid, Basingstoke, UK) for 48 hours at 37 °C under anaerobic conditions using parches (AnaeroGen®, Oxoid, Basingstoke, UK) and indicator (Oxoid, Basingstoke, UK). Prior to each experiment, the inoculum was prepared in PBS adjusted to 0.5 McF. Microbial count of *C. acnes* was performed in clostridium reinforced medium (CRM) plates, as recommended for anaerobia growth, incubated at 37 °C.

The MIC of TH and TH-NP were determined using the broth microdilution assay [56]. Briefly, double concentrated sample dilutions were prepared and added (100 µL) to double concentrated culture medium (100 µL) in a 96-well polypropylene microtiter plate (Costar, Corning Incorporated, Corning, USA). Inocula were prepared to yield a final concentration of 5 x 10^5 CFU/mL. For *S. epidermidis,* 10 µL were transferred to inoculate wells with final TH concentrations of 2 to 1024 µg/mL, followed by incubation at 37 °C for 18 to 20 h. For *C. acnes,* 20 µL was used to inoculate wells with concentrations ranging from 2 to 1000 µg/mL and the plate was incubated at 37 °C for 48 h under anaerobiosis. Thus, the MBC was performed by transferring 10 µL of each sample presenting no visible growth of *C. acnes* into BHI plates. These were further incubated as described before. Growth controls were used for the above experiments: presenting antimicrobial sterility (negative) and absent of antimicrobial (positive). Clindamycin was also used as an active control for both microorganisms.

The determination of the decimal reduction time assay, explores the antimicrobial activity of TH and its derivative TH-NP on reducing bacteria viability at determined contact times [57]. For *C. acnes*, formulations were diluted with water up to 250, 500 and 1000 µg/mL representing the MIC, 2x MIC and 4x MIC, respectively. For *S. epidermidis*, formulations were used at 1000 µg/mL, representing twice as MIC. Inocula were prepared in PBS at 10^8 CFU/mL and used to inoculate (100 µL) each experimental sample of 10 mL, incubated at 32 °C. The determined times were 0, 1, 2, 3 and 6 h or 0, 3, 8, 24 and 48 h for *C. acnes* and *S. epidermidis*, respectively. After incubations of each time set, an aliquot of 1 mL of each sample was neutralized in 9 mL of Berens diluent (Scharlab, Barcelona, Spain) for 15 minutes, then, diluted in PBS on subsequent 10-folds. Drop

count method (10 µL) was performed in CRM and TSA agar plates, *for C. acnes* and *S. epidermidis*, respectively, incubated at 37 °C as described previously. Bacterial viability was expressed as CFU/mL against time (h). The decimal reduction time, the time taken to reduce by 10 % the initial log_{10}CFU, was determined calculating the inverse of the slope (1/b).

The antimicrobial activity was also evaluated by SEM. For this, *C. acnes* was cultured for 48 h in BHI culture media in an incubator shaker (Innova® 4080, New Brunswick Scientific) at 37 °C under anaerobic conditions. The concentrated inoculum was transferred (900 µL) to each tube containing 100 µL of TH or TH-NP at 0.1 % or sterile distilled water (control) and incubated in the shaker for 1 h. After samples were centrifuged (10000 g for 5 min), supernatants were discarded and the concentrated pellets were placed into poly-l-lysine coated coverslips and kept at room temperature for 24 h [58]. Samples were fixed for 4 h with phosphate buffer 0.1 M pH 7.4, containing 4 % paraformaldehyde and 2.5 % glutaraldehyde, then post-fixed with 1 % osmium tetroxide (with potassium ferrocyanide) for 1 h, at 4 °C. After dehydration with alcohol gradients, samples were dried at critical point (Emitech K850), mounted on a conductor adhesive disc (Carbon tabs, Agar Scientific), followed by carbon coating under evaporation (Emitech 950). Images were analyzed by SEM (scanning electron microscopy, Jeol JSM-7001F).

Ex vivo antimicrobial efficacy

The bacterial viability was evaluated on treated human skin explants obtained from abdominal plastic surgery (Hospital de Barcelona, SCIAS, Barcelona, Spain), based on other researcher protocols with modifications [59]. Skin samples were cut with a cryostat (Leica Microsystems, Wetziar, Germany) in 0.6 cm^2, washed with ethanol followed by sterile PBS, for 2 and 10 s, respectively, to remove possible existing bacteria. Once dried with sterile filter paper, skins were placed into petri dishes (purchased from Fischer Scientific) with the SC facing up, onto PBS-wet sterile filter paper to keep dermis moisture. Two experiments (prevention and treatment) were set up for 24 h incubation at 32 °C, in the presence of humidity. A fresh overnight culture of *C. acnes* was suspended in PBS (1.5 x 10^8 CFU/mL) and skin samples were inoculated with 10 µL. For the pre-treatment study, TH-NP or TH were applied on skin samples (30 µL) and incubated at 32 °C

for 8 h, followed by inoculation with *C. acnes* (30 µL) for 16 h. For the post-treatment study, skin was first inoculated for 30 min and then treated with products for 24 h. At the end of the experiment, skin samples were neutralized in 1 mL Berens diluent (Scharlab, Barcelona, Spain) for neutralization (15 min) followed by extraction for 10 min using a sonication bath (JP, Selecta, Spain). The extraction method was previously optimized by testing the control at two extraction times (3 to 15 min), controlling bacteria viability by sonication process. Positive controls were also performed using PBS. 10-fold dilutions were performed and 100 µL of each sample was spread individually onto CRM agar plates and incubated under anaerobiosis at 37 °C for 48 h. Viable bacteria count was expressed as log/CFU per treated skin.

The analysis of bacterial viability on dose-dependent study on treated skin was also performed using the same technique as described above, with further modifications [59]. A fresh overnight culture of *C. acnes* was prepared in PBS and skin samples were inoculated (10 µL). After 30 min, 30 µL of TH or TH-NP were administered as a single or repeated dose (1, 2 or 3), at preselected times (0, 12 and 18 h), completing a total incubation of 24 h at 32 °C, in the presence of humidity. Then, skin samples were neutralized and extracted as described above. These were 10-fold diluted and transferred to CRM plates by drop-count method (10 µL). Plates were incubated under anaerobic conditions at 37 °C for 48 h. Viable bacteria were expressed as CFU per treated skin.

A simulation of skin infection was performed in fresh human skin explant (Hospital de Barcelona, SCIAS, Barcelona, Spain) and analyzed by transmission electron microscopy. The fat tissue of skin samples, obtained from human abdominal plastic surgery, was removed manually with sterile surgical razors. Skin samples were cut and placed on a 0.64 cm^2 Franz diffusion cell. The receptor compartment was filled with PBS, and the skin was inoculated with 20 µL of *C. acnes* (10^8 CFU/mL) and incubated for 16 h at 32 °C, followed by treatment with TH or TH-NP (100 µL) for 8 h incubation. For electron microscopy, skin samples were fixed for 2 h with 4 % paraformaldehyde and 2.5 % glutaraldehyde in 0.1 M sodium cacodylate buffer (pH 7.4), postfixed with 1 % osmium tetroxide for 2 h at 4 °C (all from Sigma Aldrich), stained in 0.5 % uranyl acetate (from Fischer Scientific) for 45 min at 4 °C and finally, dehydrated gradually in 30 to 100 % ethanol [41]. Samples were infiltered in EPON resin [Eponate 12 (23.5 g), dodecenyl succinic anhydride DDSA (12.5 g) and Methyl nadic

anhydride MNA (14 g)] (from Sigma Aldrich). Inclusions were performed gradually diluted in ethanol and finally for 3 h using a catalyst [DMP-30 (2,4,6-tris(dimethylaminomethyl)phenol), 0.37 g] (purchased from Sigma Aldrich). Polymerization was carried out for 48 h at 60 °C. Blocks were sliced in thin sections with Ultracut microtome (LEICA), further fixed on copper grids and stained with uranyl acetate 2 % for 10 min. Analysis was performed by TEM and images were obtained with Megaview III.

References

[1] A. Kapuścińska and I. Nowak, “Use of organic acids in acne and skin discolorations therapy,” *Postepy Hig. Med. Dosw.*, vol. 69, pp. 374–383, 2015, doi: 10.5604/17322693.1145825.

[2] Kampf G and Karamer A, “Epidemiologic Background of Hand Hygiene and Evaluation of the Most Important Agents for Scrubs and Rubs,” *Clin. Microbiol. Rev.*, vol. 17, no. 4, pp. 863–893, 2004, doi: 10.1128/CMR.17.4.863.

[3] S. Nishijima, I. Kurokawa, N. Katoh, and K. Watanabe, “The bacteriology of acne vulgaris and antimicrobial susceptibility of Propionibacterium aches and Staphylococcus epidermidis isolated from acne lesions,” *J. Dermatol.*, vol. 27, no. 5, pp. 318–323, 2000, doi: 10.1111/j.1346-8138.2000.tb02174.x.

[4] M. Otto, “Staphylococcus epidermidis – the ‘accidental’ pathogen,” *Nat Rev Microbiol.*, vol. 7, no. 8, pp. 557–567, 2009, doi: doi:10.1038/nrmicro2182.

[5] Ajay Bhatia, Jean-Francoise Maisonneuve, and David H. Persing, “PROPIONIBACTERIUM ACNES AND CHRONIC DISEASES - The Infectious Etiology of Chronic Diseases - NCBI Bookshelf.” 2004.

[6] J. P. Claudel, N. Auffret, M. T. Leccia, F. Poli, S. Corvec, and B. Dréno, “Staphylococcus epidermidis: A Potential New Player in the Physiopathology of Acne?,” *Dermatology*, vol. 235, no. 4, pp. 287–294, 2019, doi: 10.1159/000499858.

[7] L. Boukraâ, F. Abdellah, and L. Ait-Abderrahim, “Antimicrobial Properties of Bee Products

and Medicinal Plants," *Formatex*, no. Microbial pathogens and strategies for combating them: science, technology and education, pp. 960–970, 2013.

[8] R. Alvarez-Román, A. Naik, Y. N. Kalia, R. H. Guy, and H. Fessi, "Skin penetration and distribution of polymeric nanoparticles," *J. Control. Release*, vol. 99, no. 1, pp. 53–62, 2004, doi: 10.1016/j.jconrel.2004.06.015.

[9] A. C. Calpena, B. Clares, and F. Fernández, "Technological, biopharmaceutical and pharmacokinetic advances: New formulations of application on the skin and oral mucosa," in *Recent Advances in Pharmaceutical Sciences*, vol. 661, no. 2, D. Muñoz-Torrero, Ed. Kerala, India: Transworld Research Network, 2011, pp. 175–198.

[10] J. Shim, H. S. Kang, W. S. Park, S. H. Han, J. Kim, and I. S. Chang, "Transdermal delivery of mixnoxidil with block copolymer nanoparticles," *J. Control. Release*, vol. 97, no. 3, pp. 477–484, 2004, doi: 10.1016/j.jconrel.2004.03.028.

[11] L. Wang *et al.*, "Thymol kills bacteria, reduces biofilm formation, and protects mice against a fatal infection of Actinobacillus pleuropneumoniae strain L20," *Vet. Microbiol.*, vol. 203, pp. 202–210, 2017, doi: 10.1016/j.vetmic.2017.02.021.

[12] H. Abd-Allah, R. T. A. Abdel-Aziz, and M. Nasr, "Chitosan nanoparticles making their way to clinical practice: A feasibility study on their topical use for acne treatment," *Int. J. Biol. Macromol.*, vol. 156, pp. 262–270, 2020, doi: 10.1016/j.ijbiomac.2020.04.040.

[13] S. S. Amer *et al.*, "Cosm-nutraceutical nanovesicles for acne treatment: Physicochemical characterization and exploratory clinical experimentation," *Int. J. Pharm.*, vol. 577, no. January, p. 119092, 2020, doi: 10.1016/j.ijpharm.2020.119092.

[14] D. Trombetta *et al.*, "Mechanisms of antibacterial action of three monoterpenes," *Antimicrob. Agents Chemother.*, vol. 49, no. 6, pp. 2474–2478, 2005, doi: 10.1128/AAC.49.6.2474-2478.2005.

[15] A. Guarda, J. F. Rubilar, J. Miltz, and M. J. Galotto, "The antimicrobial activity of microencapsulated thymol and carvacrol," *Int. J. Food Microbiol.*, vol. 146, no. 2, pp. 144–150, 2011, doi: 10.1016/j.ijfoodmicro.2011.02.011.

[16] A. Nostro *et al.*, "Effects of oregano, carvacrol and thymol on Staphylococcus aureus and

Staphylococcus epidermidis biofilms," *J. Med. Microbiol.*, vol. 56, no. 4, pp. 519–523, 2007, doi: 10.1099/jmm.0.46804-0.

[17] N. V. Yanishlieva, E. M. Marinova, M. H. Gordon, and V. G. Raneva, "Antioxidant activity and mechanism of action of thymol and carvacrol in two lipid systems," *Food Chem.*, vol. 64, no. 1, pp. 59–66, 1999, doi: 10.1016/S0308-8146(98)00086-7.

[18] A. Wattanasatcha, S. Rengpipat, and S. Wanichwecharungruang, "Thymol nanospheres as an effective anti-bacterial agent," *Int. J. Pharm.*, vol. 434, no. 1–2, pp. 360–365, 2012, doi: 10.1016/j.ijpharm.2012.06.017.

[19] M. F. Nagoor Meeran, H. Javed, H. Al Taee, S. Azimullah, and S. K. Ojha, "Pharmacological properties and molecular mechanisms of thymol: Prospects for its therapeutic potential and pharmaceutical development," *Front. Pharmacol.*, vol. 8, no. JUN, pp. 1–34, 2017, doi: 10.3389/fphar.2017.00380.

[20] P. Mollarafie, P. Khadiv Parsi, R. Zarghami, M. Amini Fazl, and R. Ghafarzadegan, "Antibacterial and wound healing properties of thymol (Thymus vulgaris Oil) and its application in a novel wound dressing," *J. Med. Plants*, vol. 14, no. 53, pp. 69–81, 2015.

[21] Y. M. Zhang and C. O. Rock, "Membrane lipid homeostasis in bacteria," *Nat. Rev. Microbiol.*, vol. 6, no. 3, pp. 222–233, 2008, doi: 10.1038/nrmicro1839.

[22] R. Najafloo, M. Behyari, R. Imani, and S. Nour, "A mini-review of Thymol incorporated materials: Applications in antibacterial wound dressing," *J. Drug Deliv. Sci. Technol.*, vol. 60, no. March, 2020, doi: 10.1016/j.jddst.2020.101904.

[23] E. Medina, N. Caro, L. Abugoch, A. Gamboa, M. Díaz-Dosque, and C. Tapia, "Chitosan thymol nanoparticles improve the antimicrobial effect and the water vapour barrier of chitosan-quinoa protein films," *J. Food Eng.*, vol. 240, no. June 2018, pp. 191–198, 2019, doi: 10.1016/j.jfoodeng.2018.07.023.

[24] B. J. Juven, J. Kanner, F. Schved, and H. Weisslowicz, "Factors that interact with the antibacterial action of thyme essential oil and its active constituents," *J. Appl. Bacteriol.*, vol. 76, no. 6, pp. 626–631, 1994, doi: 10.1111/j.1365-2672.1994.tb01661.x.

[25] E. Sánchez-López *et al.*, "PEGylated PLGA nanospheres optimized by design of

experiments for ocular administration of dexibuprofen-in vitro, ex vivo and in vivo characterization," *Colloids Surfaces B Biointerfaces*, vol. 145, pp. 241–250, 2016.

[26] E. Sánchez-López *et al.*, "Memantine-Loaded PEGylated Biodegradable Nanoparticles for the Treatment of Glaucoma," *Small*, vol. 1701808, p. 1701808, 2017.

[27] E. Vega *et al.*, "Flurbiprofen PLGA-PEG nanospheres: Role of hydroxy-β-cyclodextrin on ex vivo human skin permeation and in vivo topical anti-inflammatory efficacy," *Colloids Surfaces B Biointerfaces*, vol. 110, pp. 339–346, 2013.

[28] L. Gómez-Segura, A. Parra, A. C. Calpena-Campmany, Á. Gimeno, I. G. de Aranda, and A. Boix-Montañes, "Ex vivo permeation of carprofen vehiculated by PLGA nanoparticles through porcine mucous membranes and ophthalmic tissues," *Nanomaterials*, vol. 10, no. 2, 2020, doi: 10.3390/nano10020355.

[29] D. Kim, H. El-Shall, D. Dennis, and T. Morey, "Interaction of PLGA nanoparticles with human blood constituents.," *Colloids Surf. B. Biointerfaces*, vol. 40, no. 2, pp. 83–91, Feb. 2005, doi: 10.1016/j.colsurfb.2004.05.007.

[30] X. Zhang, M. Sun, A. Zheng, D. Cao, Y. Bi, and J. Sun, "Preparation and characterization of insulin-loaded bioadhesive PLGA nanoparticles for oral administration," *Eur. J. Pharm. Sci.*, vol. 45, no. 5, pp. 632–638, 2012, doi: 10.1016/j.ejps.2012.01.002.

[31] D. Xiao, C. Gömmel, P. M. Davidson, and Q. Zhong, "Intrinsic tween 20 improves release and antilisterial properties of co-encapsulated nisin and thymol," *J. Agric. Food Chem.*, vol. 59, no. 17, pp. 9572–9580, 2011, doi: 10.1021/jf201864v.

[32] E. Sánchez-López *et al.*, "PEGylated PLGA nanospheres optimized by design of experiments for ocular administration of dexibuprofen-in vitro, ex vivo and in vivo characterization," *Colloids Surfaces B Biointerfaces*, vol. 145, pp. 241–250, 2016.

[33] A. Cano *et al.*, "Epigallocatechin-3-gallate loaded PEGylated-PLGA nanoparticles: A new anti-seizure strategy for temporal lobe epilepsy," *Nanomedicine Nanotechnology, Biol. Med.*, vol. 14, no. 4, pp. 1073–1085, 2018, doi: 10.1016/j.nano.2018.01.019.

[34] G. Abrego *et al.*, "Biopharmaceutical profile of pranoprofen-loaded PLGA nanoparticles containing hydrogels for ocular administration," *Eur. J. Pharm. Biopharm.*, vol. 95, pp.

261–270, 2015.

[35] C. Gorzelanny, C. Mess, S. W. Schneider, V. Huck, and J. M. Brandner, “Skin barriers in dermal drug delivery: Which barriers have to be overcome and how can we measure them?,” *Pharmaceutics*, vol. 12, no. 7, pp. 1–31, 2020, doi: 10.3390/pharmaceutics12070684.

[36] Q. D. Pham, S. Björklund, J. Engblom, D. Topgaard, and E. Sparr, “Chemical penetration enhancers in stratum corneum - Relation between molecular effects and barrier function,” *J. Control. Release*, vol. 232, pp. 175–187, 2016, doi: 10.1016/j.jconrel.2016.04.030.

[37] N. Akhtar, M. U. Rehman, H. M. S. Khan, F. Rasool, T. Saeed, and G. Murtaza, “Penetration enhancing effect of polysorbate 20 and 80 on the in vitro percutaneous absorption of L-ascorbic acid,” *Trop. J. Pharm. Res.*, vol. 10, no. 3, pp. 281–288, 2011, doi: 10.4314/tjpr.v10i3.1.

[38] A. Patzelt and J. Lademann, “Recent advances in follicular drug delivery of nanoparticles,” *Expert Opin. Drug Deliv.*, vol. 17, no. 1, pp. 49–60, 2020, doi: 10.1080/17425247.2020.1700226.

[39] M. N. Yukuyama, G. L. B. De Araújo, and N. A. Bou-Chacra, “Nanomaterials for hair care applications,” *Nanocosmetics*, pp. 205–225, 2020, doi: 10.1016/b978-0-12-822286-7.00010-3.

[40] Z. Zhu, T. Min, X. Zhang, and Y. Wen, “Microencapsulation of thymol in poly(lactide-co-glycolide) (PLGA): Physical and antibacterial properties,” *Materials (Basel).*, vol. 12, no. 7, 2019, doi: 10.3390/ma12071133.

[41] S. Messager, A. C. Hann, P. A. Goddard, P. W. Dettmar, and J. Y. Maillard, “Use of the ‘ex vivo’ test to study long-term bacterial survival on human skin and their sensitivity to antisepsis,” *J. Appl. Microbiol.*, vol. 97, no. 6, pp. 1149–1160, 2004, doi: 10.1111/j.1365-2672.2004.02403.x.

[42] Y. Erin Chen, M. A. Fischbach, and Y. Belkaid, “Skin microbiota-host interactions,” *Nature*, vol. 553, no. 7689, pp. 427–436, 2018, doi: 10.1038/nature25177.

[43] H. Fessi, F. Puisieux, J. P. Devissaguet, N. Ammoury, and S. Benita, “Nanocapsule

formation by interfacial polymer deposition following solvent displacement," *Int. J. Pharm.*, vol. 55, pp. R1–R4, 1989, doi: 10.1016/0378-5173(89)90281-0.

[44] R. Gonzalez-Pizarro *et al.*, "Ocular penetration of fluorometholone-loaded PEG-PLGA nanoparticles functionalized with cell-penetrating peptides," *Nanomedicine*, vol. 14, no. 23, pp. 3089–3104, 2019, doi: 10.2217/nnm-2019-0201.

[45] E. Sánchez-López *et al.*, "Dexibuprofen biodegradable nanoparticles: One step closer towards a better ocular interaction study," *Nanomaterials*, vol. 10, no. 4, pp. 1–24, 2020, doi: 10.3390/nano10040720.

[46] A. Vasconcelos, E. Vega, Y. Pérez, M. J. Gómara, M. L. García, and I. Haro, "Conjugation of cell-penetrating peptides with poly(lactic-co-glycolic acid)-polyethylene glycol nanoparticles improves ocular drug delivery," *Int. J. Nanomedicine*, vol. 10, pp. 609–631, 2015.

[47] R. Gonzalez-Pizarro, M. Silva-Abreu, A. C. Calpena, M. A. Egea, M. Espina, and M. L. García, "Development of fluorometholone-loaded PLGA nanoparticles for treatment of inflammatory disorders of anterior and posterior segments of the eye," *Int. J. Pharm.*, vol. 547, no. 1–2, pp. 338–346, 2018.

[48] E. Sánchez-López *et al.*, "Memantine loaded PLGA PEGylated nanoparticles for Alzheimer's disease : in vitro and in vivo characterization," *J. Nanobiotechnology*, vol. 16, no. 32, pp. 1–16, 2018.

[49] A. Ghasemi Pirbalouti, M. Rahimmalek, F. Malekpoor, and A. Karimi, "Variation in antibacterial activity, thymol and carvacrol contents of wild populations of Thymus daenensis subsp. daenensis Celak," *Plant Omics*, vol. 4, no. 4, pp. 209–214, 2011.

[50] M. Silva-Abreu *et al.*, "Optimization, biopharmaceutical profile and therapeutic efficacy of pioglitazone-loaded PLGA-PEG nanospheres as a novel strategy for ocular inflammatory disorders," *Pharm. Res.*, vol. 35, no. 1, p. 11, 2018.

[51] P. Carvajal-Vidal, M. J. Fábrega, M. Espina, A. C. Calpena, and M. L. García, "Development of Halobetasol-loaded nanostructured lipid carrier for dermal administration: Optimization, physicochemical and biopharmaceutical behavior, and therapeutic efficacy,"

Nanomedicine Nanotechnology, Biol. Med., vol. 20, p. 102026, 2019, doi: 10.1016/j.nano.2019.102026.

[52] H. L. Alvarado *et al.*, “Nanoemulsions for dermal controlled release of oleanolic and ursolic acids: In vitro, ex vivo and in vivo characterization,” *Colloids Surfaces B Biointerfaces*, vol. 130, pp. 40–47, 2015, doi: 10.1016/j.colsurfb.2015.03.062.

[53] K. Rehman, M. F. F. M. Aluwi, K. Rullah, L. K. Wai, M. C. I. Mohd Amin, and M. H. Zulfakar, “Probing the effects of fish oil on the delivery and inflammation-inducing potential of imiquimod,” *Int. J. Pharm.*, vol. 490, no. 1–2, pp. 131–141, 2015, doi: 10.1016/j.ijpharm.2015.05.045.

[54] N. Diaz-Garrido, M. J. Fábrega, R. Vera, R. Giménez, J. Badia, and L. Baldomà, “Membrane vesicles from the probiotic Nissle 1917 and gut resident Escherichia coli strains distinctly modulate human dendritic cells and subsequent T cell responses,” *J. Funct. Foods*, vol. 61, no. May, 2019, doi: 10.1016/j.jff.2019.103495.

[55] Y. H. Liu, Y. S. Lin, Y. W. Huang, S. U. Fang, S. Y. Lin, and W. C. Hou, “Protective Effects of Minor Components of Curcuminoids on Hydrogen Peroxide-Treated Human HaCaT Keratinocytes,” *J. Agric. Food Chem.*, vol. 64, no. 18, pp. 3598–3608, 2016, doi: 10.1021/acs.jafc.6b01196.

[56] L. M. Koeth and L. A. Miller, “Antimicrobial susceptibility test methods: dilution and disk diffusion methods,” in *Manual of Clinical Microbiology, 12th ed*, 12th ed., K. C. Carroll, M. A. Pfaller, M. L. Landy, R. Patel, A. J. McAdam, and S. . Richter, Eds. ASM Press. Washington D. C, 2019, pp. 1284–1299.

[57] A. P. MacGowan, M. Wootton, A. J. Hedges, K. E. Bowker, H. A. Holt, and D. S. Reeves, “A new time-kill method of assessing the relative efficacy of antimicrobial agents alone and in combination developed using a representative β-lactam, aminoglycoside and fluoroquinolone,” *J. Antimicrob. Chemother.*, vol. 38, no. 2, pp. 193–203, 1996, doi: 10.1093/jac/38.2.193.

[58] D. Mazia, G. Schatten, and W. Sale, “Adhesion of cells to surfaces coated with polylysine: Applications to electron microscopy,” *J. Cell Biol.*, vol. 66, no. 1, pp. 198–200, 1975, doi:

10.1083/jcb.66.1.198.

[59] S. Messager, P. A. Goddard, P. W. Dettmar, and J. Y. Maillard, “Determination of the antibacterial efficacy of several antiseptics tested on skin by an ‘ex-vivo’ test,” *J. Med. Microbiol.*, vol. 50, no. 3, pp. 284–292, 2001, doi: 10.1099/0022-1317-50-3-284.

Declarations

Ethics approval and consent to participate: not applicable

Competing interests: not applicable

Consent for publication: not applicable

Availability of data and materials: Not applicable.

Authors' contributions: CF, MLG and ACC developed, participated and coordinated the experiments carried out in this study. AMM, NDG, ACC and ME have directly participated in the experimental part of this manuscript. CF, JB, LB, MLG and ESL have written, contextualized and supervised this study.

Acknowledgements: the authors would like to acknowledge 2017SGR1477.